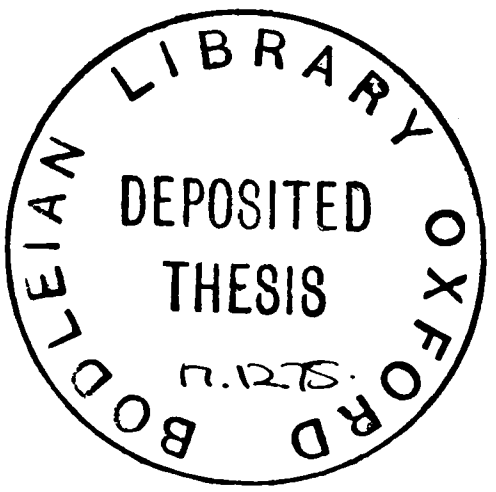
# STUDIES OF TRANSIENT INTERMEDIATES

A thesis submitted as a requirement of the degree of Doctor of Philosophy.

J.A. Robertson,

St. John's College, Oxford.

September, 1975.



ACKNOWLEDGEMENTS.

My thanks are due to Dr.M.J.Pilling for his assistance and criticism during the course of this work. I am also indebted to the Technical Staff of the Physical Chemistry Laboratory for advice and assistance.

I am indebted to my parents for their encouragement, in particular to my Mother who typed this thesis. In addition I should like to thank Christine, my fiancee, for her tolerance during its preparation.

Finally, I wish to thank the Science Research Council for a Research Studentship.

## ABSTRACT.

Ketene was flash photolysed at wavelengths greater than 160 nm. The photolysis lamp was of a four electrode pair design, with Marx - Bank circuitry, operating at 1000 J with a 1/e decay time of $< 4\ \mu s$. The photolysis products were analysed by gas chromatography. Experiments were largely limited to studies of ketene with inert gases, hydrogen, and methane, and the mixed photolysis system, ketene + azomethane. The experimental results were compared with kinetic simulations based upon Merson's method of numerical integration of coupled differential equations. The programme included a realistic simulation of the lamp profile, and varied the step length until the error in a single step was $< 10^{-4}\%$.

The major new result is the observation of "singlet products", ethane and methane, at limiting high inert gas pressures, in mixtures containing low pressures of hydrogen. Various schemes are suggested to explain this result: the most satisfactory one implicates $CH_2$ ($^1B_1$) in the reaction system. At low pressures, acetylene was formed in larger quantities than could be explained by any kinetic scheme involving $CH_2$. Its presence is attributed to heating effects or to alternative decomposition modes of $CH_2CO$ at low pressure.

The rate constants for reaction of $CH_2$ ($^3B_1$) + $CH_3$, and of $CH_2$ ($^1A_1$) with $H_2$, $CH_4$ and $CH_2CO$ are discussed. The rate constant for reaction of $CH_2$ ($^1B_1$) with $H_2$ is estimated on the assumption of a fluorescent lifetime of $10^{-6}$ s. The effect of $O_2$, NO, and CO as $CH_2$ scavengers is also discussed.

RRKM calculations for several radical - radical reactions are presented. The reactions of the various electronic states of methylene and the photolysis of ketene are discussed in terms of electronic symmetry.

CONTENTS.


| | | Page |
|---|---|---|
| | Chapter 1. Introduction. | 1. |
| 1.1. | Spectroscopic observation of the methylene radical. | 1. |
| 1.2. | Theoretical studies of the electronic states of methylene. | 5. |
| 1.3. | Generation of methylene radicals. | 9. |
| 1.4. | Reactions of methylene. | 21. |
| 1.5. | $CH_2$ ($^1A_1$) —— $CH_2$ ($^3B_1$) energy separation. | 39. |
| 1.6. | Mechanism of $CH_2(^1A_1) \longrightarrow CH_2$ ($^3B_1$) deactivation. | 42. |
| 1.7. | Theoretical studies of $CH_2$ reactions. | 48. |
| 1.8. | Aims of this work. | 55. |
| | Chapter 2. Apparatus and experimental technique. | 57. |
| 2.1. | Introduction. | 57. |
| 2.2. | Gas handling system. | 57. |
| 2.3. | Chemicals. | 58. |
| 2.4. | Gas-Liquid chromatograph. | 61. |
| 2.5. | Flash photolysis lamp. | 71. |
| 2.6. | Reaction vessels. | 81. |
| | Chapter 3. Results: A model for the vacuum U.V. photolysis of ketene. | 82. |
| 3.1. | Photolysis of $CH_2CO$ / $H_2$ / Inert gas mixtures. | 82. |
| 3.2. | Numerical solution of the kinetic scheme. | 90. |
| 3.3. | Azomethane / ketene photolysis experiments. A rate constant for $^3CH_2 + CH_3$. | 93. |
| 3.4. | Reconsideration of the $CH_2CO$ / $H_2$ / Inert gas system. | 99. |
| 3.5. | Ketene / $H_2$ system. | 99. |
| 3.6. | Physical effects. | 103. |
| 3.7. | Observation of "singlet products" at high pressure. | 106. |

Page

Chapter 4. Some Reactions of Methylene Radicals. 121.

4.1. Ketene / argon system. 121.

4.2. Reaction of $CH_2$ with $C_2H_2$. 126.

4.3. $O_2$, NO, CO as scavengers for $CH_2$. 128.

4.4. $CH_2CO$ / $CH_4$ system. 135.

4.5. Inert gases as deactivators of $^1CH_2$. 140.

4.6. Sources of $C_2H_2$. 145.

Chapter 5. Theoretical Considerations of the Reactions of Methylene and the Photolysis of Ketene. 150.

5.1. The RRKM Theory. 150.

5.1.1. Introduction. 150.

5.1.2. Decomposition of $CH_4$. 157.

5.1.3. Decomposition of $C_2H_4$. 171.

5.1.4. Decomposition of $C_2H_5$. 179.

5.2. Correlation of electronic states. 181.

5.2.1. Introduction. 181.

5.2.2. $CH_4$. 183.

5.2.3. $CH_2CO$. 185.

5.2.4. $C_2H_4$. 189.

5.2.5. $CH_3$. 191.

5.3. Collisional deactivation of $CH_2$ ($^1B_1$). 193.

Chapter 6. Suggestions for further work. 196.

6.1. A rate constant for $CH_3$ + H. 196.

6.2. $CH_2$ ($\tilde{b}^1B_1$) $\longrightarrow$ $CH_2$ ($\tilde{a}^1A_1$) fluorescence. 198.

6.3. $CH_3$ radicals. 198.

6.4. Isotope experiments. 199.

| | | Page |
|---|---|---|
| Appendix A1. | Listing of computer programme. | 200. |
| Appendix A2. | Emission spectrum of flash lamp. | 204. |
| Appendix A3. | Rate of cooling of reaction vessel. | 206. |
| Appendix A4. | Partition functions for $CH_2$ ($^3B_1$) and $CH_2$ ($^1A_1$). | 210. |
| References. | | 213. |

Note to reader

The symbols used in the figures throughout chapters 3 and 4 are described in the titles of figs. 3.1 and 3.7.
These are summarised here.

● denotes $CH_4$

○ denotes $C_2H_6$

□ denotes $C_2H_2$

△ denotes $C_2H_4$

Computer fits to the data are denoted by the following symbols:

—·—·—·—·—·— $CH_4$

— — — — — — $C_2H_6$

..... $C_2H_2$

——————— $C_2H_4$

In figures which do not show computer fits thin lines have been drawn through the points as an aid to easy interpretation of the diagram.

CHAPTER 1.

# INTRODUCTION.

Methylene: (from Greek μέθυ = wine + ὕλη = wood)
a hypothetical radical of the hydrocarbons ($CH_2$); unknown in the free state, but occurs in many compounds.

Oxford English Dictionary.
3rd Edition, 1972.

## 1.1 Spectroscopic identification of the methylene radical.

1.1.1 Observation of free methylene. Although methylene had been postulated as a reaction intermediate for many years, it was not until 1959 that Herzberg and Shoosmith [1] identified the spectrum of the methylene radical during the flash photolysis of diazomethane ($CH_2N_2$).

Three band systems were observed. Two of these, one in the red and near infrared and the other in the near ultraviolet region of the spectrum, appeared soon after the beginning of the photolysis flash. These systems were assigned to transitions between singlet electronic states of $CH_2$. The third band occurred later, in the vacuum ultraviolet near 141.5 nm. and has been assigned to a triplet transition, $^3\Sigma_u^- \leftarrow {}^3\Sigma_g^-$. Herzberg [2] found that for optimum production of the vacuum U.V. bands a mixing ratio of inert gas / $CH_2N_2$ of at least 500 / 1 was required whereas for the red bands the ratio lay between 50 / 1 and 100 / 1. Spin conservation during the photolysis requires that $CH_2$ be produced in a singlet state. The inference is that ten times as many collisions are required to bring $CH_2$ to the triplet state, where it absorbs in the vacuum U.V., than to the singlet state, where it absorbs in the red. The lifetime of $CH_2$ estimated from the vacuum U.V. bands was found to be somewhat

longer than that estimated from the red bands. These observations point to $^3\Sigma_g^-$ as the lowest state of $CH_2$.

On the basis of the observed spectral bands Herzberg [3] proposed the scheme of electronic states shown in fig.1.1. However, the spectrum gives no indication as to the magnitude of the energy separation of the triplet and singlet states. In a later paper [4] Herzberg and Johns analysed the red bands in detail and assigned them to the $\tilde{b}\,^1B_1 \leftarrow \tilde{a}\,^1A_1$ transition. The bands in the near U.V. were assigned to the $\tilde{c}\,^1A_1 \leftarrow \tilde{a}\,^1A_1$ transition. (See fig.1.1). Although it has not been possible to establish the exact relation of the singlet states to the triplet states Herzberg estimated the difference to be less than 1.0 eV.

The 141.5 nm. band represents the first member of a Rydberg series and later measurements [5] of further bands in the series led to an ionisation potential for the $CH_2$ radical of 10.396 eV., relative to the triplet ground state.

1.1.2. Electronic states of methylene. The electronic states of methylene are in accord with those predicted by molecular orbital theory. Fig.1.2 shows a molecular orbital diagram of the Walsh type [6]. Methylene possesses six valence electrons and the lowest energy configurations are:

bent ($\theta \simeq 90^\circ$) $CH_2$ : $(2a_1)^2\,(3a_1)^2\,(1b_2)^2$ : $^1A_1$

linear($\theta = 180^\circ$) $CH_2$ : $(2\sigma_g)^2\,(1\sigma_u)^2\,(1\pi_u)^2$ : $^3\Sigma_g^-,\ ^1\Delta_g,\ ^1\Sigma_g^+$

$\theta$ denotes $\widehat{HCH}$.

Consequently, if $CH_2$ is bent, the ground state might be $^1A_1$, whereas, if it is linear, Hund's rule predicts a $^3\Sigma_g^-$ state. It is evident from simple addition of orbital energies that the linear $^3\Sigma_g^-$ state and the bent $^1A_1$ state may be comparable

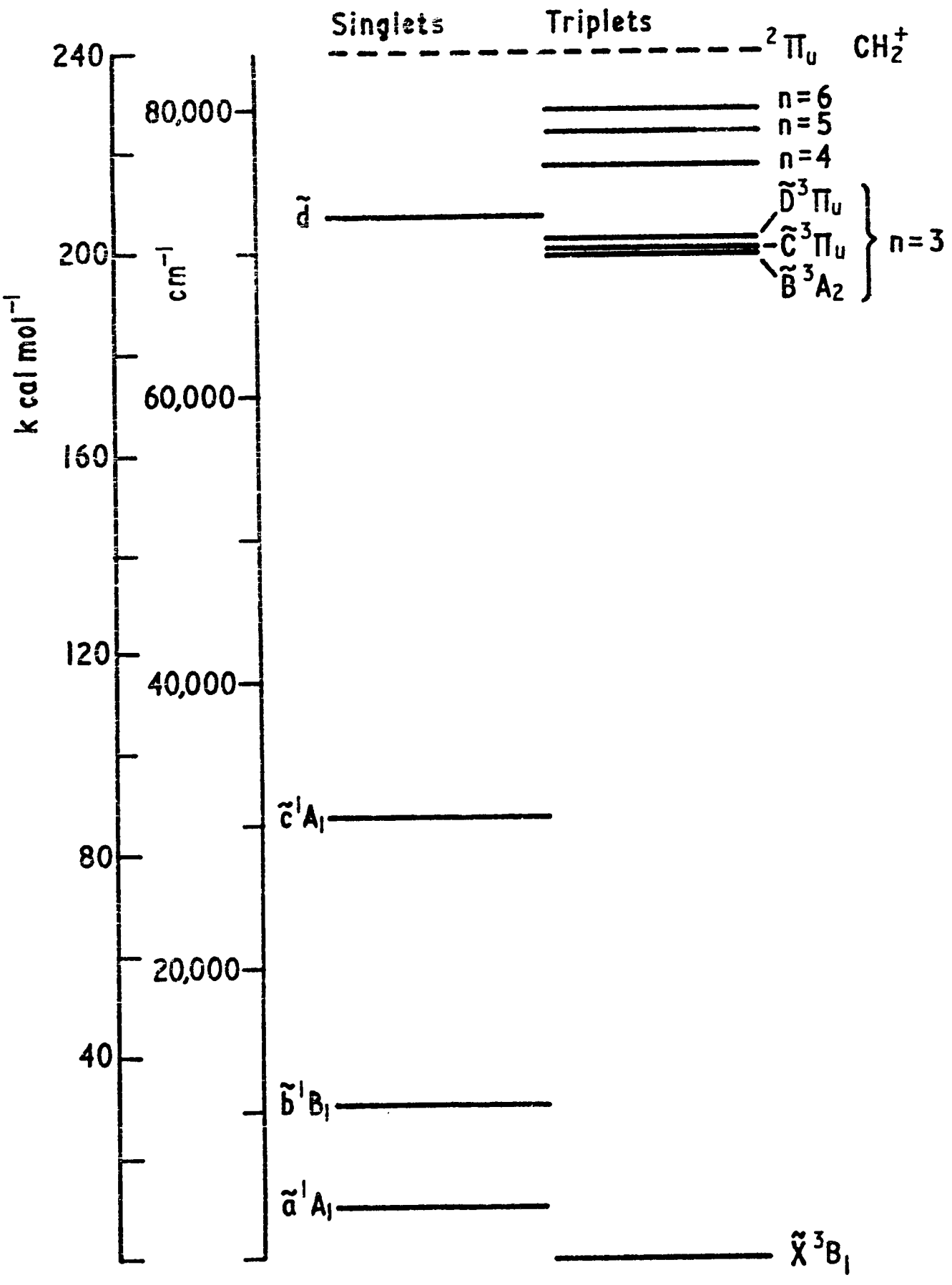



Fig. 1.1. Observed electronic states of $CH_2$ (after ref. 3). The separation between $\tilde{a}\ ^1A_1$ and $\tilde{X}\ ^3B_1$ is assumed to be 3500 $cm^{-1}$. The broken line indicates the ionisation limit corresponding to the $^2\Pi_u$ state of the $CH_2^+$ ion.

Fig. 1.2. Walsh molecular orbital diagram of an $AH_2$ molecule. The energy changes are not to scale. a = antibonding; b = bonding; n = non-bonding.

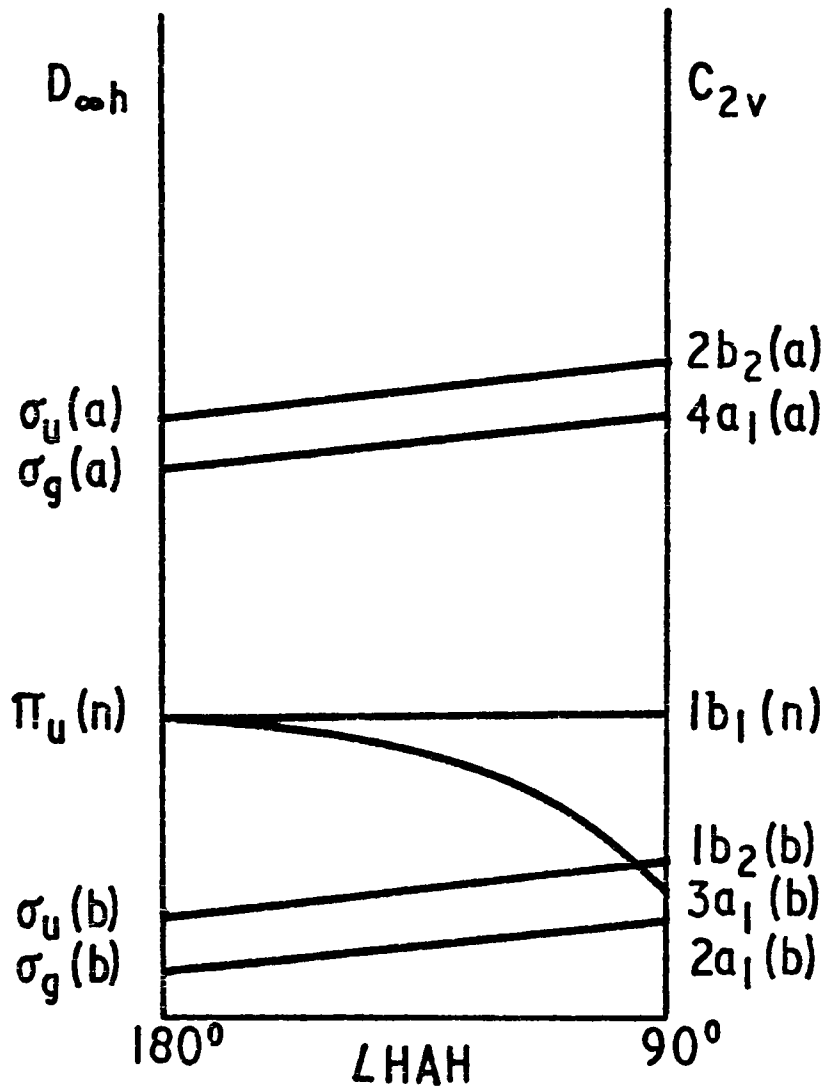
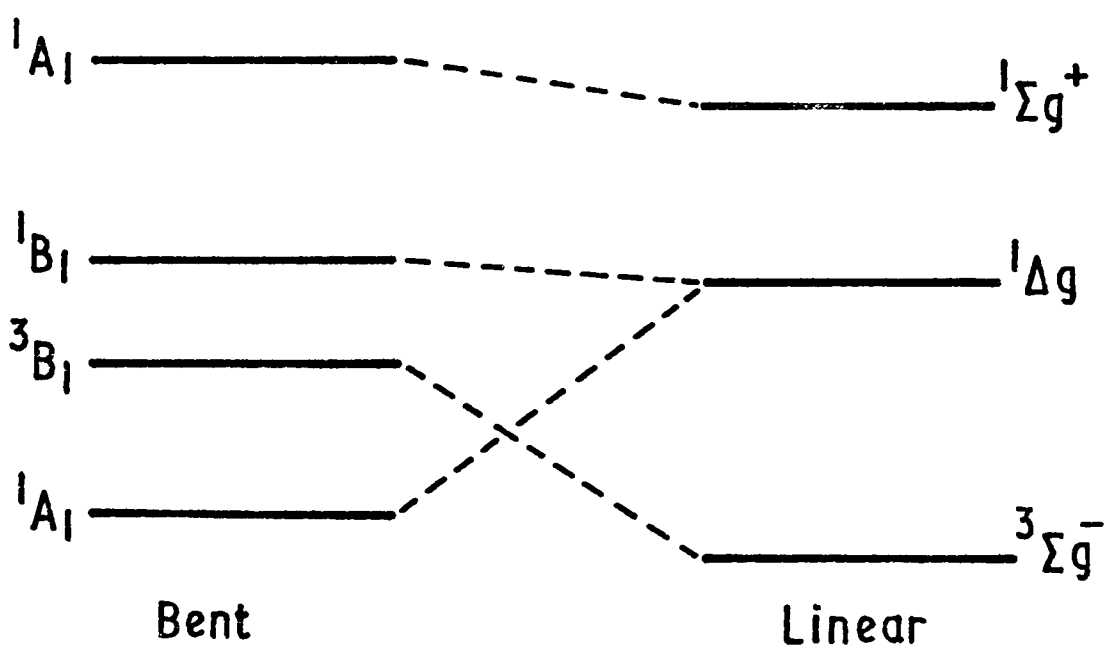



Fig. 1.3. Correlation of the electronic states of linear and bent $CH_2$.



in energy. However, if $CH_2$ is only slightly bent, the $3a_1$ and $1b_1$ molecular orbitals are nearly degenerate and the configuration,

bent ($\theta \lesssim 180^\circ$) $CH_2$ : $(2a_1)^2 (1b_2)^2 (3a_1)^1 (1b_1)^1$ : $^3B_1, ^1B_1$

may describe the ground state. Hund's rule leads to the choice of $^3B_1$ as the ground state in this case.

Recent evidence for a bent ground state comes from studies of methylene produced by photolysis of diazomethane at 4 K in a xenon matrix. Bernheim [7] et al. deduced from the electron spin resonance spectrum that the triplet ground state is slightly bent while Wasserman et al. [8, 9] calculated the angle, $\widehat{HCH}$, to be 136°. Herzberg originally analysed the rotational structure of the band at 141.5 nm. in terms of a linear molecule but in a later paper [10] he favoured interpretation of the spectrum in terms of a bent form of the radical.

Fig. 1.3 shows a correlation of the electronic states of linear and bent $CH_2$. The $^3\Sigma_g^-$ state of linear $CH_2$ correlates with the $^3B_1$ state of bent $CH_2$; the $^1\Delta_g$ state correlates with the lower $^1A_1$ state and the $^1B_1$ state. The splitting of the $^1\Delta_g$ state on bending may be thought of as produced by a strong Renner-Teller (vibronic) interaction in the linear conformation [3].

Table 1.1 summarises the information which has been obtained from the spectrum of $CH_2$.

## 1.2. Theoretical studies of the electronic states of methylene.

1.2.1. Geometries of the electronic states. Methylene is a small enough molecule to be studied by fairly sophisticated ab initio techniques. O'Neil et al. [13] have predicted

Table 1.1. Summary of the structure of $CH_2$ as deduced from the spectroscopic evidence. (refs. 2,3,4)

| Electronic state | $^3B_1$ | $^1A_1$ | $^1B_1$ |
|---|---|---|---|
| $r_{C-H}$ (Å) | 1.07 | 1.11 | 1.05 |
| $\widehat{HCH}$ | 140° | 102.4° | 140 ± 15° |
| $\nu_2{}^a$ ($cm^{-1}$) | ? | 1352.6 | 557 |

Energy separations between the electronic states are estimated as:

$$E\ (^3B_1 - {}^1A_1) < 1.0\ eV.$$

$$E\ (^1A_1 - {}^1B_1) = 0.88\ eV.\ ^b$$

(a) $\nu_2$ is the bending mode of $CH_2$. The two other normal modes are a symmetric stretch ($\nu_1$) and an asymmetric stretch ($\nu_3$).

(b) This value has been questioned by Hay et al. [15].

that there are only three bound non-Rydberg states of $CH_2$, viz. $^3B_1$, $^1A_1$, $^1B_1$, and almost all calculations deal with these states.

Foster and Boys [14], in a calculation published almost simultaneously with Herzberg's spectroscopic identification of $CH_2$, predicted the ordering of states to be $^3B_1$, $^1A_1$, $^1B_1$, with a $^3B_1 - {}^1A_1$ separation of 24.5 kcal $mol^{-1}$ and a $^1A_1 - {}^1B_1$ separation of 35.8 kcal $mol^{-1}$. The molecular geometries for the states $^3B_1$, $^1A_1$, $^1B_1$, were calculated to be (129°, 1.12 Å), (90°, 1.17 Å), (132°, 1.12 Å) respectively for ($\widehat{HCH}$, $r_{C-H}$). Since the publication of Foster and Boys' paper many calculations have been carried out with increasing sophistication and accuracy [11-20]. The following conclusions arise from all these calculations:

(i) Every calculation predicts the $^3B_1$ angle to be between 129° and 138°, with the preferred angle close to 133°. In addition, a very small barrier to linearity is predicted, being as low as 4 kcal $mol^{-1}$ in a recent calculation.[20]

(ii) The $^3B_1$ state is always the lowest energy state.

(iii) The first excited state is predicted to be the $^1A_1$ state with a bond angle between 90° and 109°. The more recent calculations favour 105°.

(iv) The second excited state is predicted to be the $^1B_1$ with a bond angle between 132° and 180°, the most recent calculations favouring 140°. This state, like the $^3B_1$, has a very shallow barrier to linearity.

1.2.2. <u>Energy separations between the electronic states.</u> The calculated energy separation between the $^1A_1$ and $^3B_1$ state,

E ($^1A_1$ - $^3B_1$), has tended to decrease as the quality of the calculations has improved. The best calculations to date are those of Hay et al. [15] who calculated 11.5 kcal mol$^{-1}$, Staemmler [20] who calculated 9.3 kcal mol$^{-1}$, and Bender et al.[17], who calculated 11.1 kcal mol$^{-1}$.

The cause of this decrease is high-lighted in the work of Bender and Schaeffer. In an early paper [12] they calculated the separation E($^1A_1$ - $^3B_1$) to be 22.2 kcal mol$^{-1}$. Their recent calculation [17] involved the same technique as the earlier one but the basis set now included functions of d-orbital symmetry. Thus, inclusion of d-orbitals in the basis set brought about a lowering in energy of the $^1A_1$ state relative to the $^3B_1$ state. (This is a differential lowering effect; an increase in the basis set tends to lower the <u>absolute</u> energies of both states.)

Harrison [21] has argued that calculations of even greater sophistication will not lower the value of this energy separation any further. Calculations of E ($^1B_1$ - $^3B_1$) are fairly straightforward, since both the $^3B_1$ and $^1B_1$ states have one electron in a non-bonding $sp^2$ orbital and another electron in a p orbital, the difference between these states being merely a change in the spin coupling of this pair of electrons. All calculations agree on a value for E ($^1B_1$ - $^3B_1$) of 36 - 50 kcal mol$^{-1}$ with a majority favouring 42 kcal mol$^{-1}$. The difficulty in calculating E ($^1A_1$ - $^3B_1$) arises since in the $^1A_1$ state the electrons occupy the same orbital and the electron correlation energy is much more important than in the $^3B_1$ state. Harrison noted that E ($^1B_1$ - $^3B_1$) $\equiv$ E ($^1B_1$ - $^1A_1$) + E ($^1A_1$ - $^3B_1$). From an analysis of the observed spectroscopic band

Herzberg [4] has estimated E ($^1B_1$ - $^1A_1$) to be 20.3 kcal mol$^{-1}$. The calculated value of E ($^1B_1$ - $^3B_1$) seems well established as 42 kcal mol$^{-1}$. This gives E ($^1A_1$ - $^3B_1$) = 21.7 kcal mol$^{-1}$, much higher in fact than the "best" calculated value.

Hay et al. [15] have questioned the validity of Herzberg's estimate for E ($^1B_1$ - $^1A_1$). Herzberg's value is based on the assumption that the lowest observed transition in the band is $^1B_1$ (060) - $^1A_1$ (000). The 0 - 0 energy was reached by an extrapolation which assumed that the $^1B_1$ state was linear and that $\nu_2$ was harmonic. Hay's calculation predicts an extremely anharmonic potential surface for bending in the $^1B_1$ state. Hay et al. suggested that the observed transition was in fact 0 - 0. This would imply a value for E ($^1B_1$ - $^1A_1$) of 30.8 kcal mol$^{-1}$ making E ($^1A_1$ - $^3B_1$) equal to 9.3 kcal mol$^{-1}$ in agreement with the"best" calculated values.

Conclusion. Theoretical calculations predict E ($^1A_1$ - $^3B_1$) to be in the region of 10 kcal mol$^{-1}$; in so doing they question the spectroscopic estimation of E ($^1B_1$ - $^1A_1$).

## 1.3. Generation of methylene radicals.

1.3.1. Heats of formation. In most gas phase experiments methylene is generated by photolysis of ketene, diazomethane, or one of the lower alkanes e.g. $CH_4$, n-$C_3H_8$, or c-$C_3H_6$. Photolysis may lead to the location of a significant amount of energy in the methylene. Translational and rotational energies are thermalised within a few collisions [22], but both vibrational and electronic excitation are less easily removed and may have a profound effect on the behaviour of

methylene. The extent of such excitation depends on the precursor and on the photolysis wavelength. The characteristics of some of the precursors of methylene are discussed in this section.

A key property in determining the energy released in any chemical reaction is the ehthalpy change. Table 1.2 lists some heats of formation of compounds discussed in this thesis. For most stable compounds these are well defined, but, until recently, the heat of formation of the methylene radical has been subject to some uncertainty.

1.3.2. Heat of formation of the methylene radical.

Several estimates of $\Delta H^{o}_{f,298}$ ($CH_2$) have been reported which rely on mass spectrometric detection of $CH_2^+$ ions produced in the photoionisation of $C_2H_4$ [27], $CH_4$ [28], and $CH_3$ [23]. In each case an appearance potential for $CH_2^+$, $V_T$, is measured.

Consider the photoionisation of $CH_3$,

$$CH_3 + h\nu \longrightarrow CH_2^+ + H + e^-$$

The appearance potential of $CH_2^+$ is given by

$$V_T = I.P.(CH_2) + \Delta H^{o}_{f,T}(CH_2) + \Delta H^{o}_{f,T}(H) - \Delta H^{o}_{f,T}(CH_3)$$

where $I.P.(CH_2)$ is the ionisation potential of $CH_2$.

Chupka and Lifshitz measured $V_T$ at a series of temperatures above T = 400 K. By extrapolation, $V_T$ at T = 0 K was obtained as 15.09 $\pm$ 0.03 eV. The ionisation potential of $CH_2$ has been measured spectroscopically [5], relative to the triplet ground state and its value is 10.396 eV. The value of $\Delta H^{o}_{f,0}$ (H) is 51.6 kcal $mol^{-1}$. Chupka and Lifshitz took a value of 35.4 kcal $mol^{-1}$ for $\Delta H^{o}_{f,0}$ ($CH_3$) which they obtained from the photoionisation threshold for

Table 1.2. Heats of formation at 298 K.

Units are kcal $mol^{-1}$.

| Compound | $\Delta H^{o}_{f,298}$ | Ref.(a) |
|---|---|---|
| $CH_2$ ($^3B_1$) | 92.2 ± 1.0 | 23 |
| H | 52.1 | |
| $CH_3$ | 34 | |
| CH | 142 | |
| $C_2H_3$ | 69 ± 2 | |
| $C_2H_5$ | 26 | |
| $CH_4$ | - 17.9 | |
| $C_2H_4$ | 12.5 | |
| $C_2H_6$ | - 20.2 | |
| $C_2H_2$ | 54.2 | |
| $n\text{-}C_3H_8$ | - 24.8 | 24 |
| $c\text{-}C_3H_6$ | 12.7 | 24 |
| $C_3H_6$ | 4.9 | 24 |
| $CH_2CO$ | - 11.4 ± 0.4 | 25 |
| $CH_2N_2$ | 54.2 | 26 |
| CO | - 26.4 | |
| $N_2$ | 0 | |
| $H_2$ | 0 | |

(a) Where a reference is not given values are taken from "Thermochemical Kinetics" by S.W. Benson, John Wiley & Sons, 1968.

production of $CH_3^+$ from $CH_4$. The value for $\Delta H^o_{f,0}$ $(CH_2)$ finally obtained is 91.9 kcal $mol^{-1}$.

In a complicated dissociation process, e.g. the elimination of $H_2$ from $CH_4$. there is a chance that excess energy will be present in the products at threshold. This is unlikely for the simple bond breaking process in the dissociation of $CH_3$ and, therefore, this measurement gives the most reliable estimate of $\Delta H^o_{f,0}$ $(CH_2)$ obtained by the photoionisation technique. The value for $\Delta H^o_{f,298} - \Delta H^o_{f,0}$ is 0.3 kcal $mol^{-1}$ giving $\Delta H^o_{f,298}$ $(CH_2)$ = 92.2 kcal $mol^{-1}$. Since the ionisation potential of $CH_2$ is relative to its triplet ground state, this value of $\Delta H^o_{f,298}$ $(CH_2)$ refers to the $^3B_1$ state of $CH_2$. This is the value which will be used throughout this thesis.

In the following discussion $CH_2$ $(^1A_1)$ will be denoted by $^1CH_2$ and $CH_2$ $(^3B_1)$ by $^3CH_2$.

1.3.3. Ketene.

1.3.3.1. Absorption spectrum. Ketene has three distinctly different electronic absorption regions [3]. These extend from 475 - 260 nm., from 213 - 193 nm., and from 185 - 130 nm.

Dixon and Kir by [29] studied the absorption of ketene in the visible region of the spectrum and found broad diffuse bands between 340 and 475 nm. which were structureless under high resolution. The mean spacing between the maxima of the diffuse bands appeared to change at 386 nm. and they interpreted this as indicating different bending modes in

two excited electronic states of ketene. Laufer and Keller [30], however, showed that the spacing between the diffuse bands changed regularly throughout the spectrum and suggested that the entire absorption is due to a $^1A_2 \longleftarrow {}^1A_1$ transition. The absorption has a maximum at 315 nm. with an extinction coefficient, $\epsilon$ , defined by $I = I_o \exp(-\epsilon c l)$, of 1 atmos$^{-1}$ cm$^{-1}$. The transition may be considered to be of the type $n \rightarrow \pi^*$.

The shorter $\lambda$ transitions have been less thoroughly analysed. There are four diffuse bands between 220 nm. and 190 nm. with a maximum extinction coefficient of 360 atmos$^{-1}$ cm$^{-1}$ at 213 nm. These correspond to $\pi \rightarrow \pi^*$ transitions.

The even stronger absorption which commences at 183 nm. extends to 130 nm. where ionisation sets in. It consists of a series of strong $^1A_1 \longleftarrow {}^1A_1$ Rydberg bands superimposed on a continuum with extinction coefficients as large as $10^3$ atmos$^{-1}$ cm$^{-1}$.

1.3.3.2. Dissociative absorption. The major primary process in the photolysis of ketene is the production of $CH_2$,

$$CH_2CO + h\nu \longrightarrow CH_2 + CO \qquad (1)$$

This reaction is endothermic by 76.9 kcal mol$^{-1}$. Dissociative absorption has been observed for light of $\lambda$ = 366 nm. which corresponds to an energy of 77.4 kcal mol$^{-1}$. The yield of CO is twice that of $C_2H_4$ [31], consistent with the primary photolysis being followed by the reaction,

$$CH_2 + CH_2CO \longrightarrow C_2H_4 + CO \qquad (2)$$

The quantum yield for dissociation, $\phi$ , increases as the photolysis wavelength decreases, being 0.04 at $\lambda$ = 366 nm. (in the limit of zero pressure) and reaching 1.0 at

270 nm.[31]. For $\lambda > 270$ nm. $\phi$ is dependent on the pressure and this has been interpreted as due to collisional stabilisation of excited ketene molecules produced in the primary process.

It appears that both $^1CH_2$ and $^3CH_2$ are produced in process (1) when ketene is photolysed with 260 nm.$\leq \lambda \leq$ 366nm. This conclusion is based on the interpretation of the observed products in ketene photolysis systems on an assumption of different chemical reactivities of $^1CH_2$ and $^3CH_2$. This aspect will be discussed fully in section 1.4.1. Although there is some disagreement on the exact fraction of methylene produced in the singlet state at any particular wavelength, the trend seems to be that the fraction of $^1CH_2$ increases as the wavelength decreases. (See table 1.3).

In order to explain the production of both $^1CH_2$ and $^3CH_2$ the following scheme has been proposed[39] :

$$CH_2CO + h\nu \longrightarrow {}^1CH_2CO^*$$

$$^1CH_2CO^* \longrightarrow {}^1CH_2 + CO$$

$$^1CH_2CO^* \longrightarrow {}^3CH_2CO^*$$

$$^3CH_2CO \longrightarrow {}^3CH_2 + CO$$

$^1CH_2CO^*$, $^3CH_2CO^*$ are excited ketene molecules in singlet and triplet states. A radiationless transition is assumed to occur from the excited singlet state of ketene to a triplet state. As $\lambda$ decreases, the probability of $^1CH_2CO^*$ decomposition increases.

Kistiakowsky and Walter[40] studied the photolysis of ketene in the U.V. absorption at $\lambda$ = 213.9 nm. The main products were $C_2H_4$ and CO, and Kistiakowsky and Walter interpreted their results on the basis of a scheme which

Table 1.3. Photolysis of ketene in the near U.V. The fraction of methylene produced in the singlet state.

| λ / nm. \ Ref. | 32 | 33 | 34 | 35 | 36 | 37 | 38 |
|---|---|---|---|---|---|---|---|
| 366 | 0.5 | 0.4 | 0.6 | | | | |
| 350 | | | | 0.13 | | | |
| 334 | | 0.39 | 0.70 | | | 0.72 | |
| 320 | | | | | 0.71 | | |
| 316 | | 0.59 | | | | | |
| 313 | | | 0.85 | | | | |
| 290 | | 0.67 | | | | | |
| 280 | 0.98 | | 0.85 | | | | 0.60 |

Table 1.4. Energy available to the photofragments in the photolysis of methylene precursors. Units are kcal $mol^{-1}$

| λ / nm. | $CH_2CO$ | $CH_2N_2$ | $n\text{-}C_3H_8$ | $c\text{-}C_3H_6$ | $CH_4$ |
|---|---|---|---|---|---|
| 450 | | 25.6 | | | |
| 400 | | 33.5 | | | |
| 350 | 4.6 | 43.8 | | | |
| 300 | 18.2 | 57.4 | | | |
| 250 | 37.3 | 76.5 | | | |
| 200 | 65.9 | 105.1 | | | |
| 175 | 86.3 | 125.5 | | 71.5 | |
| 150 | 113.6 | 152.8 | 94.0 | 98.8 | 80.7 |
| 125 | 151.7 | 190.9 | 132.1 | 136.9 | 118.8 |
| 100 | 209.0 | 248.2 | 189.4 | 194.2 | 176.1 |

implied that the 213.9 nm. radiation caused the formation of two kinds of $CH_2$ which behaved kinetically as $^1CH_2$ and $^3CH_2$ formed in the near U.V. photolysis. $^1CH_2$ / $^3CH_2$ were formed in the ratio of 7 / 3.

Braun et al. [41] used the photolysis of ketene in the far U.V. region, 170 nm. $\leq \lambda \leq$ 190 nm., to produce methylene. They monitored $^3CH_2$ by kinetic spectroscopy by its absorption at 141.5 nm., and inferred from their results that $^1CH_2$ was the major primary prduct in their system.

Laufer [42] studied ketene photolysis over a range 147 nm. $\leq \lambda \leq$ 313 nm. Molecular hydrogen was produced at all wavelengths. Laufer photolysed $CH_2CO$ / $CD_2CO$ mixtures and interpreted the production of $H_2$ and $D_2$ with little HD as evidence for an alternative primary process at $\lambda <$ 265 nm.

$$CH_2CO + h\nu \longrightarrow C_2O + H_2$$

This process accounted for 2-8% of the ketene photolysed in Laufer's experiment. However the evidence for this process is by no means conclusive.

1.3.4. Diazomethane.

1.3.4.1. Absorption spectrum. It is not surprising that the spectrum of $CH_2N_2$ is similar to that of $CH_2CO$ since the two molecules are isoelectronic and have the same geometrical structure. However, the whole spectrum is shifted to longer wavelengths.

A weak absorption begins at 475 nm. (giving $CH_2N_2$ a yellow colour in both the solid and gas phases) and extends to 320 nm. with a maximum extinction coefficient of 0.3 $atmos^{-1}$ $cm^{-1}$ at 395 nm.[43] A number of very diffuse bands in this absorption are observed beginning at 471 nm. Their

diffuse nature suggests that the dissociation energy D ($CH_2$ - $N_2$) is less than 60.8 kcal $mol^{-1}$ ( $\lambda$ equivalent = 471 nm.).

A second absorption begins at 265 nm. and extends to 200 nm. with an extinction coefficient maximum of $\simeq 10^2$ $atmos^{-1}$ $cm^{-1}$ [44] at 217.5 nm.

In the vacuum U.V. there are several discrete absorption bands beginning at 193 nm. which have been studied in detail by Merer [45].

Unfortunately the heat of formation of $CH_2N_2$ has not been measured accurately, but Laufer and Okabe [26] have set a lower limit of $\Delta H^{o}_{f,298}$ ($CH_2N_2$) $\geq$ 54.2 kcal $mol^{-1}$. This sets a limit on the dissociation energy, D ($CH_2N_2$), of D ($CH_2N_2$) $\leq$ 38.0 kcal $mol^{-1}$ ( $\lambda$ equivalent $\geq$ 753 nm.).

1.3.4.2. Dissociative absorption. The photolysis of $CH_2N_2$ has not been studied to the same extent as $CH_2CO$. The dominant process is the production of $^1CH_2$. Photolysis at longer wavelengths causes the formation of some $^3CH_2$ in the primary step. Frey [46] has found $^3CH_2$ / $^1CH_2$ $\simeq$ 0.2 at $\lambda$ = 435.8 nm., and Bell [47] has estimated $\phi\,^1CH_2$ = 1.0 at $\lambda$ = 405 nm.

1.3.5. Propane.

1.3.5.1. Absorption spectrum. Propane has a strong absorption in the vacuum U.V. beginning at $\lambda$ = 163 nm. [48], and attributed to a $\sigma$ - $\sigma^*$ type transition. The extinction coefficient at $\lambda$ = 120 nm. is $10^3$ $atmos^{-1}$ $cm^{-1}$.

1.3.5.2. Dissociative absorption. The photolysis of propane in the gas phase has been studied by several workers [49, 50, 51]. The primary processes are as follows:

$$n\text{-}C_3H_8 + h\nu \longrightarrow C_3H_7^* + H \qquad \phi_1 \qquad (1)$$

$$C_3H_6 + H_2 \qquad \phi_2 \qquad (2)$$

$$C_2H_6 + CH_2 \qquad \phi_3 \qquad (3)$$

$$C_2H_5^* + CH_3 \qquad \phi_4 \qquad (4)$$

$$C_2H_4^* + CH_4 \qquad \phi_5 \qquad (5)$$

Quantum yields for these processes have been suggested by Obi et al.[51]. These are $\phi_1 + \phi_2 = 0.67$, $\phi_3 = 0.05$, $\phi_4 = 0.11$, and $\phi_5 = 0.17$ at $\lambda = 147$ nm., and $\phi_1 + \phi_2 = 0.32$, $\phi_3 = 0.10$, $\phi_4 = 0.15$, $\phi_5 = 0.43$, at $\lambda = 123.6$ nm. The only ethanes formed in the photolysis of $C_3H_8$ / $C_3D_8$ mixtures with NO present as scavenger are $C_2H_6$ and $C_2D_6$ [49], consistent with process (3) being the only source of ethane. Koob [52] used the NO scavenged photolysis of $n\text{-}C_3H_8$ as a source of $CH_2$, and equated the $C_2H_6$ produced to the $CH_2$.

1.3.6. Cyclopropane.

1.3.6.1. Absorption spectrum. The absorption spectrum of $c\text{-}C_3H_6$ begins at $\lambda = 171$ nm. There are three regions of continuous absorption [44] with maxima at $\lambda = 120, 145$, and 159 nm. At $\lambda = 120$ nm. the extinction coefficient is close to $10^3$ atmos$^{-1}$ cm$^{-1}$.

1.3.6.2. Dissociative absorption. Photolysis of $c\text{-}C_3H_6$ has been studied at $\lambda = 147$ nm. [53]. The following primary processes are believed to occur in order of decreasing

importance:

$$c\text{-}C_3H_6 + h\nu \longrightarrow CH_2 + C_2H_4 \quad (1)$$

$$H_2 + C_3H_4 \quad (2)$$

$$H + C_3H_5 \quad (3)$$

Koob [52] has used $c\text{-}C_3H_6$ as a source of $CH_2$. In process (1) $CH_2$ and $C_2H_4$ are produced in equimolar quantities and the $C_2H_4$ therefore gives a measure of the $CH_2$ produced.

1.3.7. Methane.

1.3.7.1. Absorption spectrum. A strong absorption begins at 145 nm. and rises sharply, reaching $\epsilon = 70$ $cm^{-1}$ $atmos^{-1}$ at 137 nm. and a maximum of $\epsilon = 1500$ $cm^{-1}atmos^{-1}$ at 93 nm.[3]. Only a continuous absorption has been observed. The shape of the absorption curve has been taken to imply that several electronic transitions are responsible. A weak absorption has been reported at $\lambda > 145$ nm., but probably extends no further than 150 nm.[54].

1.3.7.2. Dissociative absorption. At photon energies below the onset of photoionisation (97 nm.) two primary processes have been proposed in methane photolysis.

$$CH_4 + h\nu \longrightarrow CH_2 + H_2 \quad (1)$$

$$CH_4 + h\nu \longrightarrow CH_3 + H \quad (2)$$

Isotopic labelling experiments [55, 56] have been interpreted as showing that process (2) has a quantum yield less than 0.02. Recent work [57] estimated the quantum yield of process (2) as zero.

Welch and Judge [58] have studied the fluorescence spectra of the products of $CH_4$ photolysis. $CH_4$ was

photolysed between 55 nm. $\leq \lambda \leq$ 124 nm. Fluorescence was observed resulting from the $\tilde{A}^2\Delta \longrightarrow \tilde{X}^2\Pi$ and $\tilde{B}^2\Sigma \longrightarrow \tilde{X}^2\Pi$ systems of the CH radical, and from the $\tilde{b}\ ^1B_1 \rightarrow \tilde{a}\ ^1A_1$ system of the $CH_2$ radical. The CH fluorescence resulted from

$$CH_4 + h\nu \longrightarrow CH\ (\tilde{A}^2\Delta) + H_2 + H \qquad (3)$$

$$CH_4 + h\nu \longrightarrow CH\ (\tilde{B}^2\Sigma) + H_2 + H \qquad (4)$$

These processes have thresholds at $\lambda$ = 104 nm. and $\lambda$ = 100 nm. respectively. The $CH_2$ fluorescence was observed at $\lambda$ = 121.6 nm. but not at $\lambda$ = 124.2 nm. It probably arose from,

$$CH_4 + h\nu \longrightarrow CH_2\ (\tilde{b}\ ^1B_1) + H_2\ (^1\Sigma_g^+) \qquad (5)$$

Braun et al. [59, 60] have suggested that CH plays an important role in the flash photolysis of $CH_4$ with high energy radiation, but some of their conclusions should be questioned.

1.3.7.3. Electronic states of $CH_4$. Karplus and Bersohn [61] have carried out crude valence bond calculations on the low lying states of $CH_4$ (point group $T_d$). They found that the ground state has symmetry $A_1$ and the first and second excited states have symmetry E and $F_2$ respectively. The strong absorption beginning at 145 nm. has been assigned to a $^1F_2 \leftarrow {}^1A_1$ transition [3]. Electric dipole transitions to a $^1E$ state are forbidden and Karplus and Bersohn suggested that the weak absorption observed at $140 < \lambda < 150$ nm. may be due to the forbidden $^1E \leftarrow {}^1A_1$ transition.

They calculated potential energy surfaces for the distortion of $CH_4$ according to $C_{2v}$ symmetry to give $CH_2 + H_2$, and according to $C_{3v}$ symmetry to give $CH_3 + H$. In their correlation diagram $CH_4\ (^1F_2)$ correlates with $CH_2\ (^1B_1) + H_2\ (^1\Sigma_g^+)$ and with $CH_3\ (^2A_2'') + H\ (^2S_g)$. The potential

gradient was steeper toward $CH_3$ + H than toward $CH_2$ + $H_2$, implying that dissociation of $CH_4$ ($^1F_2$) should lead mainly to $CH_3$ + H. This is contrary to experimental observation. Their calculation has been strongly criticised by Lindholm [62]. The correlation with $CH_2$ ($^1B_1$) is, however, supported by the experimental observation of Welch and Judge [58].

1.3.8. Energetics of photolysis. Table 1.4. shows the energy available to the photofragments in the photolyses of $CH_2CO$, $CH_2N_2$, n-$C_3H_8$, c-$C_3H_6$, and $CH_4$ to give $CH_2$ over a range of wavelengths. If the assumption is made that all the excess energy is carried by $CH_2$, one may estimate from this table which of the electronic states of $CH_2$ are energetically feasible at a particular wavelength. (As a rough estimate E ($^1A_1$ - $^3B_1$) = 10 kcal $mol^{-1}$ and E ($^1B_1$ - $^3B_1$) = 30 kcal $mol^{-1}$.) In table 1.4. entries have only been made for wavelengths where photolysis takes place.

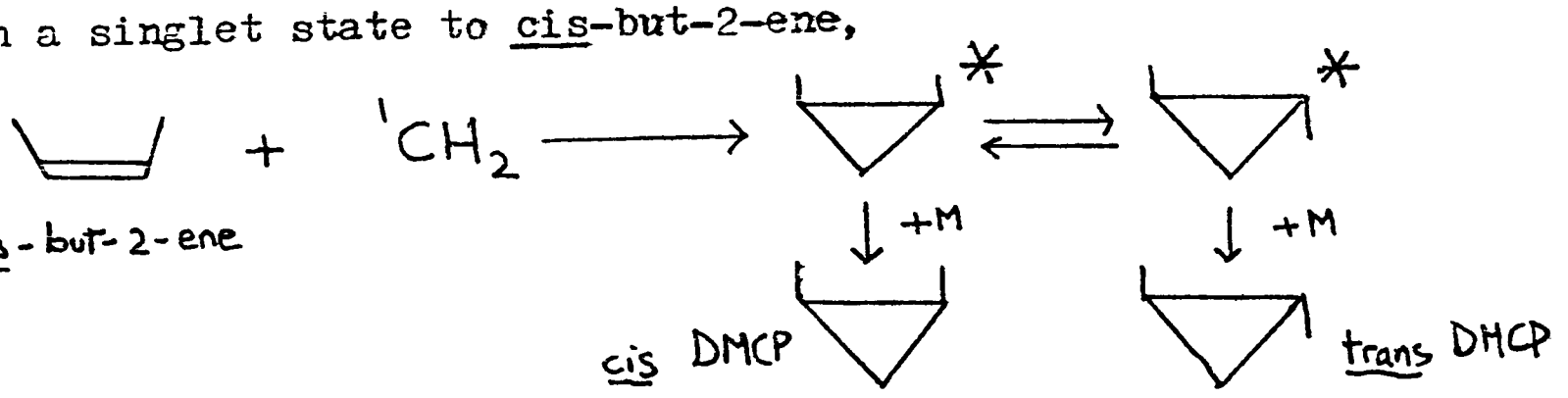
## 1.4. Reactions of methylene.

### 1.4.1. Chemical differences between $^1CH_2$ and $^3CH_2$.

In most early experiments, $CH_2$ was produced by low intensity photolysis either of ketene, with $260 \leq \lambda \leq 350$ nm., or of diazomethane with $360 \leq \lambda \leq 440$ nm. In such systems photolysis times ranged from a few minutes to several hours, and large quantities of ketene or diazomethane were required to produce sufficient product for analysis. A complicating factor in such systems was the reaction of $CH_2$ with ketene or diazomethane.

Bader and Generosa [63] photolysed small fixed amounts of diazomethane and cis-but-2-ene in the presence of increasing

pressures of inert gases. The main products arising from reaction of $CH_2$ with cis-but-2-ene were cis and trans 1,2 dimethylcyclopropane (1,2-DMCP) and several pentenes. Bader and Generosa looked particularly at the percentage yield of the trans-1,2-DMCP as a function of inert gas pressure. This showed an initial fall as the pressure increased but at high pressures it started to rise again, indicating that two mechanisms with opposite dependency on the inert gas pressure were responsible for its formation. The initial decrease in the percentage yield of the trans isomer with increasing pressure indicated that a source was the isomerisation of energised molecules. These excited molecules resulted from the addition of methylene in a singlet state to cis-but-2-ene,



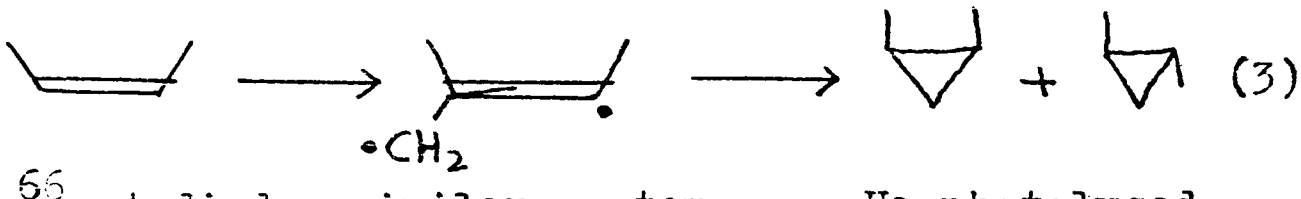

M is an inert gas molecule. * represents an energised molecule.

As the pressure was increased the energised cis-DMCP molecules were increasingly stabilised before isomerisation occurred. The subsequent rise in the yield of the trans isomer with further increase in the pressure indicated that another mechanism, one whose rate was increased by an increase in pressure, must be operating. This was attributed to a mechanism involving triplet methylene. At low pressures $^1CH_2$ formed in the initial photolysis reacted with cis-but-2-ene, but addition of inert gas caused the $^1CH_2$ to be deactivated (by collision) to $^3CH_2$. The $^3CH_2$ added to the double bond without retention of geometry.

Mechanisms for the reactions of $^3CH_2$ and $^1CH_2$ with an olefinic double bond were proposed by Skell and Woodworth [64,65]. $^1CH_2$, with a lone pair of electrons in an $sp^2$ orbital, can give the complete cyclopropane framework in a single 3-centre addition step with consequent retention of geometry.

$^1CH_2$ +  (2)

Addition of $^3CH_2$ to <u>cis</u>-but-2-ene is thought to occur via a biradical, allowing rotation about the C = C bond to occur before cyclisation takes place.

$^3CH_2$ +  (3)

Frey [66] studied a similar system. He photolysed $CH_2N_2$ / <u>cis</u>-but-2-ene mixtures and increased the pressure by increasing the <u>cis</u>-but-2-ene. No increase in the percentage of <u>trans</u>-1,2-DMCP was observed at high pressure. Bader and Generosa [63] interpreted this as being consistent with a fast reaction of $^1CH_2$ with the C = C bond. $^1CH_2$ reacts with <u>cis</u>-but-2-ene faster than it can be deactivated to $^3CH_2$.

Ring and Rabinovitch [67] used the photolysis of $CH_2N_2$ in a large excess of inert gas as a source of $^3CH_2$. They showed that $^3CH_2$ abstracts H atoms from C-H bonds at rates comparable to the rate of addition of $^3CH_2$ to C = C. They dictated caution [68] in the interpretation of the proportion of $^3CH_2$ : $^1CH_2$ from the products in such systems.

In principle, $^1CH_2$ can add to an alkene either by addition to the double bond to form an excited cyclopropane derivative, or by insertion between a carbon and a hydrogen

to form an excited propylene derivative. Frey [69] has shown that the two processes occur at comparable rates.

Bell and Kistiakowsky [70] have studied the photolysis of $CH_2N_2$ in the presence of $H_2$ and $CH_4$. The addition of $CH_2$ to $H_2$ or $CH_4$ resulted in the formation of vibrationally excited adducts which broke up to yield radical fragments. The methylene reacting in their system was expected to be $^1CH_2$.

$$^1CH_2 + H_2 \longrightarrow CH_4^* \longrightarrow CH_3 + H$$

$$^1CH_2 + CH_4 \longrightarrow C_2H_6^* \longrightarrow CH_3 + CH_3$$

At high pressures some of the vibrationally excited molecules will be stabilised.

The early work outlined above has established the following conclusions concerning the reactions of $CH_2$ in its singlet and triplet states:

(a) $^1CH_2$ adds stereospecifically to olefinic double bonds whereas $^3CH_2$ adds non-stereospecifically.

(b) $^1CH_2$ inserts into C-H bonds whereas $^3CH_2$ abstracts H atoms.

(c) $^1CH_2$ reacts with hydrocarbons faster than it is deactivated to $^3CH_2$.

1.4.2. Rates of deactivation of $^1CH_2$ to $^3CH_2$. Many experiments in low intensity systems have been carried out with small concentrations (5 - 10%) of oxygen or nitric oxide present as a scavenger for $^3CH_2$. Although $O_2$ and NO react at an appreciable rate with $^1CH_2$ [71], the high reactivity of $^1CH_2$ with other species e.g. alkanes, ensures

that little $^1CH_2$ is intercepted by the scavenger. $^3CH_2$, on the other hand, is believed to react more slowly, and will be intercepted by any scavenger present. Experiments using scavengers have been used to determine the efficiencies of different molecules in deactivating $^1CH_2$ to $^3CH_2$.

Cox and Preston [38] photolysed ketene at 249 nm. $\leq \lambda \leq$ 280 nm. Pressures were increased by addition of inert gases and they interpreted their system according to the scheme:

$$^1CH_2 + CH_2CO \xrightarrow{k_1} C_2H_4 + CO \qquad (1)$$

$$^1CH_2 + M \xrightarrow{k_2} {}^3CH_2 + M \qquad (2)$$

$$^3CH_2 + O_2 \longrightarrow CO, CO_2, H_2 \text{ etc} \qquad (3)$$

M is an inert gas molecule.

Addition of inert gas caused a reduction in $C_2H_4$ which was attributed to deactivation of $^1CH_2$ to $^3CH_2$. From the fall in $[C_2H_4]$ with increase in pressure Cox and Preston estimated $k_2 / k_1$ for various inert gases.

A selection of their results is given below:

| | He | Ar | Kr | Xe | $N_2$ | $CF_4$ | $C_2F_6$ | $SF_6$ |
|---|---|---|---|---|---|---|---|---|
| $k_2/k_1$ | 0.018 | 0.014 | 0.033 | 0.074 | 0.052 | 0.047 | 0.11 | 0.045 |

A major assumption in the above interpretation is that the excited ketene molecules formed in the primary process do not undergo a change in spin state due to collisions with inert gas molecules as in the scheme:

$$CH_2CO + h\nu \longrightarrow {}^1CH_2CO \longrightarrow {}^1CH_2 + CO$$
$$\searrow^{+M}$$
$${}^3CH_2CO \longrightarrow {}^3CH_2 + CO \qquad (4)$$

This assumption was made despite the observation of a small reduction in the total quantum yield as the inert gas pressure was increased in the absence of $O_2$. (e.g. a 10% reduction in yield as Xe was added to p = 200 Torr).

Eder and Carr [71] measured the efficiencies of inert gases as ${}^1CH_2 \longrightarrow {}^3CH_2$ deactivators relative to the rate of reaction of ${}^1CH_2$ with n-propane. They photolysed $CH_2CO$ in the presence of n-$C_3H_8$, $O_2$, and inert gas at $260 \leq \lambda \leq 350$ nm. The products, ethylene and butanes, were explained by the following scheme:

$${}^1CH_2 + CH_2CO \xrightarrow{k_1} C_2H_4 + CO \qquad (1)$$

$${}^1CH_2 + M \xrightarrow{k_2} {}^3CH_2 + M \qquad (2)$$

$${}^1CH_2 + \text{n-}C_3H_8 \xrightarrow{k_3} \text{n-}C_4H_{10}, \text{ i-}C_4H_{10} \qquad (3)$$

$${}^3CH_2 + O_2 \longrightarrow H_2, CO, CO_2 \qquad (4)$$

The i-$C_4H_{10}$ / n-$C_4H_{10}$ ratio was constant under all conditions. A decrease in product yield with increasing dilution in inert gas, M, allowed a determination of $k_2/k_3$. Results were obtained both for $CH_2$ and for $CD_2$, the latter being produced by photolysis of $CD_2CO$.

| - | He | Ar | Xe | $CF_4$ |
|---|---|---|---|---|
| $k_2/k_3$ ($CH_2$) | 0.010 | 0.030 | 0.047 | 0.043 |
| $k_2/k_3$ ($CD_2$) | 0.030 | 0.049 | 0.0167 | 0.175 |

It is apparent that values of $k_2/k_3$ are 2 - 3 times

larger for $CD_2$ than for $CH_2$.

Although there is no precise agreement between the results of Cox and Preston [38] and those of Eder and Carr [71], in both cases the same order of efficiency for deactivation of $^1CH_2$ to $^3CH_2$ is found for the monatomic species, i.e. He $\lesssim$ Ar $<$ Kr $<$ Xe, and the polyatomic "inert gases" all have efficiencies comparable to or greater than Xe. The process of deactivation of $^1CH_2$ to $^3CH_2$ is relatively inefficient occurring at rates $10^{-1}$ - $10^{-2}$ times slower than the rate of reaction of $^1CH_2$ with ketene or with alkanes.

1.4.3. Kinetic spectroscopy. The first spectroscopic determination of rate constants of $CH_2$ reactions was that of Braun et al. [41]. They used flash photolysis to generate a high concentration of $CH_2$ radicals and monitored $^3CH_2$ by its absorption at 141.5 nm. In a system containing only inert gas and $\lesssim$ 0.1 Torr $CH_2CO$, a photolysis flash which decomposed 30% of the ketene produced $C_2H_2$ as the main product. Plots of $1/[^3CH_2]$ versus time were linear supporting a bimolecular mechanism,

$$^3CH_2 + {}^3CH_2 \xrightarrow{k_1} C_2H_4{}^* \longrightarrow C_2H_2 + (H_2 \text{ or } 2H) \quad (1)$$

$k_1$ was measured as $5.3 \times 10^{-11}$ cm$^3$ molecule$^{-1}$ s$^{-1}$ which is of the order of $\frac{1}{3}$ the collision number. At the pressures used (up to 1 atmosphere) all the excited $C_2H_4$ decomposed.

In this system an absorption due to the CH radical was observed. This was initially absent and grew in as reaction (1) proceeded before decaying away. Unfortunately

the extinction coefficient for CH is unknown and [CH] could not be estimated. Its presence was attributed to a minor process,

$$C_2H_4^* \longrightarrow CH + CH_3 \qquad (2)$$

Addition of $H_2$ or $CH_4$ to this system at low inert gas pressures caused the production of $CH_3$ radicals according to the reactions,

$$^1CH_2 + H_2 \xrightarrow{k_3} CH_4^* \longrightarrow CH_3 + H \qquad (3)$$

$$^1CH_2 + CH_4 \xrightarrow{k_4} C_2H_6^* \longrightarrow CH_3 + CH_3 \qquad (4)$$

As inert gas was added, $^1CH_2$ was deactivated to $^3CH_2$. At a given time interval after the photolysis flash, $\Delta t$, the amount of $^3CH_2$ observed was proportional to the inert gas pressure provided that $\Delta t$ was sufficiently small that no reaction of $^3CH_2$ had taken place. Braun et al. estimated the following rate constants:

$^1CH_2 + He \longrightarrow {}^3CH_2 + He$ $\quad 3.0 \times 10^{-13}$ cm$^3$ molecule$^{-1}$ s$^{-1}$

$^1CH_2 + Ar \longrightarrow {}^3CH_2 + Ar$ $\quad 6.7 \times 10^{-13}$ cm$^3$ molecule$^{-1}$ s$^{-1}$

$^1CH_2 + N_2 \longrightarrow {}^3CH_2 + N_2$ $\quad 9.0 \times 10^{-13}$ cm$^3$ molecule$^{-1}$ s$^{-1}$

The ratios of these rate constants are only in fair agreement with the results of Cox and Preston [38] or Eder and Carr [71]. However they do set an absolute value on the rate of deactivation of $^1CH_2$ by collision with inert gas, showing that approximately one collision in $10^3$ is effective.

Braun et al. were also able to estimate $k_3$ and $k_4$, as $7.0 \times 10^{-12}$ and $1.9 \times 10^{-12}$ cm$^3$ molecule$^{-1}$ s$^{-1}$ respectively. They did this by setting up a competition between the reaction of $^1CH_2$ with $H_2$ or $CH_4$ and deactivation

of $^1CH_2$ by inert gas. The observation of $[CH_3]$, at a given time interval, $\triangle t$, after the flash, versus pressure gave the value of $k_3$ or $k_4$ since $k_5$ was known.

1.4.4. Steady state systems. Koob [52,74] used $n\text{-}C_3H_8$ as a precursor for $CH_2$, in a low intensity photolysis system. $O_2$ was present to scavenge $^3CH_2$, and argon was added as an inert gas. He interpreted his results according to the following reaction scheme:

$$C_3H_3 + h\nu \longrightarrow {}^1CH_2 + C_2H_6$$

$$^1CH_2 + C_3H_8 \xrightarrow{k_1} {}^3CH_2 + C_3H_8 \qquad (1)$$

$$^1CH_2 + Ar \xrightarrow{k_2} {}^3CH_2 + Ar \qquad (2)$$

$$^1CH_2 + C_3H_8 \xrightarrow{k_3} n\text{-}C_4H_{10},\ i\text{-}C_4H_{10} \qquad (3)$$

$$^1CH_2 + O_2 \xrightarrow{k_4} {}^3CH_2 + O_2 \qquad (4)$$

$$^1CH_2 + O_2 \xrightarrow{k_5} \text{Products} \qquad (5)$$

Although $O_2$ was added as a scavenger for $^3CH_2$ it does react at an appreciable rate with $^1CH_2$. Eder et al. [72] found $k_5/k_2 \lesssim 0.46$. In view of this Koob kept $[O_2] \lesssim 0.1 \times [C_3H_8]$. The system was essentially a competition between reaction of $^1CH_2$ with $C_3H_8$ and deactivation of $^1CH_2$ to $^3CH_2$. $[C_2H_6]$ measured the rate of production of $^1CH_2$ ($r_1$), and $[C_4H_{10}]$ the rate of reaction of $^1CH_2$ with $C_3H_8$ ($r_2$). In the experiment $[C_3H_8]$ and $[O_2]$ were kept constant and $[Ar]$ was increased. A plot of $r_1 / r_2$ versus $[Ar] / [C_3H_8]$ gave a straight line with a slope taken to be $k_2/k_3$. A value of 0.024 was found in good agreement with Eder and Carr's value of 0.030. Koob considered this to

be evidence that the $CH_2$ reacting in his system was in the same state as in Eder and Carr's system [71]. In that system $CH_2CO$ was photolysed at $\lambda \simeq$ 300 nm., and could have very little vibrational energy. In Koob's experiment $CH_2$ might have carried away appreciable energy from the photolysis.

The value of $k_2/k_3$ does not agree with the ratio found by Braun et al.[41]. They measured $k_2$ to be $6.7 \times 10^{-13}$ $cm^3$ $molecule^{-1}$ $s^{-1}$. An estimate of $k_3$ was obtained by Halberstadt and Crump [73] on the basis of Braun's results. They photolysed ketene at 313 nm. in the presence of a mixture of methane and propane with NO as a scavenger for $^3CH_2$ and measured a ratio of the rate constants for $^1CH_2$ reaction with the two hydrocarbons. Using Braun et al!s result for $^1CH_2$ reaction with $CH_4$ they obtained $k_3 = 6.3 \times 10^{-12}$ $cm^3$ $molecule^{-1}$ $s^{-1}$. The ratio $k_2/k_3$ is 0.106, five times higher than Koob's result.

Koob also used c-$C_3H_6$ as a precursor for $CH_2$ [75]. In the photolysis of c-$C_3H_6$ / n-$C_3H_8$ mixtures at $\lambda$ = 165 nm., where n-$C_3H_8$ does not absorb, Koob found the ratio of butanes / $CH_2$ equal to 0.6. For n-$C_3H_8$ at $\lambda$ = 123.6 nm. the ratio was again 0.6 and for n-$C_3H_8$ at $\lambda$ = 147 nm. it was 0.4. The implication is that at least 0.4 of the $CH_2$ produced in the photolysis did not insert into the propane. There were two possible explanations: (i) The primary photolysis may not produce all $CH_2$ ($^1A_1$). $CH_2$ ($^3B_1$) is known not to insert and in addition higher energy singlet states are available. (ii) Another reaction may compete with insertion e.g. reaction (1).

Koob checked possibility (i) by photolysing <u>cis</u> and <u>trans</u> - 1, 2 dimethylcyclopropane (DMCP). As discussed

earlier $^1CH_2$ adds to the double bond in but-2-ene with retention of geometry to give 1, 2 DMCP but $^3CH_2$ addition leads to a certain amount of randomisation of the geometric isomers. Koob used a similar argument for the reverse reaction. In the process,

<u>cis</u> 1,2 DMCP + $h\nu \longrightarrow$ $^1CH_2$ + <u>cis</u> but-2-ene

a mixture of <u>cis</u> and <u>trans</u> - but-2-ene might be expected if $^3CH_2$ were formed in the primary process. Experimentally, Koob found that <u>trans</u> DMCP gave <u>trans</u> but-2-ene only, and that <u>cis</u> - DMCP gave <u>cis</u> but-2-ene only. This argued against production of $^3CH_2$ in the photolysis. By analogy Koob considered formation of $^3CH_2$ in the photolysis of c-$C_3H_6$ to be unlikely. The possibility that a higher singlet state is produced in the photolysis still remains open.

It is therefore important to estimate how much energy each of the photofragments carries away from the photolysis. In the photolysis of n-$C_3H_8$ at 123.6 nm. the photofragments share 133 kcal $mol^{-1}$. This photolysis was studied by Koob over a pressure range of 2 - 760 Torr [52]. In this pressure range the $C_2H_6$ yield did not change. Failure to observe any decomposition of $C_2H_6$ at a pressure of 2 Torr implies that $C_2H_6$ carries less than 70 kcal $mol^{-1}$. This was estimated in the knowledge that the activation energy for ethane decomposition is 85 kcal $mol^{-1}$ [76]. $C_2H_6$ would be formed with a range of energies and failure to observe any $C_2H_6$ decomposition implies that no significant proportion of the $C_2H_6$ molecules carried more than 85 kcal $mol^{-1}$. $^1CH_2$ inserted into the secondary C - H bonds of n-$C_3H_8$ to give isobutane which decomposed with a measured rate constant of

$1.3 \times 10^8$ $s^{-1}$. An RRKM calculation implies that an average of 31 kcal $mol^{-1}$ must be supplied to the insertion by $CH_2$. Thus $E^*(C_2H_6) < 70$ kcal $mol^{-1}$ and $E^*(CH_2) > 31$ kcal $mol^{-1}$. The $CH_2$ is either vibrationally excited or else it may be formed in a higher singlet electronic state than $\tilde{a}\,^1A_1$.

Bell [47] has also studied the $CH_2/n\text{-}C_3H_8$ system. His source of $CH_2$ was $CH_2N_2$ photolysed at $\lambda = 405$ nm. His results are consistent with those of Braun et al. [41], and he found $k_1 = 2.4 \times 10^{-12}$ $cm^3$ $molecule^{-1}$ $s^{-1}$. This result implies that the yield of $^3CH_2$ in the system is due to the reaction

$$^1CH_2 + C_3H_8 \xrightarrow{k_1} {}^3CH_2 + C_3H_8$$

This reaction may also explain Koob's finding that only 60% of the $CH_2$ produced in $n\text{-}C_3H_8$ photolysis ended up in the butanes formed. However, it does not detract from the possibility that the $CH_2$ produced in the primary photolysis is in an excited singlet electronic state.

There appears to be a serious discrepancy between the rate constants measured by Braun et al. and those measured by Koob.

### 1.4.5. Reactivity of $^3CH_2$.

#### 1.4.5.1. Radical - radical reactions in low intensity systems.

The observation of radical - radical reactions involving $^3CH_2$ in low intensity photolysis systems, where the radical concentration is very low compared to the concentration of other molecules, supports the conclusion that $^3CH_2$ is a long lived species with a reactivity comparable to $CH_3$. Systems involving $^3CH_2$ reactions have been reported

by Frey and Walsh [77], by Rowland et al. [78], and by Dees and Setser [37].

Frey and Walsh [77] used the mercury photosensitized decomposition of ketene as a source of $^3CH_2$.

$$Hg\ (^3P_1) + CH_2CO \longrightarrow {}^3CH_2 + CO + Hg(^1S_0)$$

The principal products observed were CO, $C_2H_4$, $C_2H_2$, and $C_2H_6$, and the following scheme was suggested to account for these:

$$^3CH_2 + CH_2CO \longrightarrow C_2H_4 + CO$$

$$^3CH_2 + {}^3CH_2 \longrightarrow C_2H_4^* \longrightarrow C_2H_2 + (H_2 \text{ or } 2H)$$

$$H + CH_2CO \longrightarrow CH_3 + CO$$

$$CH_3 + CH_3 \longrightarrow C_2H_6$$

$$CH_3 + {}^3CH_2 \longrightarrow C_2H_4 + H$$

A key reaction in this scheme is the combination of $^3CH_2$ radicals. For this reaction to occur under conditions of low $^3CH_2$ and high $CH_2CO$ concentration requires the $^3CH_2$ to be very unreactive towards ketene. Frey and Walsh estimated the reaction of $^3CH_2$ with $CH_2CO$ to occur with a collision efficiency of $\simeq 10^{-7}$.

Rowland et al. [78] used radioactive precursors ($^{14}CH_2CO$, CHTCO) to provide suitably labelled methylene radicals for study. In the photolysis of $^{14}CH_2CO$ in the near U.V. in the presence of $CD_4$, ethylene $^{14}C$ was formed with 0, 1, and 2 D atoms. This was explained by a scheme where triplet methylene reacted with methyl to give excited ethyl radicals. Ethylene was then formed by loss of a hydrogen atom.

$$^3CH_2 + CH_3 \longrightarrow C_2H_5 \longrightarrow C_2H_4 + H$$

Dees and Setser [37] studied the low intensity photolysis of ketene / n-butane mixtures in the region of $300 \leq \lambda \leq 340$ nm. The products were explained by a scheme in which sec-butyl radicals were formed by $^3CH_2$ abstracting H from $n\text{-}C_4H_{10}$. The radical - radical reaction of $^3CH_2$ with sec-butyl radicals competed with the reaction of $^3CH_2$ with butane or ketene, despite the very large excess of butane and ketene.

1.4.5.2. $O_2$ as a scavenger for $^3CH_2$. Tracer experiments [79] have led to some clarification of the reactions of $^3CH_2$ with $O_2$. This reaction, highly exothermic with respect to many possible products is a reaction between two triplet species. Rowland et al. [79] have shown that the oxides of carbon account for nearly all the methylenic carbon.

$$^3CH_2 + O_2 \rightarrow \text{Intermediate(s)} \rightarrow \begin{cases} H_2 + CO + O \\ H_2 + CO_2 \\ H + CO + OH \end{cases}$$

Laufer and Bass [80] have recently measured the rate constant for this reaction in 700 Torr helium as

$$k = 1.5 \times 10^{-12} \text{ cm}^3 \text{ molecule}^{-1} \text{ s}^{-1}.$$

1.4.5.3. CO as a scavenger for $CH_2$. In some experiments CO has been used as a scavenger for $CH_2$. This is of particular interest since the reaction of $CH_2$ with CO to form $CH_2CO$ is the reverse of the photolysis of $CH_2CO$ and may lead to an increased understanding of the photolysis process.

Contrary to the results of Degraff and Kistiakowsky [33], and of Cox and Cvetanovic [81] it now appears that $^1CH_2$ reacts more rapidly with CO than does $^3CH_2$ [37]. Removal of $CH_2$ requires major amounts of CO (in comparison to the small concentration of $O_2$ required) and selective removal of $^3CH_2$

from hydrocarbon systems by CO simply reflects the extremely low probabilities for either addition or abstraction reactions of $^3CH_2$ with hydrocarbons. The mistaken conclusion of Degraff and Kistiakowsky was based on the assumption that $^1CH_2$ and $^3CH_2$ are equally reactive towards $CH_2CO$. In fact $^3CH_2$ has a very low collision efficiency with $CH_2CO$ ( $\simeq 10^{-7}$) [77], whereas $^1CH_2$ reacts quickly with an efficiency of $10^{-1}$ - $10^{-2}$ [80].

Laufer and Bass [80] have estimated a rate constant for the reaction,

$$^3CH_2 + CO \longrightarrow \text{Products}$$

of $k \leq 1.0 \times 10^{-15}$ cm$^3$molecule$^{-1}$ s$^{-1}$, at $p_{He}$ = 700 Torr

Dees and Setser found that CO did not adequately suppress $^3CH_2$ at pressures below 50 Torr. They interpreted this pressure dependence of CO scavenging in terms of the formation of chemically activated $^3CH_2CO^*$ which either redissociated or was collisionally stabilized. They estimated the half pressure for stabilization, $p_{\frac{1}{2}}$, to be 8 Torr, and, using an RRKM model, calculated an activation energy for dissociation of $^3CH_2CO^*$ of 39.5 kcal mol$^{-1}$.

By comparison, Montague and Rowland [82] have shown that addition of $^1CH_2$ to CO may be capable of forming an oxirene intermediate, $HC\overset{O}{=}CH$, which has a $p_{\frac{1}{2}}$ of 840 Torr.

1.4.5.4. NO as a scavenger for $^3CH_2$. NO is known to be a very efficient radical scavenger. The rate constant for removal of $^3CH_2$ by NO has been measured by Bass and Laufer [80] at a pressure of 700 Torr helium as $1.6 \times 10^{-11}$ cm$^3$ molecule$^{-1}$ s$^{-1}$. This is 10 times faster than the reaction

$^3CH_2 + O_2$, and $\simeq 10^4$ times faster than $^3CH_2 + CO$ under the same conditions. In all cases these rates were measured by comparison with the reaction,

$$^3CH_2 + {}^3CH_2 \longrightarrow C_2H_2 + H_2, k = 5.3 \times 10^{-11} \text{ cm}^3 \text{ molecule}^{-1} \text{ s}^{-1}$$

1.4.6. Energy carried by $^1CH_2$. An indirect method of estimating the energy carried by $^1CH_2$ has been exploited by many workers. This involves measurement of the rate of isomerisation or decomposition of the product of a $^1CH_2$ insertion in a C-H bond or addition to a double bond, and the calculation of the energy content of this excited species according to the RRKM method [153].

As an example, consider the reaction,

$$^1CH_2 + c\text{-}C_3H_6 \longrightarrow c\text{-}C_3H_5.CH_3^* \qquad (1)$$

$$c\text{-}C_3H_5.CH_3^* \xrightarrow{\omega} c\text{-}C_3H_5.CH_3 \qquad (2)$$

$$c\text{-}C_3H_5.CH_3^* \xrightarrow{k_a} \text{Butenes}$$

which has been studied by Kistiakowsky and Saunders [83]. The $^1CH_2$ inserts into a C-H bond of cyclopropane to give vibrationally excited methylcyclopropane (MCP). The "hot" MCP may isomerise to a butene or it may be collisionally stabilised. In equation (2) $\omega$ is the collision frequency and $k_a$ is the overall rate constant for isomerisation of MCP. The ratio of products formed, $[\text{Butenes}] / [\text{MCP}]$, is equal to the ratio $k_a/\omega$.

$\omega$ is proportional to the pressure in the system. Plots of the ratio $[\text{Butenes}] / [\text{MCP}]$ versus 1/pressure gave straight lines whose gradients are related to $k_a$. RRKM calculations give $k_a$ as a function of $\langle E \rangle$, the mean energy content of

the MCP, and thus, for a given $k_a$, $\langle E \rangle$ can be estimated. Subtraction of the exothermicity of reaction (1) from $\langle E \rangle$ gives the energy carried by $^1CH_2$ into the reaction. Use of monochromatic light allows measurement of $\langle E \rangle$ as a function of $\lambda$.

Table 1.5 summarises the results obtained by several workers using this technique. Although the absolute calculated value of the energy carried by $CH_2$ depends on the model used in the RRKM calculation, in any set of calculations two trends are immediately clear. Firstly, the energy carried into reaction by $CH_2$ increases as $\lambda$ decreases, and, secondly, the fraction of the available energy decreases as $\lambda$ decreases. These are consistent with $CH_2$ being formed in a vibrationally excited $^1A_1$ state and undergoing several inelastic collisions before reaction. The energy loss is greater when the total energy is greater, but the rate of reaction is sufficiently fast that $CH_2$ does not become vibrationally thermalised before reaction.

Frey [84] has speculated that the difference in energy carried by $CH_2$ in the photolysis of $CH_2CO$ at $\lambda$ = 206.2 nm. and $\lambda$ = 325 nm. may be electronic energy, i.e. at $\lambda$ =206.2nm. $CH_2$ reacts as $CH_2$ ($^1B_1$). In the photolysis of $CH_4$ [88] it is probable that $CH_2$ ($^1B_1$) is produced and this may explain the observation that the energy carried into reaction is the same at both wavelengths.

### 1.4.7. Rate of removal of vibrational energy from $^1CH_2$.

Hase et al. [89] estimated the rate of removal of vibrational energy from $^1CH_2$. In their system they photolysed $CH_2N_2$ at 435.8 nm. and $CH_2CO$ between 320 and

Table 1.5. Energy carried into reaction by $^1CH_2$.

| Precursor | λ/nm. | Reactant | Adduct | Excess energy available (kcal) | Energy carried by $CH_2$ (kcal) | Ref. |
|---|---|---|---|---|---|---|
| $CH_2CO$ | 214 | c-$C_3H_6$ | MCP [c] | 56.8 | 11.3 | |
| | 277 | | | 26.2 | 8.0 | 83 |
| | 313 | | | 14.4 | 5.9 | |
| | 330 | | | 9.6 | 5.0 | |
| $CH_2CO$ | 206.2 | c-$C_4H_8$ | MCB [d] | 61.7 | 39.6 [a] | |
| | 325 | | | 11.4 | 20.8 | 84 |
| $CH_2N_2$ | 366 | n-$C_3H_8$ | $C_4H_{10}$ | 116.5 | 24.9 | 85[b] |
| | 435.8 | | | 103.7 | 21.4 | |
| n-$C_3H_8$ | 123.6 | n-$C_3H_8$ | $C_4H_{10}$ | 135.2 | 32.6 | 86[b] |
| c-$C_3H_6$ | 165 | | | 81.8 | 31.0 | |
| $CH_2CO$ | 268.8 | $C_3H_6$ | MCP [c] | 29.8 | 3.0 | 87 |
| | 313.0 | | | 14.6 | Decreases with increasing λ | |
| | 334.0 | | | 8.6 | | |
| | 355.0 | | | 3.6 | | |
| $CH_4$ | 106 | $CH_4$ | $C_2H_6$ | 163 | Equal for the different λ s. | 88 |

Notes.

a. These values were considered to indicate an inconsistency in RRKM theory.

b. The RRKM model used was the same in these calculations.

c. MCP is methylcyclopropane.

d. MCB is methylcyclobutane.

380 nm. $O_2$ was present to scavenge any $^3CH_2$, and $^1CH_2$ reacted with cis-but-2-ene to give vibrationally excited cis-DMCP. The energy carried by $^1CH_2$ into reaction was estimated from the rate constant for isomerisation of cis-DMCP to trans-DMCP. In their model Hase et al. considered $^1CH_2$ to be produced in a $v_2 = 0$, 1, 2, or 3 level. Molecules in each level could then react, be deactivated to $^3CH_2$, or lose a single quantum of vibrational energy. The rate constant for reaction was assumed to be independent of the vibrational level. The conclusion from this oversimplified model was that 80-800 $CF_4$ or 10-100 $C_8F_{18}$ collisions remove one bending vibrational quantum from $^1CH_2$.

In view of the slow rate at which vibrational energy is removed from $CH_2$ ($^1A_1$) it is not surprising that vibrational energy is carried by $^1CH_2$ when it inserts into C-H bonds or reacts with C=C bonds.

## 1.5. $CH_2$ ($^1A_1$) —— $CH_2$ ($^3B_1$) energy separation.

No singlet-triplet transitions have been observed in the spectrum of $CH_2$ and the energy separation between the lowest singlet state ($^1A_1$) and the ground triplet state ($^3B_1$) remains unknown. This quantity is of prime importance in a discussion on the mechanism of deactivation of $CH_2$ ($^1A_1$) to $CH_2$ ($^3B_1$) by collision with an inert gas molecule. The chemical evidence has been interpreted to support both a small (2-3 kcal $mol^{-1}$) and a large (8-10 kcal $mol^{-1}$) value.

Frey [90] estimated a value of 8-10 kcal $mol^{-1}$. His argument is based on the very low reactivity of $^3CH_2$. If

equilibrium between $^1CH_2$ and $^3CH_2$ is maintained during a steady state photolysis, then the proportion of $CH_2$ reacting as $^1CH_2$ is given by the relative rates of $^1CH_2/^3CH_2$ reactions multiplied by the equilibrium constant for the reaction,

$$^3CH_2 + M \longrightarrow {}^1CH_2 + M$$

Since reactions of $^1CH_2$ are so much faster than the observed radical reactions of $^3CH_2$ [54], this must mean that K is small and E ($^1CH_2$ - $^3CH_2$) is consequently large.

In a recent paper Frey [91] put forward further evidence in favour of E ($^1CH_2$ - $^3CH_2$) = 8-10 kcal $mol^{-1}$. In the photolysis of $CH_2CO$ : cis-but-2-ene : $N_2$ mixtures, $^3CH_2$ reacted with cis-but-2-ene to give a 1 : 1 mixture of cis and trans 1,2 dimethylcyclopropane (DMCP) whereas $^1CH_2$ reacted to give cis-1,2-DMCP only[92]. On the assumption that an equilibrium ratio of $^1CH_2$ : $^3CH_2$ is maintained throughout the reaction the proportion of cis and trans-1,2-DMCP would be given by

$$\log_{10}\left\{\frac{[\text{cis-1,2-DMCP}]}{[\text{trans-1,2-DMCP}]} - 1\right\} = \log_{10}\left(\frac{2A_4}{A_3}\right) - \left(\frac{E_2-E_3}{2.3RT}\right) \qquad (1)$$

where $A_3$, $A_4$ are the Arrhenius pre-exponential factors for reaction of $^3CH_2$ and $^1CH_2$ with cis-but-2-ene. The energy of activation for the reaction of $^1CH_2$ with cis-but-2-ene has been assumed to be zero [93]. $E_3$ is the energy of activation for reaction of $^3CH_2$ with cis-but-2-ene and $E_2$ is the $^1CH_2$ - $^3CH_2$ energy separation. Frey found that a plot of the L.H.S. of eq.(1) versus 1/T gave a good straight line for 350 K $\leq$ T $\leq$ 475 K. From the gradient he obtained

$E_2 - E_3 = 1.7$ kcal $mol^{-1}$. Since the reactivity of $^3CH_2$ is similar to that of $CH_3$ he estimated $E_3$ as 7.3 kcal $mol^{-1}$, the value for the addition of $CH_3$ to but-2-ene. On this assumption $E_2$ has a value of 9.0 kcal $mol^{-1}$.

Eder and Carr[94] put forward an argument for a small E ($^1CH_2 - {}^3CH_2$). The photolysis process,

$$CH_2CO\ (^1A_1) \longrightarrow CO\ (X^1\Sigma^+) + CH_2(^3B_1)$$

was calculated to be endothermic by 81 kcal $mol^{-1}$. (Eder and Carr preferred $\Delta H^o_{f,298}\ (CH_2) = 95.0$ kcal $mol^{-1}$.) At $\lambda = 350$ nm. there is sufficient energy (81.5 kcal $mol^{-1}$) to produce $^3CH_2$. Eder and Carr interpreted their experimental results [35] as indicating the production of up to 15% $^1CH_2$ in the primary photolysis. The relative yield of $^1CH_2$ to $^3CH_2$ was expected to be

$$R = (A_3 / A_1)\ \exp\ (-(E_3-E_1)/kT)$$

where $E_1$, $E_3$ are activation energies for the decomposition of singlet and triplet ketene, and $A_1$, $A_3$ are the Arrhenius pre-exponential factors. Assuming $A_1 \simeq A_3$ and putting $R = 0.15$ Eder and Carr found $E_1 - E_3 = 1.4$ kcal $mol^{-1}$. Thus they deduced that E ($^1CH_2 - {}^3CH_2$) lay in the range 1 - 2 kcal $mol^{-1}$.

An earlier study by Halberstadt and McNesby [95] has been cited as evidence for a small E ($^1CH_2 - {}^3CH_2$). The method discussed in section 1.4.6. was used to estimate the energy carried by $^1CH_2$ into $CH_4$, and the assumption made that this was entirely electronic energy. However, this assumption is unlikely to be valid, and, in addition, Hase [76] has criticised the RRKM model which was used. This study does not give a reliable estimate of E($^1CH_2 - {}^3CH_2$).

On the basis of Eder and Carr's evidence and Frey's evidence there is a division of opinion as to whether $E\ (^1CH_2 - {}^3CH_2)$ is large or small.

## 1.6. Mechanism of $CH_2\ (^1A_1) \longrightarrow CH_2\ (^3B_1)$ deactivation.

Three possible mechanisms which can yield the observed second order kinetics for deactivation of $^1CH_2$ to $^3CH_2$ are:

(i) Rate limiting vibrational relaxation of $^1CH_2$ followed by a rapid intramolecular transition. (See fig. 1.5.)

(ii) A rapid, intramolecular radiationless transition followed by rate-limiting vibrational relaxation of $^3CH_2$. Vibrationally relaxed $^3CH_2$ would not be capable of reversibly returning to $^1CH_2$.

(iii) A bimolecular mechanism wherein the singlet - triplet transition results directly from inelastic collision of $^1CH_2$ with a suitable collision partner ( $k'_{ISC} = k_{ISC}\ [M]$ ).

Bader and Generosa [63] adopted the first approach. On the basis of Jordan and Longuet-Higgins' theoretical computations [96], they estimated that the transition occurred from the $v_2 = 1$ level of the bending mode of $^1CH_2$. They used the Landau-Zener formula [97] to show that for this level the first order rate constant for the transition was approximately $10^{11}\ s^{-1}$. The role of the inert gas, then, was to vibrationally deactivate the energy rich $^1CH_2$ initially formed in the photolysis. This approach has been criticised on two counts. Firstly, the Landau-Zener formula is not applicable to the present study since the formula was derived for transitions between a discrete

state and a continuum whereas the transition in methylene is between two discrete states. Secondly, [38] a fast, first-order crossing, being reversible, would result in the rapid establishment of an equilibrium ratio of $^1CH_2$ : $^3CH_2$. The observed rate of electronic relaxation would then be largely determined by the relative rates of vibrational quenching of singlet and triplet methylene below the energy of the crossing point.

Chang and Basch [98] have applied perturbation theory to the calculation of the rate of the singlet-triplet transition. Kinetically, the overall process is described by

$$^1CH_2 \underset{k_2}{\overset{k_1}{\rightleftharpoons}} {}^3CH_2{}^*$$

$$^3CH_2{}^* + X \xrightarrow[k_3]{} {}^3CH_2 + X$$

where X is the "inert" gas, and $k_1$ and $k_2$ are pseudo-rate constants. A steady state analysis of the system yields

$$\frac{d[^3CH_2]}{dt} = \frac{k_1 k_3}{k_2 + k_3[X]} [^1CH_2][X] \qquad (1)$$

If $k_2 \gg k_3[X]$ the rate of formation of $^3CH_2$ is bimolecular, and if $k_2 \ll k_3[X]$ the rate of formation of $^1CH_2$ is unimolecular,

The spin functions for a triplet state in symmetry $C_{2v}$ correspond to the irreducible representations $A_2$, $B_1$, $B_2$. The overall symmetries of the spin-orbital components of the $^3B_1$ state are therefore $B_2$, $A_1$, and $A_2$ respectively. Thus, in the presence of spin-orbit coupling the $A_1$

component of the triplet state may interact with the lowest state in the singlet manifold ($^1A_1$).

Chang and Basch assumed that one singlet vibronic state and one (triply degenerate) triplet vibronic state were almost degenerate, and they neglected interactions with all other vibronic states. If the system is prepared in the singlet state at time t = 0, the probability, $P_T(t)$, that the system will be in the triplet state at a subsequent time t is

$$P_T(t) = \frac{2|V_{1,s}|^2}{2|V_{1,s}|^2 + \delta^2} \sin^2\left\{\left(2|V_{1,s}|^2 + \delta^2\right)^{\frac{1}{2}} t/\hbar\right\}$$

where $2\delta$ is the energy separation of the singlet and triplet states, and $|V_{1,s}|$ is the matrix element coupling them. According to the Born-Oppenhiemer approximation $|V_{1,s}|^2$ may be approximated by

$$|V_{1,s}|^2 = |V_{1,s}^{(e)}|^2 Q$$

where Q is the Franck-Condon factor and $V_{1,s}^{(e)}$ is the matrix element for spin-orbit interaction in the absence of vibration. $|V_{1,s}^{(e)}|$ was taken as the spin-orbit interaction for the Carbon atom and Q as $10^{-2}$.

Chang and Basch distinguished two limiting cases:

Case (a): Near accidental degeneracy of the singlet and triplet states. ($\delta \simeq 0$).

$$P_T(t) \simeq \sin^2 (5 \times 10^{11} t)$$

Case (b): $\delta \simeq 10^3$ cm$^{-1}$

$$P_T(t) \simeq 4 \times 10^{-6} \sin^2 (2 \times 10^{15} t)$$

Since at atmospheric pressure the collision rate is $10^9$ s$^{-1}$, the oscillatory frequency in $P_T(t)$ is $> 10^2$ times the

collision frequency. Therefore the probabilities may be averaged over time giving:

Case (a): $P_T(t) \simeq \frac{1}{2}$

Case (b): $P_T(t) \simeq 2 \times 10^{-6}$

In case (a) the intramolecular crossover is fast, resulting in rapid establishment of an approximately 1:1 ratio of $^1CH_2$ : $^3CH_2$. Hence in eq.(1) $k_2 \gg k_3[X]$ and the observed kinetics are bimolecular. In case (b) the transition probability is very small and the overall process is likely to be unimolecular. Model (ii), then requires the near degeneracy of a singlet vibronic state and a triplet vibronic state. Fig. 1.4. shows the low lying vibrational states of $^3CH_2$ calculated assuming $\nu_1 = 2968$, $\nu_2 = 1444$, and $\nu_3 = 3000$ cm$^{-1}$ [99].

It is apparent that even at energies of 13 -14 kcal mol$^{-1}$, corresponding to the $v_2 = 1$ level of $^1CH_2$ on the assumption that E ($^1CH_2$ - $^3CH_2$) = 10 kcal mol$^{-1}$, a "near" degeneracy in the sehse of case (a) ($\delta < 30$ cm$^{-1}$) will be "accidental". However, the inclusion of rotational levels makes "accidental" degeneracy more likely. The rotational constants for $CH_2$ are $\simeq 10$ cm$^{-1}$ [2]. At 300 K the maximum population of a rotational level occurs at $J_{max}$ = 3 or 4. Rotational levels occur at 0, 20, 60, 120, ... cm$^{-1}$ thus the vibronic levels are probably fairly well populated even at energies 200 - 300 cm$^{-1}$ above the J = 0 levels shown in fig.1.4. Since deactivation of $^1CH_2$ is a slow process it is probable that $^1CH_2$ molecules are rotationally thermalised when the deactivation takes place.

Eder and Carr [71] assumed E ($^1CH_2$ - $^3CH_2$) to be small,

Fig. 1.4. Vibrational levels of $CH_2$ ($^3B_1$) calculated assuming $\nu_1$ = 2968 $cm^{-1}$, $\nu_2$ = 1444 $cm^{-1}$, $\nu_3$ = 3000 $cm^{-1}$.

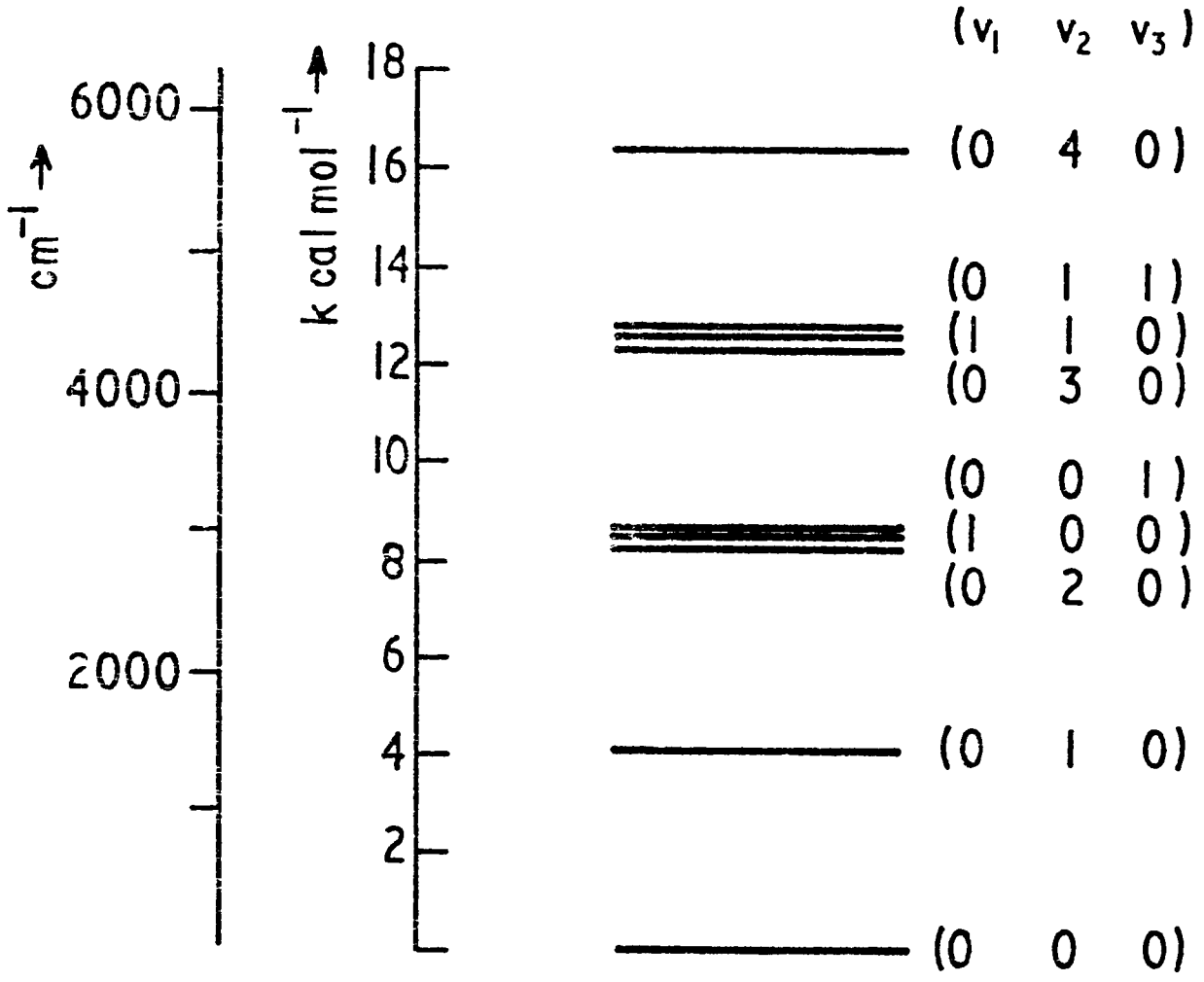
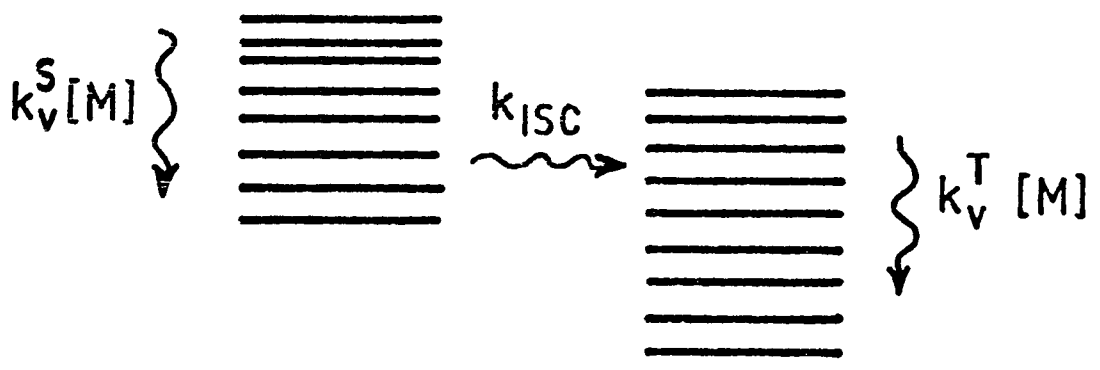



Fig. 1.5. Mechanism of $^1CH_2 \longrightarrow {}^3CH_2$ deactivation.



and favoured model (iii), since they considered an accidental degeneracy with $E(^1CH_2 - {}^3CH_2) = 1\text{-}2$ kcal $mol^{-1}$ to be unlikely. In addition, they argue that the order of efficiency of the inert gases in deactivating $^1CH_2$ (He < Ar < Xe) is the reverse of the efficiency expected on the basis of the distorted wave approximation[115]. However, Callear and Van den Bergh [100] have recently studied vibrational deactivation of excited methyl radicals by helium and argon and they found helium to be less efficient than argon.

In model (iii) the intersystem crossing is induced by collisions. The collision partner is considered to couple the methylene with a continuum of energy states. The final vibronic state of $^3CH_2$ may be energetically greater or less than the originating state in the singlet manifold, the energy difference being absorbed by the collision partner, as a difference between the initial and final relative velocities of the collision partner. Fermi's Golden Rule [101] states that

$$k_i = \left(\frac{2\pi}{\hbar}\right) \left| \langle \psi_i | V_{(r)} | \psi_f \rangle \right|^2 \rho$$

where $\left|\langle \psi_i | V_{(r)} | \psi_f \rangle\right|$ is the matrix element which, during collision, couples the initial and final states of the transition. $\rho$ is the density of final states. $\rho$ is greater for $CD_2$ than for $CH_2$ and thus $k_2$ is expected to be faster for $CD_2$ than for $CH_2$ in agreement with experimental observation [71].

Eder and Carr attempted to correlate the rate of intersystem crossing with the polarisability of the collision partner, and they speculated that van der Waals' forces may play a significant role in the mechanism. However, their

examination suffered from a paucity of experimental data.

The choice of a model for deactivation of $^1CH_2$ is obviously hampered by uncertainty in the efficiencies of the inert gases as vibrational deactivators of small molecules such as methylene and methyl radicals. However, the theory of Chang and Basch receives the most general acceptance.

## 1.7. Theoretical studies of $CH_2$ reactions.

**1.7.1. Reaction of $CH_2$ ($^3B_1$).** The simplest reaction of $CH_2$ is the reaction with $H_2$ and many theoretical studies deal with this reaction. The low reactivity of $^3CH_2$ towards $H_2$ is due to a high activation energy. Table 1.6 lists some of the theoretical estimates which have been made of this quantity.

The geometries of the different approaches are shown in fig. 1.6(i). $CH_2$ lies in the yz plane with the z-axis bisecting $\widehat{HCH}$. In the linear approach $H_2$ lies along the z-axis; in the perpendicular approach $H_2$ lies in the xz plane; and in the planar approach $H_2$ lies in the yz plane. A free motion approach may be defined as one in which the energy is minimised for each value of the reaction coordinate by optimising all the geometrical variables. Cremaschi and Simonetta [104] found that the free motion approach coincided with the linear approach in $C_{2v}$ symmetry.

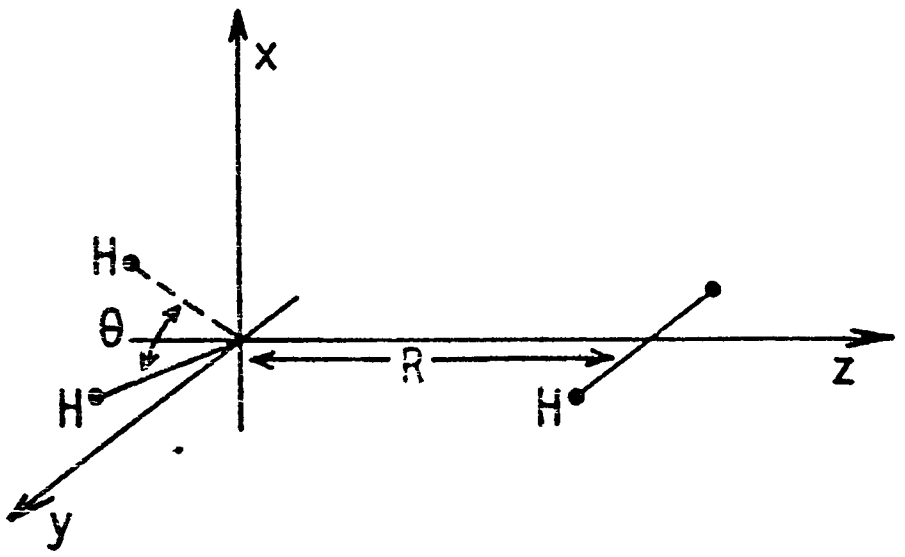
An activation energy of 19.7 kcal $mol^{-1}$ [102] corresponds to a rate constant at 300 K of $10^{-24}$ $cm^3$ $molecule^{-1}$ $s^{-1}$, which is certainly well below the upper limit of $5 \times 10^{-14}$

TABLE 1.6. Activation energy for $CH_2$ ($^3B_1$) + $H_2$.

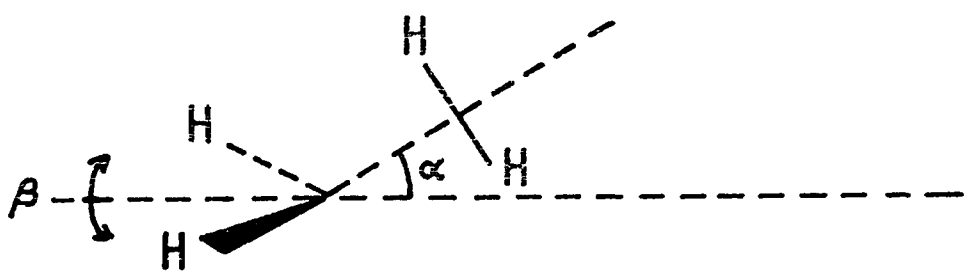
| Method used | Geometry | $E_{act}$/kcal mol$^{-1}$ | Ref. |
|---|---|---|---|
| B.E.B.O. | | 19.7 | 102 |
| Ab initio S.C.F. (configuration interaction) | $C_{2v}$ Linear approach | 15.5 | 103 |
| Ab initio S.C.F. | $C_{2v}$ Linear approach | 23.3 | 104 |
| | $C_{2v}$ Perpendicular approach | 150 | |
| | $C_{2v}$ Planar approach | 150 | |

TABLE 1.7. Activation energy for $CH_2$ ($^1A_1$) + $H_2$.

| Method used | Geometry | $E_{act}$/kcal mol$^{-1}$ | Ref. |
|---|---|---|---|
| Ab initio S.C.F. | $C_{2v}$ Perpendicular approach | 70 | 105 |
| | $C_s$ | Very small | |
| Ab initio S.C.F. | Free motion | 5.8 | 104 |
| | $C_{2v}$ Perpendicular approach | 55.2 | |
| | $C_{2v}$ Linear approach | Purely repulsive potential | |
| CNDO | Free motion | 5 | 107 |




(i) Co-ordinate system for $CH_2 + H_2$ reaction.




(ii) Kollmar's [107] model for $CH_2 + H_2$.

Fig. 1.6.

$cm^3$ $molecule^{-1}$ $s^{-1}$ estimated by Braun et al.[41].

1.7.2. Reactions of $CH_2$ ($^1A_1$). Murrell et al. [105] calculated potential energy surfaces for $^1CH_2 + H_2$. The molecular orbital correlation diagram on the assumption of $C_{2v}$ symmetry is shown in fig. 1.7. The ground state of $CH_4$ ($^1A_1$) has the configuration $(2a_1)^2 (1f_2)^6$. $CH_2$ ($^1A_1$) has the configuration $(2a_1)^2 (1b_1)^2 (4a_1)^2$. What is immediately apparent is that $CH_2$ ($^1A_1$) + $H_2$ ($^1\Sigma_g^+$) does not correlate with $CH_4$ ($^1A_1$). The highest occupied and lowest vacant orbitals cross at some point along the reaction coordinate and the reaction is symmetry forbidden in the Woodward-Hoffmann sense [106]. This crossing causes a high activation energy if the reaction is restricted to $C_{2v}$ symmetry. However, if $C_{2v}$ symmetry is relaxed to $C_s$ symmetry (only the xz symmetry plane is retained) the energy barrier is removed almost completely. (See table 1.7). In $C_s$ symmetry interaction may occur between the bonding orbital of the $H_2$ and the empty $2p\pi$ orbital of $CH_2$.

Kollmar [107] has given the following model of the reaction as occurring in two stages: (i) The empty p orbital of the $CH_2$ approaches the $H_2$ forming a 3-centre bond. The transition state is reached at a C-H distance of 2.5 Å with an activation energy of $\lesssim$ 5 kcal $mol^{-1}$. (ii) The H-H distance rapidly increases while the $CH_2$ swings round to reach the final tetrahedral geometry.

($\alpha \rightarrow 0^o, \beta \rightarrow 110^o$ in fig. 1.6 (ii) ).

Hoffmann et al. [108] used the extended Huckel method to study the potential surface for the insertion of $^1CH_2$ into $CH_4$. Their model was similar to that of Kollmar [107].

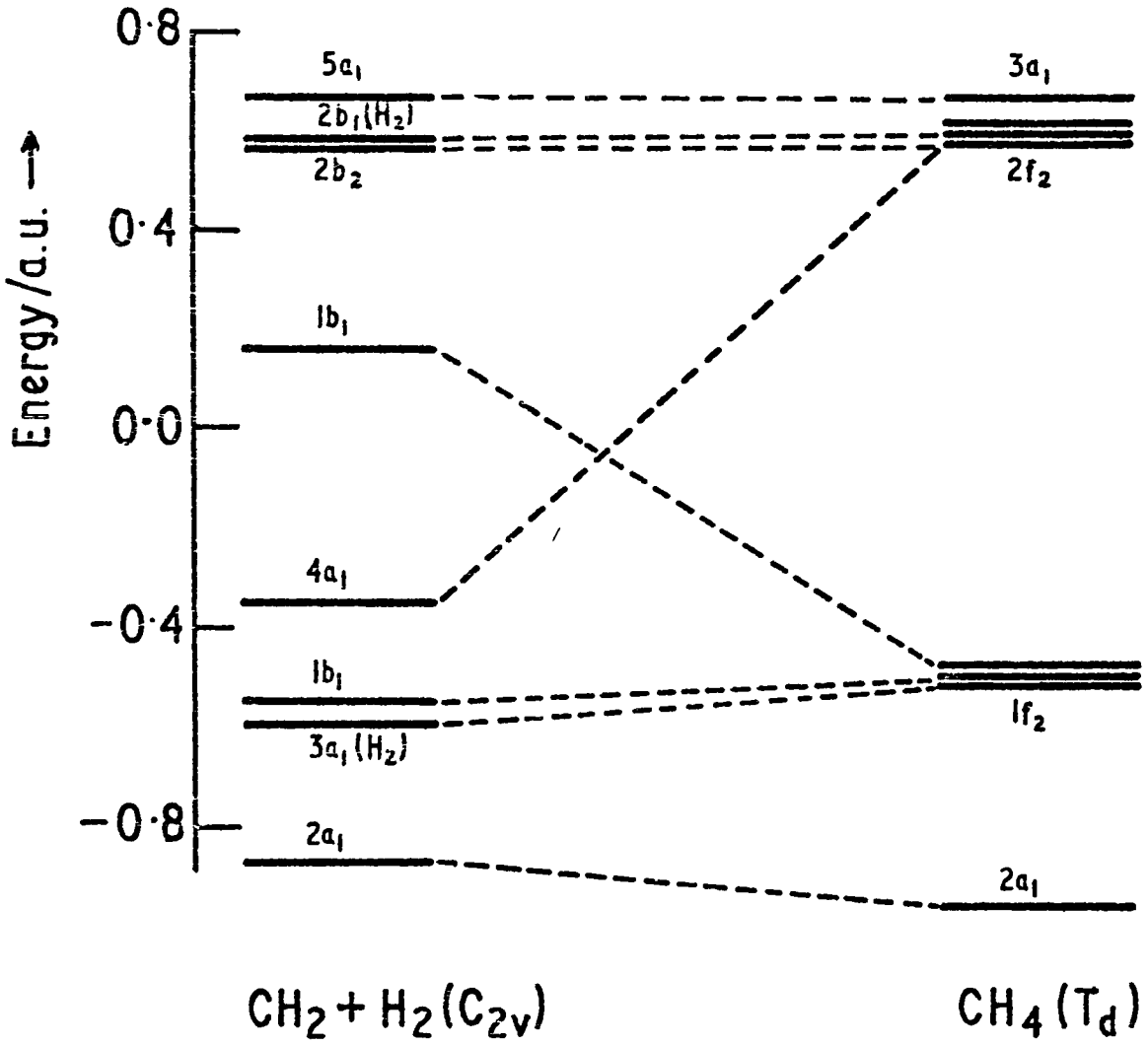



Fig. 1.7. Molecular orbital correlation diagram for $CH_4$ with $CH_2$ + $H_2$ ( $C_{2v}$ symmetry ) according to ref. 105.

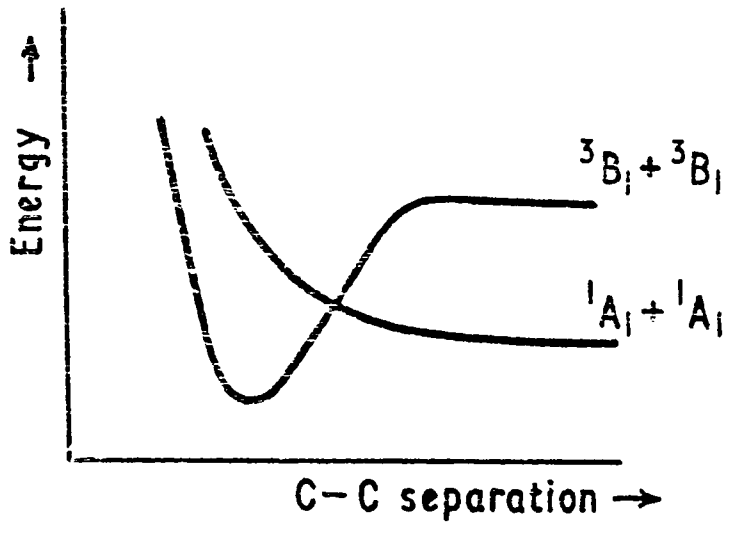
Reaction begins by an abstraction-like electrophilic attack of $CH_2$ with its empty p-orbital impinging on the H atom. In the intermediate stage of the reaction the H atom is transferred to the $CH_2$ while the C-C distance changes little. The reaction terminates in a collapse to the equilibrium ethane structure.

1.7.3. Dimerisation of $CH_2$. The dimerisation of difluoromethylene has been shown to be a slow process [109], whereas the dimerisation of methylene is known to be fast [41]. This difference has been interpreted on a qualitative basis by Simons [110]. The ground state of $CF_2$ is $^1A_1$ and the potential energy curve (fig. 1.8 (i) ) shows that the approach of two $CF_2$ ($^1A_1$) radicals is repulsive. A curve crossing must occur to form the ground electronic state of $C_2F_4$ and this presumably is a slow process. On the other hand, the ground state of $C_2H_4$ correlates with the ground state of $CH_2$ ($^3B_1$) (fig. 1.8 (ii) ) allowing a fast recombination process.

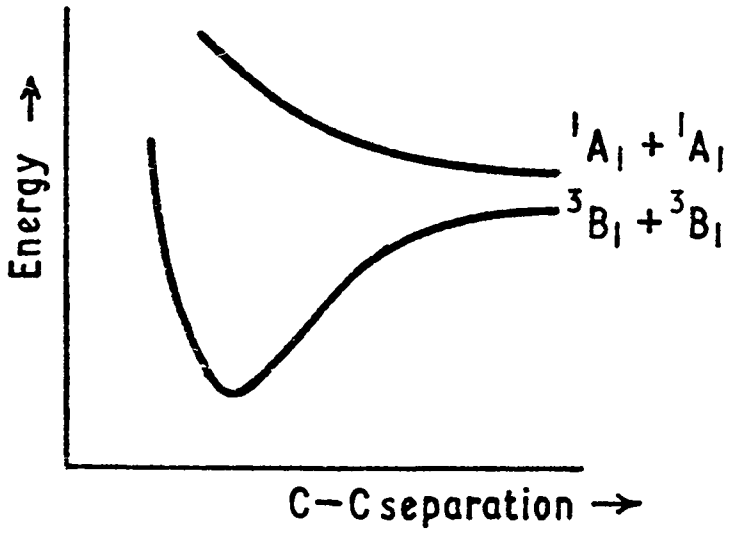
Hoffmann[111] has made a theoretical study of the dimerisation of $CH_2$ ($^1A_1$). $CH_2$ ($^1A_1$) may be considered to have a doubly occupied $\sigma$-orbital in the plane of the molecule, and an empty p-orbital at right angles to the plane. ( C atom $sp^2$ hybridised). In $D_{2h}$ symmetry the orbitals are either symmetric (S) or anti-symmetric (A) with respect to planes 1 and 2 (fig.1.8 (iii) ). The correlation of these orbitals with the orbitals of $C_2H_4$ is shown in fig.1.8 (iv). The correlation diagram exhibits a level crossing and on the basis of the Woodward-Hoffmann rules the least motion approach should be a high energy one. (It is worth noting

Fig. 1.8.

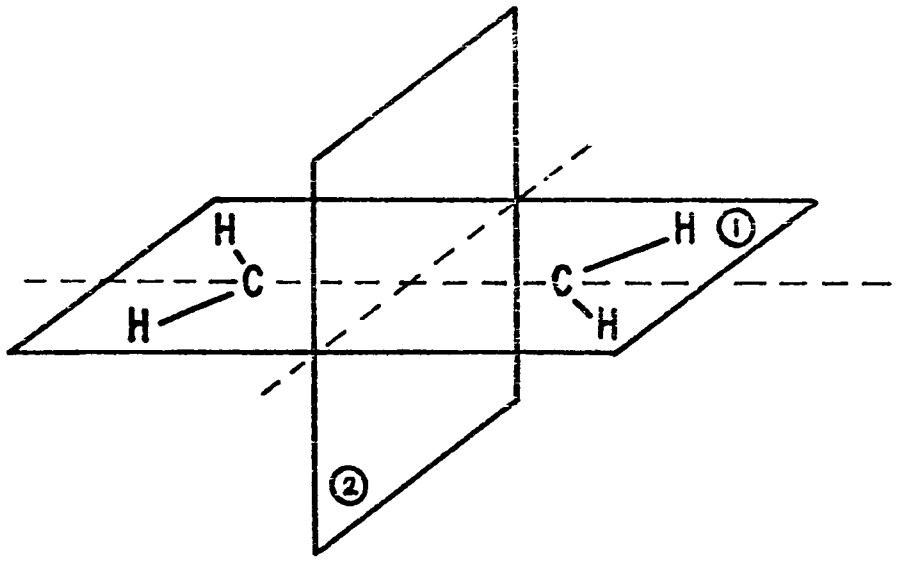
(i) Potential energy curves for the dimerisation of $CF_2$.



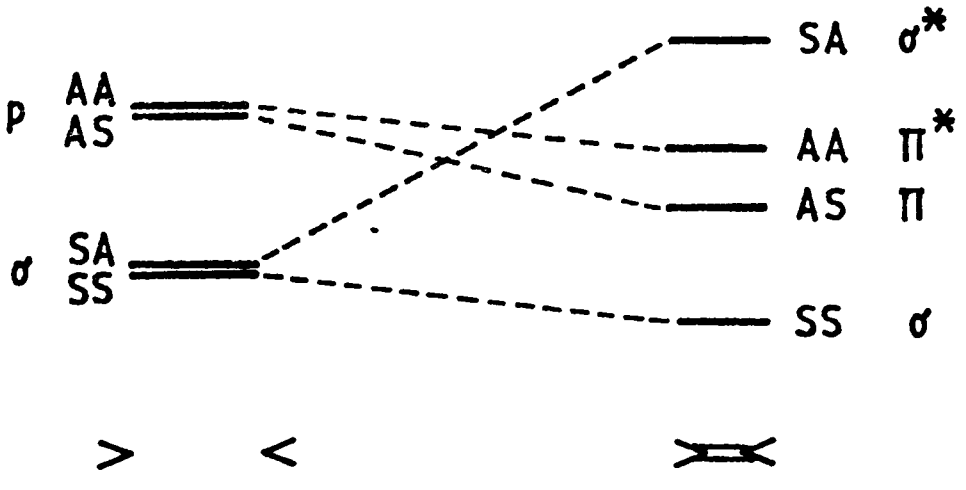

(ii) Potential energy curves for the dimerisation of $CH_2$.




(iii) Approach of two $CH_2$ radicals in $D_{2h}$ symmetry.




(iv) Correlation of $\sigma$, p orbitals in $CH_2$ with $C_2H_4$ ($D_{2h}$ symmetry).



that if the methylenes had the electron configuration $(\sigma)^1$ $(p)^1$ there would be no barrier to dimerisation in the Woodward-Hoffmann sense). On this basis $CH_2$ ($^1A_1$) + $CH_2$ ($^1A_1$) would be a slow process with a high activation energy. However, Hoffmann showed that if the approach geometry is relaxed so that the lone pair of one $CH_2$ may attack the empty p-orbital of the other, the activation energy may be reduced almost to zero. Activation energies for this free motion approach have been calculated and the results vary from almost zero to 8 kcal $mol^{-1}$ [112,113]. The activation energy for the approach in $D_{2h}$ symmetry has been estimated as 14.8 kcal $mol^{-1}$ [114].

1.7.4. Conclusions. Theoretical calculations have explained in a satisfactory way the difference in reactivities of $^1CH_2$ and $^3CH_2$ towards $H_2$. The facile dimerisation of $^3CH_2$ is also readily explained. Whether dimerisation of $^1CH_2$ occurs is less amenable to experiment since in any gas phase experiment $^1CH_2$ is a very short lived species.

## 1.8. Aims of this work.

The aim of the present work was to reinvestigate the flash photolysis of ketene in an attempt to resolve the discrepancy between the rate constants of $CH_2$ reactions measured by Koob [52,74] and those measured by Braun et al.[41].

The flash photolysis of ketene in the vacuum U.V. provides a clean source of $CH_2$ radicals. The advantages of a flash photolysis system over a steady state system relevant to the present study are: (i) in flash photolysis

high concentrations of radicals are produced favouring radical-radical reactions: (ii) In flash photolysis, problems due to secondary reaction of $CH_2$ with reaction products are minimised. (iii) Only small concentrations of ketene are required to produce sufficient $CH_2$ and consequently reactions of $CH_2$ with its precursor are minimised.

The simplest system for study is one in which only $H_2$ and inert gas are present. Two reaction pathways are then open to $^1CH_2$. It may either react with $H_2$ to give $CH_3$ + H which form "singlet products", $CH_4$ and $C_2H_6$, or it may be deactivated by the inert gas to give $^3CH_2$ which forms "triplet products", for example $C_2H_2$.

$$^1CH_2 + H_2 \xrightarrow{k_1} CH_3 + H \nearrow CH_4,\ C_2H_6$$

$$^1CH_2 + M \xrightarrow{k_2} {}^3CH_2 \nearrow C_2H_2$$

In a system with a fixed concentration of $H_2$, addition of inert gas would be expected to cause an increase in "triplet products" and a corresponding decrease in "singlet products". In the limit of high pressure the "singlet products" would be expected to disappear unless reactivation of $^3CH_2$ to $^1CH_2$ were to occur.

$$^1CH_2 + M \underset{k_{-2}}{\overset{k_2}{\rightleftharpoons}} {}^3CH_2 + M$$

Thus a measurement of singlet products at high pressures should lead to an estimate of E ($^1CH_2$ - $^3CH_2$).

CHAPTER 2

## APPARATUS AND EXPERIMENTAL TECHNIQUE

2.1 The apparatus consisted of a gas handling system, a flash photolysis lamp, and a gas-liquid chromatograph. Gas mixtures were made up in the vacuum line and then transferred to a photolysis vessel situated at the centre of the flash lamp. After photolysis a fraction of the reaction mixture was sampled on the chromatograph.

### 2.2 Gas handling system

The vacuum line was of conventional design. A vacuum approaching $10^{-6}$ Torr was achieved by means of a water-cooled mercury diffusion pump backed by a two stage rotary vacuum pump (Metrovac Type GDRI). Traps cooled by liquid nitrogen separated the mercury diffusion pump from the rotary pump and from the vacuum line. To ensure that the system was completely vacuum tight it was periodically pumped down to pressures of $10^{-5}$ - $10^{-6}$ Torr as measured on an ionisation gauge (Mullard 10G-12). However in the course of experiments it was considered sufficient to pump the system to less than $10^{-3}$ Torr. This pressure range was measured on a Pirani gauge (Birvac, Model T202).

A pressure transducer (Bell and Howell Ltd., Type 4 - 326 - 401) was used for measuring pressures from 0 - 800 Torr. This operated on a 10 Volt d.c. stabilised power supply (Weir Electronics Model W 30) and its output from 0.00 to 42.00 mV varied linearly with pressure. The output was recorded on a potentiometric chart recorder (Model RE 511.20 supplied by Goerz Electro). The transducer was calibrated against a mercury manometer and the constant of

proportionality relating pressure to output voltage was found to be invariant with the type of gas used. Linearity at low pressures was checked by expanding a gas from a high measured pressure to low pressure by means of a known volume ratio. No deviation from linearity was found down to pressures of 1 Torr. The absolute error in measuring 10 Torr was estimated as ± 2%. However the systematic error in any experiment due to error in the proportionality constant was often eliminated. For example, when a mixture of two gases was made up the ratio of gases in the mixture was independent of the proportionality constant.

Several 2-litre bulbs were available for gas storage. Where necessary these were painted black to prevent photolysis of gas mixtures by daylight. A 5-litre bulb was used for storing inert gases. A mixing vessel was used for rapid mixing of gases. This was a cylindrical glass vessel which contained a glass rotor pivoted on P.V.C. bearings at the top and bottom. A small steel bar encased in glass at the top of the rotor provided the means of rotation by a magnet rotated at high speed outside the vessel.

The section of the vacuum line connecting the mixing vessel to the photolysis vessel and also connecting the photolysis vessel to the chromatograph sampling valve was grease free. The taps used were 4 mm. quick opening in-line valves supplied by the Fischer and Porter Co. Several of the storage bulbs also had greaseless taps.

## 2.3 Chemicals

2.3.1 Ketene [116] was prepared by pyrolysis of acetic anhydride

(Analar reagent, B.D.H. Chemicals Ltd.) in a heated quartz tube. Samples of ketene of consistently high purity were obtained by controlling the temperature of the quartz tube electrically. This was done by winding Nichrome heating wire round asbestos paper surrounding the tube and binding the whole with asbestos tape. A thermocouple was placed near the quartz tube. The optimum temperature range for ketene production was 430 - 460°C. The products of the pyrolysis were passed through two traps cooled by dry ice/acetone slush baths (-78°C) to remove unpyrolysed acetic anhydride and then through a trap cooled by liquid nitrogen (-196°C) to trap the ketene. To remove small traces of $C_2H_4$ impurity the ketene was distilled to a trap at -78°C and the residual vapour pumped away.

An alternative method of ketene production from diketene [117] (Technical grade, supplied by Aldrich Chemical Co., Inc.) was attempted but this was found to produce a large fraction of allene ($\simeq$ 7%) which was difficult to remove.

The ketene was checked first by infra-red spectrocopy and then by mass spectrometry. Mass spectrometry showed samples to be better than 99.9% pure. Gas liquid chromatography showed that hydrocarbon impurities below $C_5$ were present only in quantities of 0.01%. Ketene was stored in a blackened bulb with a cold finger in liquid nitrogen. Checks on purity showed that it could be stored in this way almost indefinitely.

2.3.2 Azomethane was prepared [118] by oxidation of sym-dimethylhydrazine dichloride (supplied by Aldrich

Chemical Co., Inc.) using yellow mercuric oxide. Mass spectrometric analysis showed it to be better than 99.9% pure. It was stored in the same manner as ketene.

2.3.3 Hydrogen was supplied by B.O.C. Ltd. It was passed over a platinum catalyst to remove traces of oxygen and through a trap cooled by liquid nitrogen to remove water and condensable impurities. Experiments carried out using this source of hydrogen and using research grade hydrogen supplied by B.O.C. Ltd. in 1-litre glass bulbs gave identical results thus confirming the purity of the hydrogen.

2.3.4. Argon, helium, xenon, and sulphur hexafluoride were used as inert gases.

(i) Argon was supplied by B.O.C. Ltd. It was bubbled from the cylinder through dibutyl phthalate and samples were leaked off into the vacuum line. It was then passed through a quartz tube packed with copper shavings heated to 600°C to remove traces of oxygen and through a trap at -196°C to remove any water or condensable impurity. The copper shavings were regenerated by heating them to 250°C in an atmosphere of 150 Torr of hydrogen. Experiments were duplicated using research grade argon supplied in 1-litre glass bulbs by B.O.C. Ltd. These gave identical results and showed that the impurity level in the argon treated as above was at an acceptable level.

(ii) Helium, research grade, supplied by B.O.C. Ltd. was used without further treatment.

(iii) Xenon, research grade, supplied by B.O.C. Ltd. was used without further treatment.

(iv) Sulphur hexafluoride was supplied by B.D.H. Lab Gas Service. It was put through several freeze pump thaw cycles in a liquid nitrogen cooled trap to remove any air impurity.

2.3.5 Hydrocarbons were used mainly for calibration of the chromatograph and their purity was thus checked in the process. Methane (99%) was supplied by B.O.C. Special Gases. Ethylene (99.8%), ethane (99%), propane (99%), propylene (99%), cyclopropane (98%) and methyl acetylene (96%) were supplied by B.D.H. Lab Gas Service. Allene was supplied by K. & L. Laboratories, Inc. Industrial acetylene was used. It was distilled from a trap at -78°C to one at -196°C to remove any traces of acetone which might result from its storage.

2.3.6 Oxygen was supplied by B.O.C. Special Gases Ltd.

2.3.7 Carbon monoxide was supplied by B.O.C. Special Gases Ltd.

2.3.8 Nitric Oxide (99%) was supplied by B.D.H. Ltd. It was condensed down to a white solid at -196°C (showing the absence of nitrogen peroxides which are coloured) with a vapour pressure of $\lesssim$ 0.1 Torr. Several freeze pump thaw cycles were carried out at -196°C to ensure purity.

2.4 Gas-Liquid Chromatograph

2.4.1 The gas-liquid chromatograph (Model F 11) was supplied by Perkin Elmer Ltd. It consisted of a flame

ionisation detector (F.I.D.), an ionisation amplifier and a precision oven.

A F.I.D. comprises a hydrogen flame into which the output of the column flows. The detector output signal is produced by changes in the electrical conductivity of the flame. The conductivity of a pure hydrogen flame is negligible, but sample components entering the flame produce ions that will carry a current. A voltage is applied across the flame to collect the ions produced. A small current is thus generated, the magnitude proportional to the rate at which the sample enters the flame. This current is amplified on the ionisation amplifier and the resultant signal drives a recorder which displays the chromatogram.

F.I.D. cannot detect nitric oxide, carbon monoxide, carbon dioxide, water, hydrogen or inert gases. In these experiments it was used only to measure hydrocarbons. The area under a peak in the chromatogram was proportional to the number of moles of the corresponding sample component.

Nitrogen was chosen as the carrier gas. "White spot" nitrogen (supplied by B.O.C. Ltd.) at a pressure of typically 25 lbf $in^{-2}$ gave a flow rate through the column of 8 $cm^3$ $min^{-1}$. The flow rate depended on the length, diameter and packing of the column and on the oven temperature.

Supplies of 25 $cm^3$ $min^{-1}$ of hydrogen (B.O.C. Ltd.) and 300 $cm^3$ $min^{-1}$ of air were required for the detector. These rates of flow were achieved with pressures of 20 lbf $in^{-2}$ and 35 lbf $in^{-2}$ respectively. Compressed air was cleaned by passing it through a brass tube packed with molecular

sieve, type 4A (B.D.H. Chemicals Ltd.)

2.4.2. The gas sampling valve supplied by Perkin Elmer is designed for a flow system. It is shown schematically in fig 2.1. It was used here under vacuum conditions and, with the sampling tube in line, a vacuum of $10^{-4}$ Torr could be obtained. The rate of leak through the valve was too slow to cause any problem with the sampling technique used.

Reaction mixtures were sampled as follows. After the sample tube was pumped out to a pressure of $10^{-4}$ Torr (tap C closed and taps A and B open) tap A was closed and tap C opened thus allowing the reaction mixture into the evacuated sample tube. The gas sampling valve was then turned $60^{\circ}$ clockwise as shown in fig. 2.1 allowing the carrier gas to sweep the contents of the sample tube into the chromatograph. To check that leaks from the atmosphere into the gas sampling valve were of no importance the time between closing tap A and opening tap C was varied from a few seconds (which was the normal time) to a minute. This had no effect on the sample measured. The time between opening tap C and turning the sampling valve was also varied from a few seconds to a minute with no effect on the sample measured.

The collar with 'O' ring seals was necessary to allow for movement of the gas sampling valve when it was turned. The volume of the sample tube was 1.0 $cm^3$. The volume of the reaction vessel was generally 100 $cm^3$. If after sampling tap C was closed and the sampling procedure repeated a second time, the second sample was 85% of the first sample. Thus the relative amounts of products in a

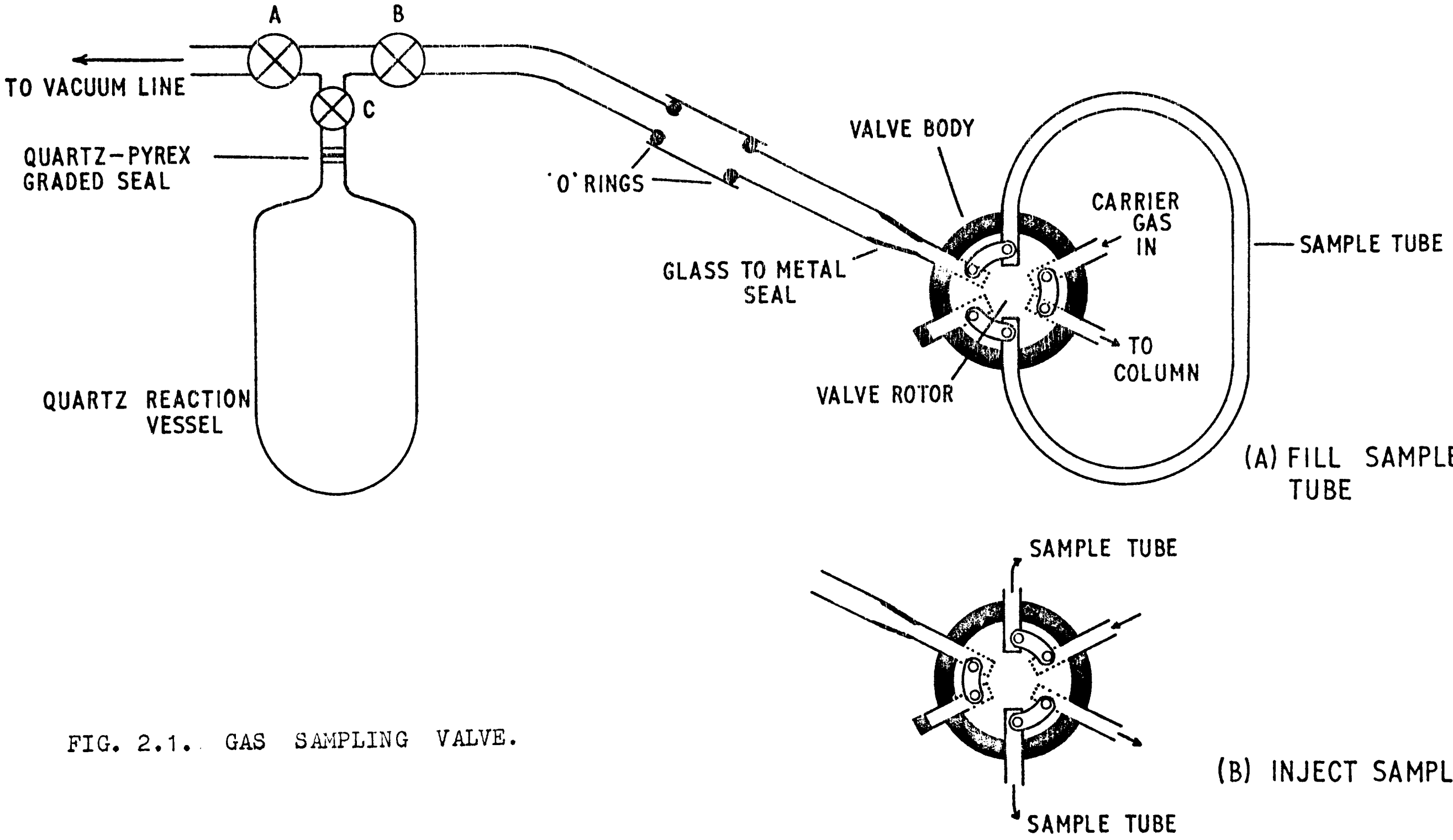



FIG. 2.1. GAS SAMPLING VALVE.

sample could be checked several times but the absolute amounts decreased by 85% on each sampling.

During the flash photolysis a small part of the reaction vessel was effectively dead volume. This was the tube leading from the reaction vessel to tap C. To check that this dead volume had no effect on the sampling, samples were taken at various times after the flash varying from a few seconds to twenty minutes. No effect on the magnitude of the sample taken was found. Presumably the turbulence which must occur when the contents of the reaction vessel are expanded into the sample tube ensures that the sample taken is representative of the contents of the reaction vessel.

2.4.3 The output signal from the chromatograph was plotted on a potentiometric pen recorder (Goerz Electric, Type RE511.20). Typical chromatograms are shown in fig 2.2. The x axis, corresponding to time, could be expanded by increasing the speed of the chart recorder. There are three methods of measuring the peak areas [119]:

(a) the peaks are cut out and weighed; if the paper has constant mass per unit area, the weight of the peak gives the area.

(b) the area is measured with a planimeter.

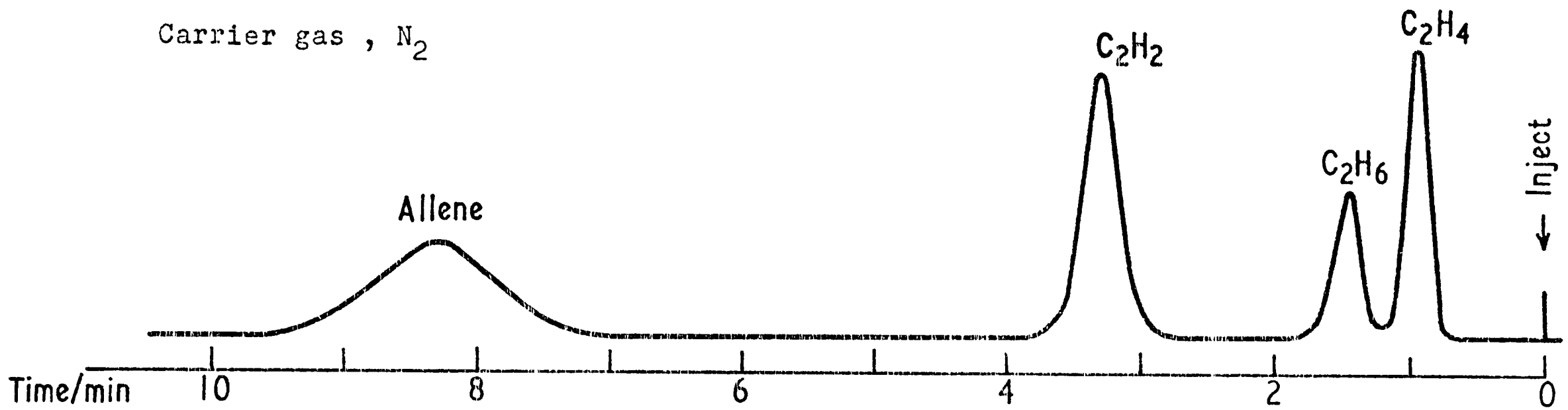
(c) the peak height and the width at half height are measured; the product of these gives an approximate measure of the peak area.

All three methods were tried and it was found that method (c) gave satisfactory results. This was convenient since method (c) involved much less labour than methods (a) or (b). The

(i) Porapak N column

Oven temperature 50 C

Carrier gas , $N_2$




(ii) Durapak column (Phenyl isocyanate / porasil C)

Room temperature

Carrier gas , $N_2$

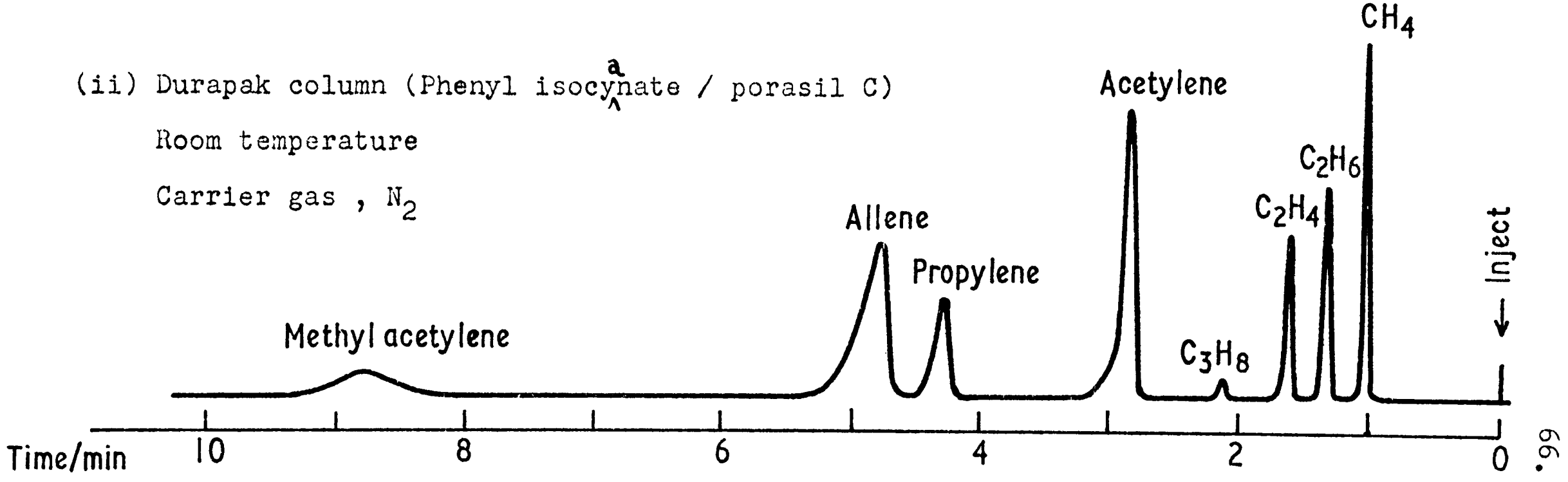
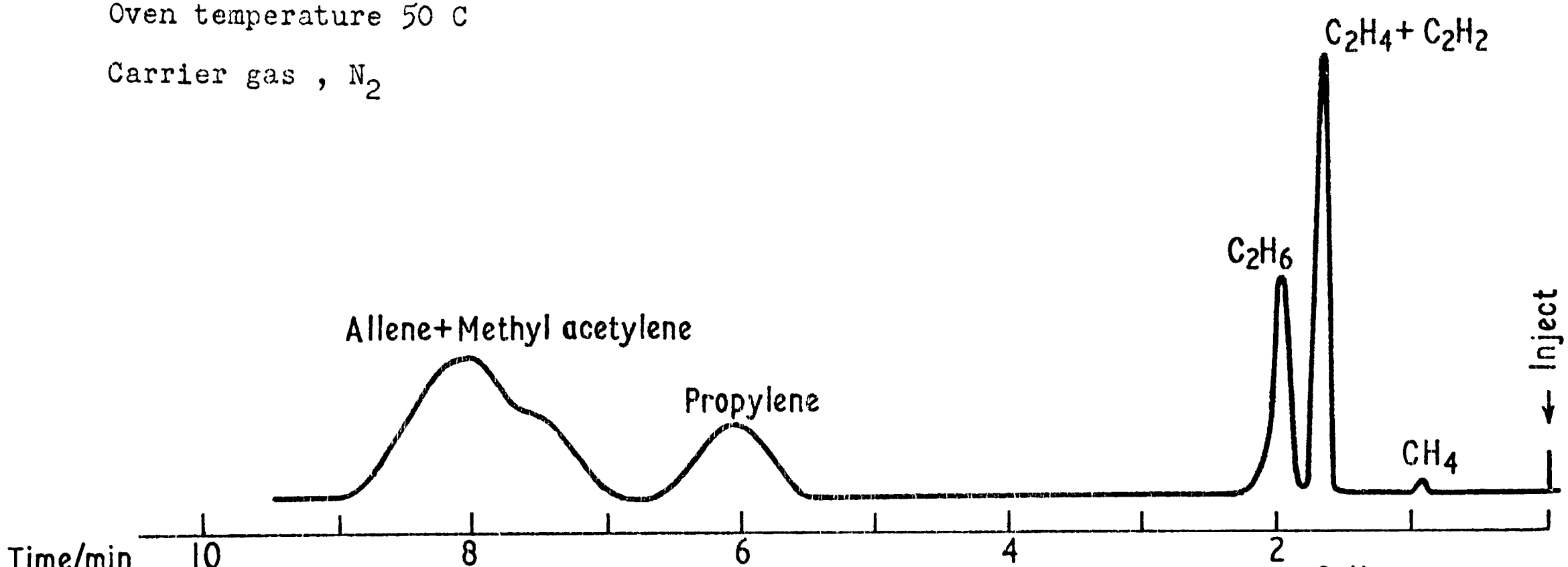



FIG. 2.2.

(iii) Porapak Q column

Oven temperature 50 C

Carrier gas , $N_2$




(iv) 3% squalane on alumina H

Room temperature

Carrier gas , $N_2$

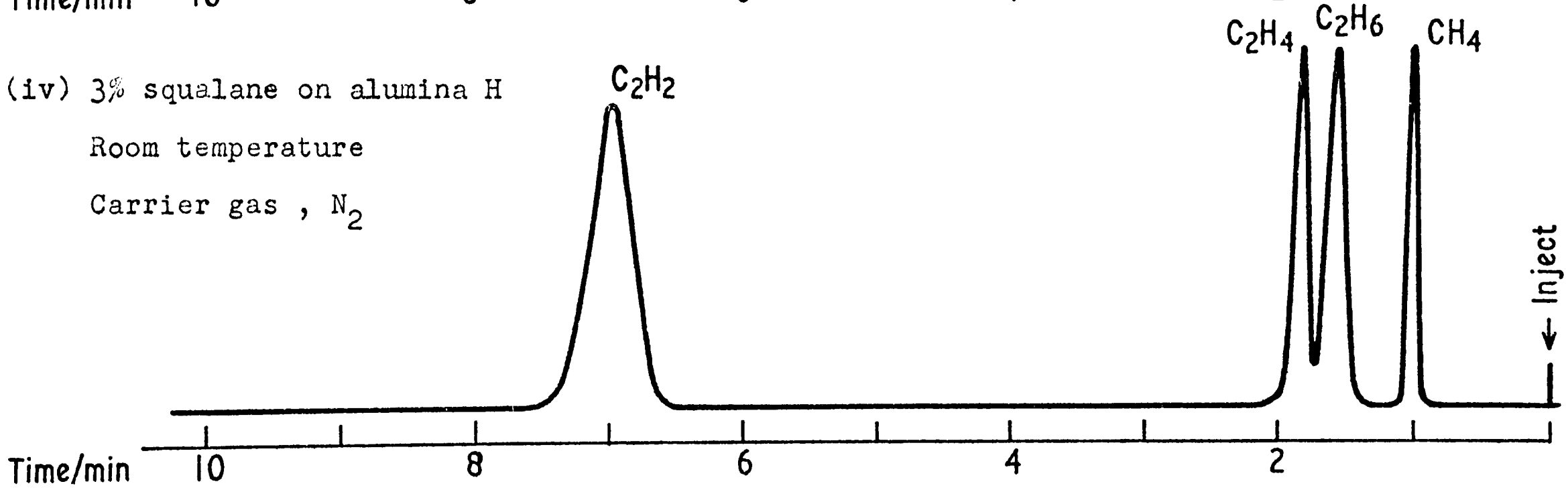



FIG. 2.2

chart paper was run at a speed of 120 mm $min^{-1}$. This typically gave peak half widths of 12 mm for $CH_4$ (which eluted first from all the columns used) and 25 mm for $C_2$ hydrocarbons. These could be measured with sufficient accuracy by eye using Vernier calipers. The reason why method (c) turned out to be satisfactory was that the peaks were fairly symmetrical about the vertical. Ideally the peaks should be Gaussian [119] in which case the areas approximated by (height X width at half height) would be 78% of the true area.

The chromatograph was calibrated by sampling mixtures of the hydrocarbons diluted in inert gas. For each calibration several mixtures were made up and samples were taken from each. Calibration was carried out over the whole range of concentrations in which the products of photolyses were present. Plots of peak areas versus concentration were linear. For $CH_4$ a peak area of 290 $mm^2$ corresponded to 1 mTorr on the most sensitive scale of the chromatograph which was used. For all the $C_2$ hydrocarbons a peak area of 580 $mm^2$ corresponded to 1 mTorr. The estimated error in measurement of 10 mTorr of any product was $\pm$ 3%. The error increased as the concentration of product decreased and it was only possible to estimate concentration of 0.1 mTorr with an error of $\pm$ 50%.

These errors in product measurement assume that there was no product present as impurity before photolysis. During experiments "blank" samples of reaction mixtures which had not been photolysed were taken at regular intervals. Such samples invariably gave a peak corresponding to methane.

The concentration of methane was worked out and was subtracted from all methane readings. The pressure of this small amount ( $<$ 1.0 mTorr) of methane could not be explained and necessarily impaired the accuracy with which methane could be measured especially for low concentrations. In general, hydrocarbons were measured in the range 0 - 30 mTorr.

The presence of a large excess of inert gas in the sample had two effects. The first was to broaden the hydrocarbon peaks; thus a peak due to 10 mTorr of $CH_4$ in 10 Torr argon might have a width at half height of 12 mm whereas in 800 Torr argon the width at half height might be 15 mm. It appeared that the peak height decreased correspondingly and no error seemed to be introduced. Secondly, though the F.I.D. was insensitive to inert gases, in the most sensitive ranges of operation a large excess of inert gas interfered with the conditions of the flame sufficiently to perturb the baseline of the chromatogram. For example, a large excess of argon gave a dip in the baseline just before the appearance of methane from a 2 m column of Porapak N with nitrogen as carrier. All that could be done to counter this effect was to adjust the carrier gas flow rate and/or the temperature of the column in order to ensure that the perturbation occurred a distance away from any of the peaks being measured.

2.4.4 The chromatograph columns were stainless steel with an outer diameter of 1/8 inch and a length of 2-4 metres. They were carefully packed by slowly pouring the packing material into one end of the tube held vertically. A

vacuum pump connected to the other end ensured that the packing material filled the tube homogeneously with no air gaps. The ends of the columns were closed with sintered metal discs. The columns were bent into spirals of approximately 3 inches in diameter and connected in the chromatograph oven with the appropriate Swagelock fittings.

Ketene eluted only slowly from the columns and sometimes this gave rise to a poor baseline on the chromatograms. To prevent this a short column (approx. 40 cm. long) of anhydrous magnesium perchlorate was placed in front of the separating column. This absorbed the ketene and had no effect on the other components of the mixture. It was replaced at intervals of a few weeks.

Various column packing materials were used. Typical chromatograms showing the separation of the hydrocarbon components in various tests are shown in fig 2.2. The Porapak and Durapak column materials were supplied by Waters Associates Inc. Porapak Q was not a useful column in the present study. It does not separate acetylene from ethylene or allene from methyl acetylene. Porapak N is less polar than Porapak Q. It provides good separation of methane, ethylene, ethane and acetylene. The $C_3$ hydrocarbons were also separated but under operating conditions which gave a separation of ethane and ethylene the $C_3$ hydrocarbons came off the column so slowly that the peaks were flat and difficult to measure quantitatively. The Durapak column gave a quick separation of the $C_2$ and $C_3$ hydrocarbons. However it proved difficult to obtain an adequate separation of ethylene from ethane.

A column of 3% squalane on alumina H was supplied by

Perkin Elmer Ltd. It gave a good separation of the $C_2$ hydrocarbons. However, under conditions which give a separation of ethylene and ethane, acetylene took 7 mins. to come off the column and $C_3$ hydrocarbons took correspondingly longer.

Most of the experiments were carried out using a 2 m column of Porapak N at a temperature of 50°C with nitrogen carrier gas flowing at 8 $cm^3$ $min^{-1}$.

## 2.5 Flash Photolysis Lamp.

2.5.1 The flash lamp was constructed from a hollow cylinder of perspex 18.5 long with an outer diameter of 20 cm and an inner diameter of 10 cm. A cross section is shown in fig. 2.3 and a photograph of the lamp in situ in fig 2.4. The cylindrical reaction vessel was situated at the centre of the lamp and was surrounded by four pairs of copper electrodes. Each electrode was secured to the body of the lamp by three screws and an 'O' ring ensured a vacuum tight seal. The electrode tips were of molybdenum, silver-soldered on to the copper. The ends of the perspex cylinder were closed by circular copper plates held in position by screws and with 'O' ring seals. A glass tube connected the lamp to the vacuum line which facilitated its filling with inert gas. A 6 mm pyrex glass tube connected to the reaction vessel via a quartz-pyrex graded seal led to a greaseless tap situated just outside the lamp (tap C in fig 2.2).

After evacuation to $10^{-3}$ Torr, the lamp was filled with 260 Torr of oxygen-free nitrogen. At this pressure the lamp fired spontaneously at 18kV and could be triggered at

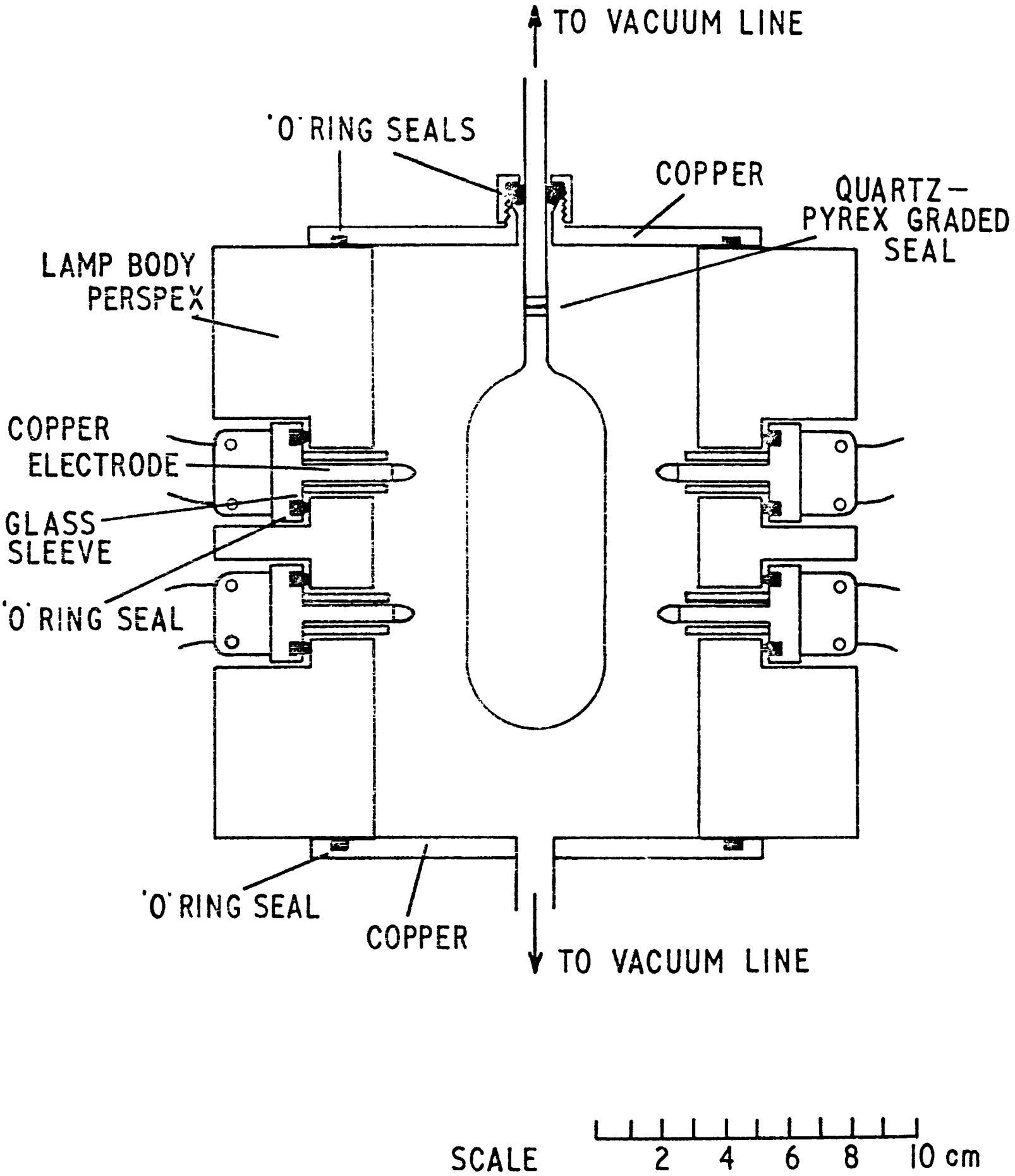
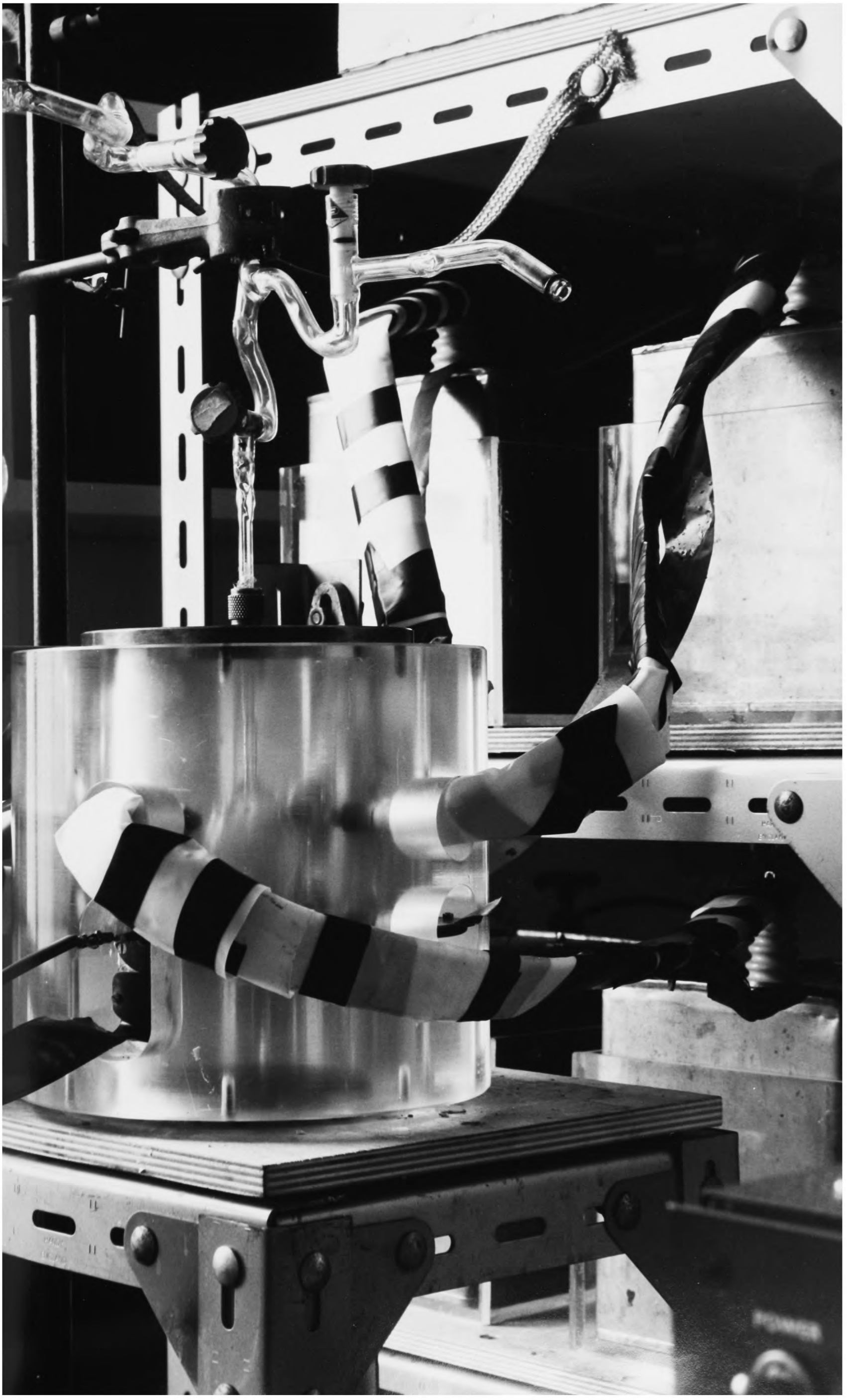



Fig. 2.3. Cross section of flash lamp.



or above 14 kV. A lower pressure of nitrogen enabled the lamp to be flashed at lower energies.

2.5.2 Four 2 μFarad rapid-discharge condensers (Hartley Measurements Ltd., model 25W068) supplied the energy for the flash. In order that each pair of electrodes discharged simultaneously a Marx-Bank circuit was used [120, 121] This is shown on fig 2.5 (i). The values of the resistors were $R_1$ = 500 kΩ and $R_2$ = 25 kΩ . A high voltage power supply unit (Hivotronic Ltd P.S.U. Type 25 - 10 - 1) was used to charge the condensers. Each electrode pair is shown encased by a dashed box. In this scheme each electrode in a pair was connected to a different condenser. Suppose the condensers are charged to a voltage of $V_o$. When a trigger pulse is applied to gap $G_1$ causing it to breakdown, a voltage equal to 2 Vo instantaneously appears across gap $G_2$. This gap immediately breaks down due to overvolting. This cycle is repeated round the circuit. Thus gap $G_4$ instantaneously receives a voltage equal to 4 $V_o$. While this circuit ensures that all the gaps break down simultaneously it is clear that the leads must be insulated to withstand a voltage four times greater than that to which the condensers are charged.

A trigger pulse of 35 kV was produced by a pulse transformer (Hartley Measurements Ltd., Model 355-50). The circuit is shown in fig 2.5 (ii). When the trigger button was depressed, the 1 μF capacitor discharged through the primary coil of the pulse transformer thus producing a 35 kV pulse in the secondary coil. The trigger pulse was fed to a pin which lay along the centre of one of the earth electrodes but which was insulated from it by a glass sleeve . The

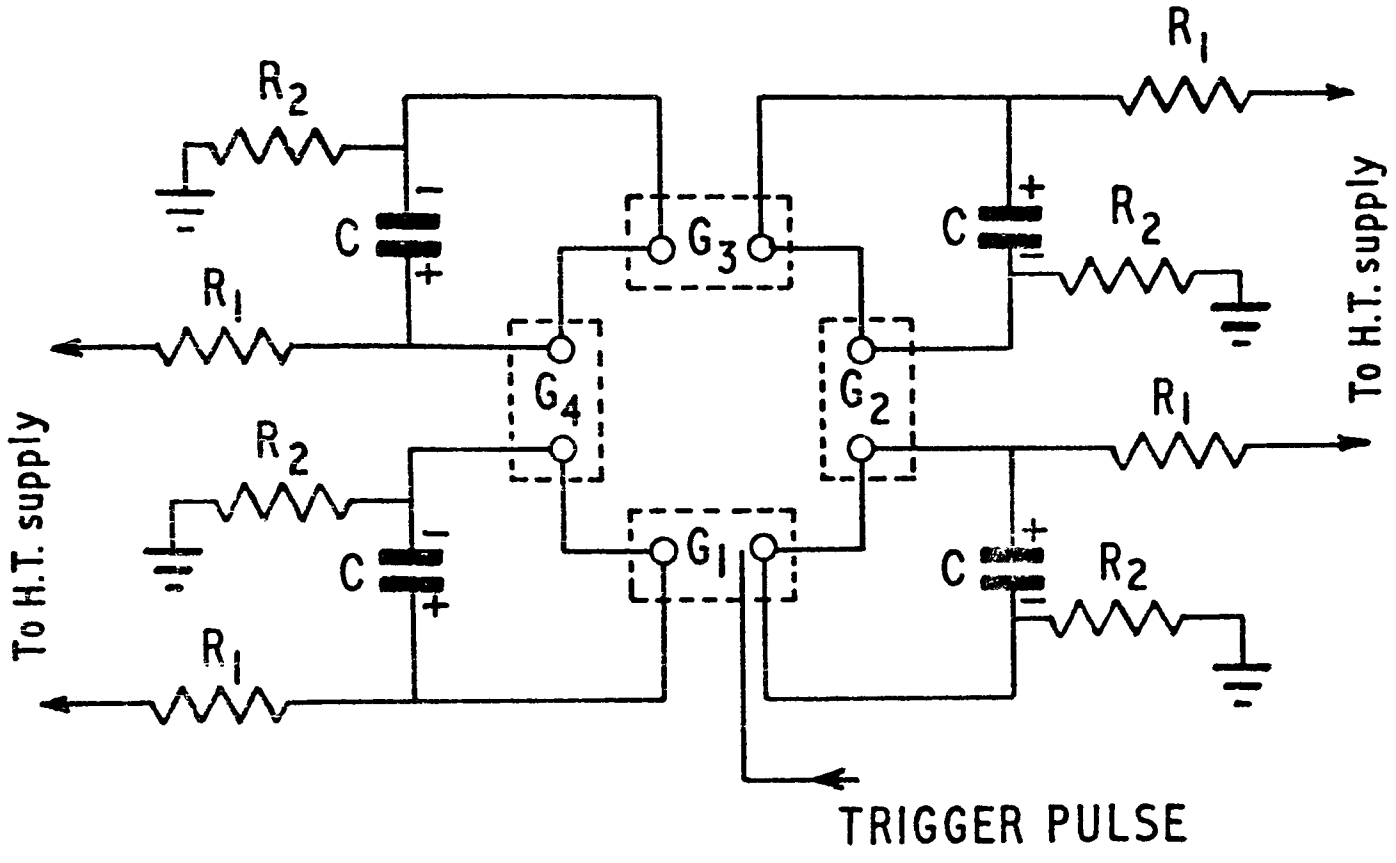



FIG. 2.5 (i) Marx-Bank circuit for flash lamp.

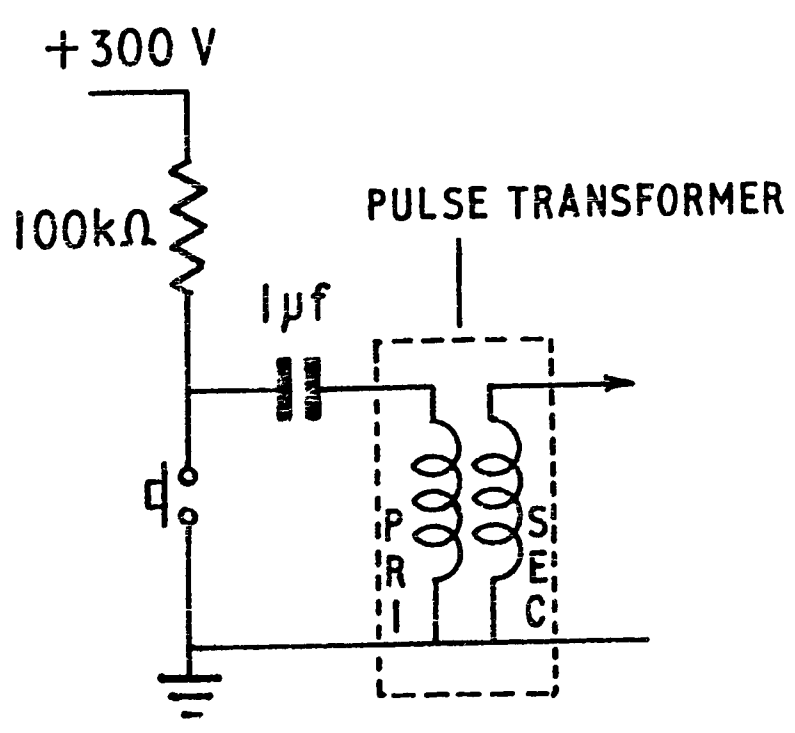



FIG. 2·5 (ii) Circuit to produce trigger pulse.

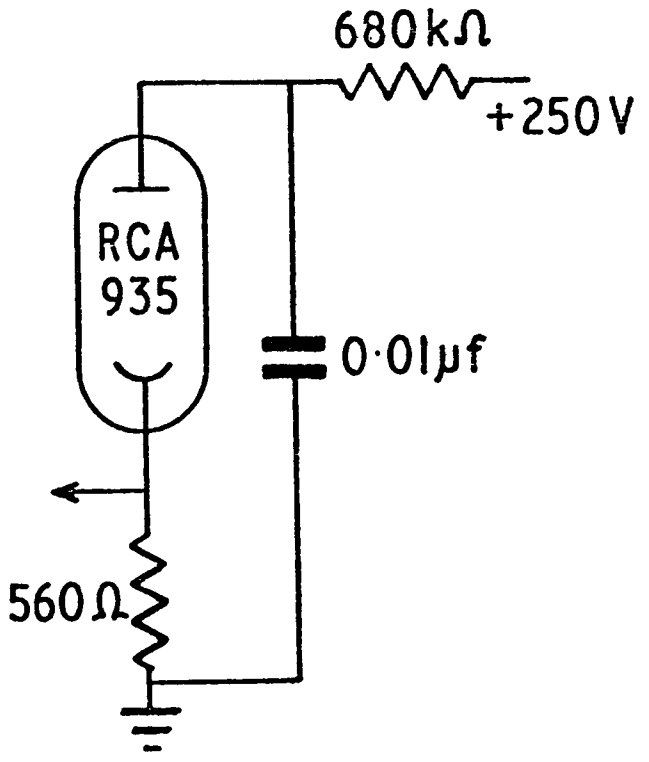



FIG. 2.5 (iii) Photodiode circuit.

trigger pin was sealed into the electrode using Araldite.

2.5.3 Each condenser stores an energy of $\frac{1}{2}CVo^2$ Joules where C is the capacitance and Vo the voltage to which the condensers are charged. Thus for Vo = 16 kV the total energy dissipated during the flash is 1024 Joules. The flash duration is determined, firstly, by the oscillatory behaviour of the electrical circuit and, secondly, by any 'afterglow' arising from long-lived excited states in the gas.

From a single electrode the oscillatory circuit is shown in fig 2.6. Little error is introduced by considering the lamp to be an Ohmic resistance [122], as it becomes reasonably Ohmic at high current density. The resistance of other parts of the circuit is normally small compared with that of the lamp. The inductance is distributed among several parts of the circuit - leads, condenser, and lamp. The condenser, charged initially to a voltage of Vo, is suddenly connected through the switch to the rest of the circuit. The current, I, which flows is governed by the equation

$$L\frac{dI}{dt} + IR + \frac{1}{C}\int_o^t I\,dt = 0$$

The solution is

$$I = \frac{V_o}{L}\exp\left(-\frac{Rt}{2L}\right)\frac{1}{\omega}\sin\omega t$$

where $$\omega = \sqrt{\frac{1}{LC} - \frac{R^2}{4L^2}}$$

The circuit is critically damped if $R = 2\sqrt{L/C}$ and is oscillatory if R is less than this. A coefficient k may be defined by $R = 2k\sqrt{L/C}$. The condition for critical damping is then k = 1.

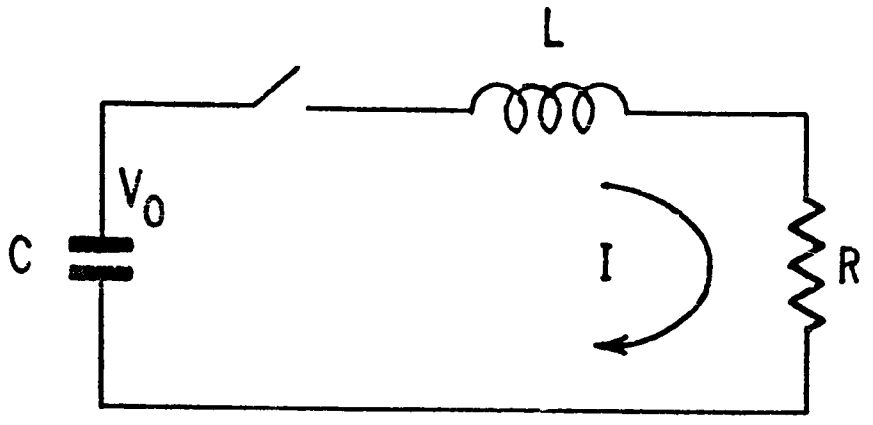



Fig. 2.6. (i) Equivalent circuit for discharge of a single electrode.

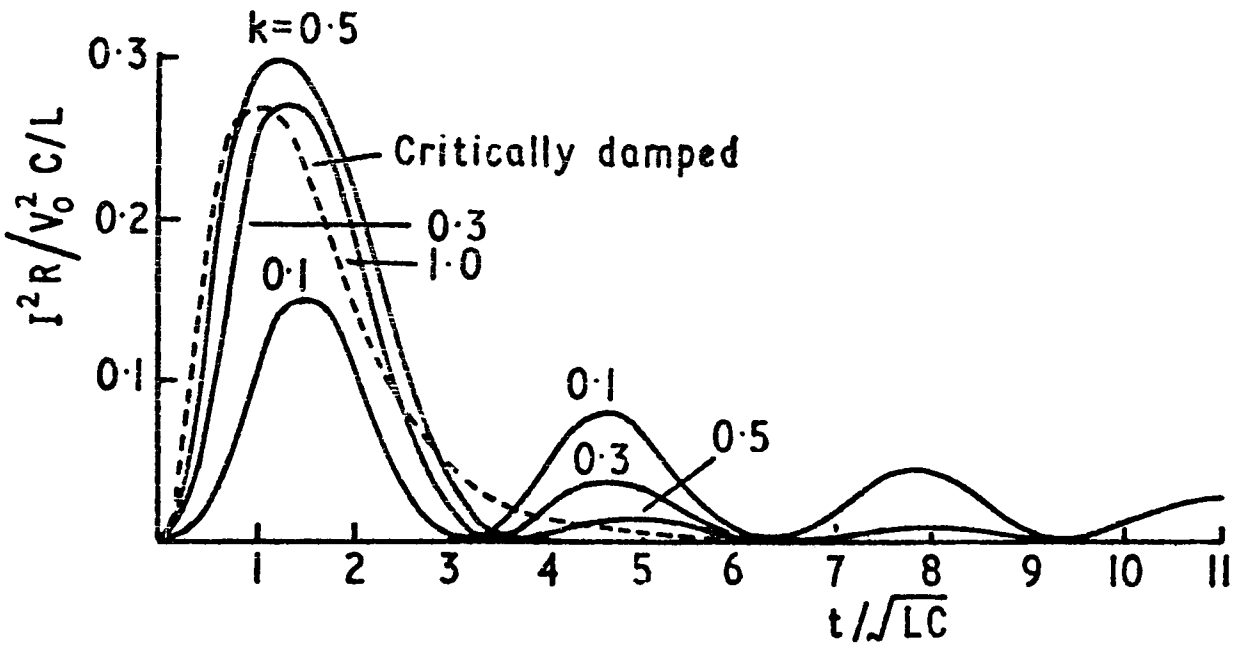



Fig. 2.6. (ii) Power dissipated in lamp as a function of time.

The power dissipated in the lamp at any moment is $I^2R$ and the fluctuation of this quantity which is closely related to the excitation energy fed into the gas is shown in fig 2.6 (ii) for various k. It can be seen that too low a lamp resistance leads to a succession of power dissipation cycles and hence to a lengthening of the light emission. The critically damped mode of operation appears to be the best for rapid power dissipation.

Damping is defined by the exponential term, $\exp(-Rt/2L)$. A conventional measure of the duration of the electrical discharge is $t_e = 2L/R$. Thus the pulse duration may be shortened by increase in R or decrease in L. One of the contributions to L is the inductance of the leads, $L_1$, connecting the condensers to the electrodes. For these leads $C_1L_1 = 1/c^2$, where c is the speed of light in vacuo. Thus to reduce $L_1$, $C_1$ must be increased. Strips of copper one inch wide and 0.004 inch thick were used for leads. The high voltage leads were insulated by PTFE film 0.010 inch thick (supplied by Crane Packing Ltd.) bound round the copper with insulating tape. To maximise $C_e$ the earth leads were bound to the high voltage leads for as long a distance as the geometry of the lamp would allow. $C_e$ was also maximised by keeping the insulation (which acts as a dielectric) to a minimum.

The light output from the lamp was monitored by a RCA 935 photodiode, Fig 2.5 (iii), the signal being displayed on an oscilloscope. During experiments flash profiles were photographed. Occasionally pulses of an abnormal shape were observed. Products from such photolyses were not recorded.

Output from a typical flash at 16 kV is shown in fig 2.7 (i). It was recorded for this purpose by a transient recorder (Datalab DL 905). The signal was recorded in 256 channels each channel corresponding to a time interval of 0.2 $\mu$sec. The main flash is over in 4 $\mu$sec but there is some oscillatory ringing and a tail which extends to 25 $\mu$sec. In order to cut down the ringing a resistance of 0.6 $\Omega$ (Nichrome wire) was included in one of the leads. This reduced the ringing considerably, the ratio of the second peak to the main peak decreasing from 0.16 (with no extra resistance) to 0.08 (with the resistance) and the third and subsequent peaks becoming negligible. However the light output from the lamp was reduced so dramatically due to power dissipated in the resistance that experiments were impossible.

In a discussion of the results it was necessary to simulate the pulse shape on the computer. The most suitable function is

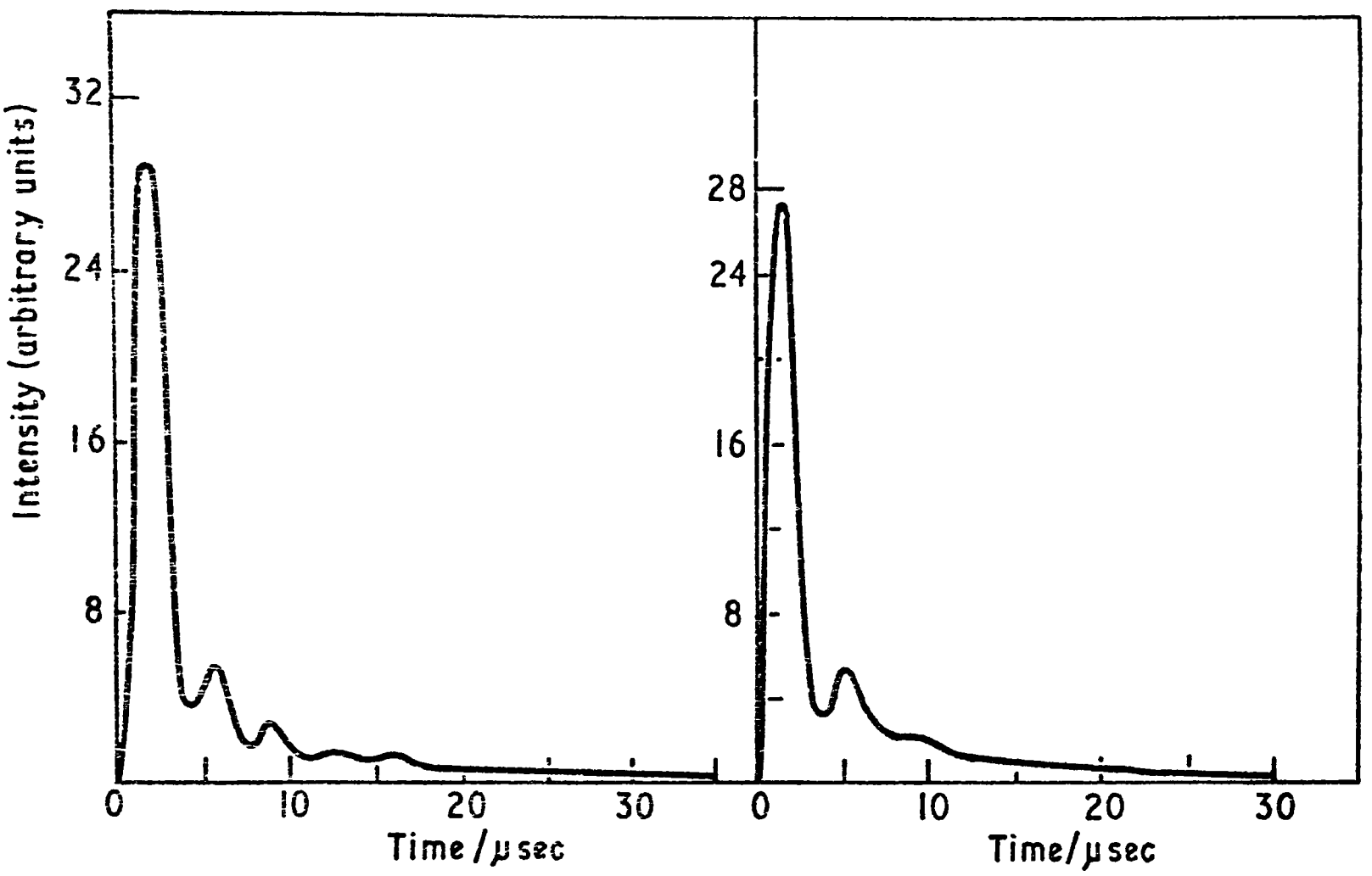
$$G(t) = 0.5\left(\frac{T_1^2 + 4T_2^2}{2T_2^3}\right)\sin^2\left(\frac{t}{T_1}\right)\exp\left(-\frac{t}{T_2}\right) + 0.5\left(\frac{1}{T_3}\right)\exp\left(-\frac{t}{T_3}\right)$$

G(t) has been normalised to unity.

$$\int_0^\infty G(t)\,dt = 1$$

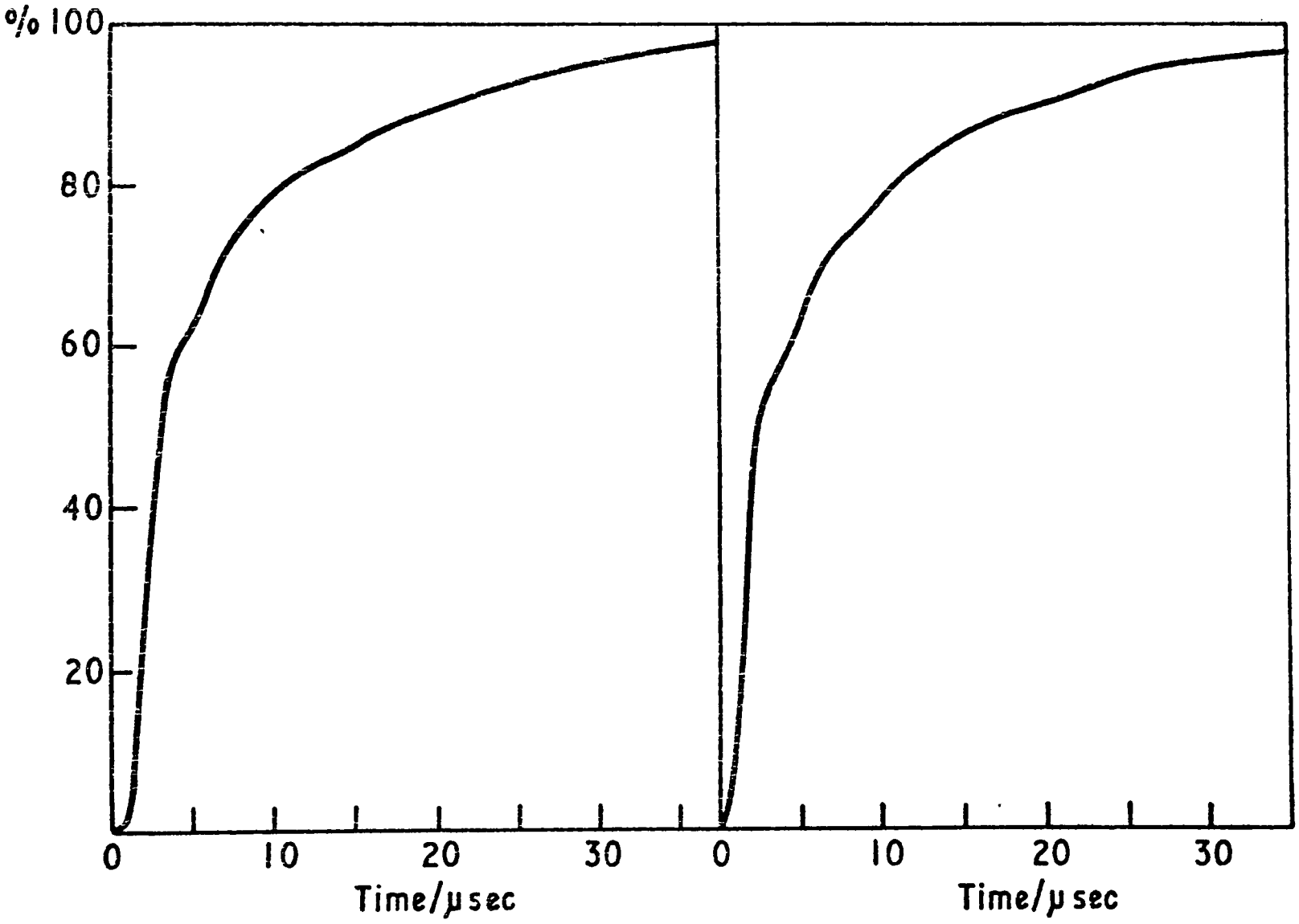
The first part of G(t) represents an oscillatory wave enveloped by an exponentially decreasing curve. Since the real pulse shape did not go to zero in the troughs it was necessary to add a more slowly decaying exponential tail in the form of the second part G(t). Fig 2.7 (ii) shows a plot of G(t) for $T_1 = 1.2$, $T_2 = 1.8$, and $T_3 = 12.0$ $\mu$sec. for comparison with fig 2.7 (i). Fig 2.7 (iii) shows the integrated flash profile (normalised to 100) and for comparison fig 2.7 (iv) shows the function $H(t) = \int_0^t G(t)\,dt$.

Nitrogen was used as the lamp gas. An attempt was made




(i) Flash profile

(ii) Simulated flash profile




(iii) Integrated flash profile.

(iv) Integral of simulated flash profile.

Fig. 2.7.

to use argon and krypton but both these allowed breakdown at very much lower voltages than nitrogen. The flash tail in nitrogen was reduced by addition of oxygen. However, since oxygen absorbs in the vacuum ultraviolet region of the spectrum which was the absorption region used in these experiments, this was not considered advisable.

## 2.6 Reaction vessels.

Reaction vessels were Spectrosil tubes supplied by Thermal Syndicate Ltd. Transmission was stated as 92% for light of wavelength above 200 nm and fell to 50% for $\lambda$ = 157 nm.

CHAPTER 3.

# RESULTS: A MODEL FOR THE VACUUM U.V. PHOTOLYSIS OF KETENE.

## 3.1 Photolysis of $CH_2CO/H_2/$ Inert Gas mixtures.

Mixtures of 200 mTorr of $CH_2CO$ in fixed pressures of $H_2$ were flash photolysed in varying pressures of added inert gas. Figures 3.1, 3.3, 3.4 and 3.5 show the hydrocarbon products of typical experiments with 5-10 Torr $H_2$, and with argon, sulphur hexafluoride, xenon, and helium as inert gases. The major hydrocarbon products were $CH_4$, $C_2H_4$, $C_2H_6$ and $C_2H_2$. The total product yield, calculated as the sum of C atoms produced, fell slightly with increasing inert gas pressure up to 100 Torr, but then remained level as the pressure was increased up to 1000 Torr. Fig. 3.2 shows the total product yield as a function of pressure for the results in fig. 3.1. In a typical experiment the total product yield showed a scatter of up to $\pm$15% due to the variability of the photolysis flash. Such a large uncertainty made it difficult to draw conclusions from plots such as fig. 3.2. Small traces of $C_3$ hydrocarbons were identified as allene, methyl acetylene, and propylene. The total of these $C_3$ products was less than 10% of the total product yield.

The most striking feature in figs. 3.1, 3.3, 3.4 and 3.5 is the initial sharp fall in the $C_2H_6$ yield with increase in inert gas pressure. The changes in the other products are much less marked.

On the basis of the work of Braun et al.[41] the following kinetic scheme would be expected to describe these systems:

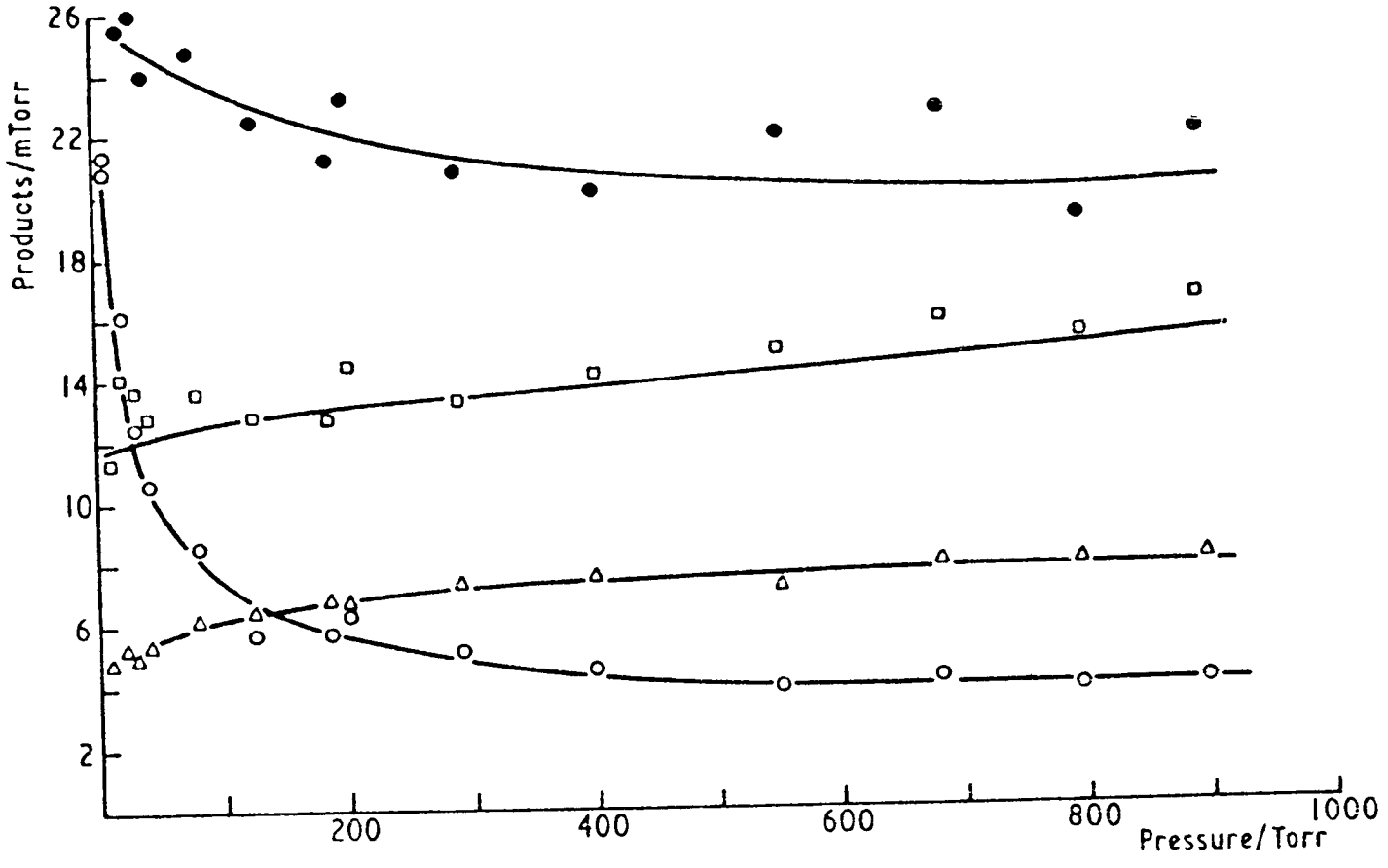



Fig. 3.1. Products from the flash photolysis of 200 mTorr $CH_2CO$, 10 Torr $H_2$, with added argon.

● $CH_4$; ○ $C_2H_6$; □ $C_2H_2$; Δ $C_2H_4$

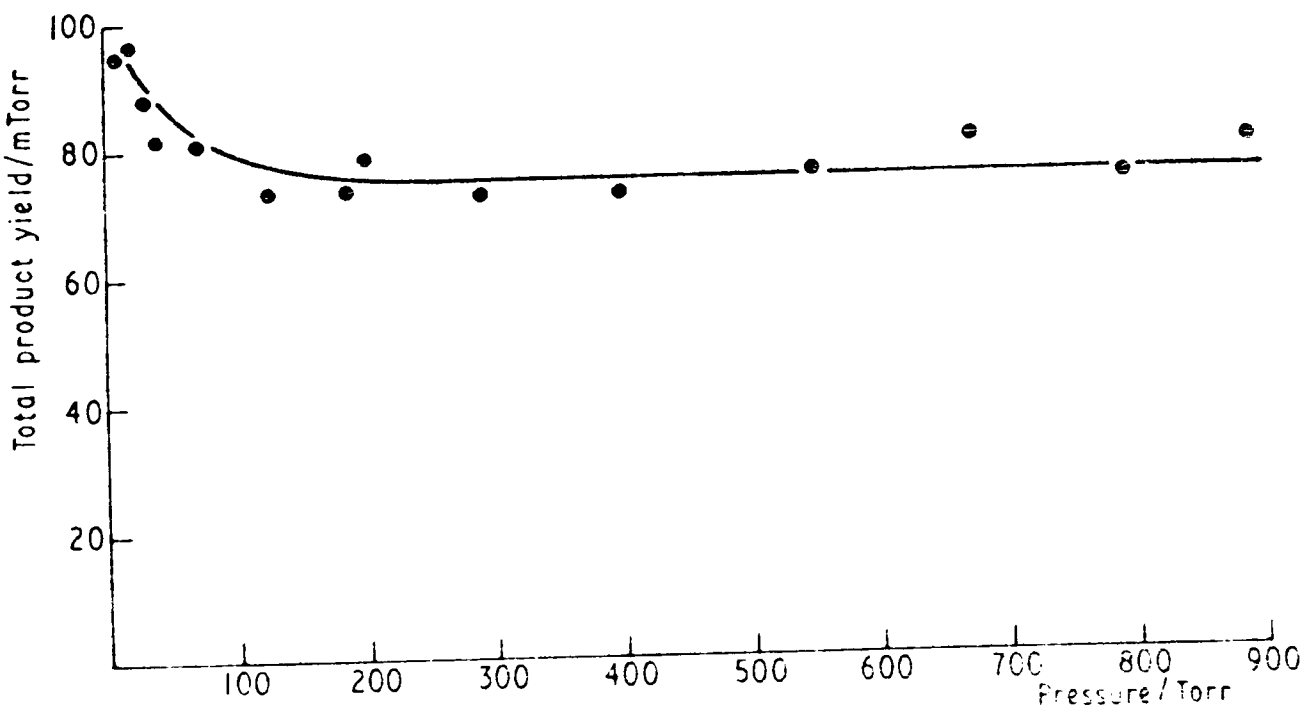



Fig. 3.2. Plot of total product yield versus pressure for fig. 3.1.

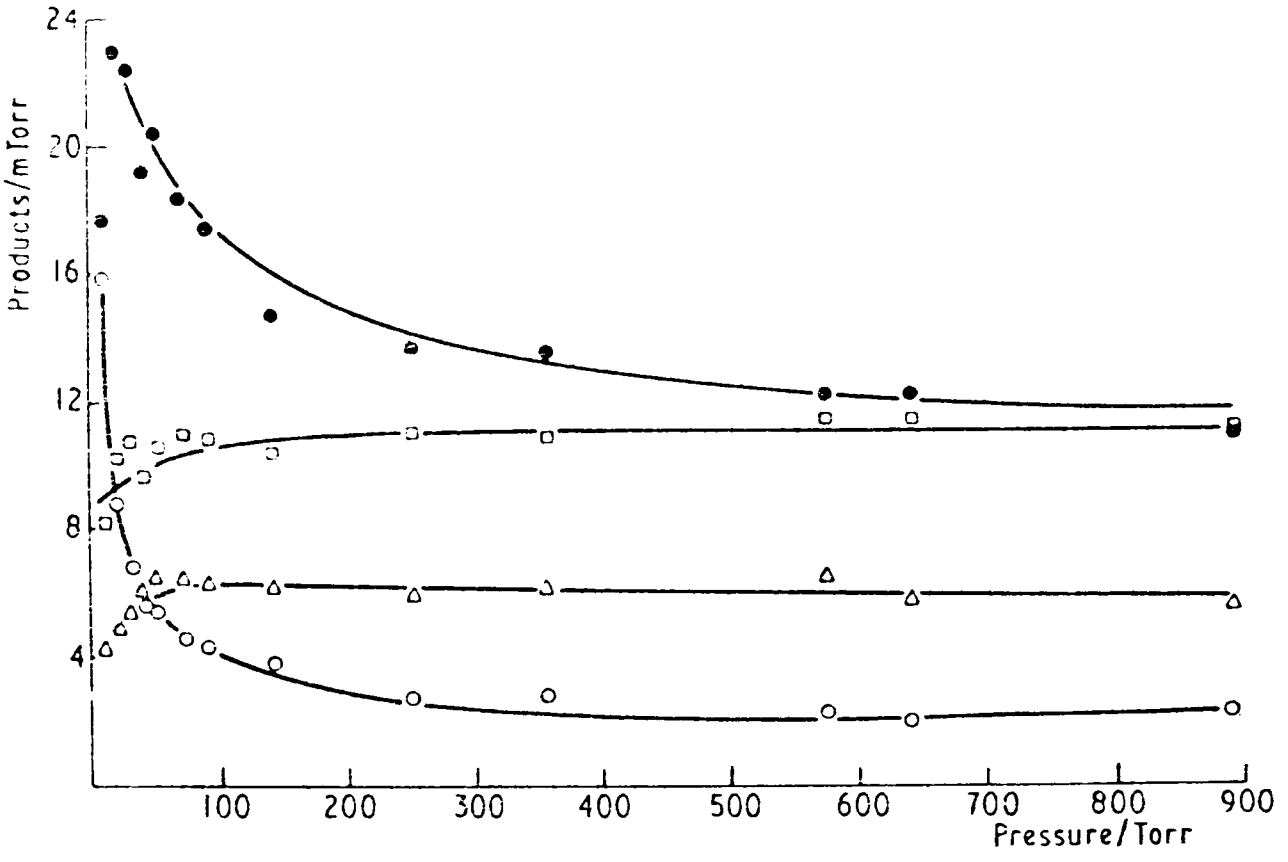



Fig. 3.3. Products from the flash photolysis of 200 mTorr $CH_2CO$, 10 Torr $H_2$ with added $SF_6$.

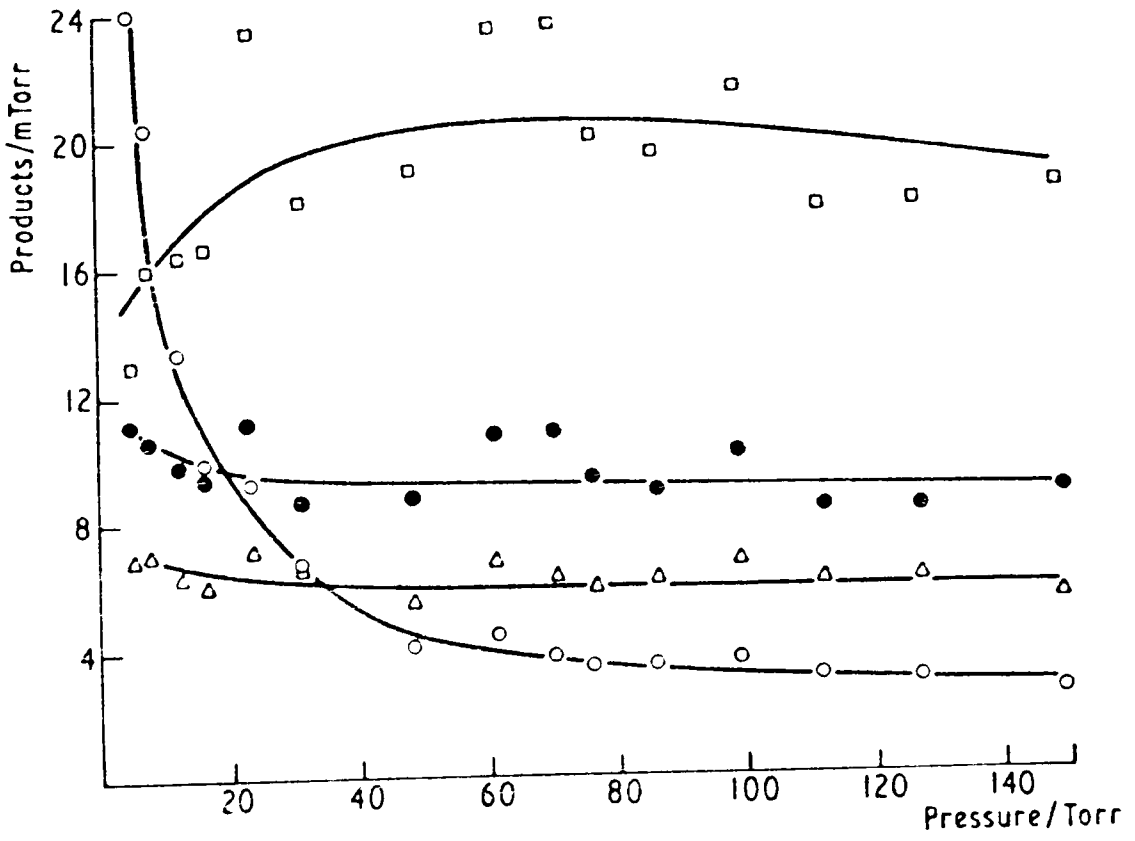



Fig. 3.4. Products from the flash photolysis of 200 mTorr $CH_2CO$, 5 Torr $H_2$, with added xenon.

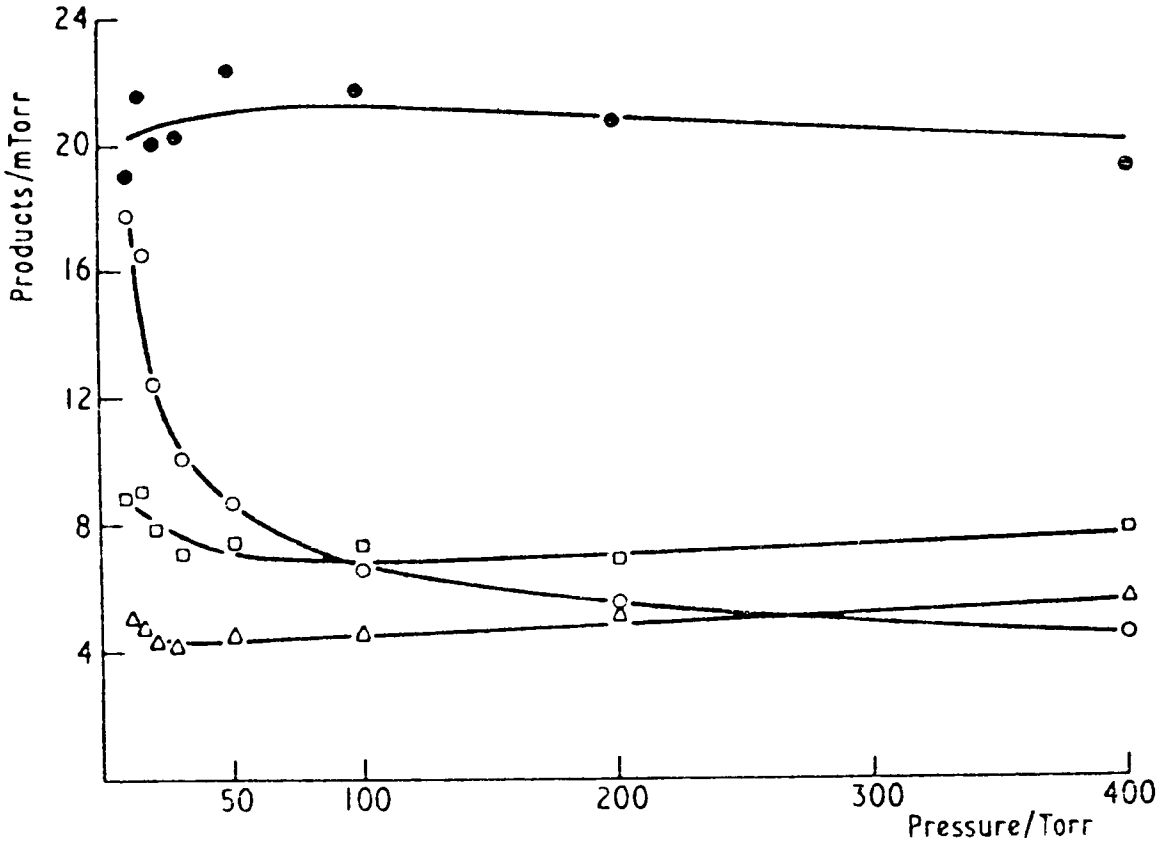



Fig. 3.5. Products from the flash photolysis of 200 mTorr $CH_2CO$, 10 Torr $H_2$, with added helium.

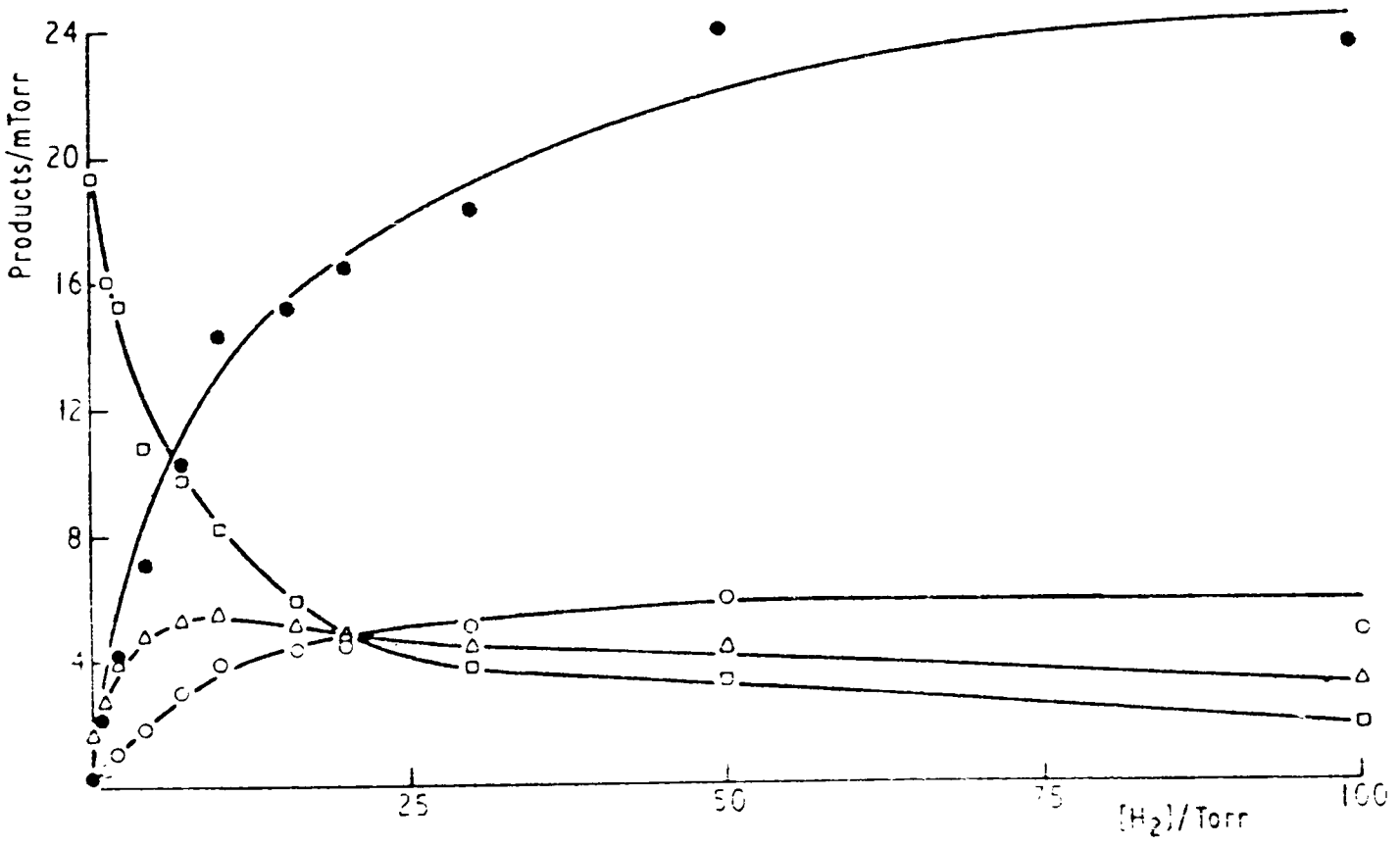



Fig. 3.6. Products from the flash photolysis of 200 mTorr $CH_2CO$, in 200 Torr argon with added $H_2$.

$$CH_2CO + h\nu \longrightarrow {}^1CH_2 + CO \qquad (1)$$

$${}^1CH_2 + M \xrightarrow{k_2} {}^3CH_2 + M \qquad (2)$$

$${}^1CH_2 + H_2 \xrightarrow{k_3} CH_3 + H \qquad (3)$$

$${}^3CH_2 + {}^3CH_2 \xrightarrow{k_4} C_2H_2 + H_2 \qquad (4)$$

$$CH_3 + CH_3 \xrightarrow{k_5} C_2H_6 \qquad (5)$$

$$CH_3 + H \xrightarrow{k_6} CH_4 \qquad (6)$$

M is an inert gas.

${}^1CH_2$ produced in the primary photolysis process may either be deactivated to ${}^3CH_2$, or it may react with $H_2$ to give $CH_3 + H$. The fall in $C_2H_6$ as $[M]/[H_2]$ is increased should be accompanied by a corresponding rise in the products from ${}^3CH_2$ reactions. In the figures 3.1, 3.3, 3.4, and 3.5 it is apparent that the fall in $C_2H_6$ is much more marked than the rise in $C_2H_2$, the expected product from ${}^3CH_2$.

Reaction (6) is expected to be pressure dependent over the pressure range investigated, and to a first approximation it may be described by a Lindemann scheme:

$$CH_3 + H \underset{k_D}{\overset{k_c}{\rightleftharpoons}} CH_4^*$$

$$CH_4^* + M \xrightarrow[k_S]{} CH_4 + M$$

The overall rate of production of $CH_4$ is,

$$\frac{d[CH_4]}{dt} = \frac{k_c}{1 + k_D/k_S[M]}[CH_3][H] = k_6[CH_3][H]$$

The apparent insensitivity of $[CH_4]$ to pressure may be explained as the result of two opposing effects: firstly, a decrease in $[CH_3] + [H]$ with increase in $[M]/[H_2]$ tends to

decrease $[CH_4]$ , and, secondly, an increase in $k_6$ with $[M]$ tends to increase $[CH_4]$.

$CH_3$ and H are produced in equal amounts and the subsequent reactions (5) and (6) will cause a surplus of H radicals. One possible route for their removal is,

$$H + CH_2CO \xrightarrow{k_7} CH_3 + CO \qquad (7)$$

This reaction may be invoked to explain the increase in total product yield at low pressure where reaction (6) is slow and H radicals are plentiful. On this basis it is unnecessary to postulate a pressure dependent quantum yield for the primary photolysis.

The scheme so far does not explain the production of $C_2H_4$. Two possible means of production are,

$$^3CH_2 + CH_3 \xrightarrow{k_8} C_2H_4 + H \qquad (8)$$

$$^1CH_2 + CH_2CO \xrightarrow{k_9} C_2H_4 + CO \qquad (9)$$

Reaction (9) has been postulated as a source of $C_2H_4$ in the low intensity photolysis of ketene [31]. In the present system $[CH_2CO] \leq 1/50[H_2]$ , and for reaction (9) to compete with reaction (3) a large value is required for $k_9/k_3$.

Reaction (8) has been suggested as a source of $C_2H_4$ in Hg - photosensitised $CH_2CO$ photolysis [77]. As a radical-radical reaction its rate might be expected to be fast, and in the present system it seems a more likely source of $C_2H_4$ than reaction (9).

The scheme of reactions (1) - (9) shown in table 3.1, provides a basis for a discussion of the data in figures 3.1 - 3.5. Included in table 3.1 are the values of rate constants which have been reported in the literature. This scheme does

Table 3.1

| Reaction | | k ($cm^3 molecule^{-1} s^{-1}$) | ref |
|---|---|---|---|
| $CH_2CO + h\nu \longrightarrow {}^1CH_2 + CO$ | (1) | | |
| ${}^1CH_2 + M \xrightarrow{k_2} {}^3CH_2 + M$ | (2) | $6.7 \times 10^{-13}$ a | 41 |
| ${}^1CH_2 + H_2 \xrightarrow{k_3} CH_3 + H$ | (3) | $7.0 \times 10^{-12}$ | 41 |
| ${}^3CH_2 + {}^3CH_2 \xrightarrow{k_4} C_2H_2 + H_2$ | (4) | $5.3 \times 10^{-11}$ | 41 |
| $CH_3 + CH_3 \xrightarrow{k_5} C_2H_6$ | (5) | $4.2 \times 10^{-11}$ | 123, 124 125 |
| $CH_3 + H \xrightarrow{k_6} CH_4$ | (6) | b | |
| $H + CH_2CO \xrightarrow{k_7} CH_3 + CO$ | (7) | $1.3 \times 10^{-13}$ c | 126 |
| ${}^3CH_2 + CH_3 \xrightarrow{k_8} C_2H_4 + H$ | (8) | ? | |
| ${}^1CH_2 + CH_2CO \xrightarrow{k_9} C_2H_4 + CO$ | (9) | $3.2 \times 10^{-11}$ d | 80 |

a. This is the value for M ≡ Ar.

b. This rate constant is pressure dependent as discussed in the text.

c. This rate constant was also measured relative to $H + C_2H_4$ by Avery and Cvetanovic [127]. If a value for $k(H + C_2H_4) = 1.6 \times 10^{-12}$ $cm^3$ $molecule^{-1}$ $s^{-1}$ is assumed [128], their value is in agreement with that given here.

d. This value does not agree with the results discussed later in this thesis.

not explain why $C_2H_2$ production is so insensitive to $[M]$ compared to $C_2H_6$. In addition, in the 10 Torr $H_2$ system, over the pressure range 500 Torr $\leq p_{Ar} \leq$ 1000 Torr, the products $CH_4$, $C_2H_4$, $C_2H_6$, which on the basis of the reaction scheme arise from $^1CH_2$, all remain fairly constant. Braun et al.[41] found $k_2/k_3 = 0.1$ and on this basis the "singlet products" would be expected to decrease by a factor of 2 over this pressure range. This is the second failure of the model.

In order to avoid the effects of a variable pressure stabilization of products, in particular via reaction (6), experiments were carried out at a fixed (high) pressure of inert gas. Figure 3.6 shows the products from the photolysis of 200 mTorr $CH_2CO$ in 200 Torr argon with varying amounts of added $H_2$. The total product yield was found to remain constant. The variation of products may be explained according to reactions (1) - (9). The production of $C_2H_4$ at zero hydrogen pressure is attributed to reaction (9). As $[CH_3]$ increases $[C_2H_4]$ from reaction (8) increases, but it reaches a maximum and begins to fall as $[^3CH_2]$ falls. The fall in $[C_2H_2]$ as $[H_2]$ is increased is mirrorred by the rise in $[CH_4] + [C_2H_6]$. In this case, then, the reaction scheme appears, at least qualitatively to explain the results.

In order to test the scheme more rigorously and to investigate its deficiencies in describing figs. 3.1, 3.3, 3.4, and 3.5 it is necessary to solve the kinetic equations describing the model. Due to the complexity of the scheme no analytical solution is available. In a flash photolysis system it is impossible to make steady state assumptions as may be done in a low intensity system. The remaining

alternative is to solve the equations numerically by computer.

## 3.2 Numerical solution of the kinetic scheme.

The computer programme used to solve the kinetic equations is listed in appendix A1. The programme, as listed, includes several equations which were used to test various kinetic schemes described later.

For the model in table 3.1 the relevant equations are:

$$\frac{d[{}^1CH_2]}{dt} = w_K G(t)[CH_2CO] - k_2[M][{}^1CH_2] - k_3[H_2][{}^1CH_2] - k_9[CH_2][CH_2CO] + w_{CH_3}[CH_3]\,G(t)$$

$$\frac{d[{}^3CH_2]}{dt} = k_2[{}^1CH_2][M] - 2k_4[{}^3CH_2] - k_8[{}^3CH_2][CH_3]$$

$$\frac{d[CH_2CO]}{dt} = -w_K G(t)[CH_2CO] - k_9[{}^1CH_2][CH_2CO] - k_7[H][CH_2CO]$$

$$\frac{d[CH_3]}{dt} = k_3[{}^1CH_2][H_2] - 2k_5[CH_3]^2 - k_6[CH_3][H] + k_7[H][CH_2CO] - k_8[{}^3CH_2][CH_3] - w_{CH_3}[CH_3]\,G(t)$$

$$\frac{d[H]}{dt} = k_3[{}^1CH_2][H_2] - k_6[CH_3][H] - k_7[H][CH_2CO] + k_8[{}^3CH_2][CH_3] + w_{CH_3}[CH_3]\,G(t)$$

$$\frac{d[C_2H_4]}{dt} = k_8[{}^3CH_2][CH_3] + k_9[{}^1CH_2][CH_2CO] - w_{C_2H_4}[C_2H_4]\,G(t)$$

$$\frac{d[C_2H_2]}{dt} = k_4[{}^3CH_2]^2 + w_{C_2H_4}[C_2H_4]\,G(t)$$

$$\frac{d[CH_4]}{dt} = k_6[CH_3][H]$$

$$\frac{d[C_2H_6]}{dt} = k_5[CH_3]^2$$

The subroutine D02ABF [129] advances the solution of the above system of ordinary differential equations,

$$\frac{dy_i}{dt} = f_i\left(y_1, y_2, \ldots, y_N\right) \quad , \; i = 1,2,\ldots,N$$

from t to $t + \Delta t$, using a number of steps of Merson's form of the Runge-Kutta method [130]. The system of equations is defined in the subroutine AUX which evaluates the derivatives $f_i$ in terms of $y_1$, $y_2$, ..., $y_N$. The subroutine D02ABF obtains an estimate of the local truncation error at each step and varies the step length automatically to keep this estimate below a preset error bound. The programme was tested by using it to solve a simple scheme of first and second order equations for which an analytical solution was available. Complete agreement was found between the computed results and the analytical solution.

The production of $^1CH_2$ is determined by the term, $w_K\left[CH_2CO\right]G(t)$. G(t) is a mathematical function given in chapter 2, which describes the shape of the flash photolysis pulse. $w_K$ is a factor determining the amount of $CH_2CO$ photolysed, given by,

$$w_K = \log_e \left\{ \left[CH_2CO\right]_f / \left( \left[CH_2CO\right]_i - \text{Pulse} \right) \right\} \quad ,$$

where $\left[CH_2CO\right]_i$ is the initial ketene concentration and Pulse is the total concentration of ketene photolysed. It was found necessary to include the generation function, G(t), to obtain accurate results for comparison with experimental data. The approximation of a $\delta$-function at time, t = 0, for the production of $^1CH_2$, gave results which differed by up to 10% from those calculated with the inclusion of G(t). This

difference occurs since reaction takes place within the photolysis flash. At maximum radical concentrations, the step length used by the programme was $\simeq 10^{-8}$ s.

It was found necessary (as will be discussed later) to include corrections for the secondary photolysis of $C_2H_4$ and $CH_3$. Both these corrections were small, however, and did not affect the computed results to any great extent. For example, it was determined experimentally that, if $C_2H_4$ were photolysed in inert gas under similar conditions to those used in obtaining the data of fig. 3.1, 40% of the $C_2H_4$ decomposed to produce $C_2H_2$. Inclusion of a term, $-w_{C_2H_4}\left[C_2H_4\right] G(t)$, in the equation for production of $C_2H_4$ caused only a 5-10% reduction in the calculated $\left[C_2H_4\right]$ since only a fraction of the $C_2H_4$ was produced during the photolysis flash. $w_{C_2H_4}$ was given by,

$$w_{C_2H_4} = -\log_e(1-f_{C_2H_4})$$

where $f_{C_2H_4}$ is the (experimental) fraction of $C_2H_4$ which was photolysed.

Although the programme gave accurate solutions to the equations it suffered from the phenomenon of "stiffness" [131]. The symptom of this was the large amount of computing time required to solve the kinetic scheme. Integration was carried out until all the radical concentrations were $<0.1$ mTorr. On this basis reaction was generally complete within 5,000 - 10,000 $\mu$s. The computer time taken to carry out a calculation for the system $\left[CH_2CO\right]$ = 200 mTorr, $\left[H_2\right]$ = 10 Torr, $\left[Ar\right]$ = 0 Torr was $\simeq$ 5 s. However when $\left[Ar\right]$ = 800 Torr the computer time increased to $\simeq$ 50 s. This is due to the difficulty of the programme in following reaction (2) which

becomes very fast at high pressures. A very short step length is required and consequently the computing time is long. It was found that at high pressures a steady state assumption,

$$\frac{d[^1CH_2]}{dt} = 0,$$

could be made without affecting the accuracy. Subroutines have been developed [132, 133] which automatically invoke a steady state assumption when the necessary conditions are fulfilled.

## 3.3 Azomethane / ketene photolysis experiments. A rate constant for $^3CH_2 + CH_3$.

In order to test the reaction scheme in table 3.1 it was necessary to obtain an estimate for $k_8$, the rate constant for $^3CH_2 + CH_3$. To do this a study was made of the azomethane / ketene photolysis system. The U.V. photolysis of azomethane is a good source of $CH_3$ radicals.

Fig. 3.7 shows the products from the photolysis of 100 mTorr azomethane in 200 Torr argon as a function of added ketene. Fig. 3.8 shows the products from the photolysis of 200 mTorr ketene in 200 Torr argon as a function of added azomethane. The kinetics may be described by the following reaction scheme:

$$CH_2CO + h\nu \longrightarrow {}^1CH_2 + CO \qquad (1)$$

$$CH_3N_2CH_3 + h\nu \longrightarrow 2CH_3 + N_2 \qquad (1b)$$

$$^1CH_2 + Ar \longrightarrow {}^3CH_2 + Ar \qquad (2)$$

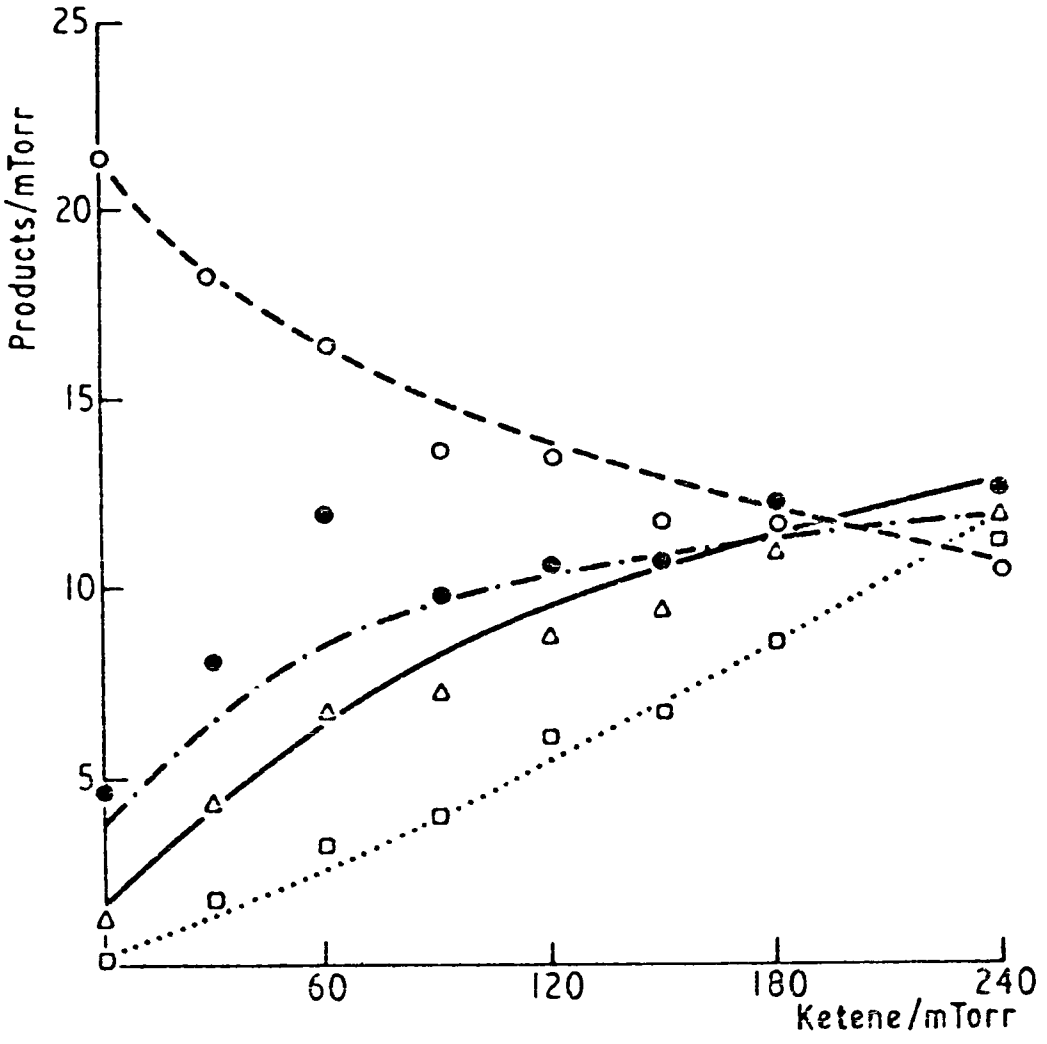



Fig. 3.7. Flash photolysis products versus $CH_2CO$ for 100 mTorr $CH_3N_2CH_3$ in 200 Torr argon with added $CH_2CO$. Curves are computer fits to the data. ..... $C_2H_2$; ------ $C_2H_6$; -·-·-·- $CH_4$; ——— $C_2H_4$

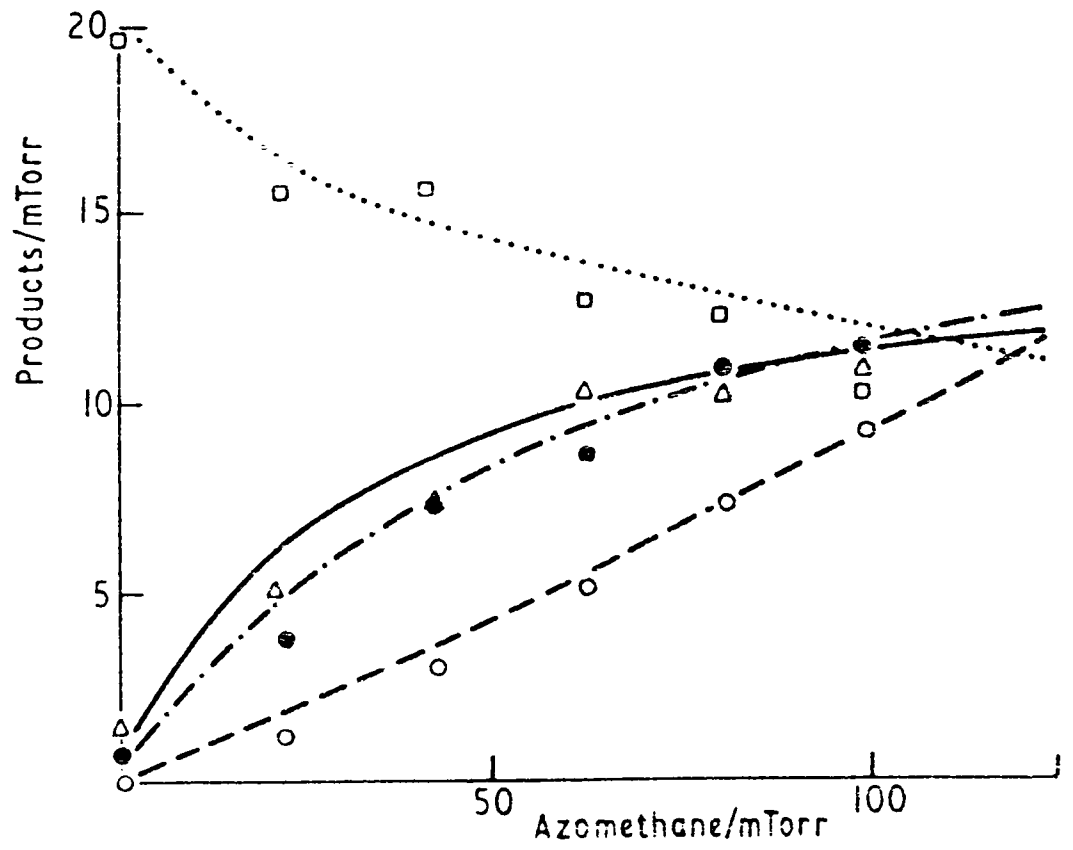



Fig. 3.8. Flash photolysis products versus $CH_3N_2CH_3$ for 200 mTorr $CH_2CO$ in 200 Torr argon with added $CH_3N_2CH_3$.

$$^3CH_2 + {}^3CH_2 \longrightarrow C_2H_4^* \longrightarrow C_2H_2 + H_2 \qquad (4)$$

$$^3CH_2 + CH_3 \longrightarrow C_2H_5^* \longrightarrow C_2H_4 + H \qquad (8)$$

$$CH_3 + CH_3 \longrightarrow C_2H_6 \qquad (5)$$

$$CH_3 + H \longrightarrow CH_4 \qquad (6)$$

$$H + CH_2CO \longrightarrow CH_3 + CO \qquad (7)$$

$$C_2H_4 + h\nu \longrightarrow C_2H_2 + H_2 \qquad (10)$$

$$CH_3 + h\nu \longrightarrow {}^1CH_2 + H \qquad (11)$$

The products observed were $CH_4$, $C_2H_6$, $C_2H_4$ and $C_2H_2$. In addition, traces of the $C_3$ hydrocarbons, methyl acetylene, allene, and propylene, were found and attributed to reaction of methylene with ethylene and acetylene. No $C_4$ hydrocarbons were observed; the absence of n-butane shows that $C_2H_5^*$ is not stablized at the pressure employed (200 Torr argon).

In addition to the primary photolyses (1) and (1b) the secondary photolyses (10) and (11) must be considered. The extent of ethylene photolysis was determined in separate experiments as $\simeq$ 30%. In the experiments with azomethane and ketene, where $C_2H_4$ is formed during and after the flash by reaction (8), the extent of $C_2H_4$ photolysis is smaller $\simeq$ 7%.

Correction for $CH_3$ photolysis was more difficult since it was impossible to carry out an experiment to determine the fraction of $CH_3$ photolysed. The methyl radical has a strong absorption band at 216 nm [3]. The upper state is predissociated to give $^1CH_2$ + H (see chapter 5). A rough value for the number of photons emitted by the lamp at 216 nm. was determined using ethylene as an actinometer, and assuming that the spectral distribution of the lamp emission could be

approximated to that of a black body at $10^4$ K [134]. The integrated absorption coefficient of the methyl radical was taken as $1.1 \times 10^{-14}$ $cm^2$ $molecule^{-1}$ [135]. These very approximate calculations (outlined in appendix A2) suggest that Some $CH_3$ was photolysed. This is supported by experiments on the photolysis of azomethane in argon, where, in addition to ethane, the minor products methane, ethylene, and acetylene are also formed, and may be accounted for by the reactions (11), (6), (8), (10). The photolysis factor for $CH_3$ was determined by computer fitting the minor products in the azomethane photolysis to the proposed secondary photolysis mechanism. The overall extent of $CH_3$ photolysis was small (10 - 15%) and was only of minor importance.

It is important in attempting a computer fit of the data that as many of the rate constants as possible are defined at the outset. A critical survey of the literature was thus necessary, and the best set of rate constants available is included in table 3.1. There is some division of opinion on $k_5$ [136], although several reliable measurements agree on the value given in table 3.1. There are no reported measurements of $k_6$ at 200 Torr pressure. RRKM calculations [137] suggest that the reaction should be approaching its high pressure limit. The collision number for $CH_3$ + H calculated on the assumption of $\sigma_{CH_3} = 3.8$ A, $\sigma_H = 0.4$ A is $3.44 \times 10^{-10}$ $cm^3$ $molecule^{-1}$ $s^{-1}$. By analogy with $CH_3 + CH_3$ the high pressure rate constant may be this value multiplied by an appropriate degeneracy factor of $\frac{1}{4}$ to account for spin. This gives $k_6 = 8.6 \times 10^{-11}$ $cm^3$ $molecule^{-1}$ $s^{-1}$ in the high pressure limit. A value of $k_6 = 10.0 \times 10^{-11}$ $cm^3$ $molecule^{-1}$ $s^{-1}$ gave

the best computer fit to the experimental data. The effect of varying $k_6$ was only of secondary importance to the other products. A variation of $k_6$ over the range 5.0 - 15.0 x $10^{-11}$ $cm^3$ $molecule^{-1}$ $s^{-1}$ was not critical to the fit obtained for the $C_2$ products.

Reaction (7) provides a route for slow removal of excess H atoms. A variation of $k_7$ over the range $10^{-15}$ - $10^{-12}$ $cm^3$ $molecule^{-1}$ $s^{-1}$ had little effect on the product distribution; provided $k_7 \lesssim 10^{-12}$ $cm^3$ $molecule^{-1}$ $s^{-1}$, any H atoms remaining at long times are converted to $CH_4$ by reaction (7) followed by (6). Even without the evidence of ref. 126, the assumption that $k_7 < 10^{-12}$ $cm^3$ $molecule^{-1}$ $s^{-1}$ is supported by comparison with other H abstraction reactions.

Using the recommended value for $k_4$ a computer fit for the experimental data was obtained with $k_8 = 5.0 \times 10^{-11}$ $cm^3$ $molecule^{-1}$ $s^{-1}$. The fit could be optimised, however, by regarding $k_4$ as a variable between the error limits quoted in ref. 41, when a best fit was obtained with $k_4 = 4.0 \times 10^{-11}$ $cm^3$ $molecule^{-1}$ $s^{-1}$ and $k_8 = 5.0 \times 10^{-11}$ $cm^3$ $molecule^{-1}$ $s^{-1}$. The value for $k_4$ primarily determines $C_2H_2$, and a variation over the range 2.7 - 5.3 x $10^{-11}$ $cm^3$ $molecule^{-1}$ $s^{-1}$ had little effect on $C_2H_4$. Varying $k_8$ over the ranges 2.5 - 5.0 x $10^{-11}$ $cm^3$ $molecule^{-1}$ $s^{-1}$ and 5.0 - 7.5 x $10^{-11}$ $cm^3$ $molecule^{-1}$ $s^{-1}$ produced changes in the $C_2H_4$ product of 36% and 25% resp.

The set of rate constants used in the computer fit is shown in table 3.2. The fits obtained are shown in figs. 3.7 and 3.8. The two sets of data are consistent with the same array of rate constants which argues that the proposed mechanism is effectively correct.

It is difficult to estimate an error in $k_5$, since it has such a complex dependence on the reliability of the other rate

Table 3.2. Optimum rate constants for the computer fit in figures 3.4 and 3.5.

| Reaction | k / $cm^3 molecule^{-1} s^{-1}$ |
|---|---|
| $^3CH_2 + {}^3CH_2 \longrightarrow C_2H_2 + H_2$ | $4.0 \times 10^{-11}$ |
| $CH_3 + CH_3 \longrightarrow C_2H_6$ | $4.2 \times 10^{-11}$ |
| $^3CH_2 + CH_3 \longrightarrow C_2H_4 + H$ | $5.0 \times 10^{-11}$ |
| $CH_3 + H \longrightarrow CH_4$ | $10.0 \times 10^{-11}$ (200 Torr Ar) |

Table 3.3. Rate constants used in the "equilibrium model" for the computer fit shown in fig. 3.13.

| Reaction | k / $cm^3 molecule^{-1} s^{-1}$ |
|---|---|
| $^1CH_2 + Ar \longrightarrow {}^3CH_2 + Ar$ | $6.7 \times 10^{-13}$ |
| $^1CH_2 + H_2 \longrightarrow CH_3 + H$ | $7.0 \times 10^{-12}$ |
| $^1CH_2 + CH_2CO \longrightarrow C_2H_4 + CO$ | $2.0 \times 10^{-11}$ |
| $^3CH_2 + CH_3 \longrightarrow C_2H_4 + H$ | $7.0 \times 10^{-11}$ |
| $^3CH_2 + {}^3CH_2 \longrightarrow C_2H_2 + H_2$ | $5.3 \times 10^{-11}$ |
| $CH_3 + H \longrightarrow CH_4$ | $10.0 \times 10^{-11}$ |
| $CH_3 + CH_3 \longrightarrow C_2H_6$ | $4.2 \times 10^{-11}$ |
| $H + CH_2CO \longrightarrow CH_3 + CO$ | $1.3 \times 10^{-13}$ |
| $^3CH_2 + Ar \longrightarrow {}^1CH_2 + Ar$ | $6.7 \times 10^{-15}$ |

constants. However no fit could be obtained outside the range 3.0 - 8.0 x $10^{-11}$ $cm^3$ $molecule^{-1}$ $s^{-1}$. The assumption of $CH_3$ photolysis is not critical and even without it the experimental data require a value for $k_5$ within this range.

## 3.4 Reconsideration of the $CH_2CO$ / $H_2$ / inert gas system.

An attempt to fit the experimentally observed products of the photolysis of 200 mTorr $CH_2CO$ in 200 Torr argon as a function of added $H_2$ using the rate constants in table 3.1 together with $k_6$ = 10.0 x $10^{-11}$ $cm^3$ $molecule^{-1}$ $s^{-1}$ and $k_5$ = 5.0 x $10^{-11}$ $cm^3$ $molecule^{-1}$ $s^{-1}$ was only partially successful. Fig. 3.9 shows the products from the photolysis of 200 mTorr of $CH_2CO$ in 800 Torr argon as a function of added $H_2$. When the same set of rate constants used for the 200 Torr system were employed, no fit could be obtained for the 800 Torr data. It was found necessary to increase the ratio $k_3/k_2$ by a factor of 5 in order to obtain even an approximate fit. This observation is in accord with the behaviour of "singlet products" noted in fig. 3.1 at high pressure, where $C_2H_6$ and $CH_4$ tend to limiting non-zero values at high inert gas pressures in the presence of 5 - 20 Torr $H_2$. Thus the simple model proposed on the basis of the work of Braun et al. [41] does not explain: (i) the behaviour of "singlet products" at high inert gas pressure (figs. 3.6 and 3.9); (ii) the production of $C_2H_2$ at low pressure (figs. 3.1, 3.3, 3.4, and 3.5).

The following sections examine possible sources of these discrepancies.

## 3.5 Ketene / $H_2$ system.

Fig. 3.10 shows the products from the photolysis of 100 mTorr $CH_2CO$ in $H_2$ as a function of pressure. Fig. 3.11

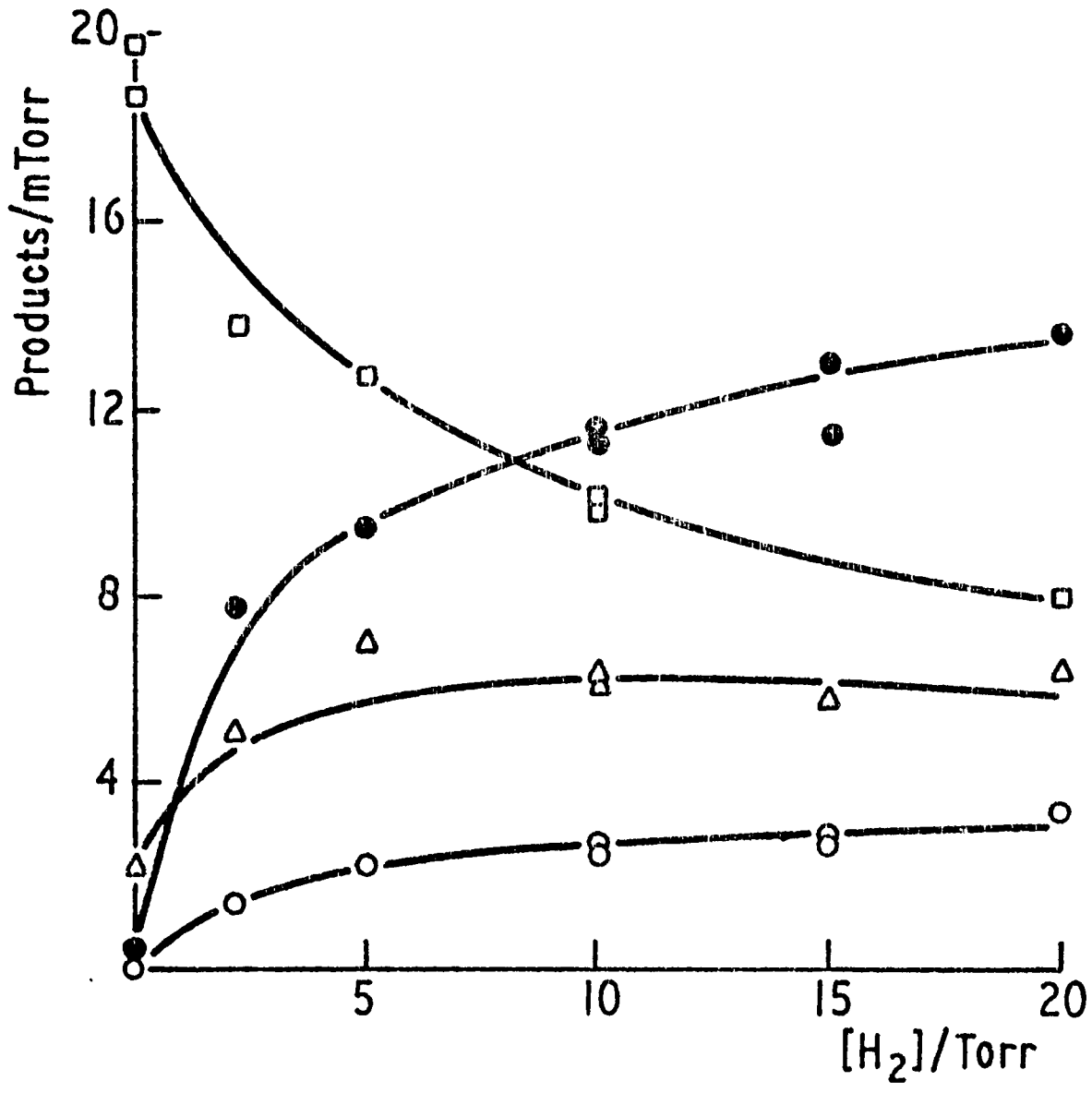



Fig. 3.9. Products from the flash photolysis of 200 mTorr $CH_2CO$ in 800 Torr argon, with added $H_2$.

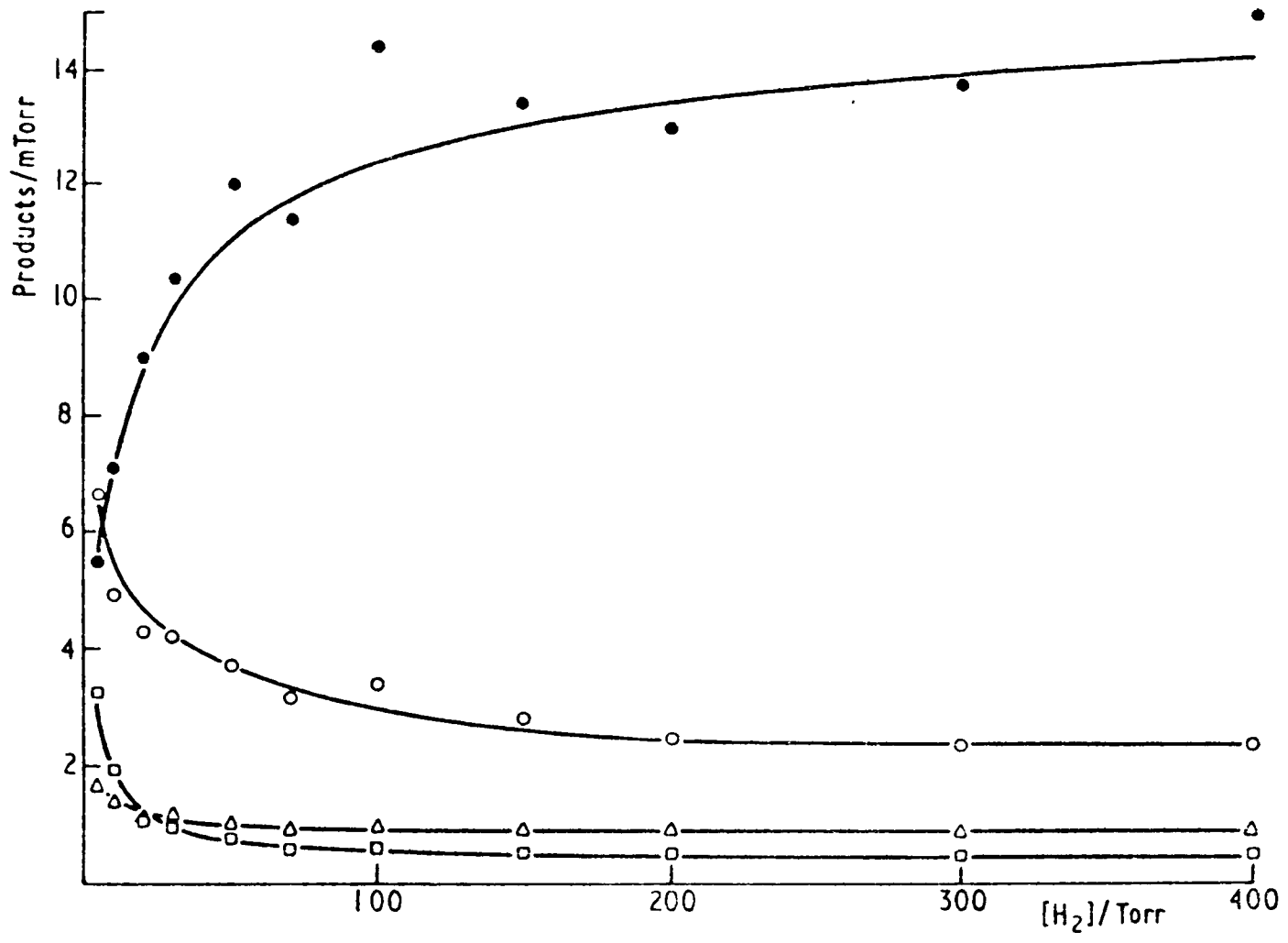



Fig. 3.10. Products from the flash photolysis of 100 mTorr $CH_2CO$ with added $H_2$.

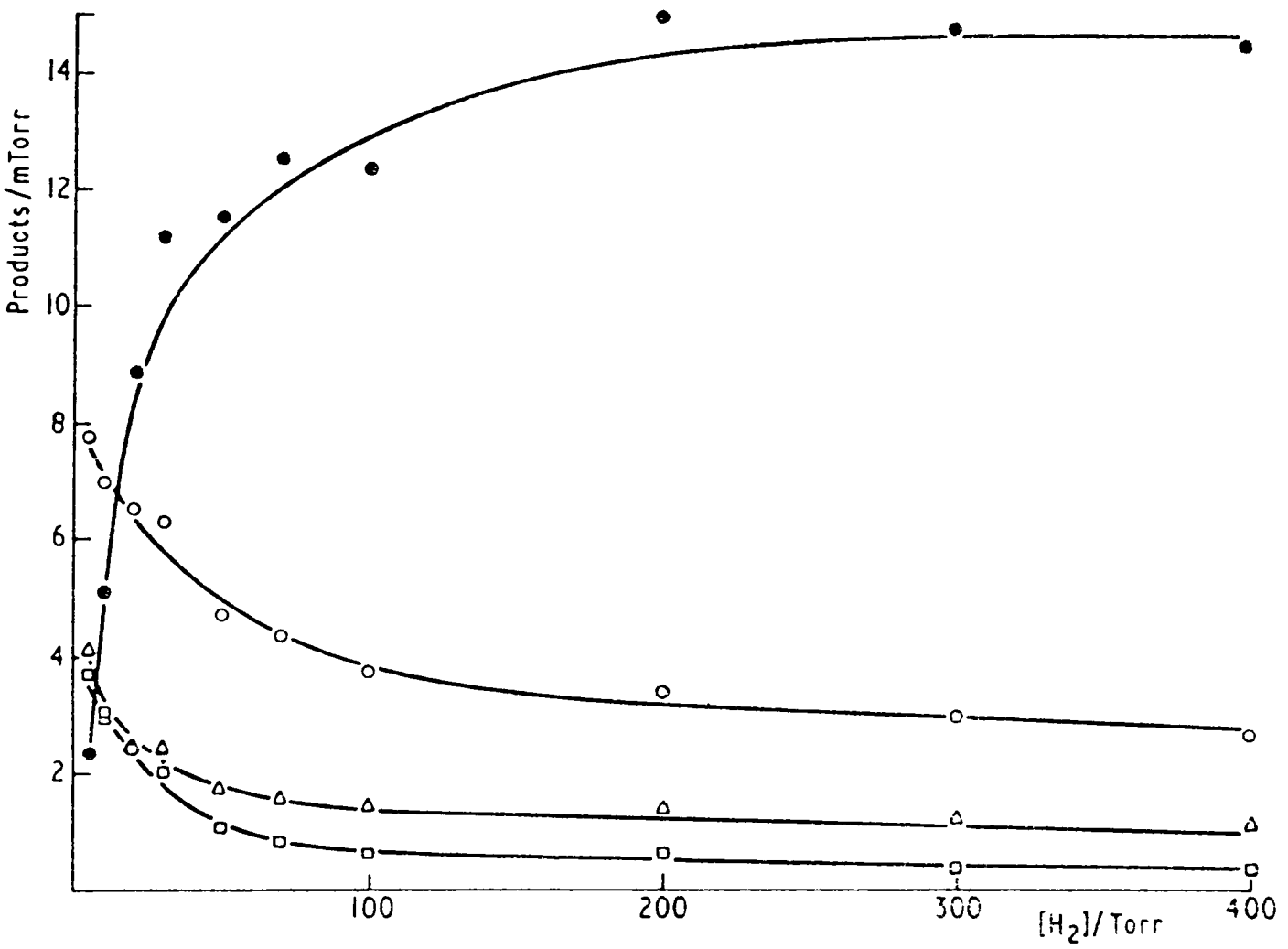



Fig. 3.11. Products from the flash photolysis of 500 mTorr $CH_2CO$ with added $H_2$.

shows a similar plot for 500 mTorr $CH_2CO$. The flash intensity was reduced at the higher ketene concentration so that the total product yields were approximately the same in both experiments. In both cases the pressure dependences of $CH_4$ and $C_2H_6$ fit a model in which $CH_4^*$ is increasingly stabilized as the pressure is increased. The $CH_4$ / $C_2H_6$ ratio at p = 5 Torr was 0.7 for 100 mTorr $CH_2CO$ and 0.3 for 500 mTorr $CH_2CO$. This difference is consistent with the enhancement of reaction (7) at the higher ketene concentration so that (at low pressures) it competes with reaction (6) for removal of H radicals. At high pressures residual H gives almost entirely $CH_4$ according to the stoichiometry,

$$2H + CH_2CO \longrightarrow CH_4 + CO$$

The increased $C_2H_4$ at low pressure may be explained by reaction (9) which is enhanced at the higher $CH_2CO$ concentration.

$C_2H_2$ and $C_2H_4$ at high pressure may be explained by reactions (4) and (8). However the model does not explain the high concentration of $C_2H_2$ at low pressure which decreases as the pressure is increased.

The kinetic scheme was investigated by means of a computer fit. One possible explanation of the $C_2H_2$ was the occurrence of radical - radical reactions as follows:

$$^1CH_2 + {}^1CH_2 \longrightarrow C_2H_2 + (H_2 \text{ or } 2H)$$

$$^1CH_2 + {}^3CH_2 \longrightarrow C_2H_2 + (H_2 \text{ or } 2H)$$

Computation shows that, even if these reactions proceeded at gas kinetic rates, they could only account for 10% of the $C_2H_2$ produced at low pressure. This conclusion is dependent on the assumed value of $k_3 = 7.0 \times 10^{-12}$ cm$^3$ molecule$^{-1}$ s$^{-1}$. If $k_3$

were a factor of 10 smaller than this, the conclusion would no longer be valid.

In a system involving mixed first and second order reactions the products of reaction are strongly dependent on the concentration of the reactants. To a first approximation, radical - molecule reactions in the present study may be considered to be first order reactions and radical - radical reactions are second order. Various experiments were carried out in which the flash photolysis intensity was varied in order to exploit this aspect of the mechanism.

Fig. 3.12 shows the result of one such experiment in a system containing 40 Torr $H_2$ and 200 mTorr $CH_2CO$. The convex slope of the $C_2H_4$ curve indicates that its production involves a first order reaction (presumably reaction (9)), whereas the concave slope of $C_2H_2$ is consistent with a second order reaction as its source.

3.6 Physical effects.

Abnormal results may result from surface reactions or from heating effects.

3.6.1. Surface reactions. In order to check the possibility of heterogeneous surface reactions experiments were carried out in a photolysis vessel which was packed with short lengths of spectrosil tube (length $\simeq$ 10 mm., outer diameter = 1 mm.). The surface / volume ratio of the system was thus increased by a factor of 10. Two experiments were carried out in this reaction vessel: (i) 200 mTorr $CH_2CO$ were photolysed in 200 Torr $H_2$ with added inert gas to various pressures; (ii) 200 mTorr $CH_2CO$ were photolysed in various pressures of $H_2$. The distribution of products in these experiments showed

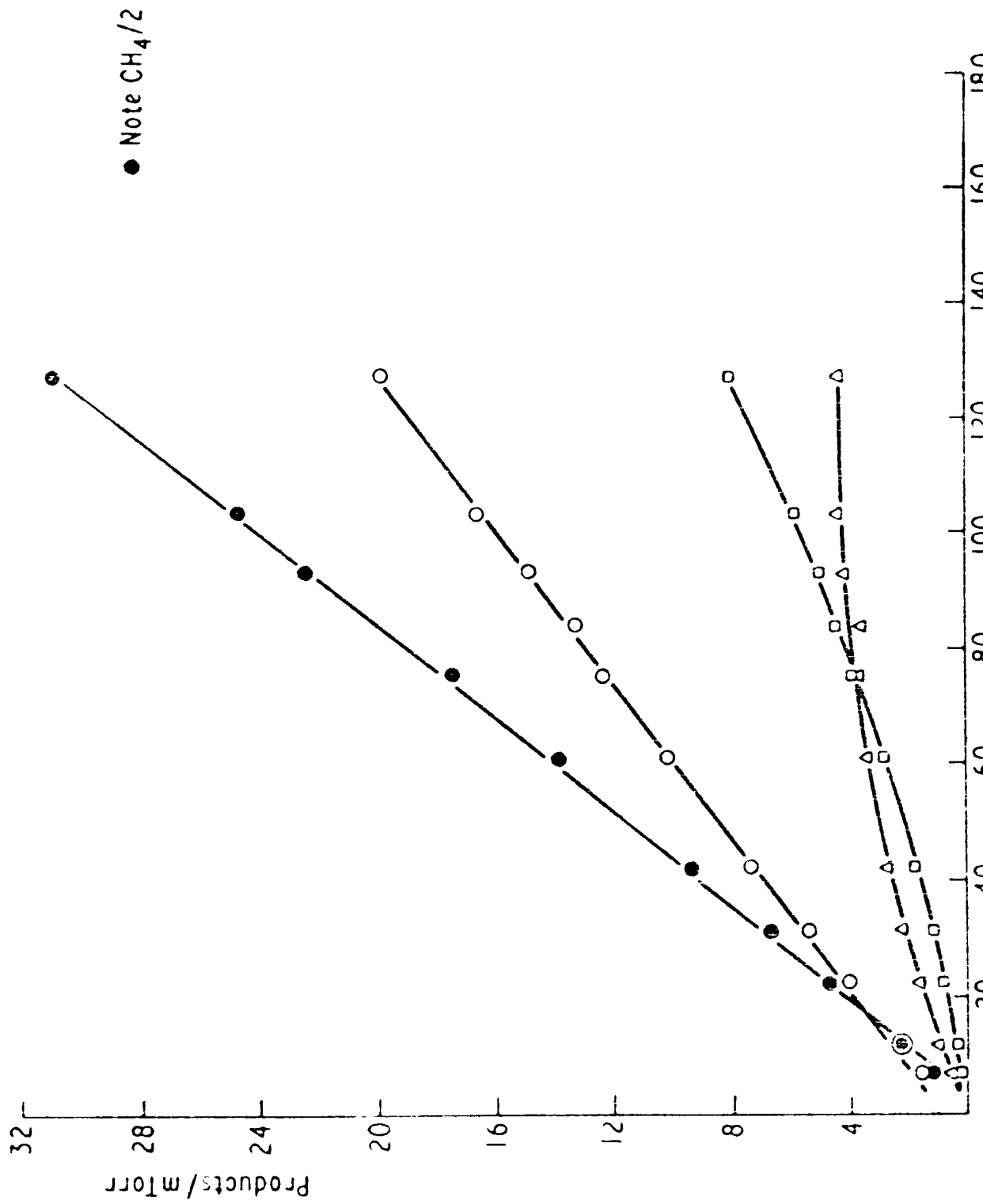



Fig. 3.12. Products from the flash photolysis of 200 mTorr $CH_2CO$ in 40 Torr $H_2$ as a function of total product yield (Variable flash intensity).

no change from the same experiments carried out in unpacked vessels, apart from a decrease in the total amount of photolysis. This was taken as evidence that surface reactions were not important in the system.

3.6.2. Heating effects. A second complication arises in flash photolysis experiments due to the heating effect of the photolysis flash. The energy available for dissipation as heat in the present system is estimated as follows.

In a typical experiment 40 mTorr of $CH_2CO$ were photolysed. The median wavelength of absorbed radiation, $\simeq$ 180 nm., corresponds to an energy of 159 kcal einstein$^{-1}$.
D ($CH_2$ - CO) is 77.4 kcal mol$^{-1}$, leaving 81.6 kcal mol$^{-1}$ to be dissipated as heat.

Heat dissipated cm$^{-3}$ = $1.75 \times 10^{-4}$ cal

For argon, $C_v$ = 3.0 cal K$^{-1}$ mol$^{-1}$

$= 1.61 \times 10^{-7}$ cal K$^{-1}$ Torr$^{-1}$

$$T = 1.09 \times 10^3 / p$$

where p is the pressure in Torr.

Thus in 10 Torr argon, $\Delta T \simeq 10^2$ K, whereas in 1000 Torr argon $\Delta T \simeq 1$ K.

Appendix A3 discusses the rate of cooling of the system. It is apparent that the reaction (which is complete in a time of approx. 5 ms.) may be complicated by a temperature change occurring during the reaction.

At low pressures a considerable temperature rise may occur during the photolysis. This should have little effect on radical recombination reactions which have zero or small activation energy, but it may have considerable effect on radical - molecule reactions which proceed with an Arrhenius activation energy of several kcal mol$^{-1}$. The low pressure

observation of $C_2H_2$ may be connected with a heating effect; further discussion on this aspect is postponed for the present.

## 3.7 Observation of "singlet products" at high pressure.

The lack of any pressure dependence of "singlet products" in $CH_2CO$ / $H_2$ / inert gas systems at high inert gas pressure demands an explanation.

3.7.1. Reactivation of $^3CH_2$ to $^1CH_2$. The uncertainty in the singlet - triplet energy separation requires that reactivation of $^3CH_2$ to $^1CH_2$, which will be important if $\Delta E$ is small, be examined as a possible reaction mechanism.

$$^3CH_2 + M \underset{k_2}{\overset{k_{-2}}{\rightleftharpoons}} {}^1CH_2 + M$$

The equilibrium constant, K, is given by

$$K = \frac{k_{-2}}{k_2} = \frac{Q_1}{Q_3} \exp\left( - (E_1 - E_3) / kT \right) \qquad (A)$$

where $Q_1$ / $Q_3$ is the ratio of the partition functions of $CH_2$ ($^1A_1$) and $CH_2$ ($^3B_1$) and $E_3 - E_1$ is the energy separation between $CH_2$ ($^3B_1$) and $CH_2$ ($^1A_1$). $Q_3$ / $Q_1$ has been calculated as 1.94 at 300 K (Appendix A4).

Fig. 3.13 shows a computed fit to the experimental data of fig. 3.9 on the basis of this "equilibrium model". The full reaction scheme is given in table 3.3. In order to obtain this fit a value of $k_{-2} = 6.7 \times 10^{-15}$ cm$^3$ molecule$^{-1}$ s$^{-1}$ was required. From equation (A) this requires $E_1 - E_3 =$ 3.1 kcal mol$^{-1}$. However the computer fit is not a good one, and none better could be found by varying the rate constants given in table 3.3 from half their quoted values to twice their

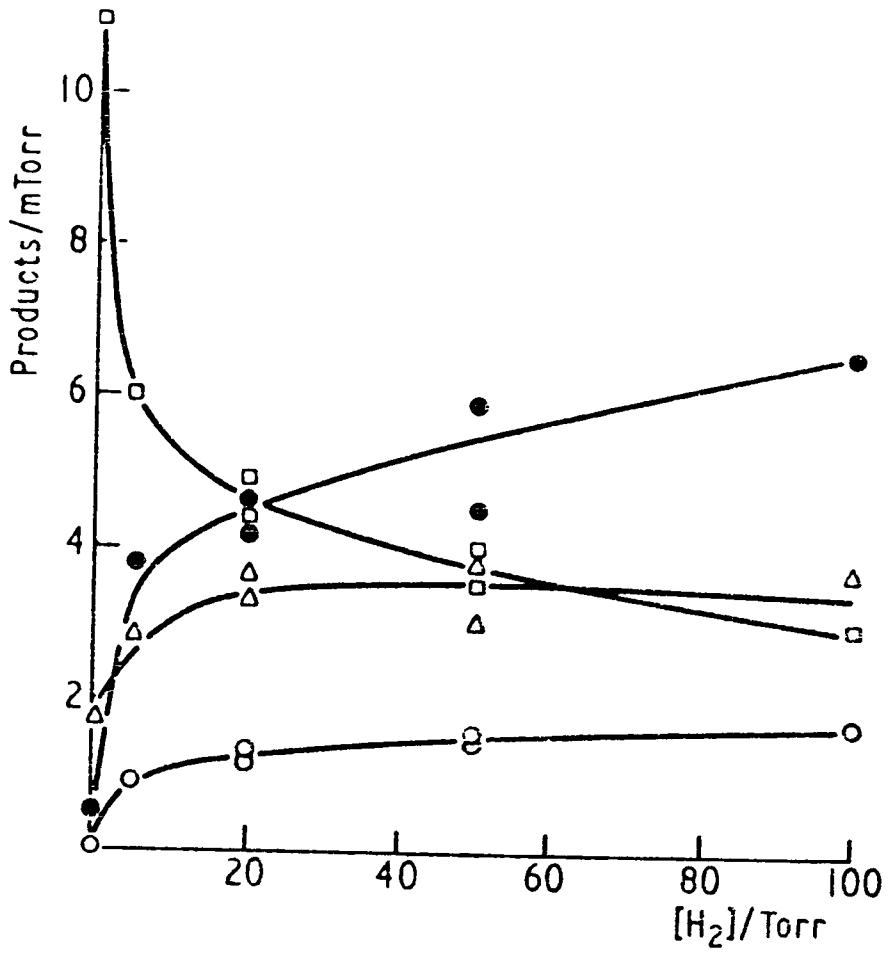



Fig. 3.14. Products from the flash photolysis of 200 mTorr $CH_2CO$ in 800 Torr xenon with added $H_2$.

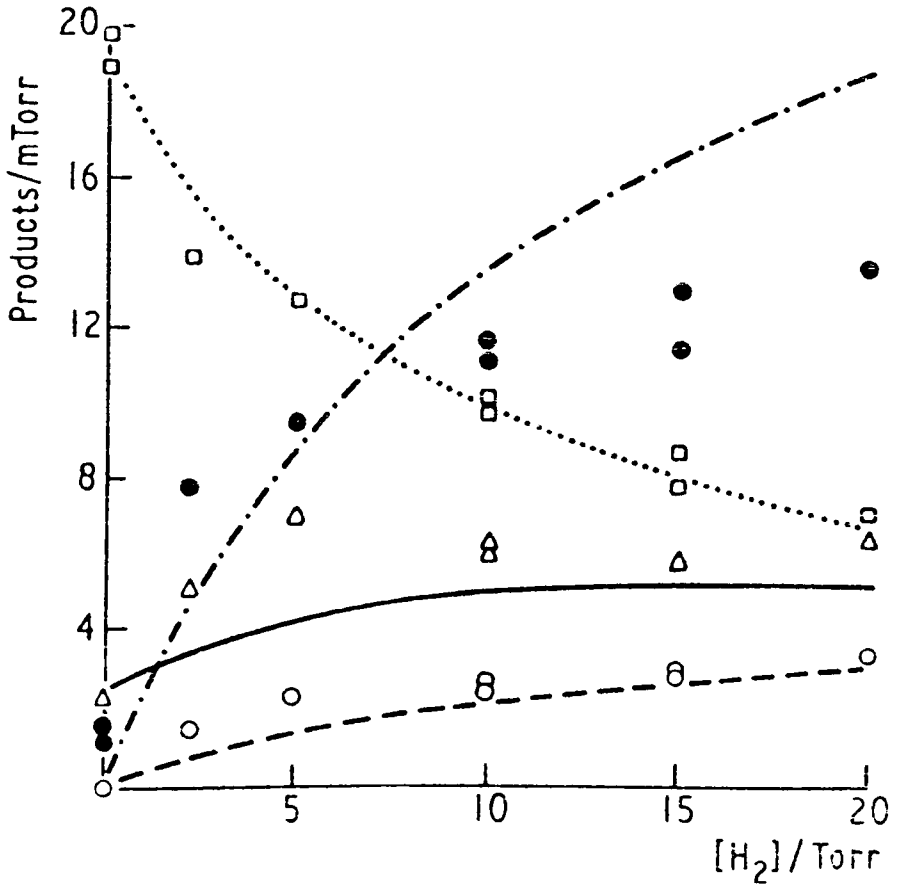



Fig. 3.13. Products from the flash photolysis of 200 mTorr $CH_2CO$ in 800 Torr argon with added $H_2$. Computer fit is for the "equilibrium model".

quoted values. The main source of error in the fit appears in the calculated $[C_2H_6]$. At low $[H_2]$, $[C_2H_6]$ calculated is very much lower than $[C_2H_6]$ experimental. An increase in $k_{-2}$ will correct this but will give far too high a value for $[C_2H_6]$ calculated at high $[H_2]$. The same difficulty was found in the fit for $CH_4$.

This behaviour is even more marked in the photolysis of 200 mTorr $CH_2CO$ in 800 Torr xenon with added $H_2$. The experimental results are shown in fig. 3.14. Addition of small concentrations of $H_2$ causes a sharp rise in $[CH_4]$ and $[C_2H_6]$, but addition of further $H_2$ then causes only a small increase in "singlet products". There is evidence that xenon deactivates $^1CH_2$ to $^3CH_2$ more efficiently than does argon [38, 71] and thus in the xenon system much higher pressures of $H_2$ would be required to intercept the singlet before deactivation than are observed experimentally. Furthermore, if an "equilibrium model" were applicable, then a monotonic increase in "singlet products" should be observed, not the sharp increase followed by a much slower rise found experimentally.

A model involving the reactivation of $^3CH_2$ to $^1CH_2$ is thus rejected on the basis that the kinetic scheme cannot give the correct variation in product distribution with added $H_2$ in a high pressure of inert gas.

3.7.2. Reaction of $CH_2$ ($^1B_1$). $CH_2$ ($^1B_1$) has been suggested as a possible intermediate in the photolysis of ketene and the lower alkanes but little is known of its chemistry. In the photolysis of ketene in the vacuum U.V. there is sufficient energy for production of this state.

A mechanism involving $CH_2$ ($^1B_1$) is capable of explaining the observed products at high pressures if the following

processes are considered to occur:

$$CH_2CO + h\nu \longrightarrow CH_2\,(^1B_1) + CO \quad \phi_x \qquad (1c)$$

$$CH_2\,(^1B_1) + H_2 \xrightarrow{k_{12}} CH_3 + H \qquad (12)$$

$$CH_2\,(^1B_1) \xrightarrow{k_f} CH_2\,(^1A_1) + h\nu \qquad (13)$$

The primary photolysis process is assumed to produce a fraction, $\phi_x$ , of $CH_2\,(^1B_1)$. $CH_2\,(^1B_1)$ may react with $H_2$, or fluoresce to $CH_2\,(^1A_1)$, but in the present model it is not deactivated by collision with inert gas to give the lower energy electronic states $^1A_1$ or $^3B_1$. The reaction scheme is shown schematically in fig. 3.15.

Before investigating such a model it is necessary to estimate the fluorescent lifetime of $CH_2\,(^1B_1)$. Fluorescence has been observed [58] but a lifetime has not been measured.

In principle the rate constant for fluorescence may be calculated from the emission spectrum. For transitions occurring from a state n to a series of states denoted by m the rate constant is given by [141],

$$k_n = \sum_m A_{nm} \qquad (B)$$

where $A_{nm}$ is the Einstein coefficient for the transition from a state n to a state m.

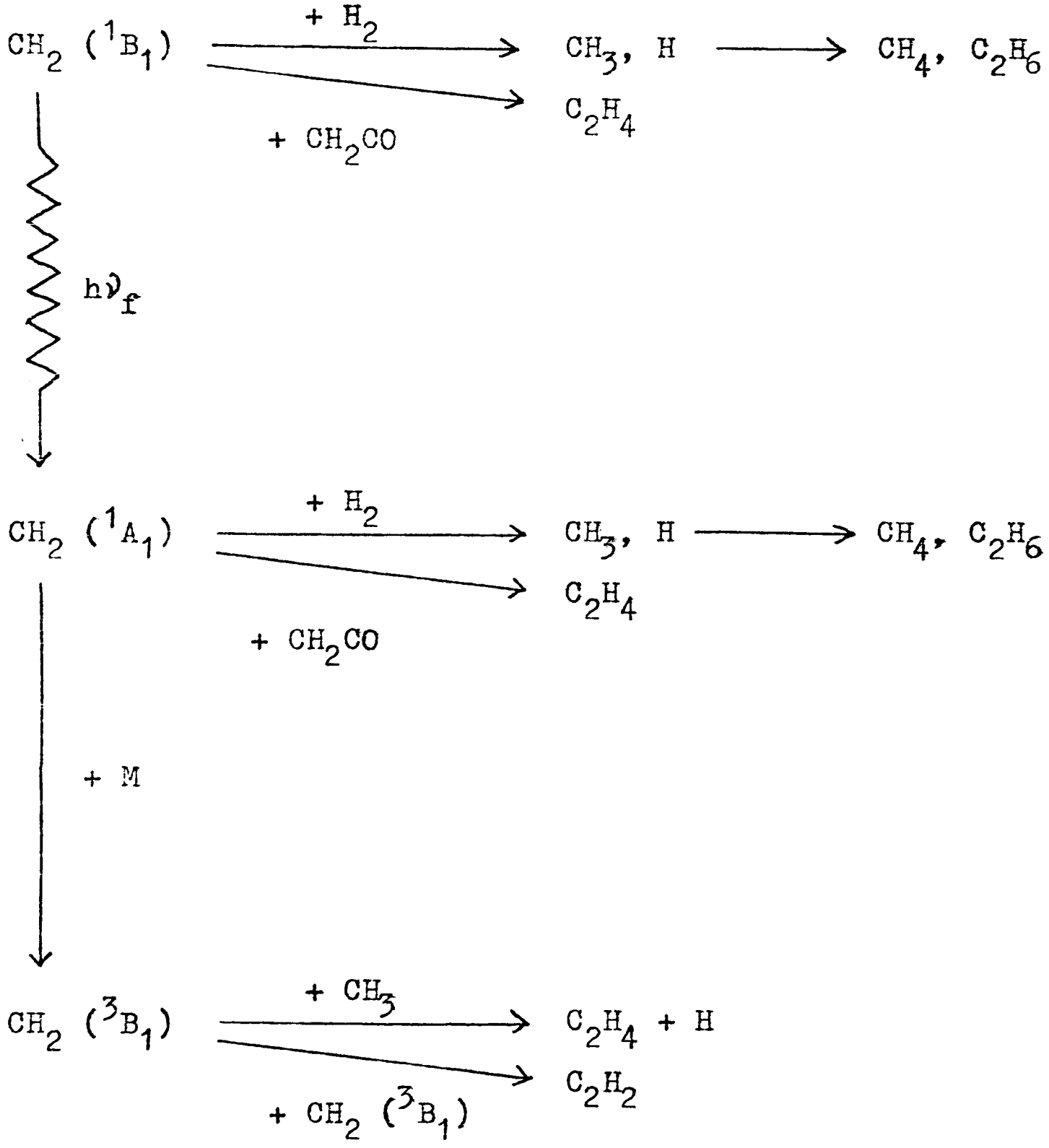
$$A_{nm} = \left(\frac{8\pi^2}{3\epsilon_0 c^3 \hbar}\right) \nu_{mn}^3 \left|d_{mn}\right|^2 \qquad (C)$$

$$\text{where } \left|d_{mn}\right|^2 = f_{mn} \Big/ (2m/3e^2\hbar)\, h\nu_{mn} \qquad (D)$$

$\left|d_{mn}\right|$ is the transition moment, $f_{mn}$ is the f - number for the transition, and $\nu_{mn}$ is the frequency of the transition. Combining equations (C) and (D), and substituting in values for the constants yields,

$$A_{nm} = 7.4 \times 10^{-22} \nu_{mn}^2 f_{mn} \qquad (E)$$

Fig. 3.15. " $CH_2$ ($^1B_1$) model ".



where $\nu_{mn}$ has units $s^{-1}$ and $f_{mn}$ is dimensionless. For each line in the spectrum $A_{nm}$ may be calculated from $\nu_{mn}$, the frequency of the transition, and $f_{mn}$ which is related to the intensity of the line. Unfortunately such detailed information is not available. The best that can be done is to assume a mean wavelength for the transition of 700 nm.[4]. For a strong transition $f \simeq 0.1$. These values give $k_n \simeq 1.4 \times 10^7\ s^{-1}$. This may be regarded as an upper limit to $k_n$ since 0.1 is probably an upper limit to f.
Thus $k_n \equiv k_f \lesssim 10^7\ s^{-1}$.

A lower limit for $k_f$ may be inferred from the work of Braun et al.[41]. They monitored $[^3CH_2]$ in an inert gas /$CH_2CO$ system, and fig. 6 of ref. 41 shows a plot of $\log_{10}\left(\frac{a-c}{a}\right)$ versus p, where a is the total concentration of $^3CH_2$ and c is the concentration of $^3CH_2$ at time, t = 6.5 $\mu$s. p is the pressure. Since the conditions in this work are similar to those in the work of Braun et al. it is reasonable to assume that any production of $CH_2$ ($^1B_1$) is comparable in both experiments. The relevant processes occurring in the inert gas system are,

$$CH_2\ (^1B_1) \xrightarrow{k_f} CH_2\ (^1A_1) + h\nu$$

$$CH_2\ (^1A_1) + M \xrightarrow{k_2} CH_2\ (^3B_1) + M$$

If the initial concentration of $CH_2$ ($^1B_1$) is a , the concentration of $CH_2$ ($^3B_1$) at time t is given by,

$$c = a - \frac{a\,k_2[M]}{k_2[M] - k_f}\exp(-k_f t) + \frac{a\,k_1}{k_2[M] - k_f}\exp(-k_2[M]\,t)$$

Rearranging,

$$\log_{10}\left(\frac{a-c}{a}\right) = \log_{10}\left\{\left(\frac{1}{k_2[M]-k_f}\right)\left[k_2\exp(-k_2t)-k_f\exp(-k_2[M]t)\right]\right\}$$

Figure 3.16 shows plots of $\log_{10}\left(\frac{a-c}{a}\right)$ versus $[M]$ for $k_2 = 6.7 \times 10^{-13}$ cm$^3$ molecule$^{-1}$ s$^{-1}$, and $k_f$ over the range $10^5 - 10^7$ s$^{-1}$. A pressure dependence comparable to that found experimentally by Braun et al. was only obtained for $k_f \gtrsim 10^6$ s$^{-1}$.

These calculations, then, suggest a reasonable value of $k_f$ to be in the range $10^6 \lesssim k_f \lesssim 10^7$ s$^{-1}$. Since an f-number of 0.1 is more generally associated with a strong Rydberg transition, a value for $k_f$ nearer $10^6$ s$^{-1}$ is probably most reasonable, and this lower limit has been used in the subsequent analysis. Using the full reaction scheme shown in table 3.4 the product distribution for the system 200 mTorr $CH_2CO$ / 800 Torr argon with added $H_2$ was computed. The values of $k_{12}$ and $\phi_x$ were adjusted to give the best fit. The set of rate constants thus obtained is given in table 3.4. The value of $k_{12}$ was chosen in order to fit the computed data to the slope of the initial fast rise in "singlet products" as $[H_2]$ is increased. The fraction of $CH_2$ ($^1B_1$) produced in the photolysis flash was also varied. This parameter effectively controls the magnitude of the initial increase in "singlet products". The following reaction was included to explain $C_2H_4$ production in the absence of $H_2$ at high inert gas pressure:

$$CH_2\ (^1B_1) + CH_2CO \xrightarrow{k_{14}} C_2H_4 + CO \qquad (14)$$

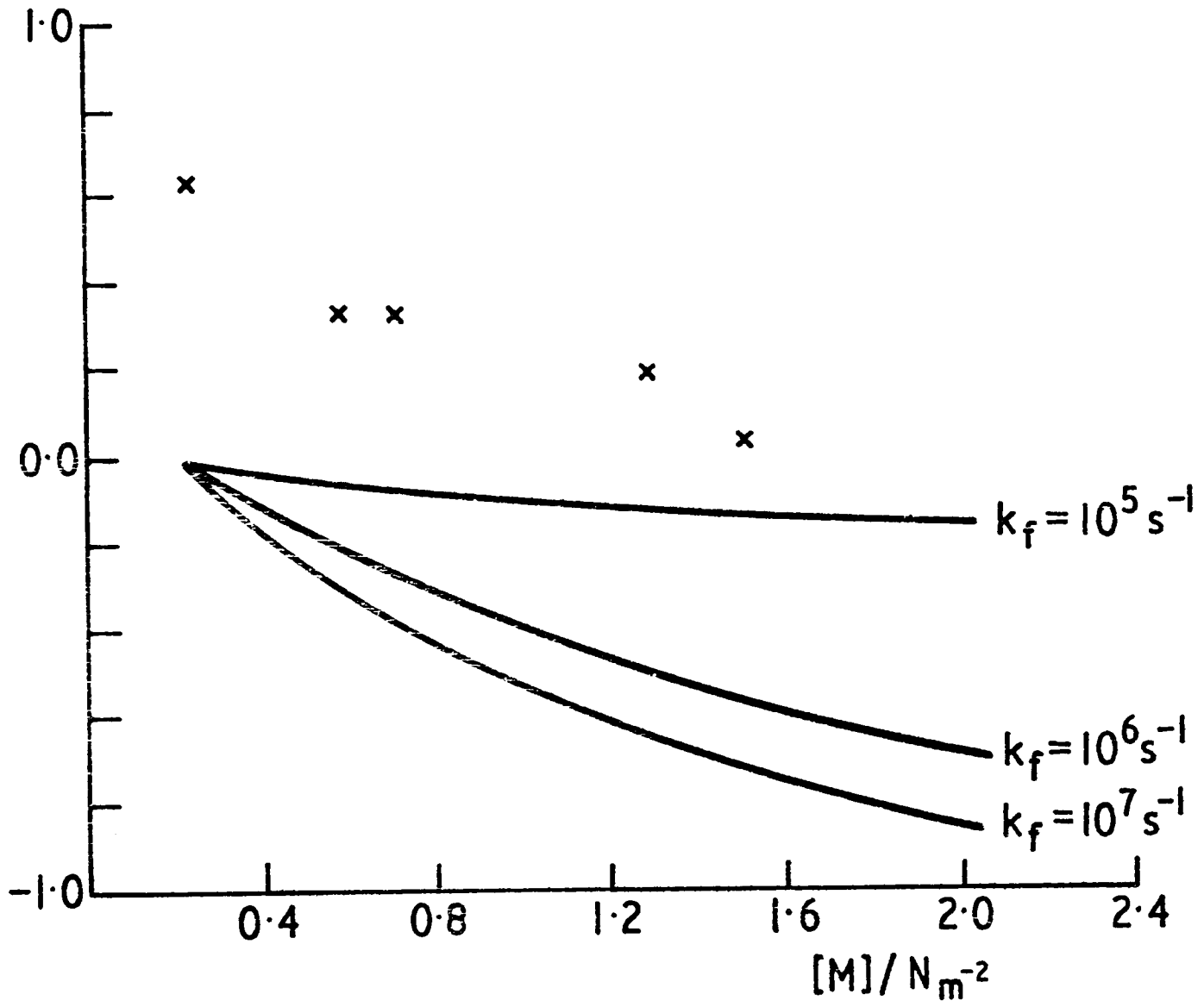



Fig. 3.16. Plot of $\log_{10}\left(\frac{a - c}{a}\right)$ versus M as calculated in equation F.

$t = 6.5\,\mu s$, $k_2 = 6.7 \times 10^{-13}$ cm$^3$ molecule$^{-1}$ s$^{-1}$.

x are results from fig. 6 of ref. 41.

These are displaced an arbitrary amount along the ordinate.

The value of $k_{14}$ was not critical to the rest of the fit. Fig. 3.17 shows the result of the computer fit.

Fig. 3.18 shows a computer fit for the system 200 mTorr $CH_2CO$ / 800 Torr xenon with added $H_2$. The same set of rate constants was used (table 3.4) except for $k_2$ which was $3.4 \times 10^{-12}$ $cm^3$ $molecule^{-1}$ $s^{-1}$. These data show even more clearly than the argon system that two mechanisms are operating, one of which gives an initial rise in "singlet products" as $[H_2]$ is increased, and the other giving a more gradual increase.

One failure common to the computer fits of figs. 3.17 and 3.18 is that the computed value of $[CH_4]$ is higher than the experimental value, i.e. the computed value of $[CH_4] / [C_2H_6]$ is slightly high. Since at 800 Torr pressure, $k_6$ must be close to its high pressure limit it seemed unreasonable to reduce this rate constant. The low experimental value for $CH_4$ may be attributed to loss mechanisms for H which are not included in the model. In the reaction scheme discussed so far all H radicals remaining at long times ( $\gtrsim 1$ ms) react with ketene to give $CH_3$ radicals which, in the presence of excess H, give $CH_4$. Thus the stoichiometry is

$$2H + CH_2CO \longrightarrow CH_4 + CO$$

Possible routes for loss of H are the following:

$$H + C_2H_4 \xrightarrow{k_{15}} C_2H_5 \qquad (15)$$

$$H + C_2H_5 \longrightarrow C_2H_6$$

$$H + C_2H_2 \xrightarrow{k_{16}} C_2H_3 \qquad (16)$$

$$H + C_2H_3 \longrightarrow C_2H_4$$

$$H + H + M \xrightarrow{k_{17}} H_2 + M \qquad (17)$$

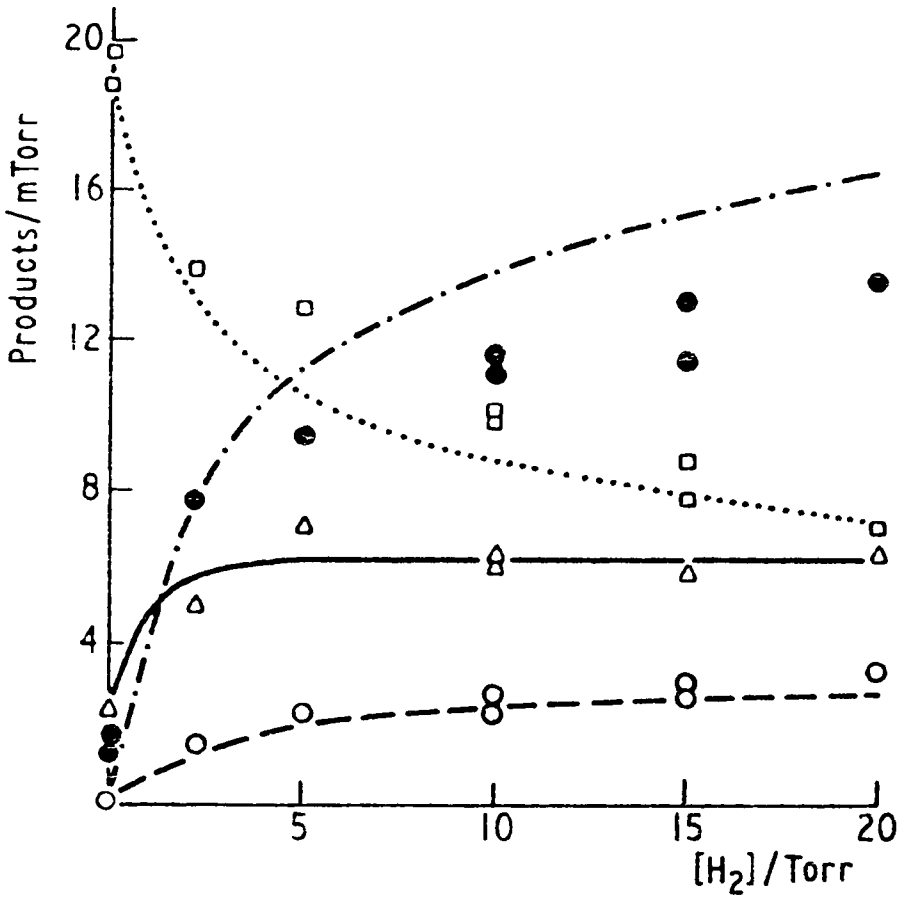



Fig. 3.17. Products from the flash photolysis of 200 mTorr $CH_2CO$ in 800 Torr argon with added $H_2$. Computer fit is for "$CH_2$ ($^1B_1$) model".

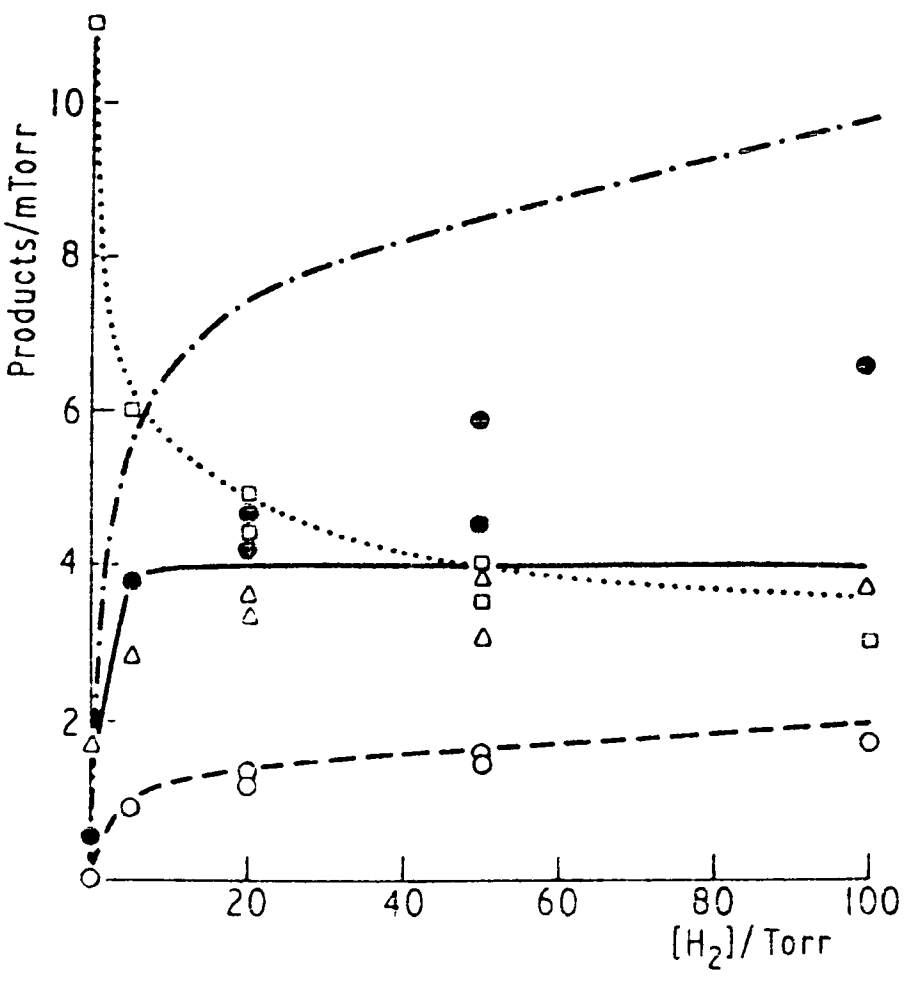



Fig. 3.18. Products from the flash photolysis of 200 mTorr $CH_2CO$ in 800 Torr xenon with added $H_2$. Computer fit is for "$CH_2$ ($^1B_1$) model".

Table 3.4. Rate constants used in the "$CH_2$ ($^1B_1$) model" for the computer fit shown in fig. 3.17.

| Reaction | k [a] |
|---|---|
| $^1CH_2 + Ar \xrightarrow{k_2} {}^3CH_2 + Ar$ | $6.7 \times 10^{-13}$ |
| $^1CH_2 + H_2 \xrightarrow{k_3} CH_3 + H$ | $7.0 \times 10^{-12}$ |
| $^3CH_2 + CH_3 \xrightarrow{k_8} C_2H_4 + H$ | $7.0 \times 10^{-11}$ |
| $^3CH_2 + {}^3CH_2 \xrightarrow{k_4} C_2H_2 + H_2$ | $5.3 \times 10^{-11}$ |
| $CH_3 + H \xrightarrow{k_6} CH_4$ | $10.0 \times 10^{-11}$ (800 Torr) |
| $CH_3 + CH_3 \xrightarrow{k_5} C_2H_6$ | $4.2 \times 10^{-11}$ |
| $CH_2(^1B_1) + H_2 \xrightarrow{k_{12}} CH_3 + H$ | $2.0 \times 10^{-11}$ |
| $CH_2(^1B_1) \xrightarrow{k_1} {}^1CH_2 + h\nu$ | $1.0 \times 10^{6}$ |
| $CH_2(^1B_1) + CH_2CO \xrightarrow{k_{14}} C_2H_4 + CO$ | $3.0 \times 10^{-11}$ |

Fraction of $CH_2(^1B_1)$ produced in flash, $\phi_X = 0.4$

a. Units are $cm^3$ $molecule^{-1}$ $s^{-1}$ for second order rate constants and $s^{-1}$ for first order rate constants.

There are many published values for $k_{15}$ and a reliable estimate is $1.6 \times 10^{-12}$ cm$^3$ molecule$^{-1}$ s$^{-1}$ [128]. Since $[CH_2CO] \gtrsim 20\ [C_2H_4]$ and $k_7 \simeq 1/10\ k_{15}$ this reaction may account for the removal of a small fraction of H at long times after the flash. However it will not occur to such an extent as to seriously affect the $C_2H_4$ or $C_2H_6$ concentrations. Reaction (16) occurs at a rate comparable to reaction (15) and similar considerations apply as to reaction (15). The rate constant for reaction (17) has been measured [142] over the pressure range 50 - 250 Torr argon where it obeys third order kinetics with $k_{17} = 1.4 \times 10^{-32}$ cm$^6$ molecule$^{-2}$ s$^{-1}$. If it is assumed that the reaction remains third order up to 800 Torr argon then $k_{17}$ (800 Torr argon) $= 4.0 \times 10^{-13}$ cm$^3$ molecule$^{-1}$ s$^{-1}$. This reaction may contribute to loss of H radicals.

Fig. 3.19 shows a computer fit to the photolysis products in the system 200 mTorr $CH_2CO$ / 10 Torr $H_2$ as a function of added argon pressure. The same set of rate constants shown in table 3.4 was used to obtain this fit. Apart from the inability to explain $C_2H_2$ at low pressures, this model gives a fairly reasonable fit to the experimental data. The rate constants used in the Lindemann scheme for $k_6$,

$$CH_3 + H \underset{k_D}{\overset{k_c}{\rightleftharpoons}} CH_4^*$$

$$CH_4^* + M \xrightarrow[k_S]{} CH_4$$

were $k_C = 2.0 \times 10^{-10}$ cm$^3$ molecule$^{-1}$ s$^{-1}$

$k_S = 1.0 \times 10^{-10}$ cm$^3$ molecule$^{-1}$ s$^{-1}$

$k_D = 1.0 \times 10^{9}$ s$^{-1}$.

The rate constants $k_{12}$, $k_{14}$ are dependent on the choice of $k_f$. Table 3.5 gives the variation in $k_{12}$ required to effect a fit when $k_f$ is varied.

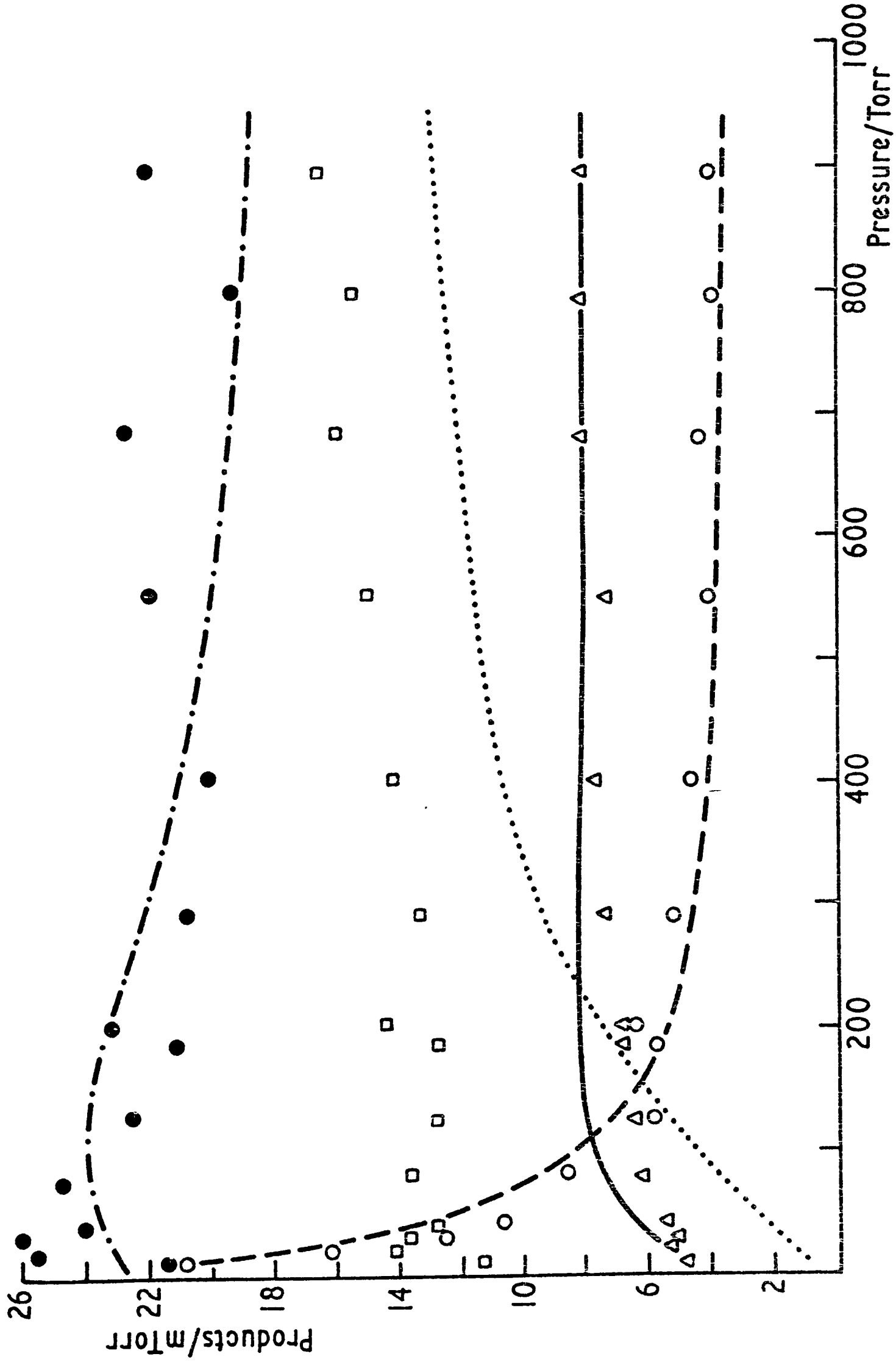



Fig. 3.19. Products from the flash photolysis of 200 mTorr $CH_2CO$ in 10 Torr $H_2$ with added argon. Computer fit to $CH_2$ ($^1B_1$) model.

Table 3.5. Variation of $k_{12}$ with $k_f$.

| $k_f$ / $s^{-1}$ | $k_{12}$ / $cm^3$ $molecule^{-1}$ $s^{-1}$ |
|---|---|
| $10^5$ | $4.0 \times 10^{-12}$ |
| $10^6$ | $2.0 \times 10^{-11}$ |
| $10^7$ | $3.0 \times 10^{-10}$ |

This model gave similarly good fits to the experimental data obtained at inert gas pressures of 200, 400, 800 Torr with addition of $H_2$.

Figs. 3.20, 3.21 show computer fits to the data of figs. 3.10, 3.11. The rate constants used in the Lindemann scheme for $k_6$ were $k_C = 2.0 \times 10^{-10}$ $cm^3$ $molecule^{-1}$ $s^{-1}$, $k_S = 4.0 \times 10^{-10}$ $cm^3$ $molecule^{-1}$ $s^{-1}$, $k_D = 1.0 \times 10^9$ $s^{-1}$. The value of $k_S$ required is $\simeq$ 4 times that in the case of argon, implying that $H_2$ is $\simeq$ 4 times more efficient than argon in deactivating $CH_4^*$.

In figs. 3.20, 3.21 $C_2H_2$ and $C_2H_4$ at high $[H_2]$ are explained by reactions (4) and (8) if a rate constant for

$$^1CH_2 + H_2 \xrightarrow{k_{18}} {}^3CH_2 + H_2 \qquad (18)$$

of $k_{18} = 1.5 \times 10^{-12}$ $cm^3$ $molecule^{-1}$ $s^{-1}$ is used. This is the upper limit placed on $k_{12}$ in ref. 41. The constancy of $[C_2H_2]$ and $[C_2H_4]$ at $200 \leq p_{H_2} \leq 400$ Torr allows a limit to be put on the rate constant for the reaction,

$$^3CH_2 + H_2 \xrightarrow{k_{19}} CH_3 + H \qquad (19)$$

of $k_{19} < 5 \times 10^{-15}$ $cm^3$ $molecule^{-1}$ $s^{-1}$.

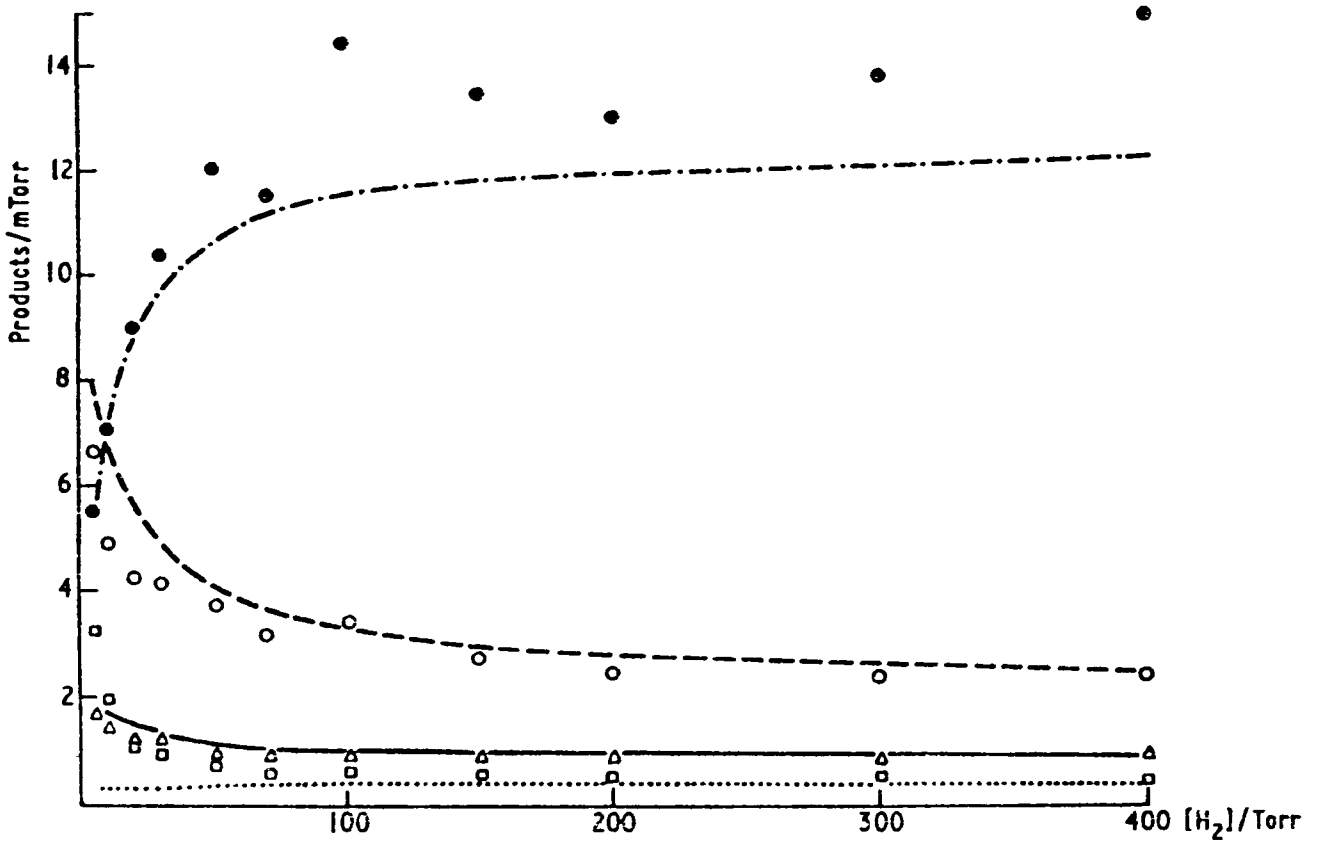



Fig. 3.20. Products from the flash photolysis of 100 mTorr $CH_2CO$ with added $H_2$.
Computer fit is for the "$CH_2$ ($^1B_1$) model".

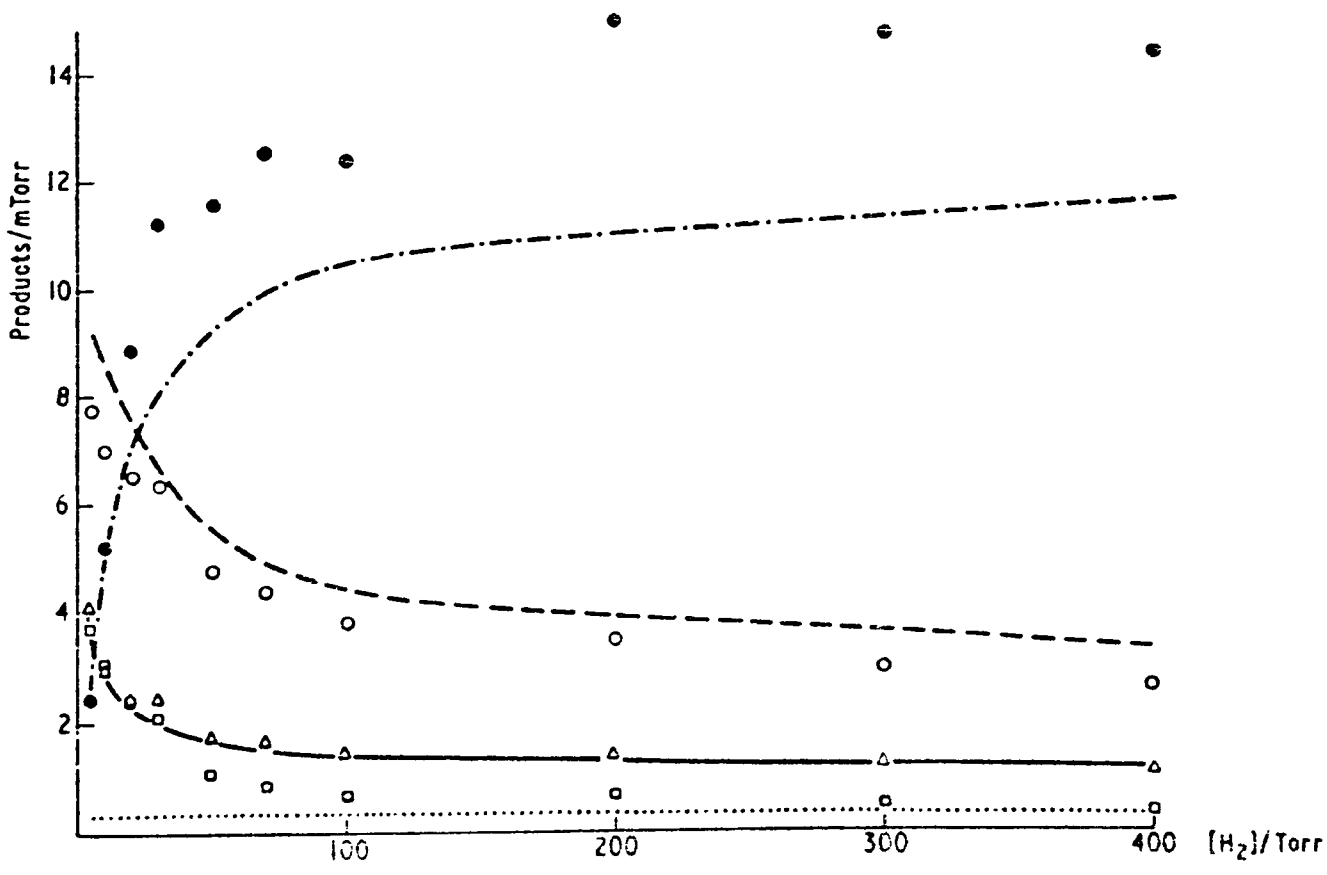



Fig. 3.21. Products from the flash photolysis of 500 mTorr $CH_2CO$ with added $H_2$.
Computer fit is for the "$CH_2$ ($^1B_1$) model".

CHAPTER 4.

## SOME REACTIONS OF METHYLENE RADICALS.

### 4.1. Ketene / argon system.

Figure 4.1 shows the products of the photolysis of 200 mTorr $CH_2CO$ in argon as a function of total pressure for $10 \leq p \leq 1000$ Torr. The total product yield remained fairly constant over the pressure range studied. The major product was $C_2H_2$. A small concentration of $C_2H_4$ was formed at low pressures and decreased as the pressure increased. Some $C_2H_6$ was formed at pressures below 100 Torr but was not detected at higher pressures. In addition traces of $CH_4$ and $C_3$ hydrocarbons were detected. $CH_4$ was detected at all pressures but its concentration was always less than 1.0 mTorr, and, due to the presence of background $CH_4$ ($\simeq$ 0.5 mTorr), it was impossible to measure accurately. The $C_3$ hydrocarbons are discussed in section 4.2.

Since the completion of the work described here Laufer and Bass [80] have reported similar results for photolysis of $CH_2CO$ in helium, but with two significant differences. Firstly they found that $C_2H_4$ was not present at high inert gas pressures, and secondly they did not report the presence of $C_2H_6$ at low inert gas pressures. Their results were consistent with the following scheme:

$$CH_2CO + h\nu \longrightarrow {}^1CH_2 + CO \qquad (1)$$

$${}^1CH_2 + CH_2CO \xrightarrow{k_9} C_2H_4 + CO \qquad (9)$$

$${}^1CH_2 + M \xrightarrow{k_2} {}^3CH_2 + M \qquad (2)$$

$${}^3CH_2 + {}^3CH_2 \xrightarrow{k_4} C_2H_2 + H_2 \qquad (4)$$

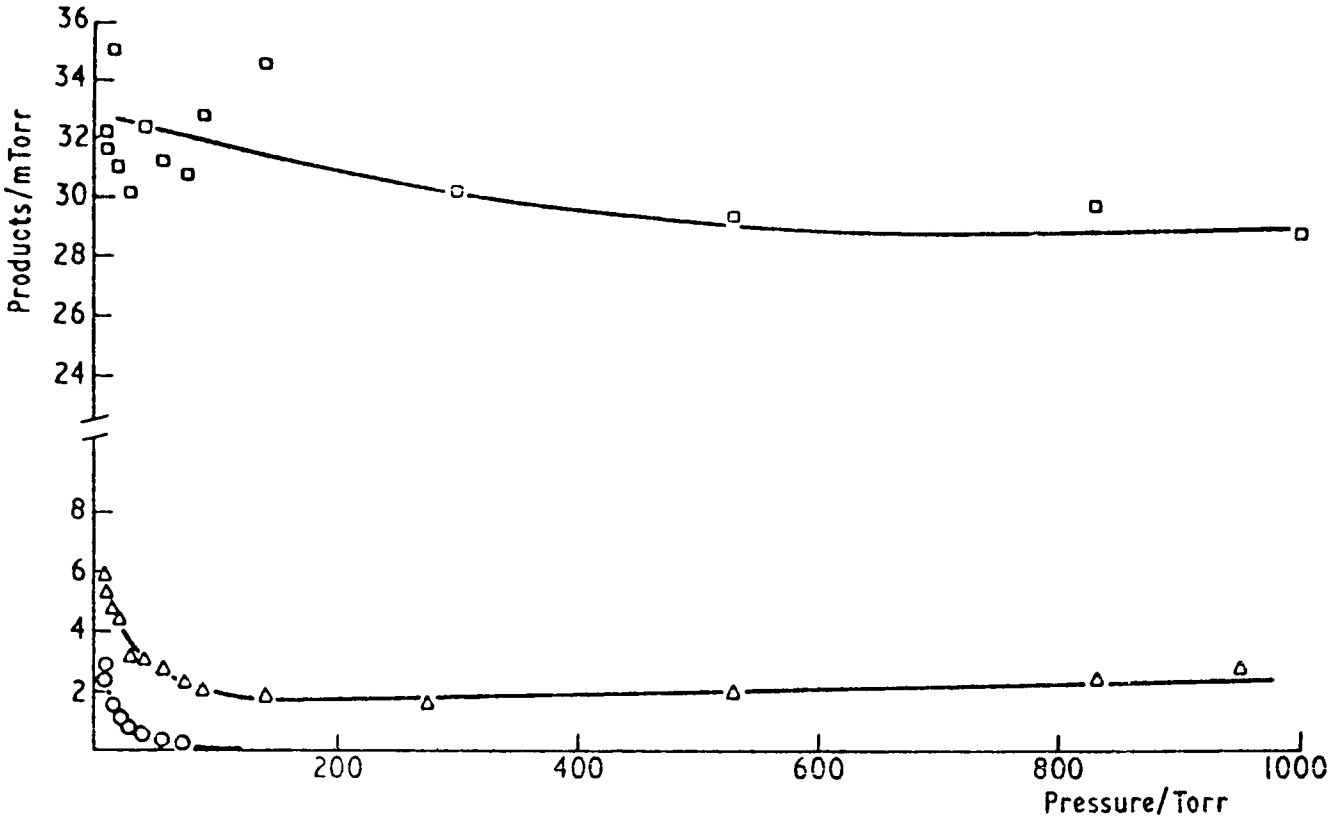



Fig. 4.1. Products from the flash photolysis of 200 mTorr $CH_2CO$ with added argon.

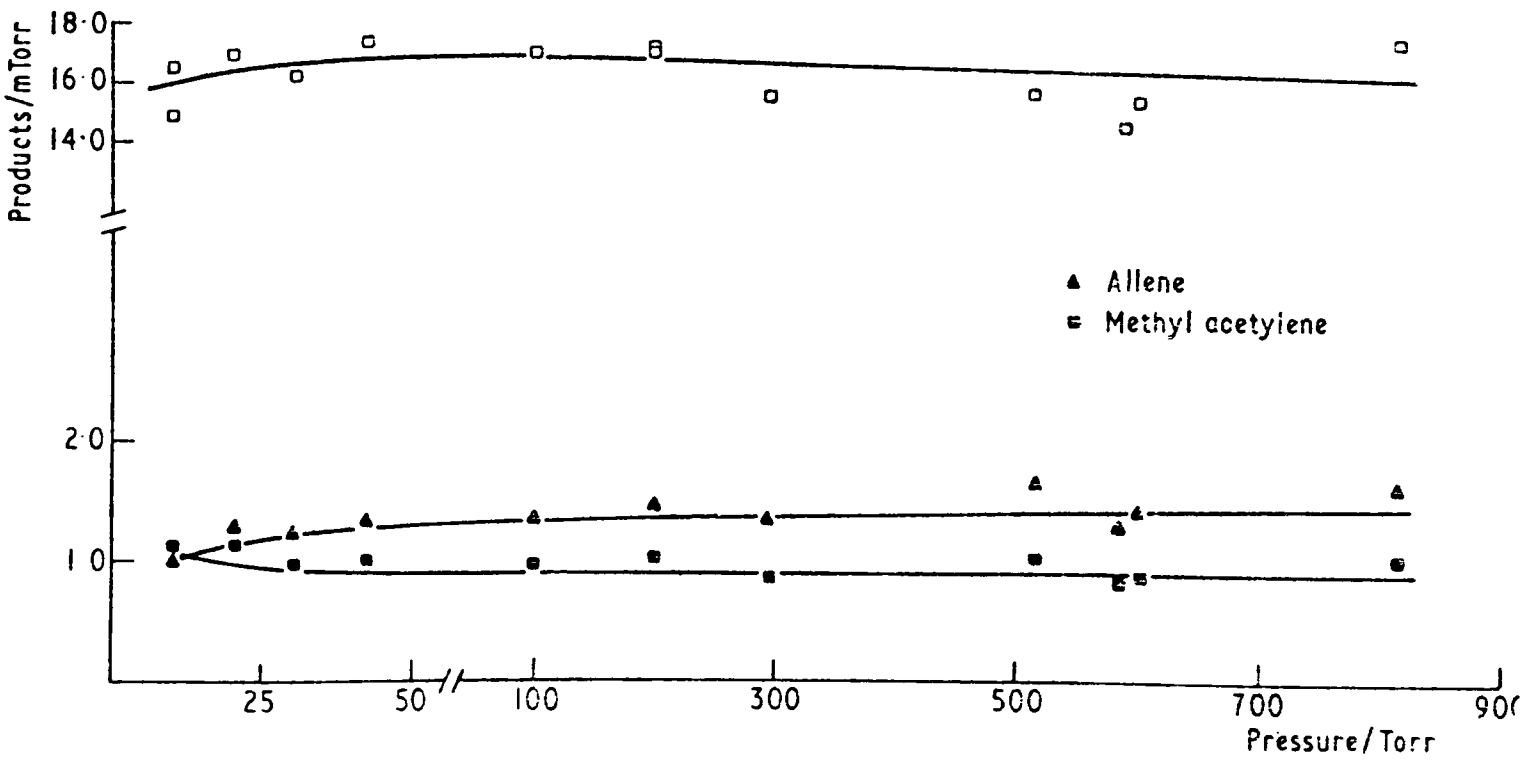



Fig. 4.2. $C_3$ products from the flash photolysis of 200 mTorr $CH_2CO$ with added argon.

M is the inert gas.

At low pressure reaction (9) was favoured and the increase in $[C_2H_4]$ at low pressures allowed the estimation of $k_9 = 3.2 \times 10^{-11}$ cm$^3$ molecule$^{-1}$ s$^{-1}$ by comparison with $k_2 = 3.0 \times 10^{-13}$ cm$^3$ molecule$^{-1}$ s$^{-1}$ for M ≡ He [41].

The data of fig. 4.1 are consistent with the following expanded scheme:

$$CH_2CO + h\nu \longrightarrow {}^1CH_2 + CO \qquad (1)$$

$${}^1CH_2 + CH_2CO \xrightarrow{k_9} C_2H_4 + CO \qquad (9)$$

$${}^1CH_2 + M \xrightarrow{k_2} {}^3CH_2 + M \qquad (2)$$

$${}^3CH_2 + {}^3CH_2 \xrightarrow{k_4} C_2H_4^* \longrightarrow C_2H_2 + (H_2 \text{ or } 2H) \qquad (4)$$

$$H + CH_2CO \xrightarrow{k_7} CH_3 + CO \qquad (7)$$

$$CH_3 + {}^3CH_2 \xrightarrow{k_8} C_2H_4 + H \qquad (8)$$

$$CH_3 + CH_3 \xrightarrow{k_5} C_2H_6 \qquad (5)$$

$C_2H_6$ is explained by the production of H radicals from $C_2H_4^*$ formed in reaction (4). Since $[C_2H_6]$ is only present at low pressures the production of H radicals is assumed to be pressure dependent, and absence of $C_2H_6$ at high pressures may be taken as evidence that at high pressures reaction (4) proceeds by molecular elimination of $H_2$. An alternative reaction which would produce $C_2H_6$ is,

$${}^3CH_2 + {}^3CH_2 \rightarrow C_2H_4^* \rightarrow CH_3 + CH \qquad (15)$$

CH radicals could then undergo the following reactions,

$$CH + CH \longrightarrow C_2H_2$$

$$CH + {}^3CH_2 \longrightarrow C_2H_2 + H$$

The kinetic scheme was investigated by computation assuming reaction (4) to be the sole source of $CH_3$ radicals (via reaction (7)). In order to fit the experimentally observed $[C_2H_6]$ at p = 10 Torr, the fraction of $C_2H_4^*$ decomposing to give $C_2H_2$ + 2H was 0.10. The following Lindemann type scheme was assumed:

$$^3CH_2 + {}^3CH_2 \xrightarrow{k_4} C_2H_4^{**} \xrightarrow{k_{17}} C_2H_2 + 2H$$

$$C_2H_4^{**} \xrightarrow{+M,\ k_{16}} C_2H_4^* \quad (E_0(1))$$

$$C_2H_4^* \longrightarrow C_2H_2 + H_2$$

$$C_2H_4^* \xrightarrow{+M} C_2H_4 \quad (E_0(2))$$

In this scheme production of H radicals is pressure dependent according to the equation,

$$\frac{d[H]}{dt} = 2 \phi k_4 \left[{}^3CH_2\right]^2$$

where $\phi = 1 / (1 + k_{16}p/k_{17})$

To fit the curve of the $[C_2H_6]$ fall off $p_{\frac{1}{2}}$ = 1.5 Torr was required. In this mechanism $CH_3$ is responsible, via reaction (8), for the production of some $C_2H_4$. The rate constant for reaction (9) required to fit the experimental $[C_2H_4]$ was now, $k_9 = 3.5 \times 10^{-12}$ cm$^3$ molecule$^{-1}$ s$^{-1}$. This is a factor of 10 smaller than the value proposed by Laufer and Bass [80].

$C_2H_4$ at high pressure may be explained either by stabilization of $C_2H_4^*$ in the above scheme, or by reaction of $CH_2$ ($^1B_1$) with $CH_2CO$.

$$CH_2\ (^1B_1) + CH_2CO \xrightarrow{k_{14}} C_2H_4 + CO \qquad (14)$$

Stabilization of $C_2H_4^*$ by collision is considered unlikely in the light of RRKM calculations discussed in chapter 5. However, such a mechanism may have contributed to the very slight rise in $[C_2H_4]$ as the pressure was increased from 300 Torr to 1000 Torr. A mechanism which fits in with the previous model is reaction (14). The rate constant required to fit $[C_2H_4]_{experimental}$ was $k_{14} = 2.0 \times 10^{-11}$ $cm^3$ $molecule^{-1}$ $s^{-1}$ (assuming $k_f = 1.0 \times 10^6$ $s^{-1}$), which may be compared with the value of $3.0 \times 10^{-11}$ suggested in chapter 3. This reaction will be a source of $C_2H_4$ at all pressures and has been taken into account in the estimation of $k_9$ above.

This scheme described the product variation with pressure adequately. It also explained (quantitatively) the product variation in a similar experiment where 100 mTorr $CH_2CO$ was photolysed in argon. It was impossible to investigate a system at much higher concentrations of $CH_2CO$ than 200 mTorr since non uniform absorption would set in, and the kinetics of the system would be complicated by a concentration gradient in $CH_2$.

The conclusion of the present study is that although reaction of $^1CH_2$ with $CH_2CO$ is required to explain $C_2H_4$ at low pressures, the system is complicated by the presence of a small concentration of $CH_3$ radicals, and any estimate of a rate constant for the reaction of $^1CH_2 + CH_2CO$ must be

treated with considerable caution. However it should be emphasised that under all conditions $C_2H_2$ is the major product accounting for $\gtrsim$ 80% of the $C_2$ hydrocarbons.

## 4.2 Reaction of $CH_2$ with $C_2H_2$.

The $C_3$ products from the photolysis of 200 mTorr $CH_2CO$ as a function of added argon pressure are shown in fig. 4.2. The ratio of $C_3$ products / $C_2H_2$ remained constant within experimental error at all pressures studied. Over most of the pressure range ( > 50 Torr) allene / methyl acetylene was close to 1.7 but at lower pressures this ratio decreased slightly, i.e. methyl acetylene appeared to be formed at the expense of allene. No trace of cyclopropene was found at any pressure.

$C_3H_4$ products are assumed to result from the reaction,

$$CH_2 + C_2H_2 \longrightarrow C_3H_4$$

where $C_2H_2$ is formed in the reaction,

$$^3CH_2 + {}^3CH_2 \xrightarrow{k_4} C_2H_2 + H_2 \qquad (4)$$

Frey [144] studied the reaction of $CH_2$ with $C_2H_2$. He photolysed $CH_2N_2$ in the presence of acetylene and found the products methyl acetylene and allene. Methyl acetylene was formed at higher concentrations than allene. Experiments carried out with deuterated acetylene were consistent with the occurrence of two competing processes,

$$CH_2 + CH\equiv CH \longrightarrow CH_3-C\equiv CH \qquad (i)$$

$$CH_2 + CH\equiv CH \longrightarrow \underset{\diagdown\ \diagup}{CH=CH}\ (CH_2) \longrightarrow \begin{matrix} CH_3-C\equiv CH \\ + \\ CH_2=C=CH_2 \end{matrix} \qquad (ii)$$

The cyclopropene formed in process (ii) was not stabilized at $p \leq 250$ Torr. The $CH_2$ reacting in Frey's system was presumably mainly $^1CH_2$.

The same mechanism was proposed by Terao et al. [145] who photolysed $CH_2CO$ in the near U.V. in the presence of $C_2H_2$. Again no inert gas was present and $CH_2$ would react mainly as $^1CH_2$. Terao et al. found methyl acetylene / allene = $1.5 \pm 0.3$ over the pressure range 40 - 920 Torr. No cyclopropene was detected even at 1500 Torr.

Both these results should be contrasted with the experiments of Jacox and Milligan [146] who photolysed $CH_2N_2$ in an argon matrix at 4 K. The predominant product of the reaction of $CH_2$ with $C_2H_2$ was allene. There was no spectroscopic evidence for either methyl acetylene or cyclopropene. Under these conditions $CH_2$ would be expected to react as $^3CH_2$.

These results suggest that $^3CH_2$ reacts with $C_2H_2$ to give allene as the major product whereas $^1CH_2$ reaction with $C_2H_2$ produces more methyl acetylene than allene. However this conclusion must be regarded as tentative since no account has been taken of the large temperature difference in the two cases.

The results of the present study where allene was formed in larger amounts than methyl acetylene are consistent with $CH_2$ reacting as $^3CH_2$. The kinetic scheme was assumed to be

$$^3CH_2 + {}^3CH_2 \xrightarrow{k_4} C_2H_2 + H_2 \qquad (4)$$

$$^3CH_2 + C_2H_2 \xrightarrow{k_{18}} C_3H_4 \qquad (18)$$

where $C_3H_4$ includes allene and methyl acetylene. The

expected concentrations of products were computed assuming $k_4 = 5.3 \times 10^{-11}$ cm$^3$ molecule$^{-1}$ s$^{-1}$ [41] and varying $k_{18}$. In order to fit the experimentally observed products $k_{18} = 4.0 \times 10^{-12}$ cm$^3$ molecule$^{-1}$ s$^{-1}$ was required.

The production of $CH_2$ ($^1B_1$) did not affect the above result even with a rate constant for $CH_2$ ($^1B_1$) + $C_2H_2$ of $10^{-10}$ cm$^3$ molecule$^{-1}$ s$^{-1}$ (assuming $k_f = 10^6$ s$^{-1}$). Reaction of $^1CH_2$ is most important at low pressures and even at a pressure as low as 10 Torr, $^1CH_2$ + $C_2H_2$ accounted for only 50% of the observed $C_3H_4$ when a rate constant of $1.0 \times 10^{-10}$ cm$^3$ molecule$^{-1}$ s$^{-1}$ was used. By comparison with other $^1CH_2$ reactions with hydrocarbons, this is improbable and the effect is not considered important.

Laufer and Bass [80] recently reported the formation of allene / methyl acetylene in the ratio of 2 / 1 in a similar system. This is consistent with the results given here. They estimated $k_{18} = 7.5 \pm 1.0 \times 10^{-12}$ cm$^3$ molecule$^{-1}$s$^{-1}$ but their estimation assumed a $\delta$ pulse for $^3CH_2$ production which would cause $k_{18}$ to be too high.

## 4.3 $O_2$, NO, CO as scavengers for $CH_2$.

Figure 4.3 shows the effect of added NO to the photolysis of 200 mTorr $CH_2CO$ in 200 Torr argon. Addition of approximately 100 mTorr NO caused a halving in the yield of $C_2H_2$. NO presumably scavenges $^3CH_2$ according to the reaction,

$$^3CH_2 + NO \xrightarrow{k_{19}} CH_2NO \qquad (19)$$

The addition product was not isolated. Based upon a competition mechanism between reaction (4) and reaction (19)

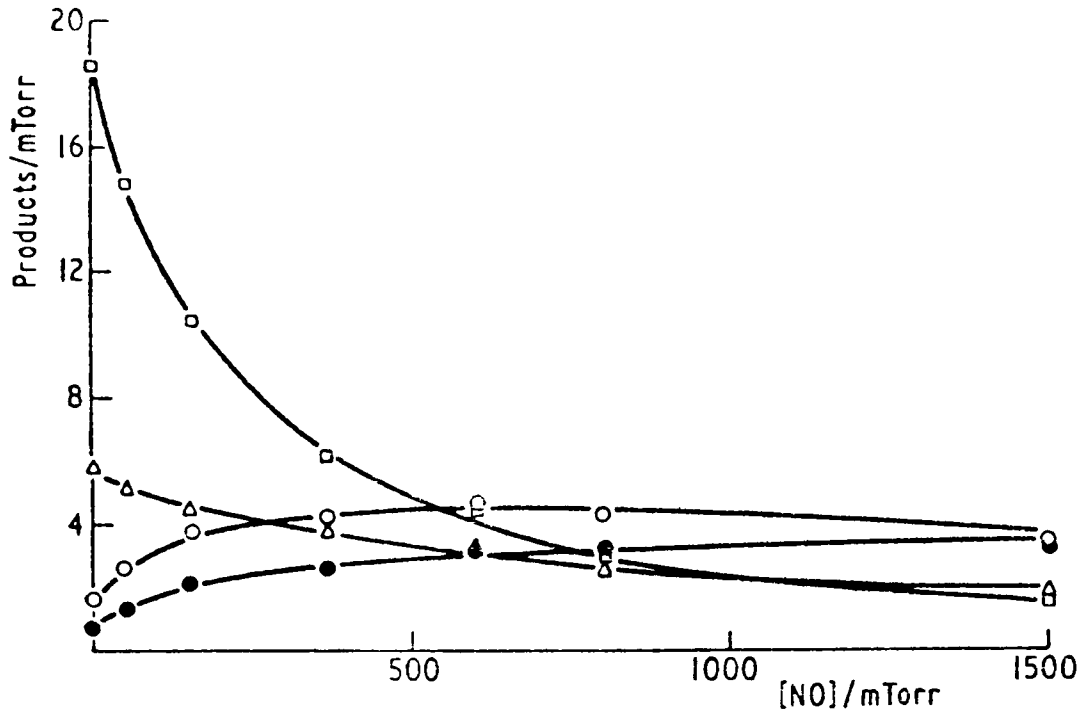



Fig. 4.4. Products from the flash photolysis of 200 mTorr $CH_2CO$ in 10 Torr argon with added nitric oxide.

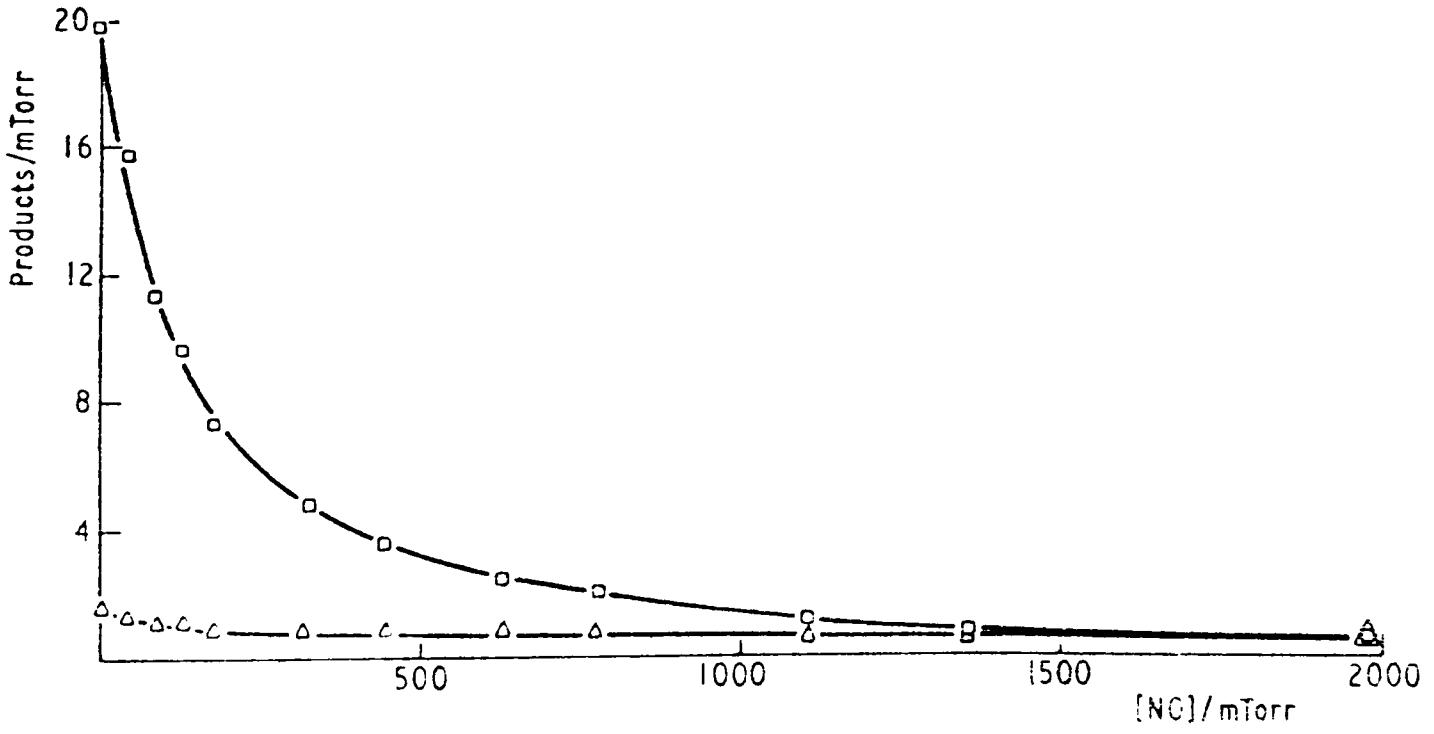



Fig. 4.3. Products from the flash photolysis of 200 mTorr $CH_2CO$ in 200 Torr argon with added nitric oxide.

a rate constant for reaction (19) was determined as $k_{19} = 1.0 \times 10^{-11}$ cm$^3$ molecule$^{-1}$ s$^{-1}$ at 200 Torr argon. This is in close agreement with Laufer and Bass [80] whose value was $1.6 \times 10^{-11}$ cm$^3$ molecule$^{-1}$ s$^{-1}$ over the pressure range 50 - 700 Torr helium.

This rate constant was determined from the fall off in $C_2H_2$ as NO was added. An important assumption was that NO did not reduce the product yield either by scavenging excited ketene molecules, or by reducing the total photolysis by absorption. The experiment was carried out in a quartz cell with a cut off in the region of 170 - 180 nm. Above 180 nm. NO has a series of absorptions [147], but all consist of sharp lines and it was considered unlikely that they would interfere to any great extent with the $CH_2CO$ absorption.

Figure 4.4 shows the products from a similar experiment carried out at a total pressure of 10 Torr argon. A rather surprising feature of this experiment was the rise in $CH_4$ and $C_2H_6$ product as NO was added. Presumably the product of the reaction between $^3CH_2$ and NO breaks up at low pressures. One of the possible fragments, H radicals, may react with $CH_2CO$ to give $CH_3$ and hence $CH_4$ and $C_2H_6$. From the fall off in $C_2H_2$ a rate constant for $^3CH_2$ + NO was determined as $k_{19} = 5.0 \times 10^{-12}$ cm$^3$ molecule$^{-1}$ s$^{-1}$ at 10 Torr argon. A fall off in $k_{19}$ at low pressures is not surprising. A similar scavenging reaction, $CH_3$ + NO, has a half pressure for stabilization of $p_{\frac{1}{2}} \simeq 500$ Torr [148].

The product $C_2H_4$ is less strongly affected by addition of NO, indicating that one of its sources is the reaction,

$$^1CH_2 + CH_2CO \longrightarrow C_2H_4 + CO$$

$^1CH_2$ reacts with $CH_2CO$ before any scavenging may take place.

However, due to the presence of minor products involving $CH_3$ radicals, it was not considered worth while to investigate the system further via a computer model.

$O_2$ is a less effective scavenger of $^3CH_2$ than NO. In the photolysis of 200 mTorr $CH_2CO$ at a pressure of 400 Torr argon, 1 Torr of $O_2$ was required to halve the yield of $C_2H_2$ (fig. 4.5) compared to 0.1 Torr of NO. In order to fit the observed fall off in $C_2H_2$ as $O_2$ was added, according to the scheme,

$$^3CH_2 + {}^3CH_2 \xrightarrow{k_4} C_2H_2 + H_2 \qquad (4)$$

$$^3CH_2 + O_2 \xrightarrow{k_{20}} \text{Products} \qquad (20)$$

a value of $k_{20} = 1.2 \times 10^{-12}$ $cm^3$ $molecule^{-1}$ $s^{-1}$ was required. This is in close agreement with the value of $1.5 \times 10^{-12}$ $cm^3$ $molecule^{-1}$ $s^{-1}$ reported by Laufer and Bass [80] over the pressure range 50 - 700 Torr helium. The addition product(s) of reaction (20) was not isolated. Rowland et al. [79], using tracer techniques, have shown that the oxides of carbon account for nearly all the methylenic carbon and suggested the following products:

$$^3CH_2 + O_2 \longrightarrow \text{Intermediate(s)} \rightarrow \begin{cases} H_2 + CO_2 \\ H_2O + CO \\ H + OH + CO \end{cases}$$

$O_2$ has two absorption bands above the quartz cut off [149], which might interfere with the ketene absorption. The weak Herzberg dissociation continuum extends from 175 - 260 nm. but

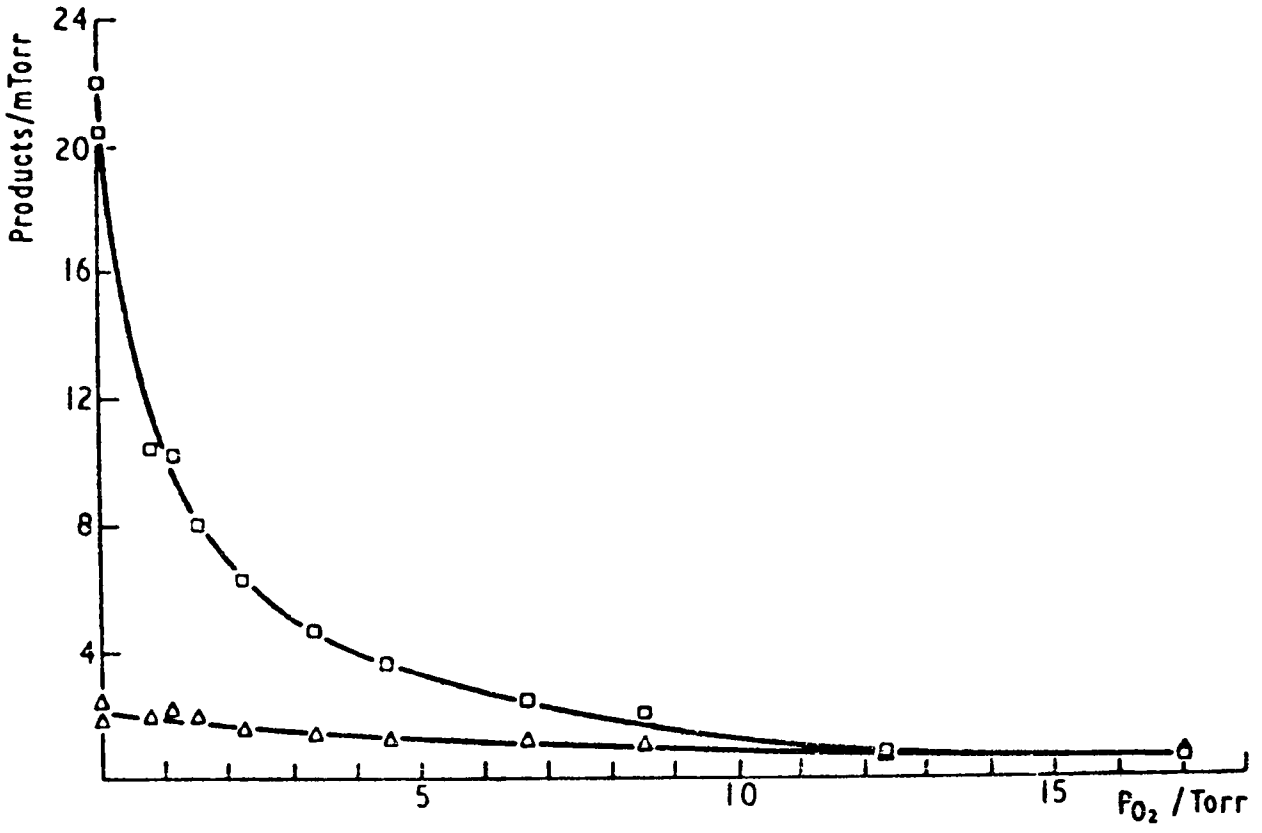



Fig. 4.5. Products from the flash photolysis of 200 mTorr $CH_2CO$ in 400 Torr argon with added oxygen.

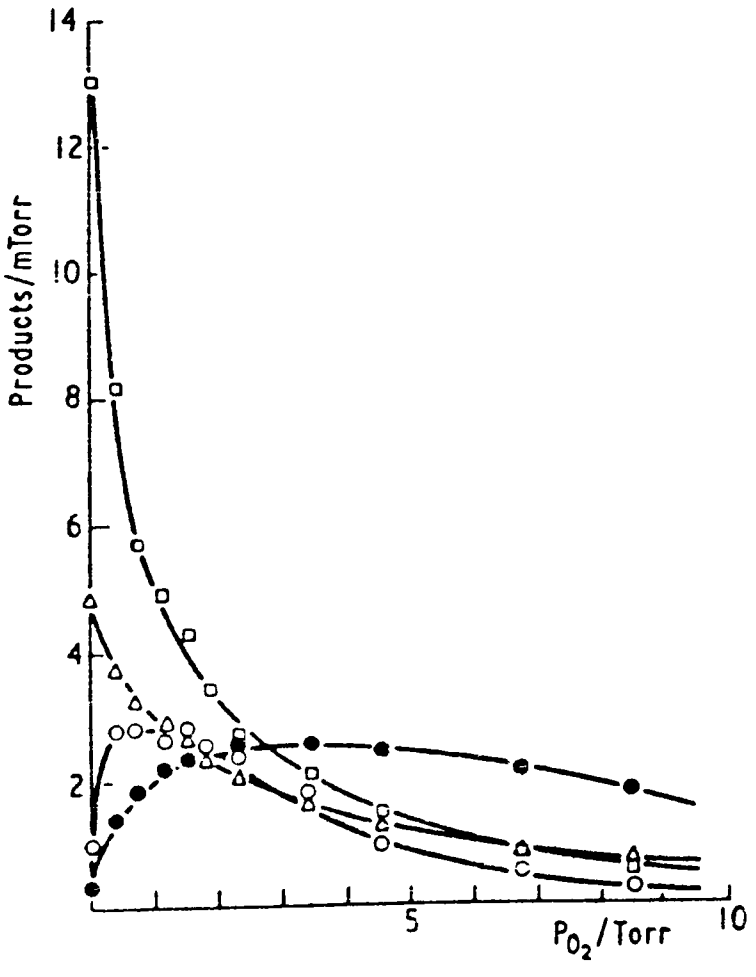



Fig. 4.6. Products from the flash photolysis of 200 mTorr $CH_2CO$ in 10 Torr argon with added oxygen.

since pressures of 1 atmosphere and path lengths of up to 10 m are necessary for measurable absorption, the absorption in the present experiments will not be significant. The absorption bands of the Schumann - Runge system extend from 175 - 200 nm. These consist of well separated rotational lines and are therefore unlikely to have a large effect on the absorption.

Figure 4.6 shows the products from photolysis of 200 mTorr $CH_2CO$ in 10 Torr argon with added $O_2$. To fit the fall in $C_2H_2$ required a value of $k_{20} = 1.2 \times 10^{-12}$ $cm^3$ $molecule^{-1}$ $s^{-1}$, the same value as at 200 Torr. As in the case of scavenging by NO at low pressure, scavenging is accompanied by an increase in $C_2H_6 + CH_4$ formed from $CH_3$ radicals, thus implying the production of H radicals in the fragments at low pressure.

Figure 4.7 shows the products from photolysis of 200 mTorr $CH_2CO$ in 10 Torr $H_2$ as a function of added CO. If the reactions of $CH_2$ ($^1B_1$) are discounted, the addition of CO has three possible effects: scavenging of $^1CH_2$; deactivation of $^1CH_2$ to $^3CH_2$; scavenging of $^3CH_2$. It is apparent from fig. 4.7, where $[C_2H_2]$ increases as $[CO]$ is increased, and does not fall off even at $[CO]$ = 300 Torr, that scavenging of $^3CH_2$ is not a fast process, and that the main effect of CO is to deactivate $^1CH_2$ to $^3CH_2$ which goes on to give $C_2H_2$.

The major difference between fig. 4.7 and, for example, fig. 3.1, where argon is added in place of CO, is that in the CO system $CH_4$ falls rapidly and $C_2H_6$ tends to zero at high pressure. The absence of "singlet products" at high pressure implies either that CO is a good scavenger for $CH_3$, or that CO intercepts $CH_2$ ($^1B_1$) before reaction with $H_2$.

This system was not investigated further due to the large

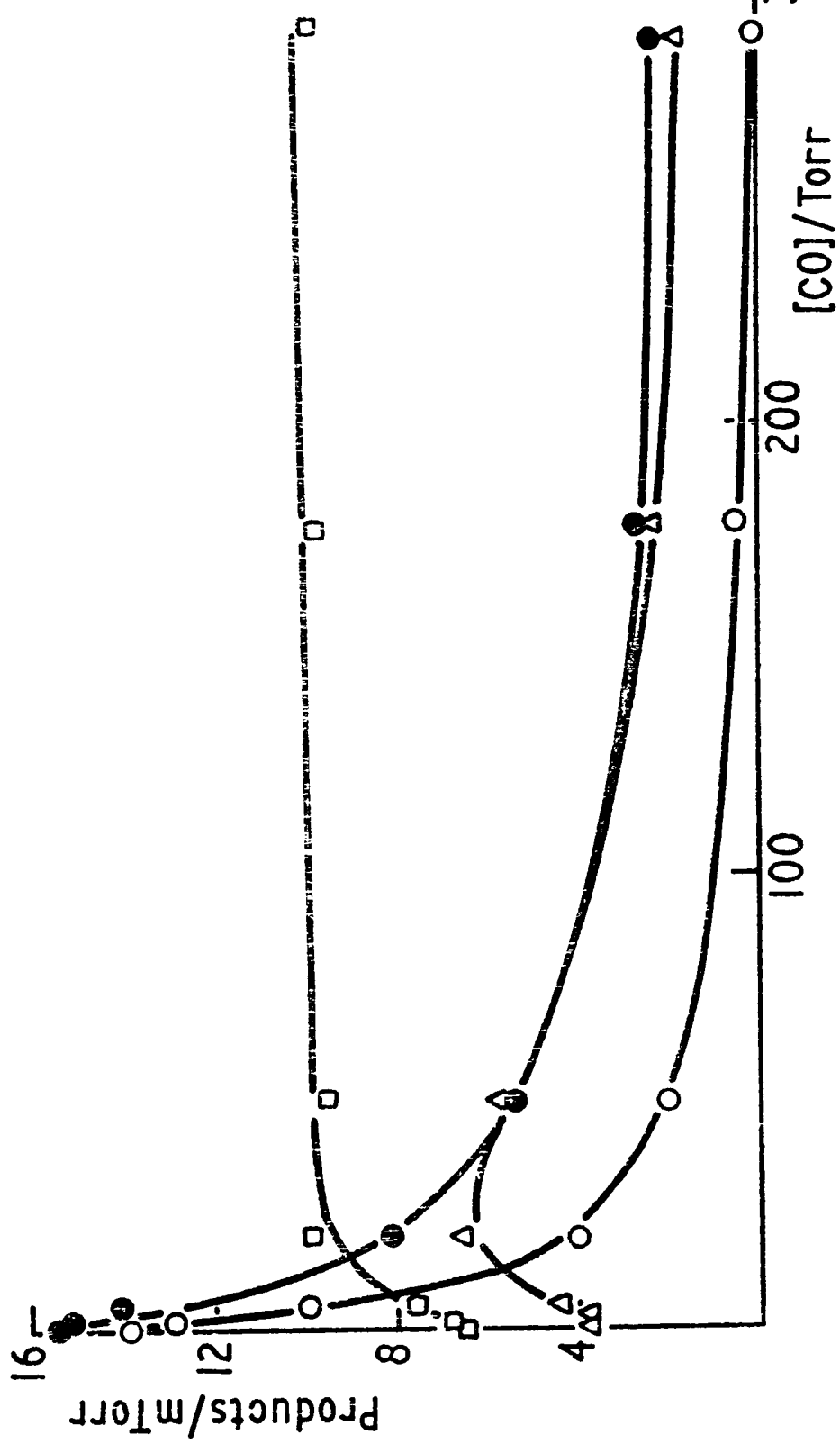



Fig. 4.7. Products from the flash photolysis of 200 mTorr $CH_2CO$ in 10 Torr $H_2$ as a function of added CO.

number of unknown rate constants in the mechanism. However the evidence that CO is a poor scavenger for $^3CH_2$ seems conclusive.

## 4.4 $CH_2CO$ / $CH_4$ system.

Reaction of $^1CH_2$ with $CH_4$ is known [70] to give vibrationally excited $C_2H_6$ which may decompose to give $CH_3$ radicals or which may be collisionally stabilized. This reaction does not produce H radicals which were a complicating feature of the $CH_2CO$ / $H_2$ system and this ought to lead to some simplification of the system. Experiments were limited to relatively small pressures ( $\leq$ 5 Torr) of $CH_4$ for two reasons. Firstly, it was difficult to obtain completely pure $CH_4$. Even 10 Torr of 99.99% pure $CH_4$ may contain 10 mTorr $C_2H_6$ as impurity which would introduce large errors to the experimental results. Secondly, on the columns used in the gas chromatographic separation it proved difficult to separate the $C_2$ hydrocarbons from $CH_4$ if more than 5 Torr of $CH_4$ were present. One disadvantageous feature was the impossibility of measuring any $CH_4$ produced or consumed in reaction (since this is a small difference between two large quantities). A sample of $CH_4$ photolysed in a suprasil reaction vessel did not yield any hydrocarbon products showing that there was no photolysis of $CH_4$ on its own. Figures 4.8 and 4.9 show the products from the photolyses of 200 mTorr $CH_2CO$ in added argon with 5 Torr, and 1 Torr $CH_4$ respectively. In both cases there was no variation in the products at pressures above 200 Torr argon. The presence of "singlet products", $C_2H_6$ and $C_2H_4$, at high pressure is not unexpected

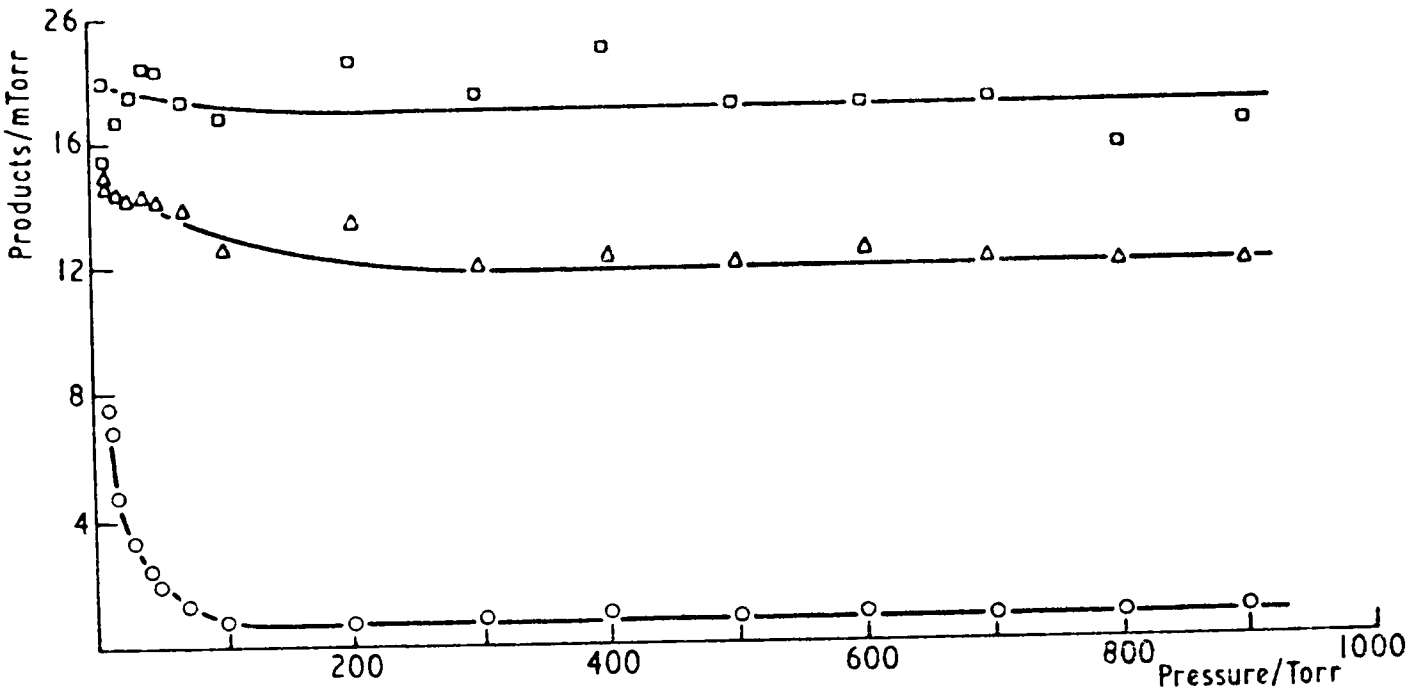



Fig. 4.9. Products from the flash photolysis of 200 mTorr $CH_2CO$ in 1 Torr $CH_4$ with added argon.

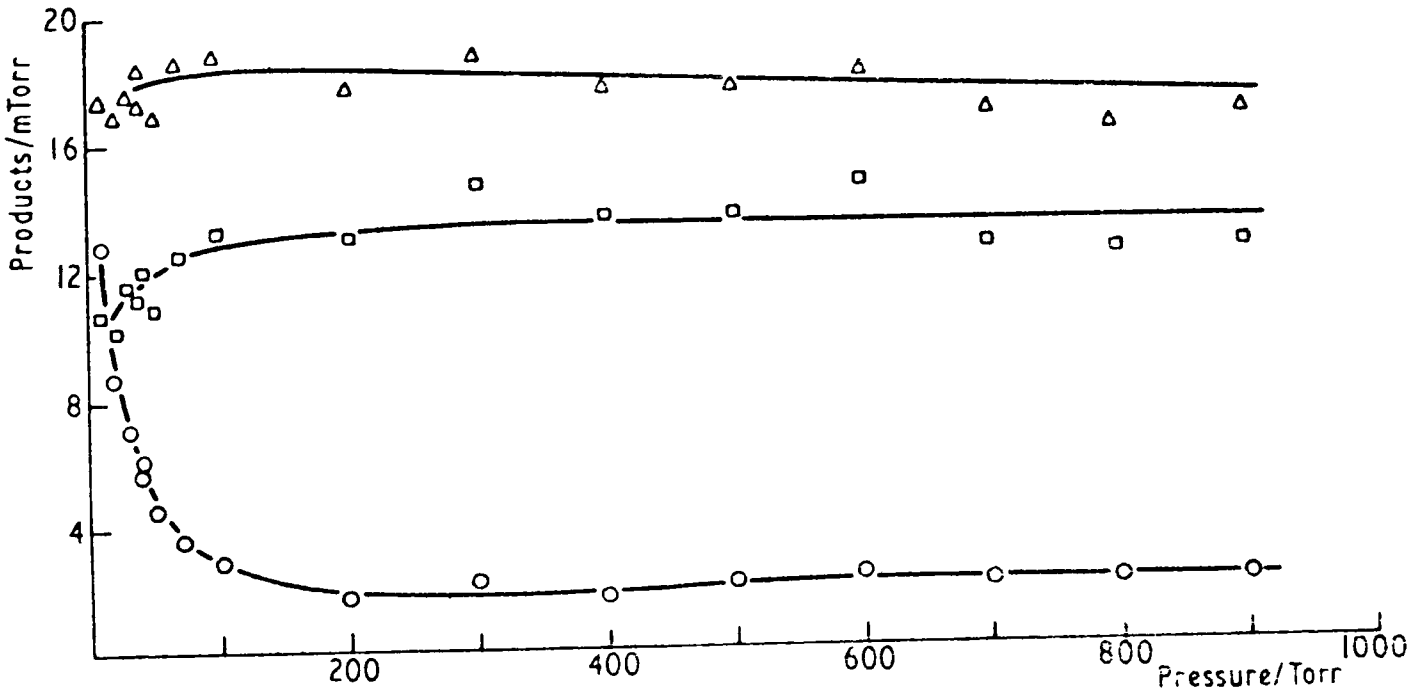



Fig. 4.8. Products from the flash photolysis of 200 mTorr $CH_2CO$ in 5 Torr $CH_4$ with added argon.

after the discussion of similar experiments with $H_2$ in place of $CH_4$.

By comparison with the $H_2$ system the expected reaction scheme is as follows:

$$CH_2CO + h\nu \longrightarrow {}^1CH_2 + CO \qquad \phi_1$$

$$CH_2CO + h\nu \longrightarrow CH_2\ ({}^1B_1) + CO \qquad \phi_2$$

$${}^1CH_2 + CH_4 \xrightarrow{k_{21}} C_2H_6^* \xrightarrow{+M} C_2H_6 \qquad (21)$$
$$\downarrow$$
$$2CH_3$$

$${}^1CH_2 + Ar \xrightarrow{k_2} {}^3CH_2 + Ar \qquad (2)$$

$${}^1CH_2 + CH_2CO \xrightarrow{k_9} C_2H_4 + CO \qquad (9)$$

$$CH_3 + CH_3 \xrightarrow{k_5} C_2H_6 \qquad (5)$$

$${}^3CH_2 + {}^3CH_2 \xrightarrow{k_4} C_2H_2 + H_2 \qquad (4)$$

$$CH_3 + {}^3CH_2 \xrightarrow{k_8} C_2H_4 + H \qquad (8)$$

$$H + CH_3 \xrightarrow{k_6} CH_4 \qquad (6)$$

$$H + CH_2CO \xrightarrow{k_7} CH_3 + CO \qquad (7)$$

$$CH_2\ ({}^1B_1) \xrightarrow{k_f} {}^1CH_2 + h\nu) \qquad (13)$$

$$CH_2\ ({}^1B_1) + CH_2CO \xrightarrow{k_{14}} C_2H_4 + CO \qquad (14)$$

$$CH_2\ ({}^1B_1) + CH_4 \xrightarrow{k_{22}} C_2H_6^* \xrightarrow{+M} C_2H_6 \qquad (22)$$
$$\downarrow$$
$$2CH_3$$

In this scheme the "singlet products" at high pressure are accounted for by reactions (22) and (14). At first sight this mechanism seems to be reasonable. As the pressure of $CH_4$ is increased from 1 Torr to 5 Torr, the "singlet

products" at high pressure increase and $C_2H_2$ decreases. The increase in $C_2H_6$ at low pressure is attributed to reaction (21).

Estimates of all the rate constants in the scheme with the exception of $k_{21}$ and $k_{22}$ were available from the work described earlier and, using these, the expected products were computed. At high pressure, $k_{22}$ was varied to fit the observed $C_2H_6$. This procedure led to an underestimate in $[C_2H_4]$ by approximately a factor of $\frac{1}{2}$, and an overestimate in $[C_2H_2]$ by a factor of 2. (The computed total photolysis yield was adjusted to give the correct overall yield.)

In the model the main reactions which determine the products from $^3CH_2$ and $CH_3$ are (4), (5), and (8). The "best" estimates of rate constants for these reactions are $k_4 = 5.3 \times 10^{-11}$ cm$^3$ molecule$^{-1}$ s$^{-1}$, $k_5 = 4.2 \times 10^{-11}$ cm$^3$ molecule$^{-1}$ s$^{-1}$, and $k_8 = 5.0 \times 10^{-11}$ cm$^3$ molecule$^{-1}$ s$^{-1}$. In order to compute a fit to the experimental products it was found necessary to reduce $k_4$ to $1.5 \times 10^{-11}$ cm$^3$ molecule$^{-1}$ s$^{-1}$, and to increase $k_8$ to $10.0 \times 10^{-11}$ cm$^3$ molecule$^{-1}$ s$^{-1}$, i.e. the ratio of $k_8$ / $k_4$ required an increase by a factor of 7. Such an increase lies outside the expected error in $k_8$ and $k_4$, and indicated that the mechanism was not entirely correct. $C_2H_4$ appears to be formed by some other reaction. An obvious candidate is reaction (14). From the previous fits in the $H_2$ / $CH_2CO$ system $k_{14}$ was estimated as $3.0 \times 10^{-11}$ cm$^3$ molecule$^{-1}$ s$^{-1}$. An increase in $k_{14}$ to the gas kinetic value of $5.0 \times 10^{-10}$ cm$^3$ molecule$^{-1}$ s$^{-1}$ was barely sufficient to account for the discrepancy and, in view of the results for the $H_2$ / $CH_2CO$ system such a value seems unlikely.

Another possible source of $C_2H_4$ is the decomposition of $C_2H_6^*$ according to the reaction,

$$C_2H_6^* \longrightarrow C_2H_4 + H_2 \qquad (23)$$

Such a reaction has been postulated to explain $C_2H_4$ in the vacuum U.V. photolysis of $CH_4$ [55]. In NO scavenged photolysis of $CH_4$, $C_2H_6$ was found to increase with pressure up to approximately 1 atmosphere and this was attributed to stabilization of vibrationally excited $C_2H_6$ formed in the reaction of $^1CH_2$ with $CH_4$. $C_2H_4$ was also formed but did not have a strong dependence on pressure. Ausloos et al. [55] interpreted the absence of a pressure effect to indicate that the excited ethane intermediate had a shorter lifetime than the one leading to the formation of two methyl radicals, and suggested that a difference in the degree of excitation of the methylenes participating in the two reactions would be sufficient to account for this observation. Laufer [42] has argued against such a process, but his evidence, based on the analysis of isotopic hydrogen produced during photolysis, seems to be complicated by wall reactions. A process such as (23) would explain the observed results in the system described here.

The rise in $C_2H_6$ at pressures less than 10 Torr was attributed to reaction of $^1CH_2$ with $CH_4$ before its deactivation by argon to $^3CH_2$. A value for $k_{21}$ of $1.0 \times 10^{-12}$ cm$^3$ molecule$^{-1}$ s$^{-1}$ was required (which is a factor of 2 less than the value measured by Braun et al. [41]) to simulate the rise in $C_2H_6$. However this value does not allow for any stabilization of $C_2H_6^*$. Bell and Kistiakowsky [70] measured a half pressure for stabilization, $p_{\frac{1}{2}}$, of 2.6 Torr in

$CD_4$, and their value increases to 150 Torr when allowance is made for the secondary isotope effect. Braun et al.[41] measured $p_{\frac{1}{2}}$ = 450 Torr.

## 4.5 Inert gases as deactivators of $^1CH_2$.

The estimation of the efficiencies of the inert gases as deactivators of $^1CH_2$ from the pressure dependence of the products of an inert gas / $H_2$ / $CH_2CO$ system is complicated by the pressure dependent reaction between $CH_3$ and H. Unfortunately computer fits to the experimental data did not prove exact enough to provide unequivocal values for the rate constants of reactions,

$$^1CH_2 + M \longrightarrow {}^3CH_2 + M$$

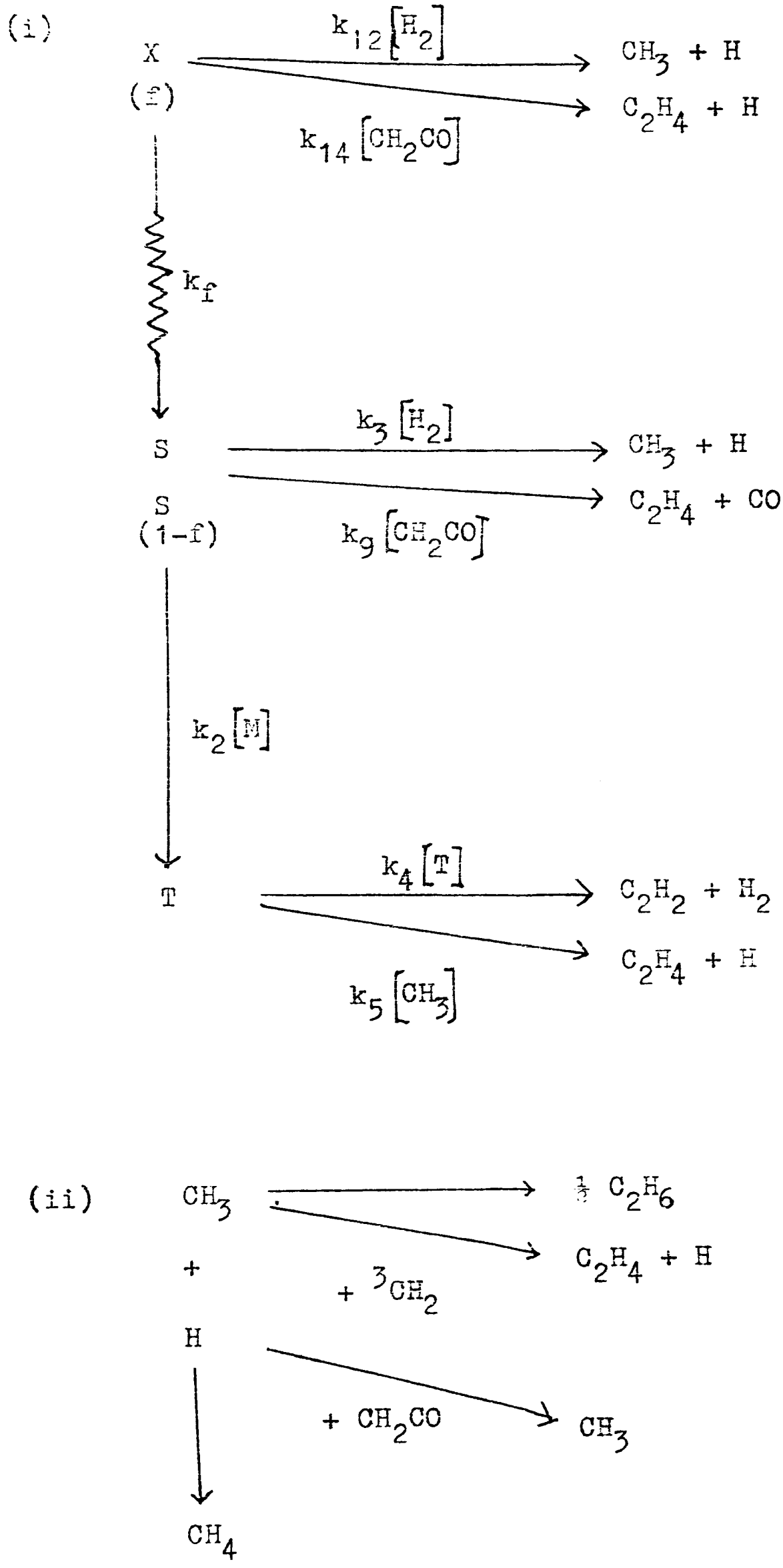
where M is an inert gas.

The reason for this is that the fall in $C_2H_6$ as pressure is increased (e.g. fig. 3.1) is critically affected by changes in the half pressure for $CH_4^*$ stabilization from $CH_3$ + H, and this quantity also depends on the nature of M.

The full reaction scheme is illustrated in fig. 4.10(i). X represents $CH_2$ ($^1B_1$); S represents $CH_2$ ($^1A_1$); and T represents $CH_2$ ($^3B_1$). $\phi_x$ is the fraction of $CH_2$ ($^1B_1$) produced in the photolysis and hence $1 - \phi_x$ is the fraction of $CH_2$ ($^1A_1$). That the inert gases have different efficiencies in deactivating $^1CH_2$ and in stabilizing $CH_4^*$ is apparent by inspection of figs. 3.1, 3.3, 3.4, and 3.5. An estimate of the efficiencies of deactivation may be made according to the following considerations.

Suppose x mTorr of $CH_3$ and x mTorr of H are produced

Fig. 4.10. Reaction scheme for " $CH_2$ ($^1B_1$) model ".



in the system. The fate of $CH_3$ is shown schematically in fig. 4.10(ii). H radicals may react with $CH_3$ to give $CH_4$, or they may react with $CH_2CO$ to give $CH_3$ + CO. $CH_3$ radicals may give $C_2H_6$ by self combination, or they may react with $^3CH_2$ to give $C_2H_4$ + H. Suppose x mTorr ( $CH_3$ + H ) leads to the formation of y mTorr $C_2H_6$ + w mTorr $CH_4$ + z mTorr $C_2H_4$. Symbolically,

$$x\left\{CH_3 + H\right\} \longrightarrow y\left\{C_2H_6\right\} + w\left\{CH_4\right\} + z\left\{C_2H_4\right\}$$

y mTorr of $C_2H_6$ is formed from 2y mTorr $CH_3$.
z mTorr of $C_2H_4$ is formed from z mTorr $CH_3$ and in addition produces z mTorr H.

$$\text{Thus } x\left\{CH_3 + H\right\} \longrightarrow y\left\{C_2H_6\right\} + z\left\{C_2H_4\right\} + (x-2y-z)\left\{CH_3\right\} + (x+z)\left\{H\right\}$$

If it is assumed that the $CH_3$ and H remaining form $CH_4$ (the excess H forming $CH_3$ by reaction with $CH_2CO$), the amount of $CH_4$ produced is (x - y) mTorr.

$$x\left\{CH_3 + H\right\} \longrightarrow y\left\{C_2H_6\right\} + z\left\{C_2H_4\right\} + (x-y)\left\{CH_4\right\}$$

thus the sum of $\left[CH_4\right] + \left[C_2H_6\right]$ gives an estimate of x.

From fig. 4.10(i),

$$\left[CH_3\right] + \left[H\right] = \text{Pulse}\left\{\frac{\Phi_x k_{12}\left[H_2\right]}{X} + \left[\frac{\Phi_x k_f}{X} + (1-\Phi_x)\right]\frac{k_3\left[H_2\right]}{k_3\left[H_2\right] + k_9\left[CH_2CO\right] + k_1\left[M\right]}\right\}$$

where Pulse = Total $CH_2$ produced

and $X = k_{12}\left[H_2\right] + k_{14}\left[CH_2CO\right] + k_f$

Since $[CH_3] + [H] \equiv [CH_4] + [C_2H_6]$ ,

we have

$$[CH_4] + [C_2H_6] - \frac{\text{Pulse } \phi_x k_{12} [H_2]}{X} = \left[\frac{\phi_x k_f}{X} + (1 - \phi_x)\right] \cdot \frac{\text{Pulse } k_3[H_2]}{k_3[H_2] + k_9 [CH_2CO] + k_2[M]}$$

$$\therefore \left\{[CH_4] + [C_2H_6] - Y\right\}^{-1} = Z\left\{1 + \frac{k_9 [CH_2CO]}{k_3 [H_2]} + \frac{k_2 [M]}{k_3 [H_2]}\right\}$$

where $Y = \frac{\text{Pulse } \phi_x k_{12} [H_2]}{X}$ is simply the singlet product in the limit of high pressure i.e. $[CH_4] + [C_2H_6]$ at high pressure.

$Z = \text{Pulse } \frac{\phi_x k_f}{X} + (1-\phi_x)$ is a constant term.

A plot of $\left\{[CH_4] + [C_2H_6] - Y\right\}^{-1}$ versus $[M]$ should give a straight line with

$$\text{Slope / Intercept} = \frac{k_2}{k_3 [H_2] + k_9 [CH_2CO]}$$

For $[H_2]$ = 5 or 10 Torr, $k_3[H_2] > k_9[CH_2CO]$

and $\text{Slope / Intercept} \simeq \frac{k_2}{k_3 [H_2]}$

Thus plots of $\left\{[CH_4] + [C_2H_6] - Y\right\}^{-1}$ versus $[M]$ should allow estimates of $k_2 / k_3$. Figure 4.11 shows several such plots where Y was estimated by visual inspection of figs. 3.1, 3.3, 3.4, and 3.5.

The scatter of points is large and large errors in the

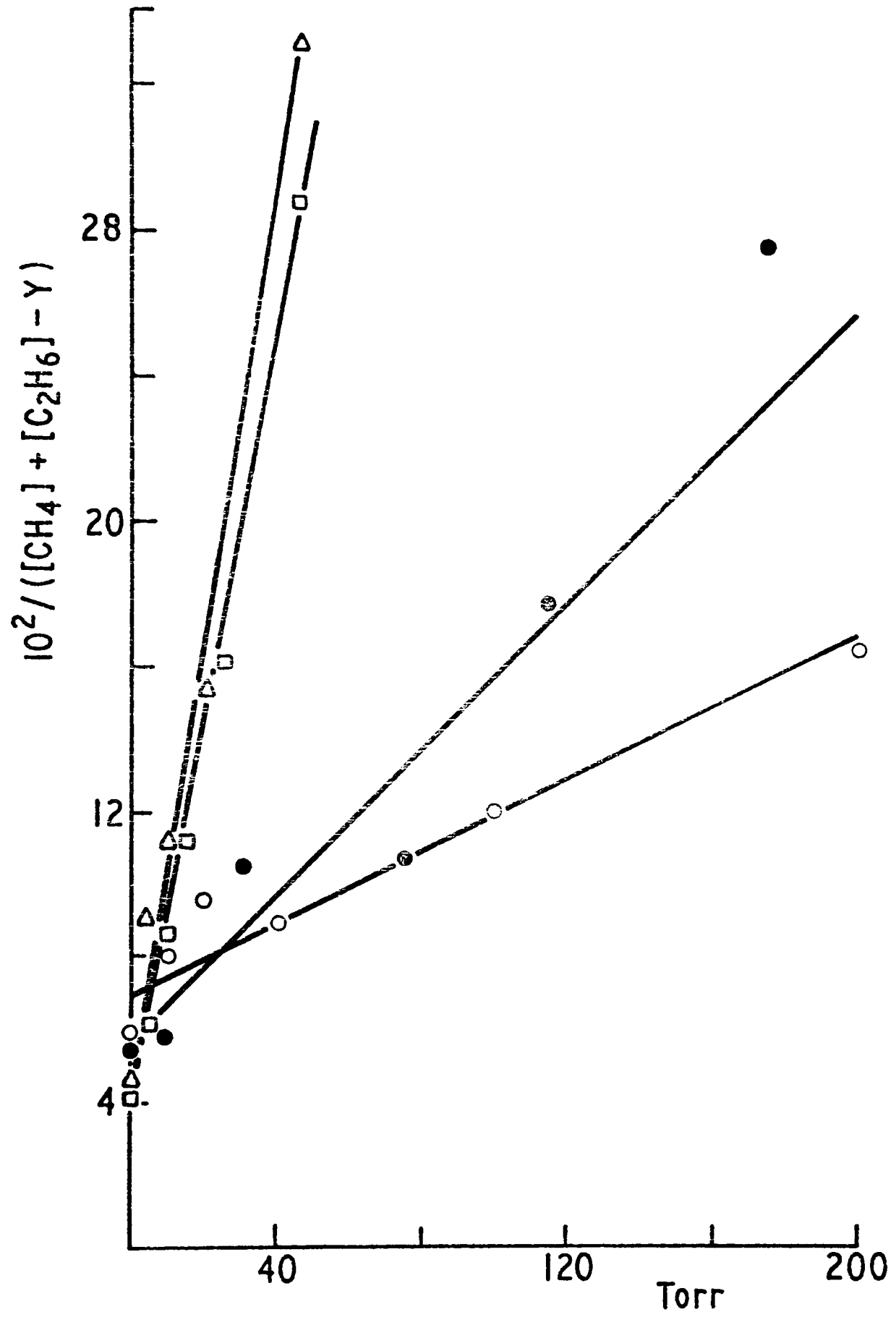



Fig.4.11. Plot to determine the efficiencies of various inert gases as deactivators of $^1CH_2$.

- ○ helium, 10 Torr $H_2$
- ● argon, 10 Torr $H_2$
- △ sulphur hexafluoride, 5 Torr $H_2$
- □ xenon, 5 Torr $H_2$

values of $k_2 / k_3$ arise particularly due to uncertainties in the intercept. However it is immediately obvious that the values of $k_2 / k_3$ take the order,

$$He < Ar < SF_6 \sim Xe$$

The actual values obtained are :

| | He | Ar | $SF_6$ | Xe |
|---|---|---|---|---|
| $k_2 / k_3$ | 0.07 | 0.17 | 0.73 | 0.67 |

The values of $k_2 / k_3$ obtained from the work of Braun et al.[41] are 0.04 for helium and 0.10 for argon. Due to the complexity of the system values of $k_2 / k_3$ cannot be obtained with a high degree of accuracy.

## 4.6 Sources of $C_2H_2$.

The origin of $C_2H_2$ at low pressures is not accounted for in any of the models discussed so far.

Kistiakowsky and Walter [40] in a study of the photolysis of ketene at 213.9 nm. attributed the production of $C_2H_2$ to the following mechanism:

$$^1CH_2 + CH_2CO \longrightarrow C_2H_4^* + CO$$

$$C_2H_4^* \longrightarrow C_2H_2 + H_2$$

$$C_2H_4^* + M \longrightarrow C_2H_4 + M$$

At high pressures $C_2H_2$ decreased due to stabilization of $C_2H_4^*$. An additional source of $C_2H_4$ was required in the analysis of their results. This was,

$$^1CH_2 + CH_2CO \longrightarrow C_2H_4 + CO$$

This interpretation suggests the existence of two types of $^1CH_2$,

one being more energetic than the other. Analysis of the results of Kistiakowsky and Walter is difficult since, under the low intensity conditions of their experiment, with high pressures ( > 10 Torr ketene), most of the absorption occurs within 1 - 2 mm. of the cell window. (In addition polymer formation was observed on the window of the photolysis vessel.)

A further source of $C_2H_2$ suggested by Kistiakowsky and Walter was via the mechanism,

$$^3CH_2 + CH_2CO \longrightarrow CH_3 + CHCO$$

$$CHCO + CHCO \longrightarrow C_2H_2 + 2CO$$

A consideration of the concentrations of $CH_2$ produced in the experiments makes the following route for $C_2H_2$ formation equally likely:

$$^3CH_2 + {}^3CH_2 \longrightarrow C_2H_2 + H_2$$

$$^3CH_2 + CH_2CO \longrightarrow C_2H_4 + CO$$

At high pressures of $CH_2CO$, $C_2H_4$ is favoured over $C_2H_2$. This consideration is based on an estimated collision efficiency for $^3CH_2 + CH_2CO$ of $\simeq 10^{-7}$ [77].

In the present system there appears to be evidence against the reaction of $^1CH_2 + CH_2CO$ being a source of $C_2H_2$ at low pressure. Consider the data of figs. 3.20 and 3.21 where 100 mTorr and 500 mTorr of $CH_2CO$ respectively was flash photolysed in $H_2$. At a pressure of 5 Torr $H_2$ (the lowest pressure used in these experiments) the $C_2H_4$ is higher in the 500 mTorr $CH_2CO$ system than in the 100 mTorr $CH_2CO$ system when the total photolysis is approximately the same in both cases. This is consistent with $^1CH_2 + CH_2CO$ being a source of $C_2H_4$.

The amount of $C_2H_2$ is roughly equal in these experiments. This implies that $^1CH_2 + CH_2CO$ is not a source of $C_2H_2$. A loophole in this argument is the possibility that $CH_2CO$ might be a very efficient deactivator of $C_2H_4^*$. Thus,

$$^1CH_2 + CH_2CO \longrightarrow C_2H_4^* \longrightarrow C_2H_2 + (H_2 \text{ or } 2H)$$

$$C_2H_4^* \xrightarrow{+\,CH_2CO} C_2H_4$$

For this mechanism to explain the experimental results would require $CH_2CO$ to be $\gtrsim 10^2$ times more efficient than $H_2$ as a deactivator for $C_2H_4^*$.

Other possibilities for $C_2H_2$ production are considered in the following discussion. The result of the variable intensity experiment (fig. 3.12) suggests that $C_2H_2$ is formed in a second order reaction. Possibilities include $CH_2$ ($^1B_1$) + $CH_2$ ($^1B_1$), $CH_2$ ($^1B_1$) + $CH_2$ ($^1A_1$), $CH_2$ ($^1B_1$) + $CH_2$ ($^3B_1$), $CH_2$ ($^1A_1$) + $CH_2$ ($^1A_1$), $CH_2$ ($^1A_1$) + $CH_2$ ($^3B_1$), and $CH_2$ ($^1B_1$) + $CH_3$. These possibilities were tested using a computer model on the assumption that all proceeded at rates equal to the calculated collision numbers. Given the accepted values for k ($^1CH_2 + H_2$) [41] and k ($CH_2$ ($^1B_1$) $\longrightarrow$ $CH_2$ ($^1A_1$)), none of the above reactions provides sufficient $C_2H_2$ (all give less than 10% of the observed $C_2H_2$).

An alternative approach to the problem is to consider the primary process. If $^3CH_2$ were produced in the photolysis flash, a finite amount of $C_2H_2$ would be expected at low pressures. In the $H_2$ / $CH_2CO$ system the decrease in $C_2H_2$ with added $H_2$ would then be explained by a slow reaction of

$^3CH_2$ with $H_2$. The model was tested by computation. In order to fit the initial fall off curve for $C_2H_2$ (this model now does not explain the production of $C_2H_2$ at high pressures of $H_2$) requires $\simeq$ 50% $^3CH_2$ to be produced in the flash, and if the reaction,

$$^3CH_2 + CH_3 \longrightarrow C_2H_4 + H$$

occurs at a rate $> 10^{-11}$ cm$^3$ molecule$^{-1}$ s$^{-1}$, the model predicts a yield of $C_2H_4$ well in excess of that observed experimentally. The model is therefore rejected.

The remaining alternative seems to be the production of some other species in the photolysis flash. Possible candidates are:

$$CH_2CO + h\nu \longrightarrow CHCO + H$$

$$CH_2CO + h\nu \longrightarrow H_2 + C_2O$$

$$CH_2CO + h\nu \longrightarrow CH + H + CO$$

$$CH_2CO + h\nu \longrightarrow C_2H_2 + O$$

The production of CH radicals was observed spectroscopically in the flash photolysis of $CH_2CO$ by Braun et al. [41], but the concentration could not be estimated since the extinction coefficient for CH has not been measured. Furthermore, CH appeared to increase as the reaction proceeded suggesting that it was produced in reaction and not in the primary process.

CHCO production was considered unlikely by Kistiakowsky and Walter [40] in the photolysis of $CH_2CO$ at $\lambda$ = 213.9 nm. This conclusion is also supported by Laufer [42], who, however, suggested $C_2O$ as a possible photolysis product. The reactions

of $C_2O$ with olefines have been studied by Bayes et al. [150]. The ground state of $C_2O$ is $\tilde{X}^3\Sigma$, and a low-lying excited state, $^1\Delta$, also exists.

In $H_2$ the reaction of $C_2O$ ($^1\Delta$) has been suggested as follows [151]:

$$C_2O\ (^1\Delta) + H_2 \longrightarrow {}^1CH_2 + CO$$

This would not explain the production of $C_2H_2$.
Although the reaction [152],

$$O\ (^3P) + C_2H_2 \longrightarrow C_2O\ (^3\Sigma) + H_2$$

has been proposed, the reverse reaction is expected to be endothermic by $\simeq$ 20 kcal $mol^{-1}$.

The origin of $C_2H_2$ is not clear. It must be produced in a mechanism inhibited by increase in pressure, since as $[C_2H_6]$ decreases additional $^3CH_2$ is produced which goes on to give $C_2H_2$. There is no observed rise in $C_2H_2$. Thus processes which form and remove $C_2H_2$ must approximately balance over this pressure range. The production via $C_2H_4^*$ (from $^1CH_2 + CH_2CO$) is attractive, but it must be remembered that over the pressure range in question the temperature rise following the flash photolysis is quite large and it may be that radical / molecule reactions with comparatively high activation energies are occurring and that these are responsible for $C_2H_2$ production. As the pressure is increased the temperature rise is moderated and any such reactions will become less important.

CHAPTER 5.

# THEORETICAL CONSIDERATIONS OF THE REACTIONS OF METHYLENE AND THE PHOTOLYSIS OF KETENE.

The purpose of this chapter is to rationalise some of the suggestions made in chapters 3 and 4 concerning, (a) the rates of decomposition of vibrationally excited molecules and the chance of collisional stabilization, and, (b) the production of various electronic states in a photolysis process and the reactivity of these states.

## 5.1. The RRKM theory.

5.1.1. Introduction. The Rice-Ramsperger-Kassel-Marcus (RRKM) theory [153] provides a method of calculating the rate of decomposition of vibrationally excited molecules. Like all statistical theories of unimolecular reactions it is based on the assumption that internal energy is statistically redistributed among all the degrees of freedom of the energised molecule on a time scale which is short compared to the lifetime for unimolecular decomposition or isomerisation. This assumption has been tested experimentally and appears to be a reasonable one. For most molecules randomisation of energy occurs in less than $5 \times 10^{-12}$ s [154].

Unimolecular decomposition of an energised molecule, $A^*$, is assumed to occur via an activated complex, $A^\dagger$.

$$A^* \longrightarrow A^\dagger \longrightarrow \text{Products}$$

The rate constant is given by,

$$k_a(E^*) = L \frac{1}{hN^*(E^*)} \sum_{E^\dagger_{vr}=0}^{E^\dagger} P(E^\dagger_{vr}) \qquad (5.1)$$

$E^*$ is the non-fixed energy contained in the active degrees of freedom of the energised molecule, $A^*$. $E_o$ is the critical energy below which reaction cannot occur. The total non-fixed energy of the activated complex, $A^\dagger$, is denoted by $E^\dagger$. $N^*(E^*)$ is the density of quantum states of $A^*$ at energy $E^*$. $\sum P(E^\dagger_{vr})$ is the number of quantum states of $A^\dagger$ at all energies up to and including $E^\dagger$. L is the statistical factor which may be considered as the number of equivalent reaction paths which lead to the formation of an activated complex. The terminology is illustrated in fig. 5.1.

Rotational energy poses a problem. It may well contribute to reaction (e.g. centrifugal force may assist a bond breaking reaction), but there may be limitations due to the requirement of conservation of angular momentum. If, as a result, a rotational degree of freedom stays in the same quantum state during the reaction (adiabatic mode), there is no random exchange of energy between that mode and the other degrees of freedom. In figure 5.1, $E_J$ is the energy of the adiabatic rotational degrees of the molecule, and $E^\dagger_J$ is the corresponding quantity for the activated complex. $E_J$, $E^\dagger_J$ are related by,

$$E_J I = E^\dagger_J I^\dagger \qquad (5.2)$$

Hence $\Delta E_J = E^\dagger_J - E_J = E^\dagger_J ( 1-I^\dagger / I )$

Energy level of reacting molecule.

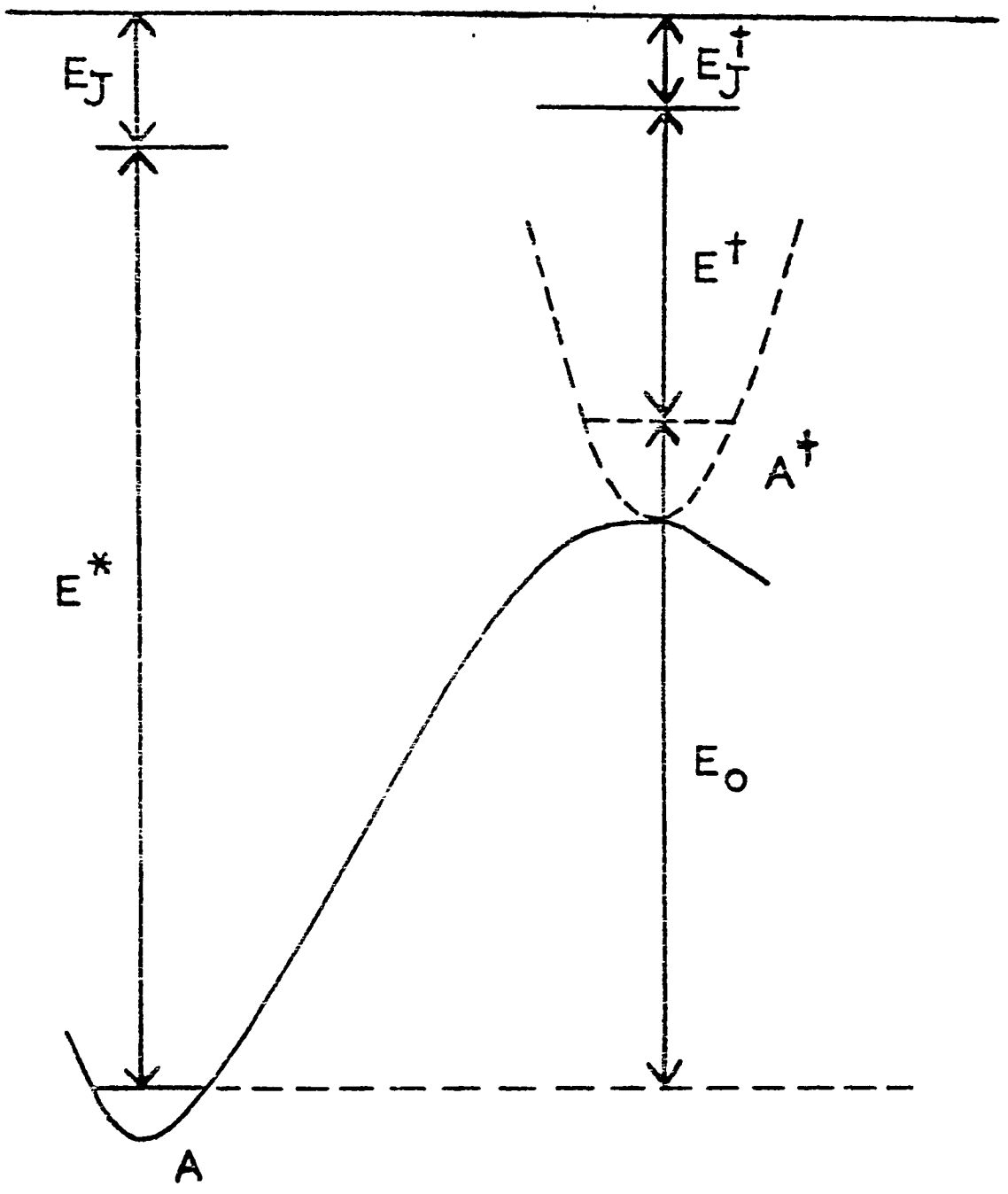



Fig. 5.1. Illustration of the energy terminology for a unimolecular reaction.

and $$\langle \Delta E_J \rangle = \langle E_J^\dagger \rangle \ ( 1 - I^\dagger / I ) \qquad (5.3)$$

where $\langle \ \rangle$ denote mean values.

$\langle E_J^\dagger \rangle$ , the average value of $E_J$ for molecules which react has been shown to be [155]

$$\langle E_J^\dagger \rangle = 1/2 \ kT \qquad (5.4)$$

where l is the number of adiabatic degrees of freedom.

From fig. 5.1,

$$E^\dagger = E^* - E_o - \Delta E_J \qquad (5.5)$$

Thus if $I^\dagger$ is considerably larger than I, $E^\dagger$ may be increased by a significant amount due to a flow of energy from the adiabatic rotations into the active degrees of freedom.

In general, all vibrations in the activated complex are treated as active and it is assumed that energy is exchanged freely between them. External rotations are generally treated as adiabatic, and internal rotations as active. However, there are cases where external and internal rotations are strongly coupled, and the assumption of an active internal rotation may necessarily imply an active external rotation. One such case is $C_2H_6$. Here the internal rotation about the C - C bond has been considered to be active [156], and hence a case could be made for treating the external rotation about the C - C bond as active. There is no rigorous method by which to decide whether a mode is active, adiabatic, or inactive.

In equation 5.1 the terms $N^*(E^*)$ and $\sum P(E^\dagger_{vr})$ may be calculated by a direct count of the vibrational states which are assumed to be harmonic. This process, however, quickly becomes time consuming at high energies, and approximate formulae (e.g. the Whitten-Rabinovitch approximation [157]) are often used. Approximations have been developed to correct for anharmonicity in the vibrations [158].

The main deficiency of RRKM theory is that the structure of the critical configuration and the vibration frequencies must be determined primarily by intuition. One constraint on the critical configuration is that the high pressure Arrhenius A factor calculated for a given critical configuration ought to agree with the experimentally measured A factor for the reaction.. However in no sense does this constraint predict a unique critical configuration. For the molecules considered in this chapter no reliable experimental data exist. A better approach is to allow RRKM theory to prescribe its own critical value of the reaction coordinate [159]. The critical configuration is chosen such that the number of internal states of the molecule is minimised. The rationale for this is the observation [160] that this type of bottleneck in molecular phase space is a prerequisite to the truth of the underlying RRKM assumptions about the randomness of molecular lifetimes.

The condition for minimum state density is

$$\frac{\partial N(E^\dagger)}{\partial r^\dagger} = 0 \qquad (5.6)$$

where $r^\dagger$ is the reaction coordinate.

In recent years RRKM theory has developed from the status

of a specialised theory to a fairly routine computational technique. A computer programme [161] has recently been made available which carries out a full RRKM calculation either for a critical configuration prescribed by the user or via the criterion of minimum state density. In the latter case the input data required are as follows:

(i) the potential energy as a function of the reaction coordinate, $V(r^{\dagger})$;

(ii) the variation of the moments of inertia of the molecule as a function of reaction coordinate. (Some of these may vary with $r^{\dagger}$);

(iii) the variation of vibrational frequencies as a function of $r^{\dagger}$.

If the reaction coordinate is chosen as the extension of a single bond, the potential energy may be based on a Morse function for a diatomic molecule [162],

$$V(r^{\dagger}) = D_e \left[1 - \exp\left(-\beta (r^{\dagger} - r_e)\right)\right]^2 \qquad (5.7)$$

where $r_e$ is the value of r corresponding to the minimum of the potential well, $D_e$ is the bond dissociation energy measured from the well minimum and $\beta$ is given by

$$\beta = 1.2177 \times 10^7 \, \omega_e \sqrt{\mu / D_e} \qquad \text{cm}^{-1} \qquad (5.8)$$

$\mu$ is the reduced mass (atomic weight units), $\omega_e$ is the frequency ($\text{cm}^{-1}$) extrapolated to the hypothetical $v = -\frac{1}{2}$ level, and $D_e$ is the bond dissociation energy ($\text{cm}^{-1}$).

In the case of a polyatomic molecule allowance must be made for zero point energy in modes other than the reaction coordinate. This is illustrated in section 5.1 .2.

The moments of inertia, $I(r^{\dagger})$, may be calculated by standard techniques [163].

The variation of vibration frequencies with $r^{\dagger}$ is a more difficult problem. In a molecule the vibration frequencies may be related to a set of force constants for a given force field. (Often a valence force field is used [164].) Empirical rules suggested by Badger and Pauling [165] relate force constants to bond length.

Pauling's definition of bond order, $n$, is

$$R = R_s - 0.60 \log_{10} n$$

where R is the bond length and $R_s$ is the length of the corresponding single bond. Badger's rule may be stated as

$$F = F_s \, 10^{(R_s - R)/b_{ij}} = F_s \, n^{0.6/b_{ij}}$$

where F is the stretching force constant between a pair of atoms i and j, and $F_s$ is the force constant for the corresponding single bond. $b_{ij}$ is a constant determined by the rows of the periodic table in which atoms i and j occur; for first row atoms $b_{ij} = 0.60$.

For a given set of force constants the frequencies may then be determined by the method of Wilson et al.[166] This procedure gives good results for bond extensions over the molecular range e.g. C - C, C = C, C ≡ C distances, but extrapolation of the formula to the much larger distances encountered in critical configurations has little empirical or theoretical justification. This method has also been used (in the absence of any other available method) to bending frequencies, but there appears to be little basis for

this since the empirical rule developed by Badger applies only to stretching frequencies.

5.1.2. Decomposition of $CH_4$. Estimates of the rate constant for the reaction,

$$CH_3 + H \xrightarrow{k_6} CH_4$$

and its pressure dependence were discussed in chapter 3. Due to the complex nature of the photolysis system, these cannot be relied on with great confidence. A suggestion is made in chapter 6 for a more direct method of measuring $k_6$, and in this section, some foundations are laid for the analysis of such projected experimental results using the RRKM technique. The approximate results obtained in chapter 3 provide a rough guide as to the likely success of such a treatment.

$CH_4$ (symmetry $T_d$) has four C - H stretching vibrations (symmetry $a_1 + f_2$) and five $CH_3$ deformations (symmetry $e + f_2$). Decomposition to $CH_3$ + H may be considered to occur with retention of $C_{3v}$ symmetry. The reaction coordinate is taken to be a C - H stretch. The remaining three C - H stretches remain as C - H stretches in the $CH_3$ radical and their frequencies are effectively unchanged. Two of the $CH_3$ deformation frequencies may be associated with the doubly degenerate $H_3 \equiv$ C - H bend. These decrease as the reaction coordinate is extended. The other three $CH_3$ deformation modes remain in the $CH_3$ radical with little change in frequency, although the frequency of one of these may decrease somewhat. ($\nu_2$ in $CH_3$ has been determined as 611 $cm^{-1}$ [167].) Table 5.1 shows the model used. In the activated complex the C - H stretching frequency is taken as

Table 5.1. RRKM Calculation on $CH_4$ decomposition.

Minimum state density calculation.

| Molecule | | | Complex | | |
|---|---|---|---|---|---|
| Motion | Number of modes | $\nu/cm^{-1}$ | Motion | Number of modes | $\nu/cm^{-1}$ |
| C-H stretch | 1 | 2914.2 | C-H stretch | 3 | 2994 |
| | 3 | 3020.3 | | | |
| Deform: :ations | 2 | 1526 | Deform: :ations | 3 | 1394 |
| | 3 | 1306.2 | | | |
| | | | $H_3C$-H bend | 2 | variable |
| Moments of inertia / amu Å$^2$ $I_x = I_y = I_z = 3.19$ | | | Moments of inertia / amu Å$^2$ $I_x = 3.19$ $I_y = I_z$ = function of r | | |

a mean of the C - H stretches in $CH_4$, and a similar procedure is adopted for the $CH_3$ deformations. The main problems with the present approach lie in estimating the variation with $r^\dagger$ of the frequencies, of $V(r^\dagger)$, and of $I^\dagger(r^\dagger)$, and the approach used is discussed at some length in the rest of this section.

The variation of the bending frequency with $r^\dagger$ may be estimated by considering the activated complex to be a triatomic molecule.

$$H_3 \equiv C \text{ --------} H$$

For a linear triatomic molecule defined by the geometry below,




the bending frequency, $\nu$ , is given by [168],

$$4\pi\nu^2 = \frac{1}{l_1^2 l_2^2}\left(\frac{l_1^2}{m_Z} + \frac{l_2^2}{m_X} + \frac{(l_1 + l_2)^2}{m_Y}\right) k_\delta \ ,$$

where $k_\delta$ is the force constant for the bend. In the present case this expression becomes,

$$\nu^2 = 1.2756 \times 10^{18}\left(\frac{0.1496}{r^2} + \frac{0.0609}{r} + 0.4167\right) k_\delta$$

where $k_\delta$ has an order of magnitude of $10^{-11} - 10^{-12}$ dynes cm radian$^{-1}$. The value of $k_\delta$ required to give $\nu$ = 1394 cm$^{-1}$ at r = 1.09 Å (equilibrium geometry) was $2.55 \times 10^{-12}$ dynes cm radian$^{-1}$.

According to Badger's rule $k_\delta$ falls off with r according to the expression,

$$k_\delta = 2.55 \times 10^{-(r-1.09)\ /\ 0.6}$$

This yields the expression for $\nu$ ,

$$\nu^2 = 3.2466.10^6 \left( \frac{0.1496}{r^2} + \frac{0.0609}{r} + 0.4167 \right) 10^{-(r-1.09)\ /\ 0.6} \qquad (5.9)$$

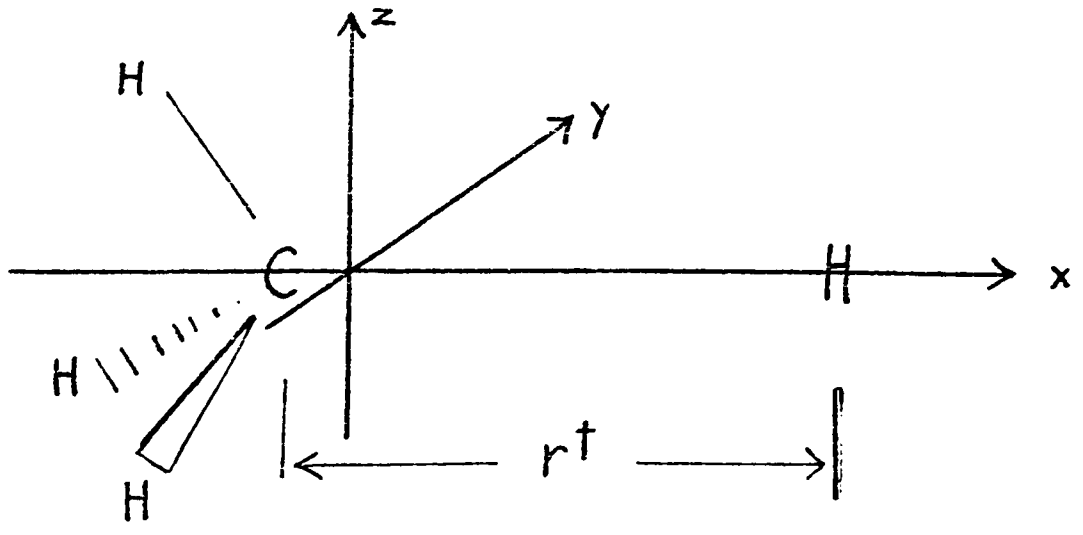
For large r ( $r \gtrsim 2.0$ A ) this reduces to the expression,

$$\nu \simeq 1394 \exp \{ -\alpha(r-1.09) \) \qquad (5.10)$$

where $\alpha \simeq 2.0$.

Equation (5.10) was used to generate $\nu$ as a function of r in preference to (5.9) and the effect of varying $\alpha$ was tested in the model. This empirical approach was followed since Badger's rule has little foundation here, and it was considered important to know how the model reacted to different frequency variations.

$CH_4$ is a spherical top with moments of inertia $I_x = I_y = I_z = 3.19$ amu $\mathring{A}^2$. If the reaction coordinate is the extension of the C - H bond lying along the x - axis then $I_x$ changes only slightly as $r^\dagger$ increases. ( In the limit, as $r^\dagger \rightarrow \infty$ and $CH_3$ becomes planar, $I_x$ increases to 3.59 amu $\mathring{A}^2$.) In the present model $I_x$ was assumed constant.



As $r^{\dagger}$ increases, the centre of mass of the molecule moves along the x - axis and $I_y$ and $I_z$ increase. A consideration of the moment of inertia of the $CH_3$ group in its fixed geometry [169] and application of the theorem of parallel axes [170] leads to the result,

$$I_y = I_z = 0.9375\ r^{\dagger 2} + 0.0683\ r^{\dagger} + 1.9779 \qquad \text{amu } \mathring{A}^2$$

The potential energy was based on a Morse function. From fig. 5.2,

$$D_e = \Delta H_{T=0} + E_z(\text{r.c.}) + E_z(CH_4) - E_z(CH_3) \qquad (5.11)$$

where $E_z(CH_3)$ is the zero point energy of $CH_3$, $E_z(CH_4)$ is the zero point energy of $CH_4$ excluding vibration in the reaction coordinate, and $E_z(\text{r.c.})$ is the zero point energy corresponding to the vibration in the reaction coordinate. $\Delta H_{T=0}$ is the enthalpy at T = 0 K of the reaction,

$$CH_4 \longrightarrow CH_3 + H$$

The lower curve in fig. 5.2 is a Morse potential based on $D_e$ = 111.1 kcal $mol^{-1}$ calculated by eq. (5.11). The upper curve was calculated by addition to the lower curve of the zero point energies of all modes except the reaction coordinate. In eq. (5.1) $E^*$ is calculated from a zero energy corresponding to the v = 0 level in this potential. This energy scale is shown in fig. 5.2. Since the frequencies of various modes change as the molecule moves along the reaction coordinate, the zero point energies of these modes change too, and to that extent cannot be considered

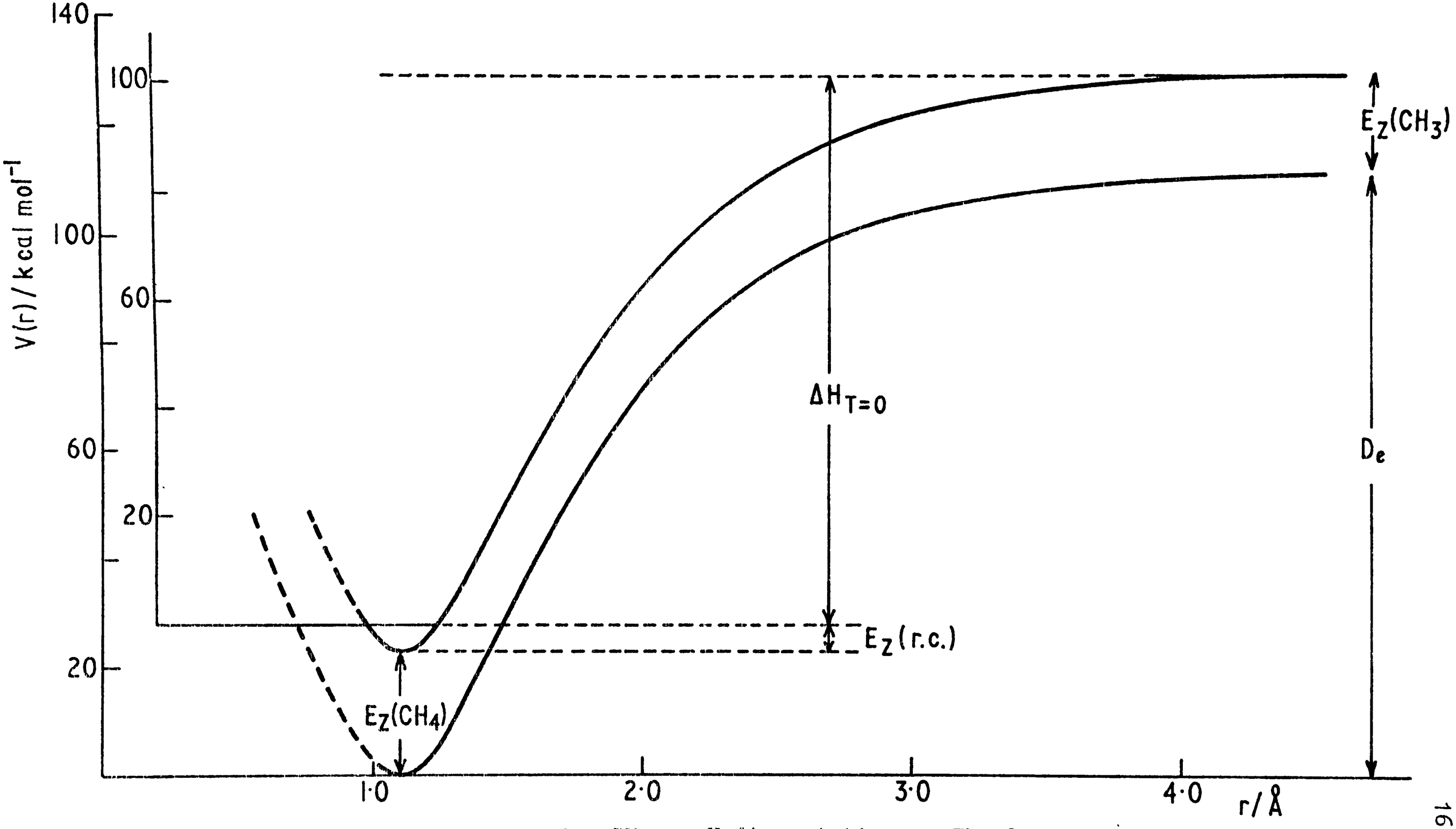



Fig.5.2. Potential energy curve for $CH_3$....H dissociation. The lower curve is a Morse potential. The upper curve corresponds to $V(r^{\dagger})$.

to be of fixed energy. The frequencies of the bending modes were assumed to vary according to eq. (5.10) (putting $\alpha$ = 2.0), and the frequency of one of the $CH_3$ deformations was assumed to decrease smoothly from 1394 $cm^{-1}$ to 611 $cm^{-1}$ in an arbitrary manner. The latter assumption introduces little error into the procedure since the zero point energy of this mode only changes by approximately 1 kcal $mol^{-1}$.

The rate constants for $CH_4$ decomposition were computed over a range of energies for various values of $\alpha$ in eq.(5.10) using the criterion of minimum state density. A selection of results is shown in table 5.2. The rate constants given are for $E^*$ = 102.5 kcal $mol^{-1}$ corresponding to $\Delta H_{T=0} + \frac{3}{2}RT$, which may be considered as an estimate of the mean energy of $CH_4^*$. Included in table 5.2 are values of $\langle E_o \rangle$. This value of the critical energy varied with the energy, $E^*$, of the dissociating molecules. As $E^*$ increased a minimum in the state density was found at smaller values of $r^\dagger$ and consequently $\langle E_o \rangle$ decreased.

As $\alpha$ is increased the value of $r^\dagger$, at which a minimum state density occurs, decreases due to the increased steepness with which the frequency falls as $r^\dagger$ is increased. Table 5.2 includes results for a model similar to that predicted by Rabinovitch and Setser [137]. They postulated an activated complex in which $CH_3$ undergoes free tumbling motions about the y and z axes. (The model is described quantitatively in table 5.3.)

Transition state theory allows the calculation of rate constants for the recombination process,

$$CH_3 + H \longrightarrow CH_4$$

Table 5.2. Rate constants for $CH_4^*$ decomposition, and for $CH_3$ + H combination for various models of the activated complex.

| $\alpha$ | $r^\dagger$/Å | $I^\dagger$/amu Å$^2$ | $\nu$/cm$^{-1}$ | $\langle E_o \rangle$/kcal mol$^{-1}$ | k/s$^{-1}$ ($E^*$=102.5kcalmol$^{-1}$) | $k_{T.S.T.}$(a) |
|---|---|---|---|---|---|---|
| 1 | 3.52 | 13.83 | 122.7 | 99.45 | $1.7 \times 10^{10}$ | $7.67 \times 10^{-11}$ |
| 1.5 | 3.20 | 11.80 | 58.7 | 97.66 | $1.3 \times 10^{11}$ | $2.16 \times 10^{-10}$ |
| 2.0 | 2.94 | 10.28 | 34.4 | 95.29 | $8.6 \times 10^{11}$ | $4.89 \times 10^{-10}$ |
| Free rotor model | 3.64 | 14.60 | ---- | 101.6 | $2.4 \times 10^{10}$ | $5.81 \times 10^{-10}$ |

(a) Units are cm$^3$ molecule$^{-1}$ s$^{-1}$.

Table 5.3. RRKM calculation on $CH_4$ decomposition.

Free rotor model [164].

| Molecule | | | Complex | | |
|---|---|---|---|---|---|
| Motion | Number of modes | $\nu$/cm$^{-1}$ | Motion | Number of modes | $\nu$/cm$^{-1}$ |
| C–H stretch | 4 | 2993 | C–H stretch | 3 | 3023 |
| Deform: :ations | 2 | 1526 | Deform: :ations | 2 | 1420 |
| | 3 | 1306 | | 1 | 950 |
| Moments of inertia / amu Å$^2$<br>$I_x = I_y = I_z = 3.19$ | | | Moments of inertia / amu Å$^2$<br>$I_x = 3.50$<br>$I_y = I_z = 14.60$<br>Internal rotations I = 1.75 | | |

The transition state theory expression is [171],

$$k_{T.S.T.} = \frac{kT}{h} \frac{Q_{CH_4}\dagger}{Q_{CH_3} Q_H}$$

where $Q_{CH_4}\dagger$ , $Q_{CH_3}$, $Q_H$ are the partition functions for $CH_4\dagger$ , $CH_3$, H respectively. To a first approximation Q may be factorised into partition functions for electronic, vibrational, rotational, and translational motion. Thus, for example,

$$Q_{CH_4} = q_{trans}^3 q_{rot}^3 q_{vib}^8 q_{electronic}$$

Calculated values of $k_{T.S.T.}$ are given in table 5.2. In the case of the free rotor model some attention must be paid to the symmetry numbers for the internal rotations.

$$Q_{CH_4} = q_{trans}^3 q_{rot}^3 q_{int.rot.}^2 q_{vib}^6 q_{electronic}$$

In the case of a molecule as simple as $CH_4$ the best approach is via a consideration of the occupied energy levels. Symmetry numbers really apply to classical partition functions, and allow for energy levels which are absent because of symmetry restrictions arising from the nuclear statistics, and the requirement that the overall wavefunction must be symmetrical (bosons) or antisymmetrical (fermions) with respect to exchange of nuclei. If the classical partition function cannot be applied (e.g. $H_2$ at low temperatures) then the symmetry number has no meaning.

Consider, for example, the case of $CH_3$ ($D_{3h}$ symmetry). Fig. 5.3 shows the rotational energy levels together with

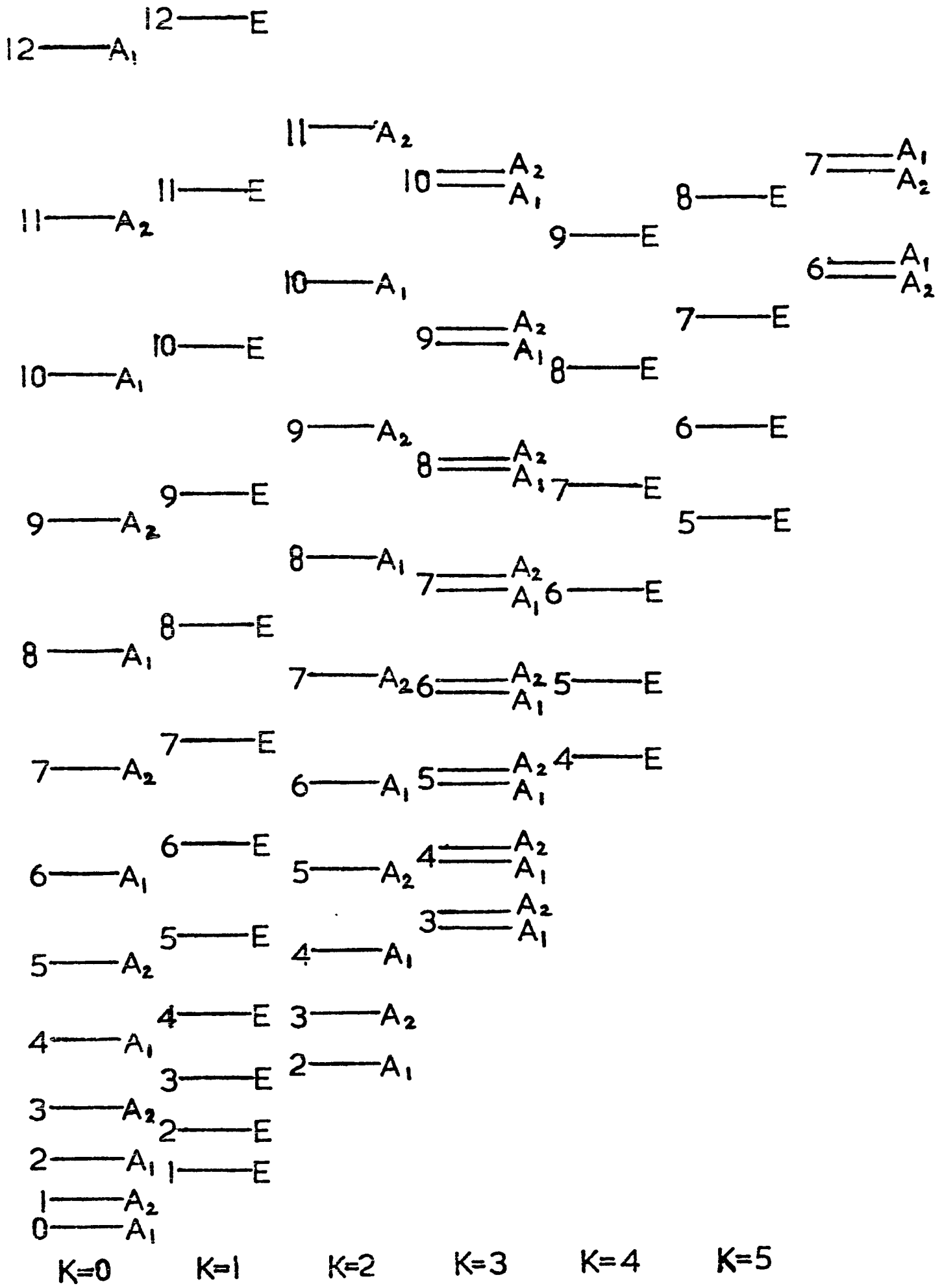
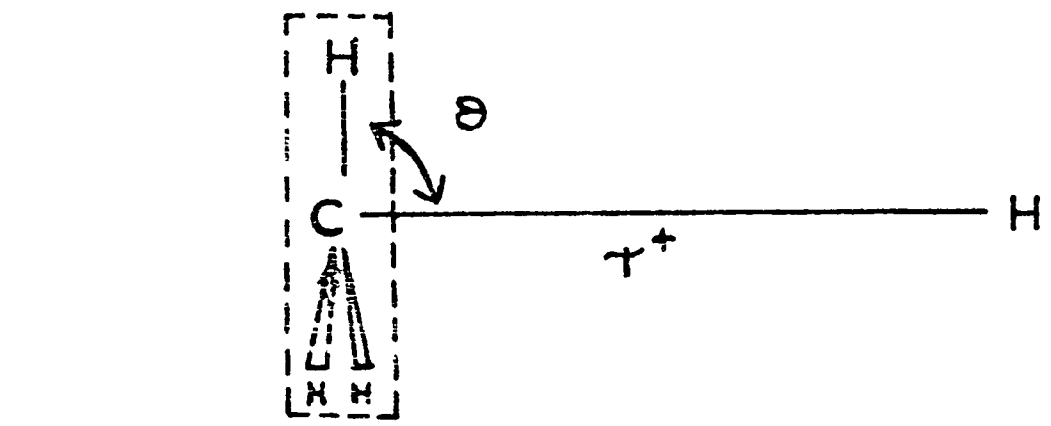


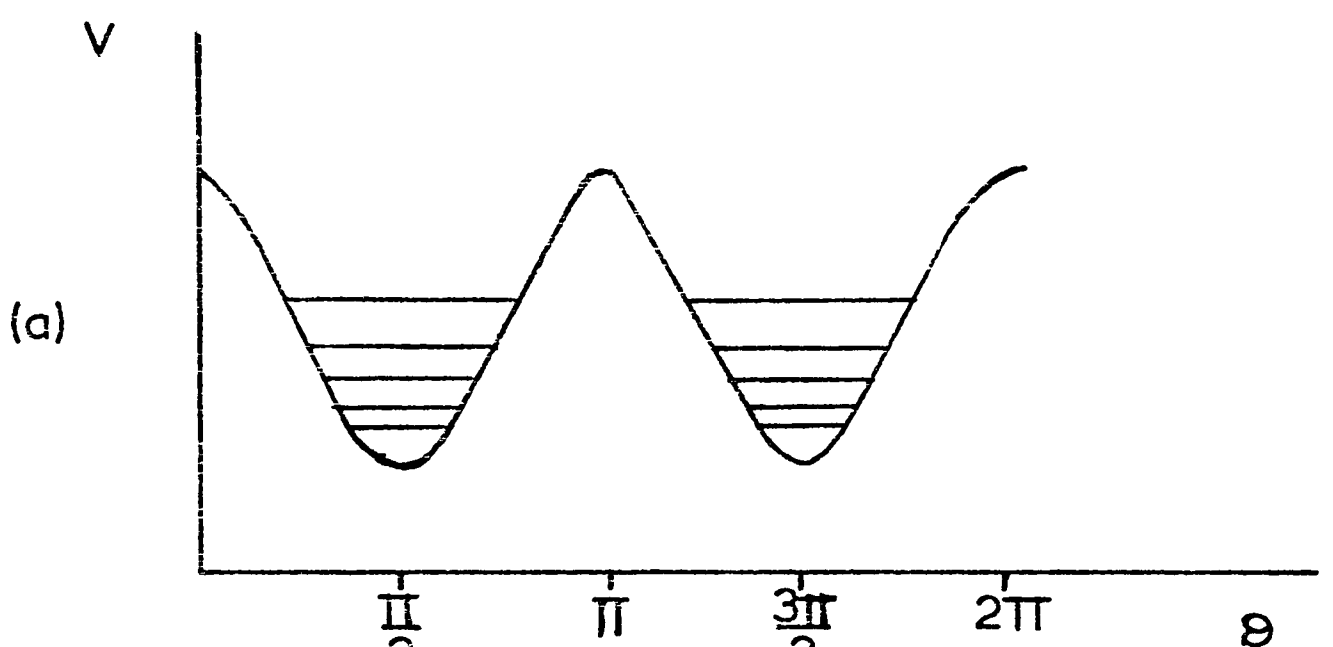

Fig. 5.3. Symmetry properties of the rotational levels of molecules with a 3-fold axis in a totally symmetric vibronic state

symmetry assignments for the molecule in a totally symmetric vibronic state. All the energy levels are present but with different nuclear spin weightings. Since we are only concerned with the fraction of levels absent, the easiest approach is to consider H as a boson of nuclear spin zero. In this hypothetical case, some of the levels are totally absent, but the fraction of disallowed levels, taking into account the nuclear spin degeneracy in the real case, is the same in both cases. Only levels with symmetry $A_1$ are allowed. Thus K = 1, 2, 4, 5, 7, 8, ... levels are absent, as are half of the K = 0, 3, 6, 9, ... levels. Hence the rotational symmetry number is 6.

In the free rotor model of $CH_4$, the $CH_3$ group will be planar (if completely free). Hence the symmetry number for internal rotation is 2, and for the figure axis 3, giving an overall symmetry number of 6. Figure 5.4 (a) shows a schematic representation of the potential as a function of $\theta$ . Both sets of levels are present. The proper point group to use is still $D_{3h}$ even though the molecule is non planar. Thus the symmetry number is still 6. (This is effectively tunnelling cf. $NH_3$ [173].) As $r^\dagger$ decreases $CH_3$ becomes non-planar and the potential wells lose their symmetry. (Fig. 5.4 (b)) In $CH_4$ one set of levels is inaccessible. Thus there is an overall reduction of 2 in the available levels and the symmetry number becomes 12. (The point group is now $T_d$.)

Table 5.2 includes calculated values of the rate constant for $CH_3$ + H combination, $k_{T.S.T.}$, for the various models. The best agreement with the values suggested in chapter 3 occurs for the model with $\alpha = 1$. The free rotor model predicts a similar half pressure for $CH_4^*$ stabilization



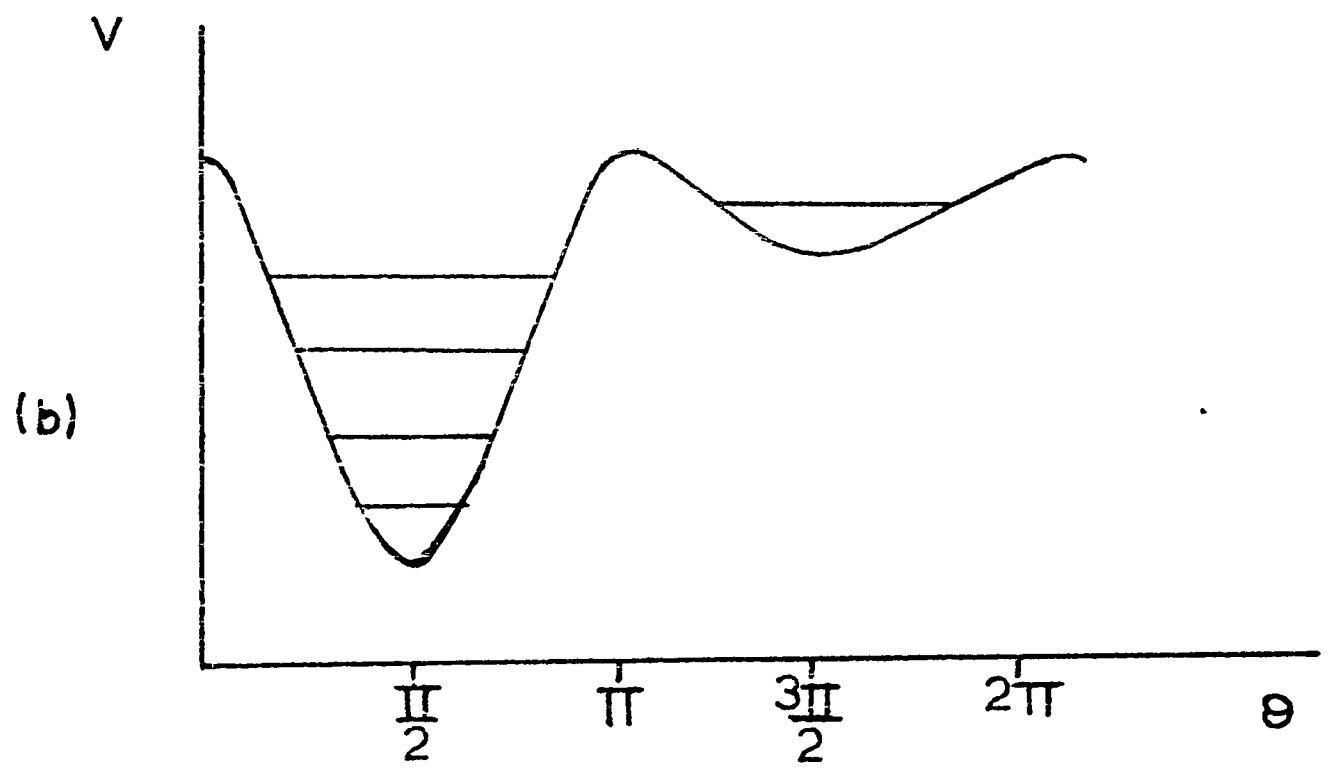
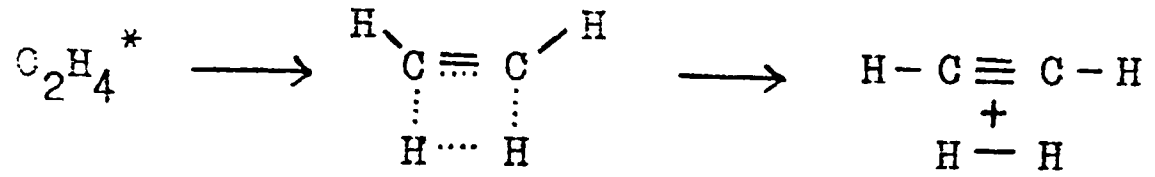



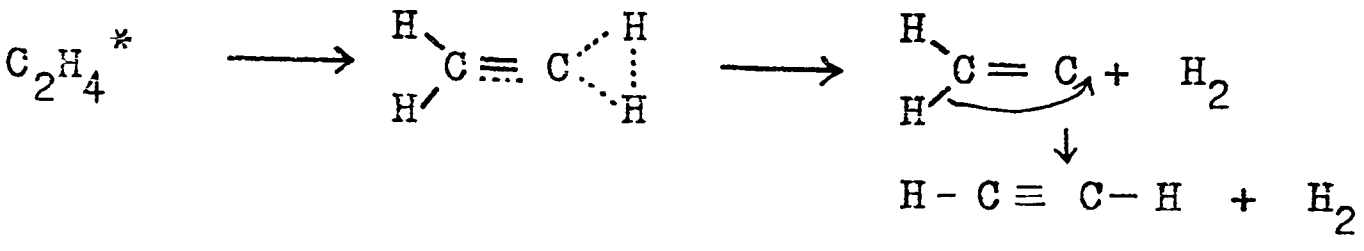

Fig. 5.4. Schematic representation of the potential energy for the internal rotations in $CH_4^+$.

but the rate constant for $CH_3$ + H combination predicted by this model is a factor of 8 higher than for the $\alpha = 1$ model. In order to compare these theoretical results with experimental data it would be necessary to average $k_a(E)$ over the distribution of energies of $CH_4^*$. The experimental data at this stage are too unreliable to merit such a treatment.

Conclusion. The calculations suggested in this section have been performed in outline only. They do, however, serve to illustrate the problems associated with the minimum density of states approach, arising largely out of a lack of knowledge of $V(r^\dagger)$ near the dissociation limit, and of the variation of the vibrational frequencies with the reaction coordinate. However, reliable experimental data could be inverted to provide information on just these parameters. This would be especially true if the reaction were studied as a function of temperature, such that the value of $\langle E_o \rangle$ were varied, and the potential function scanned over a range of $r^\dagger$ values. Alternatively, and probably more realistically, ab initio calculations of potential surfaces are now becoming fairly reliable, and computed potential parameters, coupled with experimental data, would provide a test of the RRKM method, free of arbitrary assumptions, other than those fundamental to the application of this statistical technique.

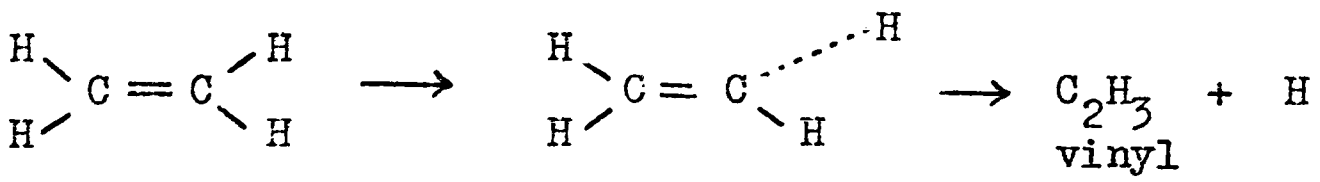
5.1.3. Decomposition of $C_2H_4$. At high pressure $C_2H_4^*$ formed by rection of $^3CH_2 + {}^3CH_2$ decomposed by molecular elimination of $H_2$ (see section 4.1). There are various possibilities for the activated complex. These include a 4 - centre structure and a 3 - centre structure.





Unfortunately, it is very difficult to assign frequencies to the transition states shown above, and RRKM calculations were not carried out.

At low pressures there is the possibility of H atom elimination, according to the mechanism,



An RRKM calculation was carried out using the model in table 5.4, to examine the possibility of producing vinyl radicals in the above reaction.

The reaction coordinate was considered to be a C - H stretch. The remaining three C - H stretches in the activated complex were assigned a mean frequency. The C = C stretch is unchanged in the activated complex, but the C = C torsion may decrease. Each $CH_2$ group in $C_2H_4$ has associated with it a "wag" (out of the molecular plane), a "rock" (in plane), and a "scissor" motion. In the

Table 5.4. RRKM Model for $C_2H_4$ decomposition [a].

| Molecule | | | Complex | | |
|---|---|---|---|---|---|
| Motion | Number of modes | $\nu$/ cm$^{-1}$ | Motion | Number of modes | $\nu$/ cm$^{-1}$ |
| 1. C-H stretch | 4 | 3055.8 | C-H stretch | 3 | 3055.8 |
| 2. C=C stretch | 1 | 1622.9 | C=C stretch | 1 | 1622.9 |
| 3. C=C torsion | 1 | 1023.0 | C=C torsion | 1 | 500 |
| 4. $CH_2$ wags | 2 | 943.0<br>949.3 | $CH_2$ wag | 1 | 946.2 |
| 5. $CH_2$ scissors | 2 | 1342.2<br>1443.5 | $CH_2$ scissor | 1 | 1392.9 |
| 6. $CH_2$ rocks | 2 | 826.0<br>1222.0 | $CH_2$ rock | 1 | 1024.0 |
| 7. | | | =C...H bend | 2 | 100 |
| 8. | | | =C-H bend | 1 | 1150 |
| Moments of inertia / amu Å$^2$<br>3.68, 16.96, 20.46 | | | Moments of inertia / amu Å$^2$<br>11.04, 20.52, 31.56 | | |

(a) $C_2H_4$ frequencies are from ref. 174.

activated complex one of each of these remains effectively unchanged, but the "scissors" motion associated with the $C\begin{smallmatrix}H\\H\end{smallmatrix}$ group will undergo a drop in frequency, and so too will one of the bends. Thus the two frequencies which introduce the greatest uncertainties into the model are no. (7) in table 5.4. These become small and therefore give a fast decomposition rate. $E_o$, the critical energy for reaction, was estimated as 109 kcal $mol^{-1}$ from the heats of formation of H, $C_2H_4$, and $C_2H_3$ (table 1.2). (This value has an error of $\pm$ 2 kcal $mol^{-1}$ due to uncertainty in the estimate for the heat of formation of $C_2H_3$.)

The moments of inertia of the molecule were calculated for the equilibrium geometry. In the activated complex the simplifying assumption was made that the centre of mass was fixed at the centre of the C = C bond. The C···· H distance in the activated complex described in table 5.4 was 3 x $r_o$(C - H) where $r_o$(C - H) is the internuclear distance in the v = 0 level.

The reaction,

$$^3CH_2 + {}^3CH_2 \longrightarrow C_2H_4$$

is exothermic by 171.9 kcal $mol^{-1}$. The result of the RRKM calculation based on the model described here was a rate constant for decomposition of 4.0 x $10^{12}$ $s^{-1}$. Even if the calculation is in error by a factor of $10^2$, there is little chance of stabilization of $C_2H_4$ at pressures up to 1 atmosphere.

The RRKM approach allows an estimation of the translational energy distribution of the products. The probability of translational energy, $E_{trans}$, shared between

the products is

$$P\ (E_{trans}) = \frac{\text{Density of states at energy } E^{\dagger} - E_{trans}}{\text{Total number of states for } 0 \leq E \leq E^{\dagger}}$$

$E^{\dagger}$ = 62.9 kcal $mol^{-1}$. Calculation gave a mean value of $E_{trans}$, $\langle E_{trans} \rangle$, of 7.9 kcal $mol^{-1}$. Since $M_{C_2H_3} \gg M_H$, this energy will be carried almost entirely by H. Thus, in a statistical model $C_2H_3$ will carry 55.0 kcal $mol^{-1}$ as vibrational and rotational energy. However if, for example, the H atom moves away along a repulsive potential surface, it may well carry away more than its statistical share of energy, and 55.0 kcal $mol^{-1}$ is likely to be an upper limit to the energy carried by $C_2H_3$. A RRKM calculation was carried out on $C_2H_3$.

The vibration frequencies of $C_2H_3$ have not been measured experimentally and were therefore estimated by comparison with $C_2H_4$ and $C_2H_2$. The values used are shown in table 5.5. The estimation of the in plane bends and out of plane bends presented a problem. An attempt to calculate these bending frequencies using the F and G matrix approach was hampered by a lack of reliable force constants in the literature. Instead the approach shown in table 5.5 was used. This assumes no coupling between the $=C-H$ bend and the $H_2=C=$ bend.

The model used in the RRKM calculation is shown in table 5.6. One of the bends associated with the C···· H group will become very low in frequency. The moments of inertia of the molecule were calculated assuming the structure below [176]

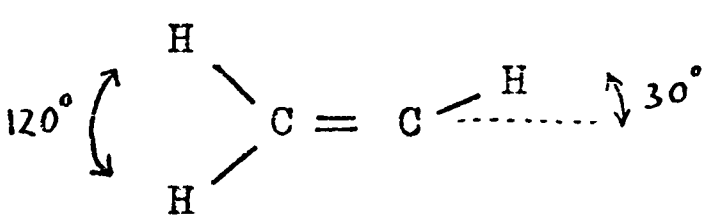


Table 5.5. Assignment of vibration frequencies to $C_2H_3$ (a)

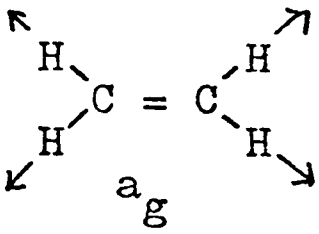
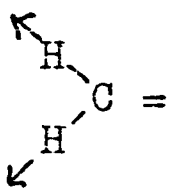
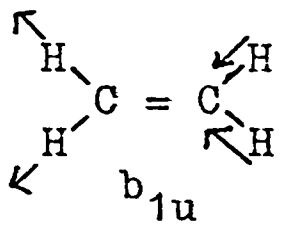
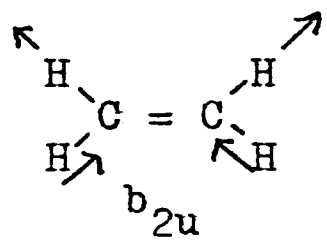
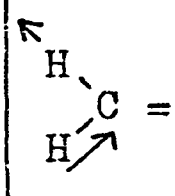
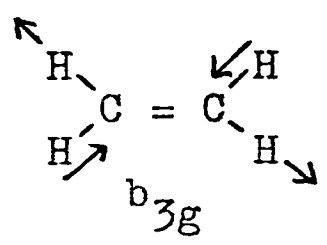
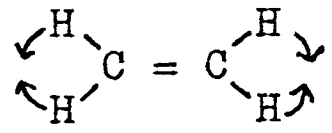
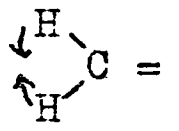
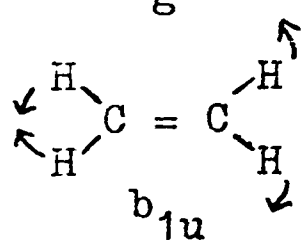
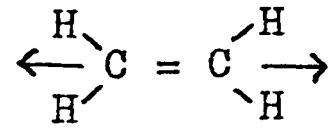
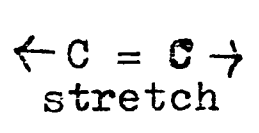
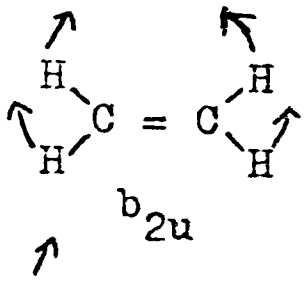
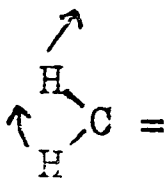
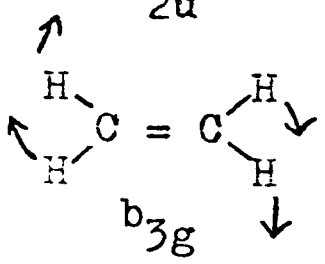
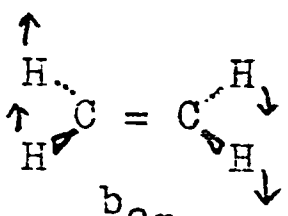
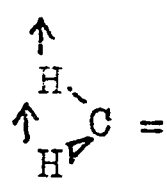
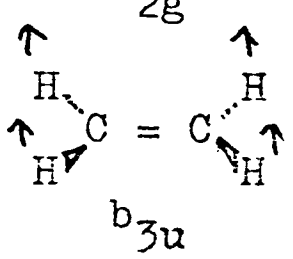
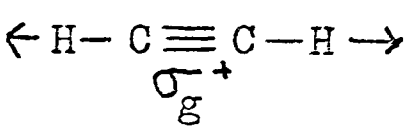
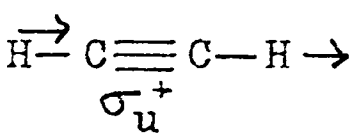
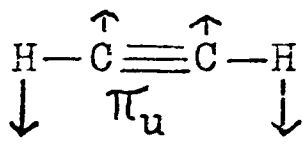
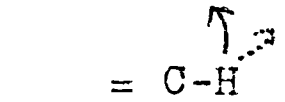
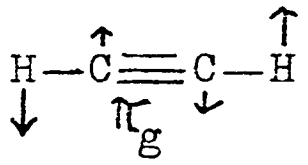
| Vibrations used in estimation | | $C_2H_3$ | |
|---|---|---|---|
|  $a_g$ | 3026.4 $cm^{-1}$ |  | 3007.6 $cm^{-1}$ |
|  $b_{1u}$ | 2988.7 $cm^{-1}$ | | |
|  $b_{2u}$ | 3105.5 $cm^{-1}$ |  | 3104.0 $cm^{-1}$ |
|  $b_{3g}$ | 3102.5 $cm^{-1}$ | | |
|  $a_g$ | 1342.2 $cm^{-1}$ |  | 1392.9 $cm^{-1}$ |
|  $b_{1u}$ | 1443.5 $cm^{-1}$ | | |
|  $a_g$ | 1622.9 $cm^{-1}$ |  stretch | 1622.9 $cm^{-1}$ |

Table 5.5. continued

| Vibrations used in estimation | | $C_2H_3$ |
|---|---|---|
|  $b_{2u}$ | 826.0 $cm^{-1}$ |  1024.0 $cm^{-1}$ ($CH_2$ "rock" in plane) |
|  $b_{3g}$ | 1222.0 $cm^{-1}$ | |
|  $b_{2g}$ | 943.0 $cm^{-1}$ |  946.2 $cm^{-1}$ ($CH_2$ "wag" o.o.plane) |
|  $b_{3u}$ | 949.3 $cm^{-1}$ | |
|  | 3373.7 $cm^{-1}$ | = C-H→ 3350.5 $cm^{-1}$ |
|  | 3287.0 $cm^{-1}$ | |
|  | 729.1 $cm^{-1}$ |  670.5 $cm^{-1}$ (doubly degenerate) |
|  | 612.0 $cm^{-1}$ | |

(a) $C_2H_4$ frequencies are from ref.174.

$C_2H_2$ frequencies are from ref.175.

Table 5.6. RRKM model for $C_2H_3$ decomposition.

| Molecule | | | Complex | | |
|---|---|---|---|---|---|
| Motion | Number of modes | $\nu$/cm$^{-1}$ | Motion | Number of modes | $\nu$/cm$^{-1}$ |
| C-H stretch | 2 | 3008<br>3104 | C-H stretch | 2 | 3330 |
| | 1 | 3330 | | | |
| C=C stretch | 1 | 1623 | C=C stretch | 1 | 1800 |
| Bends o.o.p. | 2 | 946<br>670 | Bends o.o.p. | 2 | 807<br>670 |
| Bends in plane | 3 | 1393<br>1024<br>670 | Bends in plane | 3 | 900<br>670<br>50-100 |

o.o.p. = out of plane.

and using the C = C and C — H bond lengths in $C_2H_4$. The simplifying assumption was made that the centre of mass lay at the centre of the C = C bond. The values thus obtained were 16.27, 2.06, and 18.33 amu $Å^2$. In the activated complex a C···· H bond length of 3 x $r_o$(C - H) was assumed giving corresponding moments of inertia of 21.53, 11.12, and 32.65 amu $Å^2$.

The reaction,

$$C_2H_3 \longrightarrow C_2H_2 + H$$

has an endothermicity of 37.3 kcal $mol^{-1}$. The activation energy for the back reaction is probably $\simeq$ 2 kcal $mol^{-1}$ (cf. H + $C_2H_4$, $E_{act}$ = 1.6 kcal $mol^{-1}$ [128]) and a reasonable estimate for $E_o$ is therefore 39.0 kcal $mol^{-1}$. On this basis an RRKM calculation was carried out and, over the range 40 kcal $mol^{-1} \leq E^* \leq$ 55 kcal $mol^{-1}$, the value of $k_a(E^*)$ was 1.0 x $10^{10}$ $s^{-1} \leq k_a(E^*) \leq$ 3.5 x $10^{13}$ $s^{-1}$.

If $C_2H_3$ is formed with energy in excess of $E_o$ by even a few kcal $mol^{-1}$ there is little chance of its collisional stabilization. Experimentally, no products were observed which need be attributed to $C_2H_3$ and this is consistent with the result found here. If the decomposition of $C_2H_4^*$ does occur at a rate of $k_a > 10^{12}$ $s^{-1}$ as the calculation suggests, there is little likelihood that any energy will be removed before its decomposition. These considerations suggest that the translational energy carried from the decomposition of $C_2H_4$ by H is less than 23 kcal $mol^{-1}$.

5.1.4. Decomposition of $C_2H_5$. Vibrational frequencies of $C_2H_5$ were assigned by comparison with $C_2H_6$. The values used are shown in table 5.7. The modes which are affected most when the energised molecule goes over to the activated complex are: (a) the C - C stretch whose frequency increases; (b) the free internal rotation which becomes a C = C tortion; (c) two of the $CH_3$ deformations whose frequencies decrease.

The reaction of H with $C_2H_4$ is known to have a small activation barrier ( $\simeq$ 1.6 kcal $mol^{-1}$) [128]. In this case a Morse potential cannot be used to approximate the potential energy along the reaction coordinate. Instead an arbitrary potential curve was drawn with a potential hump at $r^\dagger$ = 3.5 Å. The variations of molecular frequencies with $r^\dagger$ are not known and were also represented by arbitrary curves. The frequencies which are most critical to the model are the $CH_3$ deformation frequencies which become very small as the reaction coordinate is increased. These were represented by an expression of the form,

$$\nu = 1441 \exp(-2(r-r_e))$$

Using this rather arbitrary procedure a minimum in the density of states was found at $r^\dagger$ = 2.7 Å for $E^*$ = 100 kcal $mol^{-1}$.

$C_2H_5$ formed in the reaction of $CH_3$ with $^3CH_2$ has 100 kcal $mol^{-1}$ excess energy. This model predicted $k = 2 \times 10^{14}$ $s^{-1}$ at $E^*$ = 100 kcal $mol^{-1}$. Very substantial changes in the form of frequency variation with $r^\dagger$ were required to reduce this value by a factor of $10^2$. The conclusion is that there is very little chance of $C_2H_5^*$ stabilization at pressures up to 1 atmosphere.

Table 5.7. RRKM model for $C_2H_5$ decomposition.

| Molecule | | | Complex | | |
|---|---|---|---|---|---|
| Motion | Number of modes | $\nu$ / $cm^{-1}$ | Motion | Number of modes | $\nu$ / $cm^{-1}$ |
| C-H stretch | 5 | 2961 | C-H stretch | 4 | 2961 |
| C-C stretch | 1 | 993 | C=C stretch | 1 | 993-1623 |
| Bends | 2 | 1155 | Bends | 2 | 1155 |
| | 2 | 821 | | 2 | 821 |
| $CH_2$ scissor | 1 | 1393 | $CH_2$ scissors | 2 | 1393 |
| $CH_3$ deform: :ations | 3 | 1441 | C···H bends | 2 | 100 |
| Internal rotation | 1 | --- | C=C torsion | 1 | 1020 |

The energy available to $C_2H_4$ formed in the dissociation of $C_2H_5^*$ is $E_{C_2H_4} = 100 - 38.6 - E_H$ kcal $mol^{-1}$ where $E_H$ is the energy carried away from the reaction by H as translational energy. $E_H$ calculated on a statistical basis was 10 kcal $mol^{-1}$, and $E_{C_2H_4}$ is therefore $\simeq 50$ kcal $mol^{-1}$. The reaction,

$$C_2H_4 \longrightarrow C_2H_2 + H_2$$

is 41.7 kcal $mol^{-1}$ endothermic. Although further decomposition of $C_2H_4$ is thermodynamically possible, it is unlikely due to an additional energy barrier which has been estimated as 20 kcal $mol^{-1}$ [177].

## 5.2. Correlations of electronic states.

5.2.1. Introduction. The basis of this treatment involves an examination of the adiabatic correlations of reactants and products in terms of their symmetry. Adiabatic correlations allow one to predict which reactions are likely to be rapid and also the electronic states of the product molecules. This method requires a full knowledge of the term manifolds of both reactants and products. Clearly, without detailed calculations to construct complete potential energy surfaces, activation energies and hence absolute rates cannot be predicted ab initio. However where a surface leads directly and exothermically to products, very low or negligible activation energies are generally observed.

An important consideration in discussing correlation is the non-crossing rule [178]. For diatomic molecules, potential curves of the same species do not cross. If in a certain

approximation they do cross, the effect of the neglected terms in the wave equation will always be that the levels "repel" each other, and, therefore, that in fact they do not cross. For polyatomics this will not necessarily be the case as the greater number of degrees of freedom allows simultaneous occurrence of the conditions for crossing. Thus a pair of 3-dimensional surfaces may intersect along a line. Nevertheless although the non-crossing rule does not rigorously apply for polyatomic molecules, the larger number of degrees of freedom involved gives rise to the situation under which non-crossing of states with the same species does effectively hold. Therefore, the lowest electronic configuration of the reactants correlates with the lowest product configuration of the same symmetry.

Correlation diagrams were constructed using the tables in Appendices I - IV of ref. 3. Consider, for example, the dissociation of $CH_4$ ($T_d$ symmetry). Lowering of the symmetry to $C_{2v}$ causes a splitting of states of $F_2$ symmetry to states of $A_1$, $B_1$, $B_2$ symmetries (table 60), and a state of symmetry $A_1$ ($T_d$) becomes $A_1$ ($C_{2v}$). It is now necessary to consider the dissociation products $CH_2 + H_2$. The ground state of $H_2$ ($^1\Sigma_g^+$) ($D_{\infty h}$) resolves to $A_1$ symmetry ($C_{2v}$) (table 59). $CH_2$ has states $^3B_1$, $^1A_1$, $^1B_1$. The states resulting from a combination of 2 symmetry species in a particular point group are the products of the species. From table 57,

$B_1 \times A_1 \longrightarrow B_1$, $A_1 \times A_1 \longrightarrow A_1$.

Thus $H_2$ ($^1A_1$) + $CH_2$ ($^3B_1$) correlates with $CH_4$ ($^3B_1$) (a component of $^3F_2$). $H_2$ ($^1A_1$) + $CH_2$ ($^1A_1$) correlates with $CH_4$ ($^1A_1$). $H_2$ ($^1A_1$) + $CH_2$ ($^1B_1$) correlates with $CH_4$ ($^1B_1$) (a component of $^1F_2$).

5.2.2. $\underline{CH_4}$. Figure 5.5 shows the correlation of the low lying states of $CH_4$ ($T_d$) with $CH_2 + H_2$ ($^1\Sigma_g^+$) ($C_{2v}$) and with $CH_3 + H$ ($^2S_g$) ($C_{3v}$).

The ground state of $CH_4$ ($\tilde{X}\ ^1A_1$) correlates in $C_{2v}$ symmetry with $CH_2$ ($^1A_1$) + $H_2$ ($^1\Sigma_g^+$). In fig. 1.7 the correlation of molecular orbitals is shown. From this figure, it is apparent that the ground state of $CH_4$ $(2a_1)^2(1f_2)^6$ correlates with $CH_2$ $(2a_1)^2(1b_2)^2(1b_1)^2$ + $H_2(3a_1)^2$ i.e. with $CH_2$ ($\tilde{c}^1A_1$) + $H_2$ ($^1\Sigma_g^+$). This implies that $CH_2$ ($\tilde{a}^1A_1$) + $H_2$ ($^1\Sigma_g^+$) correlates with a higher state of $CH_4$. However due to the non-crossing rule these states do not cross, and so the situation shown in fig. 5.5 is correct. The molecular orbital approach breaks down at large separations. However this orbital crossing may lead to an activation barrier for the reaction of $CH_2$ ($^1A_1$) + $H_2$. The experimental value for the rate constant, $^1CH_2 + H_2$, at 298 K, $k = 7.0 \times 10^{-12}$ $cm^3$ $molecule^{-1}$ $s^{-1}$ [41] combined with a bimolecular A factor assumed equal to the collision rate ($7.0 \times 10^{-10}$ $cm^3$ $molecule^{-1}$ $s^{-1}$) leads to an estimate of the activation energy, $E_{act} = 2.8$ kcal $mol^{-1}$. Since the collision rate is the upper limit to $A_{bim}$, 2.8 kcal $mol^{-1}$ is the upper limit of $E_{act}$.

$CH_2$ ($^3B_1$) + $H_2$ correlates with $CH_4$ ($^3F_2$). There is obviously a large activation barrier to formation of $^3CH_4$ and the observed reaction of $CH_2$ ($^3B_1$) + $H_2$ probably occurs on a different potential surface altogether [103]. Similarly $CH_2$ ($^1B_1$) + $H_2$ correlates with $CH_4$ ($^1F_2$). Any reaction on a potential surface of $C_{2v}$ symmetry would have an extremely high activation energy. The reaction postulated in chapter 3 must occur on a surface of different symmetry e.g. $CH_2$ ($^1B_1$) + $H_2$ might be an abstraction type reaction.

$H_2(^1\Sigma g^+) + CH_2$ $CH_4$ $H(^2Sg) + CH_3$

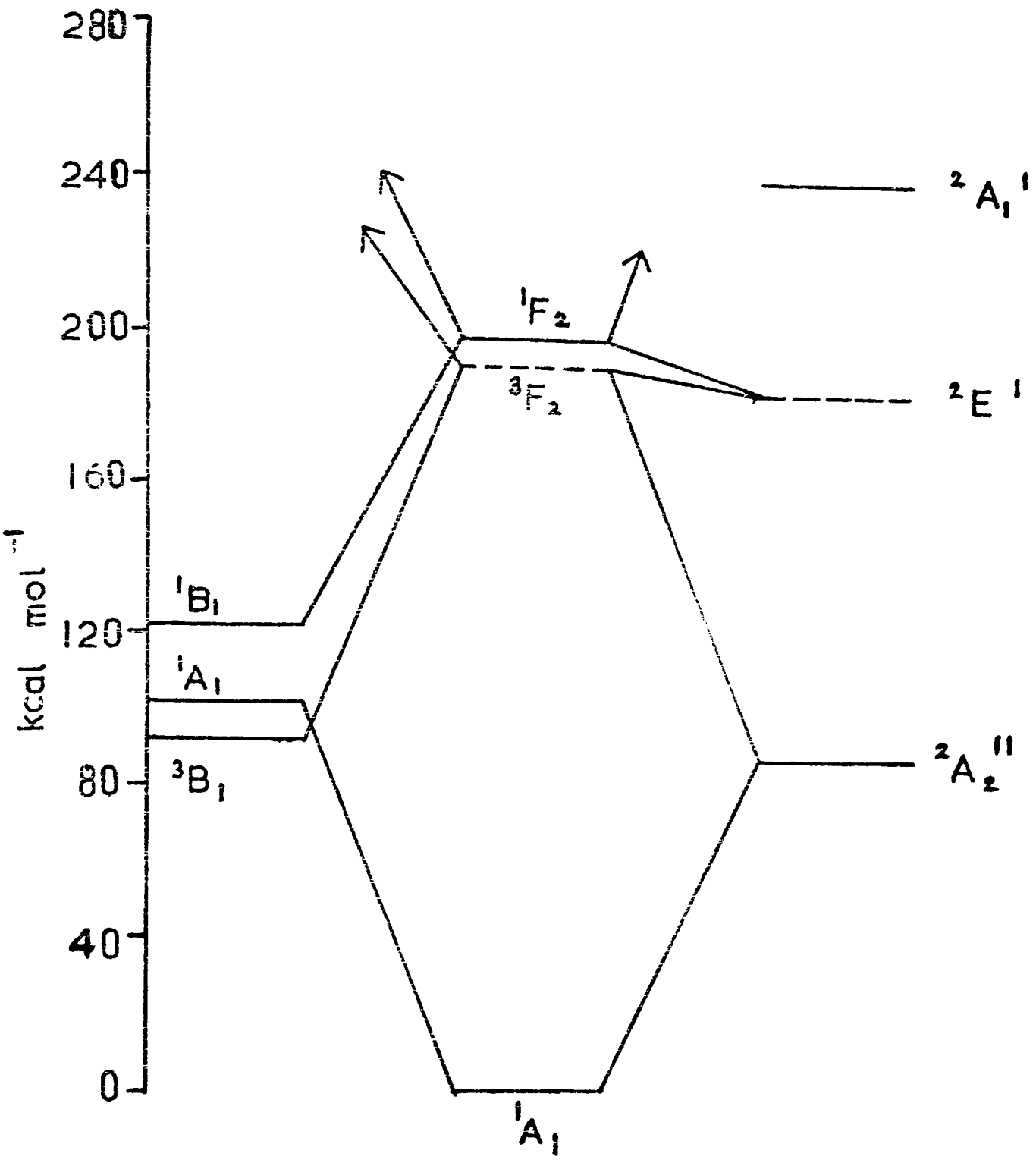



Fig. 5.5. Correlation of electronic states of $CH_4$ with $CH_2 + H_2$ ($C_{2v}$ symmetry) and with $CH_3 + H$ ($C_{3v}$ symmetry).
(Dashed lines indicate states whose energy is uncertain)

$CH_3$ ($^2A''_2$) + H ($^2S_g$) correlates with $CH_4$ ($\tilde{X}\ ^1A_1$) and with $CH_4$ ($^3F_2$). Thus in the combination reaction between $CH_3$ + H, $\frac{3}{4}$ of the reactants will move on a repulsive triplet surface, and $\frac{1}{4}$ on an attractive singlet surface.

Absorption of radiation causes a transition $^1F_2 \leftarrow {}^1A_1$. The $^1F_2$ state of $CH_4$ correlates with $CH_2$ ($\tilde{b}\ ^1B_1$) thus explaining the observation of $CH_2$ ($\tilde{b}\ ^1B_1$) $\rightarrow$ $CH_2$ ($\tilde{a}\ ^1A_1$) fluorescence in the photolysis of $CH_4$ [58]. It is interesting to speculate that any $CH_3$ produced as a minor product in the photolysis should on the basis of this correlation be produced in an excited $^2E'$ state unless crossover to the $^3F_2$ surface were to occur. There are no reported observations of $CH_3$ ($^2E'$).

5.2.3. $CH_2CO$. Molecular orbital calculations predict the following ordering of states in $CH_2CO$ [179] ($C_{2v}$ symmetry):

$$(1a_1)(2a_1)(3a_1)(4a_1)(5a_1)(6a_1)(1b_2)(7a_1)(1b_1)(2b_2)(2b_1)(3b_2)(3b_1)$$

The $7a_1$ and $1b_2$ orbitals lie close in energy and in some calculations their order is reversed. The ground state of ketene has the configuration,

$$....(1b_2)^2(7a_1)^2(1b_1)^2(2b_2)^2(2b_1)^2 \qquad : {}^1A_1$$

The highest occupied orbital of $b_1$ symmetry ($\pi$ orbital) is principally a bonding orbital between the C atoms and is somewhat anti-bonding in the C - O group [180]. The lowest unoccupied orbitals have $b_2$ and $b_1$ symmetries. The orbital of $b_2$ symmetry is antibonding in the C - O group, and the orbital of $b_1$ symmetry is antibonding both with respect to C - C and to C - O [180].

Promotion of an electron from the $2b_1$ orbital to the

$3b_2$ orbital produces the states $^3A_2$ and $^1A_2$. The electric dipole transition $^1A_2 \leftarrow {}^1A_1$ is symmetry forbidden. However calculations [180] predict that both the states $^1A_2$ and $^3A_2$ have planar geometries in which the C - O bond is bent in the plane of the molecule ($C_s$ symmetry). Optical transitions to the $^1A''$ state are then allowed and explain the absorption $260 < \lambda < 385$ nm.

Promotion of an electron from the $2b_1$ orbital to the $3b_1$ orbital produces the states $^3A_1$ and $^1A_1$. These states are less well studied but Del Bene [180] has predicted that $^3A_1$ has an equilibrium structure in which the C - O bond bends out of the plane of the $CH_2$ group giving a molecular geometry with non-planar $C_s$ symmetry.

CO ($\tilde{X}\ ^1\Sigma^+$) is described by the configuration,

$$(1\sigma)^2(2\sigma)^2(3\sigma)^2(4\sigma)^2(5\sigma)^2(1\pi)^4$$

Resolving from symmetry $C_{\infty v}$ to $C_{2v}$ this becomes

$$(1a_1)^2(2a_1)^2(3a_1)^2(4a_1)^2(5a_1)^2(1b_1)^2(1b_2)^2$$

The "addition" of this configuration to the low lying states of $CH_2$ is considered here. From chapter 1, the low lying states of $CH_2$ are

$(a_1)^2(a_1)^2(b_2)^2(a_1)^2$ : $\tilde{a}^1A_1$

$(a_1)^2(a_1)^2(b_2)^2(a_1)^1(b_1)^1$ : $\tilde{b}^1B_1$ , $\tilde{X}^3B_1$

$(a_1)^2(a_1)^2(b_2)^2\ \ (b_1)^2$ : $\tilde{c}^1A_1$

$CH_2$ ($\tilde{a}\ ^1A_1$) + CO ($^1\Sigma^+$) correlates (in the molecular orbital description) with $CH_2CO$ ($^1A_1$). This state has the configuration,

$$\ldots (8a_1)^2(2b_2)^2(1b_1)^2$$

and is not the ground state of $CH_2CO$.

$CH_2$ ($\tilde{X}\ ^3B_1$) + CO ($^1\Sigma^+$) correlates with $CH_2CO$ ($^3B_1$).

$CH_2$ ($\tilde{b}\ ^1B_1$) + CO ($^1\Sigma^+$) correlates with $CH_2CO$ ($^1B_1$).

$CH_2$ ($\tilde{c}\ ^1A_1$) + CO ($^1\Sigma^+$) correlates with $CH_2CO$ ($^1A_1$), which is the ground state of $CH_2CO$.

A suggested potential energy diagram based on these correlations, and on correlations with states of higher energy, is shown in figure 5.6. Due to the non-crossing rule $CH_2$ ($\tilde{a}\ ^1A_1$) + CO ($^1\Sigma^+$) does correlate with the ground state of $CH_2CO$ ($\tilde{X}\ ^1A_1$). However in $C_{2v}$ symmetry the non-adiabatic behaviour of the molecular orbitals may be expected to give rise to an energy barrier for the combination of $CH_2$ ($\tilde{a}\ ^1A_1$) + CO ($^1\Sigma^+$). It is impossible to estimate the height of this barrier but its existence is compatible with the slow reaction of $^1CH_2$ + CO. In this diagram $CH_2$ ($\tilde{X}\ ^3B_1$) + CO ($^1\Sigma^+$) gives only a repulsive surface. Relaxation of the symmetry, e.g. to $C_s$, would allow a crossing to the $^3A_2$ state and the reaction $^3CH_2$ + CO might produce a bound state of $CH_2CO$.

It is important to note that the ground $^1A_1$ state of ketene does correlate with the lowest energy $^1A_1$ state of combined $^1CH_2$ + CO. This is contrary to early descriptions[33,37] but is confirmed in a recent paper by Basch [181].

As discussed earlier, absorption in the near U.V. occurs to a $^1A''$ state ($^1A_2$). Production of $CH_2$ ($\tilde{a}\ ^1A_1$) must then occur by mixing of the $^1A_2$ and $^1A_1$ states. Production of $CH_2$ ($\tilde{X}\ ^3B_1$) requires a crossing from $CH_2CO$ ($^1A_2$) to $CH_2CO$ ($^3B_1$) either directly or via the $^3A_2$ state. The $^1A'' \leftarrow {}^1A_1$ transition is governed by the selection rules for

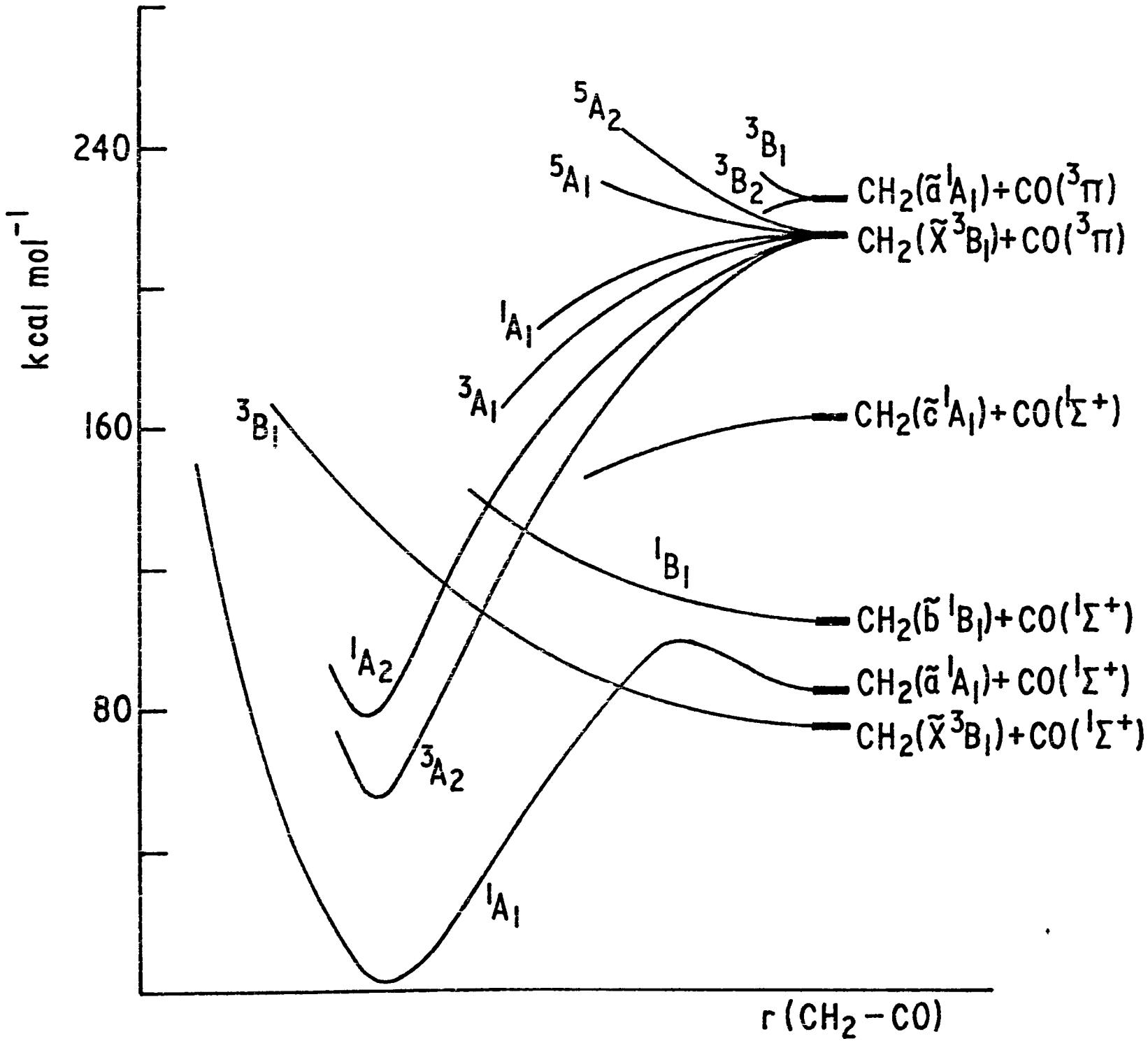



Fig.5.6. Potential energy curves for $CH_2CO$ ($C_{2v}$ symmetry) as a function of $CH_2$— CO separation.

the joint point group $C_s$. However the transition will still be very weak since the "vertical" i.e. Franck-Condon allowed part of the transition will obey selection rules in $C_{2v}$ symmetry.

There appear to be no low lying $^1B_1$ states of ketene. This suggests that $CH_2$ ($\tilde{b}\ ^1B_1$) + CO ($^1\Sigma^+$) interact on a repulsive surface. A $^1B_1 \leftarrow {}^1A_1$ transition is electronically allowed. This transition to a repulsive state would give rise to a continuum absorption in the far U.V. ( $\lambda <$ 200 nm.) accompanied by production of $CH_2$ ($\tilde{b}\ ^1B_1$).

5.2.4. $C_2H_4$. Figure 5.7 shows the correlation of the electronic states of $CH_2 + CH_2$ with those of $C_2H_4$ in $D_{2h}$ symmetry. The order of the electronic states of $C_2H_4$ is taken from Merer and Mulliken's paper [173], and is consistent with a consideration of molecular orbitals.

The ground state of $C_2H_4$ is

$$K^2K^2(2a_g)^2(2b_{1u})^2(1b_{2u})^2(1b_{3g})^2(3a_g)^2(1b_{3u})^2 \quad : {}^1A_g$$

The lowest excited states have the configuration:

$$K^2K^2(2a_g)^2(2b_{1u})^2(1b_{2u})^2(1b_{3g})^2(3a_g)^2(1b_{3u})^1(1b_{2g})^1 : {}^{1,3}B_{1u}$$

Higher electronic states arise from the configurations:

$$\ldots\ldots\ldots(1b_{3u})^1(3b_{1u})^1 \quad : {}^1B_{2g},\ {}^3B_{2g}$$

$$\ldots\ldots\ldots(1b_{3u})^1(4a_g)^1 \quad : {}^1B_{3u},\ {}^3B_{3u}$$

$$\ldots\ldots\ldots(3a_g)^1(1b_{3u})^2(1b_{2g})^1 \quad : {}^1B_{2g},\ {}^3B_{2g}$$

$$\ldots\ldots\ldots(3a_g)^1(1b_{3u})^2(3b_{1u})^2 \quad : {}^1A_g,\ {}^3A_g$$

Reaction of two ground state methylene molecules ($\tilde{X}\ ^3B_1$) may occur on a singlet, triplet, or quintet surface.

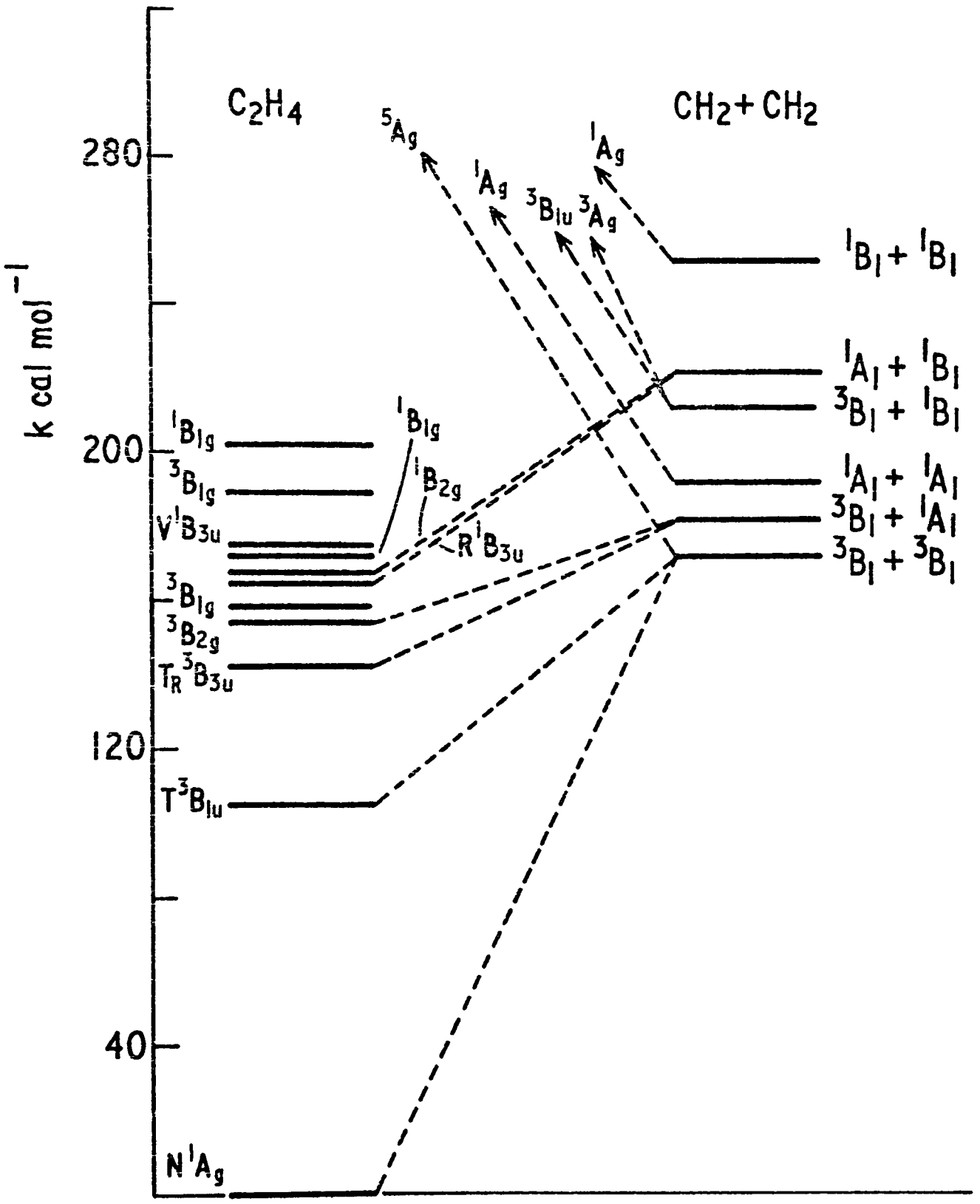



Fig.5.7. Correlation of the electronic states of $CH_2 + CH_2$ with those of $C_2H_4$ in $D_{2h}$ symmetry.

From fig. 5.7 it is apparent that the triplet and singlet surfaces may lead to stable $C_2H_4$. The measured rate constant for $^3CH_2 + {}^3CH_2$ is consistent with a value of 4/9 times the collision rate. The combination of excited $CH_2$ radicals is less certain though $^3B_1 + {}^1A_1$, and $^1A_1 + {}^1B_1$ may well lead to formation of bound states of $C_2H_4$.

5.2.5. $CH_3$. A minor aspect of the mechanism proposed in chapter 3 was the photolysis of methyl radicals. It is pertinent, therefore, to examine the probable electronic state of the methylene produced.

Spectroscopic evidence implies that $CH_3$ is planar in its ground electronic state. The electronic configurations of the lowest states of $CH_3$ in $D_{3h}$ symmetry are:

$(a_1')^2(a_1')^2(e')^4(a_2'')^1$ : $^2A_2''$

$(a_1')^2(a_1')^2(e')^3(a_2'')^2$ : $^2E'$

$(a_1')^2(a_1')^2(e')^4(a_1')^1$ : $^2A_1'$

No transitions to the $^2E'$ state have yet been observed. (The $^2E' \leftarrow {}^2A_2''$ transition is electronically forbidden.) The longest wavelength transition of $CH_3$ occurs at 216 nm. and has been assigned to the $^2A_1' \leftarrow {}^2A_2''$ transition [2]. The strong diffuseness observed in the absorption bands is apparently produced by predissociation in the upper state.

Figure 5.8 shows a Walsh diagram for the correlation of orbitals between a planar and non-planar molecule of type $XH_3$. It is apparent from this diagram that the $^2E'$ state may well be non-planar in its equilibrium state. This has been confirmed by calculation [182], and it has been predicted that if $D_{3h}$ symmetry is imposed on the molecule the $^2E'$ state

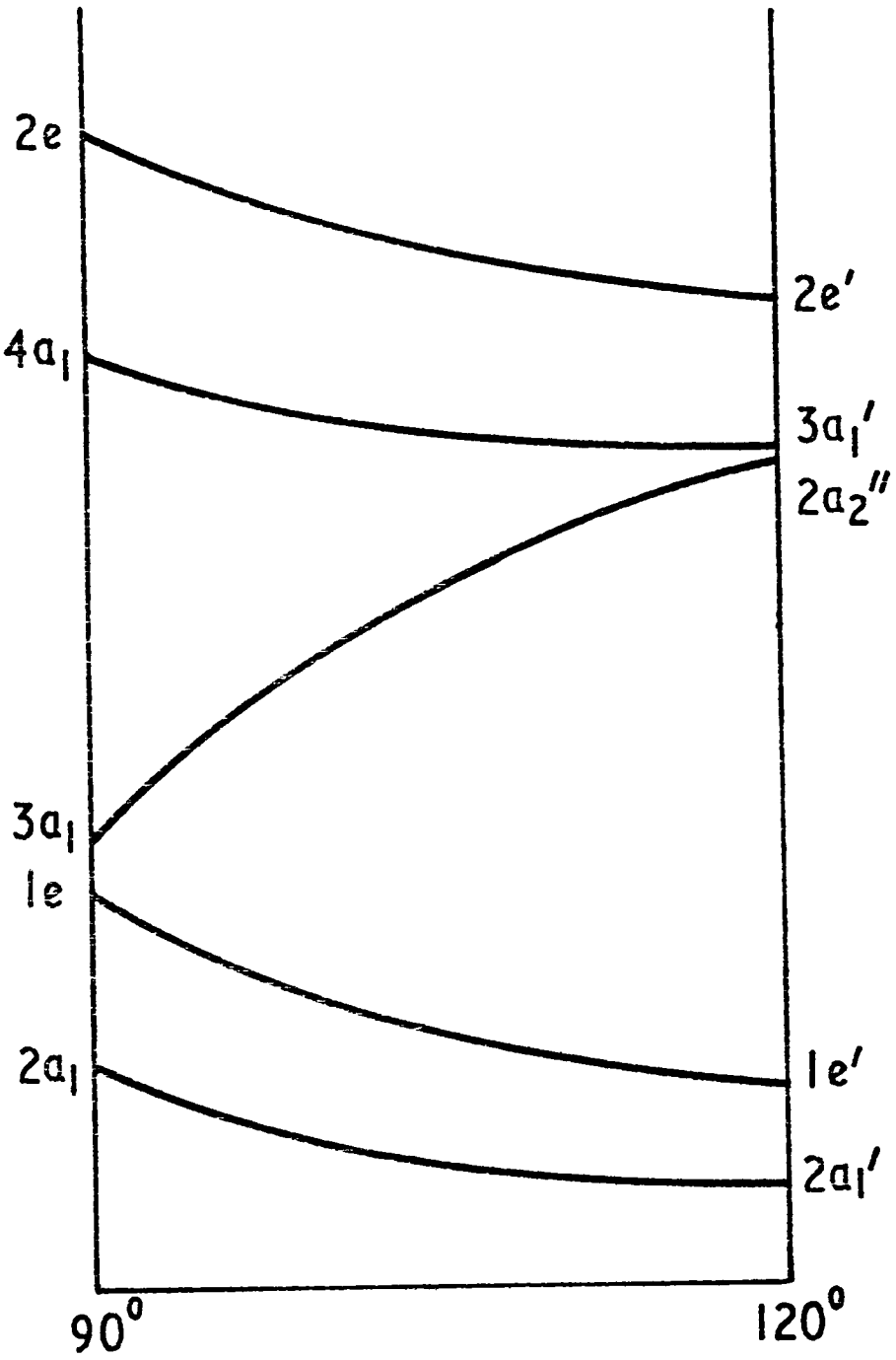



Fig.5.8. Walsh diagram for the correlation of orbitals between planar and non-planar $XH_3$. (As in ref.3.) The angle on the abscissa is $\widehat{HXH}$ ; $120^{o}$ corresponds to the planar conformation. The 1s orbital of X is not included.

lies above the $^2A_2''$ state.

Figure 5.9 shows the correlation between $CH_2$ + H ($C_{2v}$ symmetry) and $CH_3$ ($D_{3h}$ symmetry). In order to explain the predissociation in the $^2A_1'$ state it is necessary to assume that $CH_3$ ($^2A_1'$) correlates with a higher electronic state than $CH_2$ ($\tilde{a}\ ^1A_1$) but that the non-crossing rule forces a correlation to the $\tilde{a}\ ^1A_1$ state. In this case a consideration of the molecular orbital correlation does not give a clear indication of the higher electronic state involved. It is quite clear, however, that the predissociation of $CH_3$ ($^2A_1'$) leads to the production of $CH_2$ ($\tilde{a}\ ^1A_1$) and <u>not</u> $CH_2$ ($\tilde{X}\ ^3B_1$).

## 5.3. Collisional deactivation of $CH_2$ ($^1B_1$).

In section 1.6 the collisional deactivation of $CH_2$ ($^1A_1$) to $CH_2$ ($^3B_1$) was discussed. The total symmetry of the electronic wave function (spin + orbital motion) of $CH_2$ ($^3B_1$) has components $B_2$, $A_1$, and $A_2$, and it was presumed that the coupling of the $A_1$ component with the electronic wave function of $CH_2$ ($^1A_1$) causes a mixing between states and allows collisional deactivation. Since the electronic wave function of $CH_2$ ($^3B_1$) does not have a component of $B_1$ symmetry collisional deactivation of $CH_2$ ($^1B_1$) to $CH_2$ ($^3B_1$) is not expected.

The discussion thus far has dealt only with electronic motion and has neglected vibrational and rotational motion. As in an electronically forbidden electric dipole induced transition, vibronic considerations may lead to a mixing of states which does not occur in the absence of vibration. The 3 vibrations in $CH_2$ have symmetry $A_1$, $A_1$, and $B_2$ for the

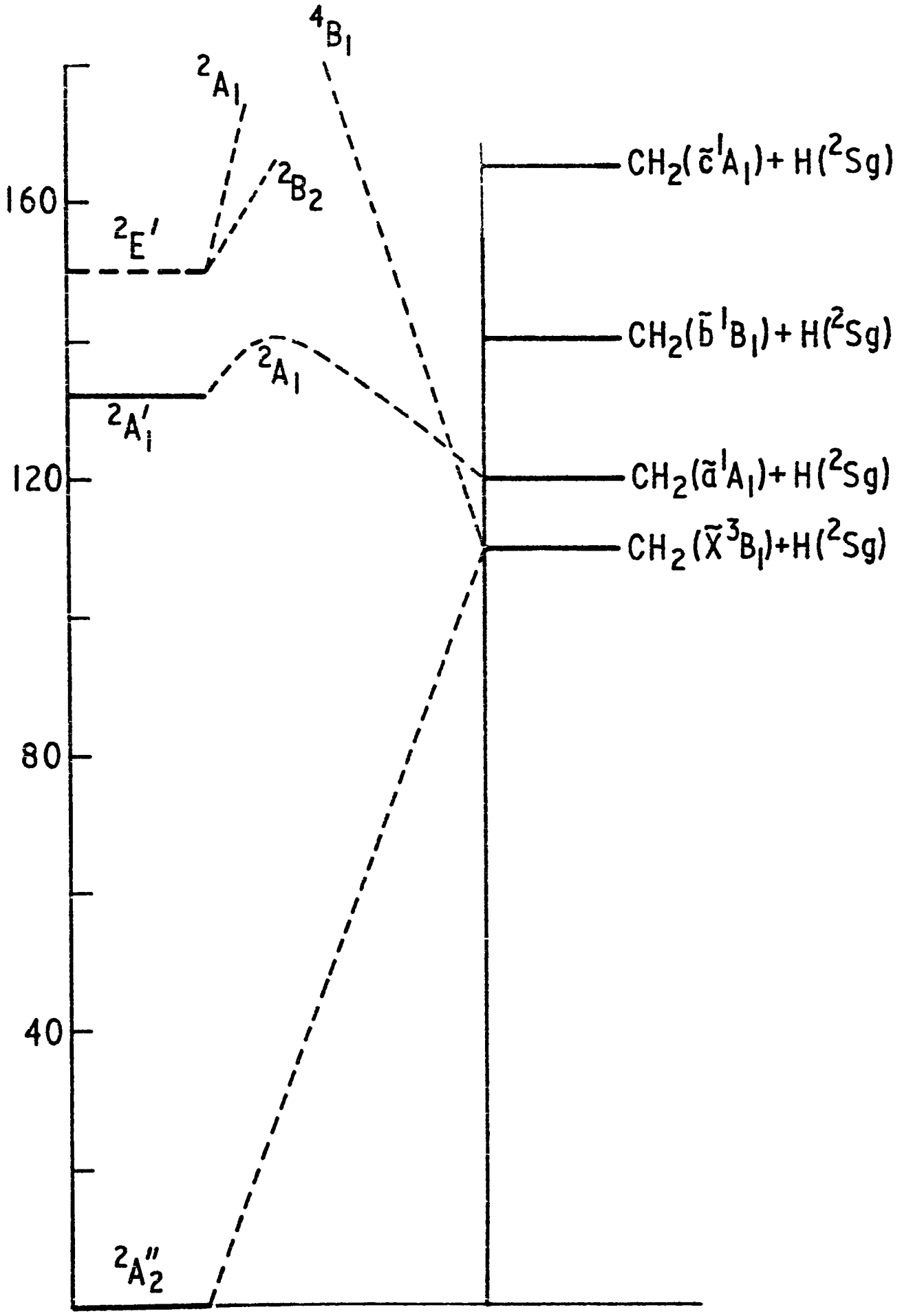



Fig.5.9. Correlation of the electronic states of $CH_3$ ($D_{3h}$) with $CH_2$ + H ($C_{2v}$)

symmetric stretch ( $\nu_1$), bend ( $\nu_2$), and asymmetric stretch ( $\nu_3$) respectively.

Since the asymmetric stretch and bend are totally symmetric they will not interfere with any of the symmetry arguments. The asymmetric stretch ( $\nu_3$) may, however, be important. In the $^1B_1$ state the $v_3 = 1, 3, 5, \ldots$ states have symmetry $A_2$ ($B_1 \times B_2$) (electron spin + orbit + nuclear vibration). Thus for these states there may be interaction with the $^3B_1$ state, and collisional deactivation may be important. In a similar way the $v_3 = 1, 3, 5, \ldots$ levels of $^3B_1$ have overall symmetry $B_1$ and may therefore interact with the lowest vibrational state of $^1B_1$.

$^1B_1$, $^1A_1$ arise from the same $^1\Delta$ state, the degeneracy being lifted by the bending mode. Conversely, the bending mode may mix the $^1B_1$, $^1A_1$ states effectively via coupling between the rotational motion and the electronic motion.

The conclusion is that it is not possible to rule out mixing of $^1B_1$ with either $^1A_1$ or $^3B_1$. However, interactions require either vibronic or rovibronic interactions. A small molecule like $CH_2$ also relies heavily on accidental degeneracy of states with closely related rotational quantum numbers [183]. Whether or not this occurs can only be ascertained once detailed spectroscopic analyses are available.

CHAPTER 6.

# SUGGESTIONS FOR FURTHER WORK.

In this chapter some experiments are suggested which would help to substantiate the conclusions reached in this thesis.

## 6.1. A rate constant for $CH_3$ + H.

One of the unknowns which has hampered the interpretation of the systems described in chapters 3 and 4 is the pressure dependent rate constant for the reaction,

$$CH_3 + H \longrightarrow CH_4$$

A simple experiment is described here which would set more definite limits on this rate constant.

The experiment consists of two parts:

(a) Consider the photolysis of azomethane and iodine,

$$CH_3N_2CH_3 + h\nu \longrightarrow 2CH_3 + N_2 \qquad (1)$$

$$I_2 + h\nu \longrightarrow 2I \qquad (2)$$

In a quartz reaction vessel, $CH_3N_2CH_3$ is photolysed in the U.V. ( $\lambda < 200$ nm.), and $I_2$ is photolysed in the range $400 < \lambda < 500$ nm. [44]. In this mixed photolysis system the radicals produced ( $CH_3$ and I ) undergo the following reactions:

$$CH_3 + CH_3 \longrightarrow C_2H_6 \qquad (3)$$

$$I + I \longrightarrow I_2 \qquad (4)$$

$$CH_3 + I \longrightarrow CH_3I \qquad (5)$$

Rate constants for reactions (3) and (4) are known. By

measuring the products of reactions (3) and (5) using gas chromatographic separation followed by flame ionisation detection, a rate constant for reaction (5) may be obtained by a computer simulation of the reaction scheme. This rate constant is pressure dependent, and, by carrying out the photolysis in an inert gas bath at different total pressures, the rate constant could be obtained as a function of pressure.

(b) Now consider the flash photolysis of the mixed system HI / $CH_3N_2CH_3$. Hydrogen iodide has a dissociative absorption in the range $180 < \lambda < 300$ nm. [44].

$$CH_3N_2CH_3 + h\nu \longrightarrow 2CH_3 + N_2 \qquad (1)$$

$$HI + h\nu \longrightarrow H + I \qquad (6)$$

The radical products of the photolysis undergo the following reactions,

$$CH_3 + CH_3 \longrightarrow C_2H_6 \qquad (3)$$

$$CH_3 + I \longrightarrow CH_3I \qquad (5)$$

$$I + I \longrightarrow I_2 \qquad (4)$$

$$CH_3 + H \longrightarrow CH_4 \qquad (7)$$

Rate constants for reactions (3), (5), and (4) are known. Thus a measurement of the products $C_2H_6$, $CH_3I$, and $CH_4$ over a range of pressure would lead to an estimate of a rate constant for reaction (7) as a function of pressure.

There are two complications to the above experiment. Firstly, I atoms are produced in two different electronic states, $^2P_{\frac{1}{2}}$ and $^2P_{\frac{3}{2}}$. These states react at different rates

and must be considered as different species in the reaction scheme. However the reactions of these species are fairly well characterised [184]. The second complication is that H atoms produced in HI photolysis are translationally "hot". At low pressures they may not be thermalised before reaction. This may lead to difficulty in interpretation of results at low pressures, but should not affect the validity of the high pressure rate constant.

## 6.2. $CH_2$ ($\tilde{b}\ ^1B_1$) → $CH_2$ ($\tilde{a}\ ^1A_1$) fluorescence.

The model adopted to describe the experimental results involves the production of $CH_2$ ($^1B_1$). Fluorescence attributed to $CH_2$ ($^1B_1$) → $CH_2$ ($^1A_1$) has been observed in the photolysis of $CH_4$ [58]. Observation of this fluorescence in the photolysis of $CH_2CO$ would confirm the production of $CH_2$ ($^1B_1$) in the primary process. The lifetime of $CH_2$ ($^1B_1$) could be measured by monitoring the decay of fluorescence from $CH_2$ ($^1B_1$) produced in a pulsed experiment. This determination would allow the measurement of absolute rate constants for $CH_2$ ($^1B_1$) reactions with $H_2$ and $CH_2CO$ from the ratios measured in this work.

A study of the intensity of fluorescence as a function of the wavelength of the photolysis radiation might lead to a better understanding of the highly excited states of $CH_2CO$.

## 6.3. CH radicals.

It has been assumed that the photolysis of $CH_2CO$ leads entirely to production of $CH_2$. It is therefore important that a spectroscopic search should be carried out for the presence of other radicals in the system e.g. $C_2O$, CHCO, CH.

The observation of CH has already been reported [41], but knowledge of the absolute concentration awaits the measurement of the extinction coefficients for CH absorption.

## 6.4. Isotope experiments.

One of the unexplained results in ref. 41 was the presence of $CD_3$ in the photolysis of $CH_2CO$ / $D_2$ systems at high pressures. No satisfactory explanation has been proposed to account for the presence of $CD_3$.

A very tentative suggestion involves a reaction of $CH_2$ ($^1B_1$) with $D_2$,

$$CH_2\ (^1B_1) + D_2 \longrightarrow CD_2 + H_2$$

This postulate, that one of the reaction pathways open to $CH_2$ ($^1B_1$) + $D_2$ involves an exchange of the H atoms, must be regarded only as a speculation. Careful work on the photolysis of isotopically substituted $CH_2CO$ in $H_2$ / $D_2$ systems using mass spectrometric analysis might lead to more insight into the system.

In 1974, Schaeffer [103] forecast that a crossed molecular beam experiment involving $CH_2$ was a real possibility within the next few years. "The potential importance of experiments of this kind with respect to the discernment of the dynamics of $CH_2$ reaction can hardly be over-emphasised."

APPENDIX A1.

A listing of the computer programme which solves the kinetic equations for the reactions of $CH_2$ produced in the vacuum U.V. photolysis of ketene in an excess of $H_2$ and/or inert gas.

```
*FORTRAN OPT
      MASTER JIM
      EXTERNAL AUX
      REAL K
      DIMENSION K(29)
      DIMENSION Y(11),G(11),YO(11),E(11),A(11),B(11),C(11),D(11)
      COMMON/BLOCK1/K,P,WMET,WAZO,WC2H4,WCH3,PH,ZETA3,
     1FI1,FI2,FI3,FI4,ZETA,FRACT1,FRACT2
      COMMON/BLOCK2/THETA1,THETA2
C
C     THIS PROGRAM SOLVES THE KINETIC EQUATIONS FOR THE REACTIONS OF
C     METHYLENE PRODUCED IN THE VACUUM UV PHOTOLYSIS OF KETENE
C     HYDROGEN AND/OR INERT GAS ARE PRESENT IN CONCENTRATIONS MANY
C     TIMES GREATER THAN THAT OF METHYLENE
C
C
C     INPUT DATA IS IN FREE FORMAT AS FOLLOWS:
C     29 RATE CONSTANTS ARE READ INTO DIMENSION K
C     NEW LINE
C     NUM-THE NUMBER OF CALCULATIONS TO BE CARRIED OUT FOR
C         A PARTICULAR SET OF RATE CONSTANTS
C     EACH CALCULATION REQUIRES TWO SETS OF DATA
C     NEW LINE
C     P-PRESSURE(TORR),Z-KETENE CONC(MTORR),PULSE-KETENE PHOTOLYSED(MTORR),
C     FACTOR-PHOTOLYSIS FACTOR FOR C2H4,HO-PRINT OUT STEP LENGTH(MICROSEC),
C     NO-THE NUMBER OF STEP LENGTHS (HO*NO=TOTAL TIME INTERVAL OVER WHICH
C        THE CALCULATION IS CARRIED OUT)
C     NEW LINE
C     ZA-AZOMETHANE CONC(MTORR),PULSEA-AZOMETHANE PHOTOLYSED(MTORR),
C     PH-HYDROGEN PRESSURE(TORR),DES-A PHOTOLYSIS FACTOR FOR CH3,
C     FRACT2-THE FRACTION OF XCH2 PRODUCED
C
C
12    FORMAT('HO,5X,23HINITIAL KETENE PRESSURE= ,F5.1)
1     FORMAT(6000.0)
10    FORMAT( 10X,1PE .2)
13    FORMAT('HO,5X,23HREQD NO OF CALCULATIONS= ,I2)
14    FORMAT('HO,5X,1 HPRESSURE= ,F6.1)
506   FORMAT( 5X,20HPHOTOLYSIS OF C2H4= ,F5.3)
507   FORMAT( 5X,,5HTIME INTERVAL= ,F5.2)
508   FORMAT( 5X,13HNO OF STEPS= ,I3)
511   FORMAT( 5X,29HINITIAL AZOMETHANE PRESSURE= ,F6.1)
512   FORMAT( 5X,18HAZOMETHANE PULSE= ,F6.1)
522   FORMAT( 5X,19HHYDROGEN PRESSURE= ,F6.2)
526   FORMAT( 5X,19HPHOTOLYSIS OF CH3= ,F8.3)
550   FORMAT( 5X,18HFRACTION OF XCH2= ,F5.3)
15    FORMAT('HO)
16    FORMAT('HO,3X,1HT,8X,4HCH2,7X,4H3CH2,7X,4HXCH2,7X,
     13HCH3,8X,1HH,7X,5HKETEN,2X,3HAZO,5X,3HCH4,
     25X,4HC2H4,3X,4HC2H6,3X,4HC2H2)
17    FORMAT(1H1)
18    FORMAT('HO,5X,7HPULSE= ,F5.1)
501   FORMAT( 6X,47H*----------------------------------------)
502   FORMAT( 6X,1H*,45X,1H*)
503   FORMAT( 6X,1H*,3X,27H1CH2+AR-------3CH2+AR     K2,3X,1PG9.2,3X,1H*)
504   FORMAT( 6X,1H*,3X,27H1CH2+KETEN----C2H4+CO     K3,3X,1PG9.2,3X,1H*)
505   FORMAT( 6X,1H*,3X,27H3CH2+3CH2------C2H4**     K4,3X,1PG9.2,3X,1H*)
513   FORMAT( 6X,1H*,3X,27H1CH2+KETEN-3CH2+KETEN     K1,3X,1PG9.2,3X,1H*)
```

```
514   FORMAT( 6X,1H*,3X,2HH3CH2+CH3-------C2H4+H     K5,3X,1PG9.2,3X,1H*)
515   FORMAT( 6X,1H*,3X,2HCH3+CH3---------C2H6*      K6,3X,1PG9.2,3X,1H*)
516   FORMAT( 6X,1H*,3X,2HCH3+H-----------CH4*       K7,3X,1PG9.2,3X,1H*)
517   FORMAT( 6X,1H*,3X,2HH+KETEN--------CH3+CO      K8,3X,1PG9.2,3X,1H*)
518   FORMAT( 6X,1H*,3X,2HC2H4+*---------C2H2+2H     K9,3X,1PG9.2,3X,1H*)
519   FORMAT( 6X,1H*,3X,2HC2H4+**+AR-----C2H4+*AR   K10,3X,1PG9.2,3X,1H*)
520   FORMAT( 6X,1H*,3X,2HCH3+H----------CH3+H      K11,3X,1PG9.2,3X,1H*)
521   FORMAT( 6X,1H*,3X,2HCH3+*AR--------CH4+AR     K12,3X,1PG9.2,3X,1H*)
523   FORMAT( 6X,1H*,3X,2HICH2+H2---------CH3+H     K13,3X,1PG9.2,3X,1H*)
524   FORMAT( 6X,1H*,3X,2HICH2+H2-------3CH2+H2     K14,3X,1PG9.2,3X,1H*)
525   FORMAT( 6X,1H*,3X,2H                          K15,3X,1PG9.2,3X,1H*)
527   FORMAT( 6X,1H*,3X,2HCH3+*+H2--------CH4+H2    K16,3X,1PG9.2,3X,1H*)
528   FORMAT( 6X,1H*,3X,2HC2H4+---------C2H2+H2     K17,3X,1PG9.2,3X,1H*)
529   FORMAT( 6X,1H*,3X,2HC2H4+*AR------C2H4+AR     K18,3X,1PG9.2,3X,1H*)
530   FORMAT( 6X,1H*,3X,2HC2H4+*+H2----C2H4+*H2     K19,3X,1PG9.2,3X,1H*)
531   FORMAT( 6X,1H*,3X,2HC2H4+*+H2------C2H4+H2    K20,3X,1PG9.2,3X,1H*)
532   FORMAT( 6X,1H*,3X,2HC2H6+*H2------C2H6+H2     K21,3X,1PG9.2,3X,1H*)
533   FORMAT( 6X,1H*,3X,2HC2H6+*AR------C2H6+AR     K22,3X,1PG9.2,3X,1H*)
534   FORMAT( 6X,1H*,3X,2HC2H6+---------CH3+CH3     K23,3X,1PG9.2,3X,1H*)
535   FORMAT( 6X,1H*,3X,2HXCH2+H2---------CH3+H     K24,3X,1PG9.2,3X,1H*)
536   FORMAT( 6X,1H*,3X,2HXCH2-----------1CH2       K25,3X,1PG9.2,3X,1H*)
537   FORMAT( 6X,1H*,3X,2HXCH2+3CH2--------C2H2     K28,3X,1PG9.2,3X,1H*)
538   FORMAT( 6X,1H*,3X,2HXCH2+XCH2--------C2H2     K29,3X,1PG9.2,3X,1H*)
539   FORMAT( 6X,1H*,3X,2HXCH2+CH3-------C2H4+H     K27,3X,1PG9.2,3X,1H*)
540   FORMAT( 6X,1H*,3X,2HXCH2+KETEN----C2H4+CO     K26,3X,1PG9.2,3X,1H*)
C
C     NUMBER IS NO. OF K'S TO BE READ
C     N IS NO. OF EQUATIONS
C
      NUMBER=29
      N=11
C
C     READ IN RATE CONSTANTS
C
      READ(5,*) (K(I),I=1,29)
      DO 693 IJ=1,2
      WRITE(6,17)
      WRITE(6,501)
      WRITE(6,502)
      WRITE(6,515) K(1)
      WRITE(6,503) K(2)
      WRITE(6,524) K(14)
      WRITE(6,502)
      WRITE(6,504) K(3)
      WRITE(6,525) K(15)
      WRITE(6,517) K(8)
      WRITE(6,525) K(15)
      WRITE(6,514) K(5)
      WRITE(6,502)
      WRITE(6,505) K(4)
      WRITE(6,518) K(9)
      WRITE(6,519) K(10)
      WRITE(6,528) K(17)
      WRITE(6,529) K(18)
      WRITE(6,530) K(19)
      WRITE(6,531) K(20)
      WRITE(6,502)
      WRITE(6,516) K(7)
      WRITE(6,520) K(11)
      WRITE(6,521) K(12)
      WRITE(6,527) K(16)
      WRITE(6,502)
      WRITE(6,515) K(6)
      WRITE(6,532) K(21)
      WRITE(6,533) K(22)
      WRITE(6,534) K(23)
      WRITE(6,502)
      WRITE(6,535) K(24)
      WRITE(6,536) K(25)
      WRITE(6,537) K(28)
      WRITE(6,538) K(29)
      WRITE(6,539) K(27)
      WRITE(6,540) K(26)
      WRITE(6,502)
      WRITE(6,501)
693   CONTINUE
C
C     FIRST ORDER RATE CONSTANTS ARE CONVERTED TO UNITS OF (MICROSEC)-1
C     AND SECOND ORDER RATE CONSTANTS TO (MTORR -1(MICROSEC)-1
C
      DO 2 I=1,NUMBER
      K(I)=K(I)*3.24E 7
      IF(K(I).LT.1.0) GO TO 2
      K(I)=K(I)/3.24E 13
2     CONTINUE
C
C     G(J) ARE ERROR BOUNDS
C     A MIXED TEST IS USED
C     IF E(J) IS THE ESTIMATED LOCAL TRUNCATION ERROR IN Y(J),THEN
C     FOR Y(J).LT.1.0,E(J).LT.G(J)
C     FOR Y(J).GT.1.0,E(J).LT.G(J)*Y(J)
C
      IT=1
      DO 3 J=1,N
      G(J)=1.0E-5
3     CONTINUE
      READ(5,1) NUM
      WRITE(6,15) NUM
      DO 100 I=1,NUM
      WRITE(6,17)
      READ(5,*) P,Z,PULSE,FACTOR,HO,NO
      READ(5,*) ZA,PULSEA,PH,DES,FRACT2
      WRITE(6,512) PULSEA
      WRITE(6,511) ZA
      WRITE(6,522) PH
      WRITE(6,526) DES
      WRITE(6,550) FRACT2
C
C     FRACT1 IS THE FRACTION OF 1CH2 PRODUCED IN PHOTOLYSIS
C     FRACT2 IS THE FRACTION OF XCH2 PRODUCED IN PHOTOLYSIS
C
      FRACT1=1.0-FRACT2
C
C     PH IS CONVERTED TO MTORR
C     P IS CONVERTED TO MTORR
C
```

```
      PH=PH*1.0E 3
      WRITE(6,14) P
      P=P*1.0E 5
      WRITE(6,12) Z
      WRITE(6,16) PULSE
      WRITE(6,506) FACTOR
C
C     IF K(9)=0.0 THE PROGRAM TREATS THE SCHEME AS IF 3CH2+3CH2=C2H2+H2
C     WITH RATE CONSTANT K(4). K(10),K(17),K(18),K(19),K(2A) ARE THEN
C     IRRELEVANT.
C     IF K(9).NE.0.0 THEN K(17),K(10) AND/OR K(19),K(18) AND/OR K(20)
C     MUST BE ASSIGNED
C
      FI1=0.0
      FI2=1.0
      FI3=0.0
      FI4=1.0
      IF(K(9).EQ.0.0) GO TO 69
      FI1=1.0/(1.0+((K(10)*P+K(19)*PH)/K(9)))
      FI2=1.0-FI1
      FI4=1.0/(1.0+((K(18)*P+K(20)*PH)/K(17)))
      FI3=1.0-FI4
69    CONTINUE
C
C     IF K(11)=0.0 THEN THE PROGRAMME ASSUMES THE RATE CONSTANT FOR
C     CH3+H TO BE THE HIGH PRESSURE VALUE I.E. K(7) ;OTHERWISE
C     A LINDEMANN MODEL IS ASSUMED AND K(12) AND/OR K(16) MUST
C     BE NON ZERO
C
      ZETA3=K(7)
      IF(K(11).EQ.0.0) GO TO 70
      ZETA3=K(7)/(1.0+(K(11)/(K(12)*P+K(16)*PH)))
70    CONTINUE
C
C     IF K(23)=0.0 THEN THE PROGRAM ASSUMES THE RATE CONSTANT FOR
C     CH3+CH3 TO BE THE HIGH PRESSURE VALUE I.E. K(6) ;OTHERWISE A
C     LINDEMANN MODEL IS ASSUMED AND K(22) AND/OR K(21) MUST BE NON ZERO
C
      ZETA=K(6)
      IF(K(23).EQ.0.0) GO TO 71
      ZETA=K(6)/(1.0+(K(23)/(K(22)*P+K(21)*PH)))
71    CONTINUE
C
C     Y(1)=1CH2     Y(7)=H
C     Y(2)=3CH2     Y(8)=CH4
C     Y(3)=CH2CO    Y(9)=C2H6
C     Y(4)=C2H4     Y(10)=CH3N2CH3
C     Y(5)=C2H2     Y(11)=XCH2
C     Y(6)=CH3
C
C      NORMALLY ALL INITIAL CONCENTRATIONS ARE ZERO EXCEPT FOR KETENE
C     AND/OR AZOMETHANE
C
      DO 7 J=1,N
      Y(J)=0.0
7     CONTINUE
      Y(3)=Z
      Y(10)=ZA
C
C     WKET AND WAZO ARE SET SO THAT THE AMOUNTS OF KETENE AND
C     AZOMETHANE PHOTOLYSED ARE PULSE AND PULSEA RESPECTIVELY
C
C     WC2H4 AND WCH3 CORRECT FOR PHOTOLYSIS OF C2H4 AND CH3
C     FACTOR AND DES ARE THE FRACTIONS OF C2H4 AND CH3 WHICH WOULD BE
C     PHOTOLYSED THROUGHOUT THE WHOLE PHOTOLYSIS FLASH
C
      WKET=0.0
      WAZO=0.0
      IF (Z.LT.0.1) GO TO 67
      WKET=ALOG(Z/(Z-PULSE))
67    CONTINUE
      IF (ZA.LT.0.1) GO TO 68
      WAZO=ALOG(ZA/(ZA-PULSEA))
68    CONTINUE
      WC2H4=ALOG(1.0-FACTOR)
      WC2H4=-WC2H4
      WCH3=ALOG(1.0-DES)
      WCH3=-WCH3
C
C     THETA1,THETA2 ARE NORMALISING CONSTANTS FOR FUNCTION GEN(T)
C
      TAU1=1.7
      TAU2=1.3
      TAU3=12.0
      GAMP=TAU1**2.0+4.0*TAU2**2.0
      GAMP=GAMP/(2.0*TAU2**3.0)
      THETA1=GAMP*0.5
      THETA2=0.5/TAU3
C
C     INTEGRATION STARTS AT T=0.0
C     IFAIL=0.0 SETS HARD FAILURE
C     THE INITIAL STEP LENGTH IS H=1.0E-3
C
      T=0.0
      IFAIL=0
      H=1.0E-3
      WRITE(6,507) HO
      WRITE(6,508) NO
      WRITE(6,15)
      WRITE(6,16)
      WRITE(6,15)
      DO 4 L=1,NO
      CALL DO2AUF(T,Y,G,IT,N,IFAIL,HO,H,AUX,YO,E,A,B,C,D)
      WRITE(6,5)T,Y(1),Y(2),Y(11),Y(6),Y(7),Y(3),Y(10),
     1Y(8),Y(4),Y(9),Y(5),H
5     FORMAT(1X,0PF6.1,1X,5(1PG10.3,1X),2(0PF6.1,1X),5(0PF6.3,1X))
4     CONTINUE
100   CONTINUE
      STOP
      END
C
C
C
C     THE SUBROUTINE AUX EVALUATES THE DERIVATIVES F(I) IN TERMS OF Y(J)
C
C
C
```

```
      SUBROUTINE AUX(F,Y,T)
      REAL K
      DIMENSION K(29)
      DIMENSION F(11),Y(11)
      COMMON/BLOCK1/K,P,WKET,WAZO,WC2H4,WCH3,PH,ZETA3,
     1FI1,FI2,FI3,FI4,ZETA,FRACT1,FRACT2
      CCC=0.0
      A=0.0
      AA=0.0
      AF=0.0
      AAA=0.0
      AG=0.0
      IF(T.GT.50.0) GO TO 999
      CCC=GEN(T)
      A=CCC*Y(3)*WKET*FRACT1
      AA=CCC*Y(4)*WC2H4
      AF=CCC*Y(10)*WAZO
      AAA=CCC*Y(3)*WKET*FRACT2
      AG=CCC*Y(6)*WCH3
999   CONTINUE
      B=0.0
      C=0.0
      DA=0.0
      DB=0.0
      ADD=0.0
      F(1)=0.0
      IF(T.GT.50.0.AND.Y(1).LT.1.0E-3)GO TO 998
      B=K(3)*Y(1)*Y(3)
      C=K(2)*P*Y(2)
      DA=K(13)*PH*Y(1)
      DB=K(14)*PH*Y(1)
      ADD=K(15)*Y(1)*Y(3)
      F(1)=A-C-DB-DA-B+AG-ADD
998   CONTINUE
      AAB=0.0
      AAC=0.0
      AAD=0.0
      AAE=0.0
      AAF=0.0
      AAG=0.0
      IF(Y(11).LT.1.0E-4.AND.T.GT.50.0) GO TO 700
      AAB=K(29)*Y(11)*PH
      AAC=K(25)*Y(11)
      AAD=K(28)*Y(11)*Y(2)
      AAE=K(29)*Y(11)*Y(11)
      AAF=K(27)*Y(11)*Y(6)
      AAG=K(26)*Y(11)*Y(3)
700   CONTINUE
      BA=K(8)*Y(3)*Y(7)
      E=K(4)*Y(2)*Y(2)
      BB=FI1*E
      BC=FI3*FI2*E
      BD=FI2*FI4*E
      AC=K(5)*Y(2)*Y(6)
      AD=ZETA*Y(6)*Y(6)
      AE=ZETA3*Y(6)*Y(7)
      F(1)=F(1)+AAC
      F(2)=C-2.0*E-AC+DB+BD-AAD
      F(3)=-A-BA-B-AAG-AAA-ADD
      F(4)=AC-AA+B+BC+AAG
      F(5)=AA+BB+BD+AAD+AAE+AAF+ADD
      F(6)=2.0*AF-2.0*AD-AE-AC+BA+DA-AG+AAB-AAF
      F(7)=AC-AE-BA+DA+2.0*BB+AG+AAB+AAF
      F(8)=AE
      F(9)=AD
      F(10)=-AF
      F(11)=AAA-AAD-AAC-AAD-AAF-AAG-2.0*AAE
      RETURN
      END
C
C
C
C     FUNCTION GEN(T) SIMULATES THE PHOTOLYSIS FLASH
C
C
C
      REAL FUNCTION GEN(T)
      COMMON/BLOCK2/THETA1,THETA2
      GEN=THETA1*(SIN(T/1.2))**2.0*EXP(-T/1.8)+THETA2*EXP(-T/12.0)
1001  CONTINUE
      RETURN
      END
      FINISH
*LINK LIB NAGF
*END BIN CICERO5
****
```

APPENDIX A2

## Emission spectrum of flashlamp.

The emission spectrum from a black body at temperature T K is given by [143]

$$U_\lambda = 15N\left(\frac{hc}{\pi kT}\right)^4 \frac{1}{\lambda^5} \frac{1}{\exp(hc/\lambda kT) - 1}$$

where $U_\lambda$ is normalised such that

$$\int_o^\infty U_\lambda d\lambda = N$$

N may be considered as the total number of photons incident on the reaction vessel.

Fig. A2.1 shows a plot of $U_\lambda$ versus $\lambda$ on the assumption that the flash has a black body temperature of $10^4$ K.

$C_2H_4$ may be used as an actinometer to obtain a rough estimate of N. Fig. A2.2 shows a plot of $I_{abs}$ versus $\lambda$, where $I_{abs}$ has been calculated as

$$I_{abs} = U_\lambda \epsilon_\lambda t_\lambda c l.$$

$\epsilon_\lambda$ is the extinction coefficient of $C_2H_4$ and $t_\lambda$ is the transmission coefficient of spectrosil. c the concentration of $C_2H_4$ was taken as 10 mTorr and l the optical path as 3 cm. If the quantum yield for $C_2H_4$ photolysis is 1.0 the area under this plot should be equal to the concentration of $C_2H_4$ which is photolysed.

$$\left[C_2H_4\right]_{\text{photolysed}} \simeq 4.0 \text{ mTorr}$$

$$\text{Area} \simeq 3.2 \times 10^{-4} \text{ N photons}$$

$$N = \frac{4 \times 3.24 \times 10^{13}}{3.2 \times 10^{-4}} = 4.0 \times 10^{17} \text{ photons}$$

It is now possible to estimate the photolysis of $CH_3$ at

$\lambda$ = 216 nm.

At 216 nm. $U_\lambda = 7.2 \times 10^{23}$ photons $m^{-1}$

The oscillator strength for the transition, $f = 1.2 \times 10^{-2}$

i.e. $$\int k_\nu d\nu = 0.833 \times 10^{-12} \times 1.2 \times 10^{-2}$$
$$\simeq 10^{-13} \text{ molecule}^{-1} \text{ cm}$$

$$\underset{(O.D.)}{\text{Optical density}} = \ln k_\nu$$

where l is the optical path length, n is the number density of absorbing species.

$$\int O.D.\ d\nu = l \times n \times 10^{-13}$$

$$\int O.D.\ d\lambda = n\, l\, 10^{-13} / 2.14\, 10^{11} = 4.7 \times 10^{-25}\, n\, l$$

since $d\nu = 1/\lambda^2\, d\lambda$

Hence $$-I_o \times O.D. = U_\lambda \times 4.7 \times 10^{-25}\, n\, l$$
$$= 33.8\, n\, l$$

$$\frac{I_{abs}}{n} = \frac{I_o \times O.D.}{n} = 33.8\, l$$

Thus even for an optical path l = 0.01 cm.,

$I_{abs} / n = 0.338$ , which implies that a significant fraction of $CH_3$ radicals absorb radiation.

Fig. A2.1. Emission spectrum from a black body at T = $10^4$ K.

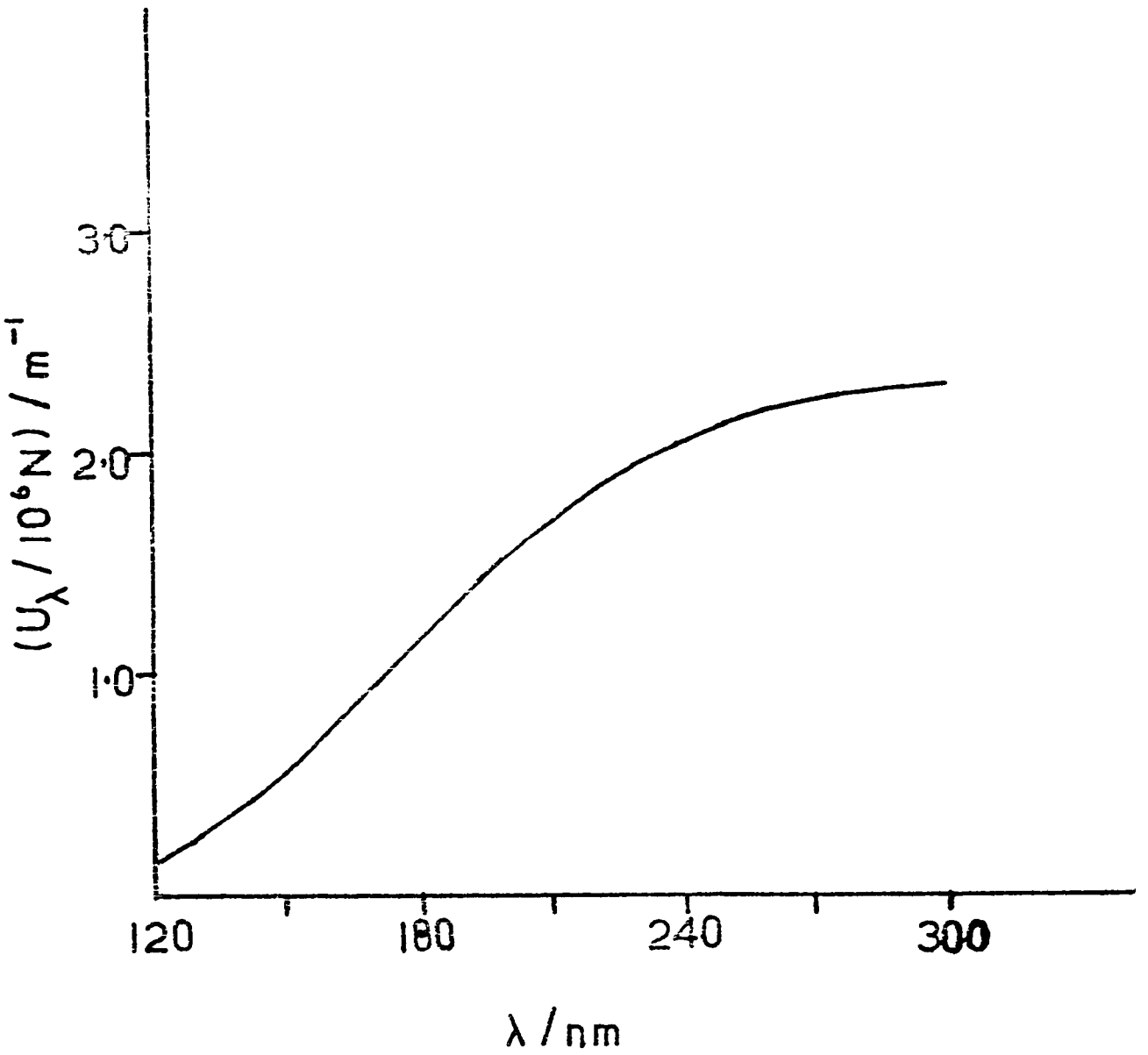
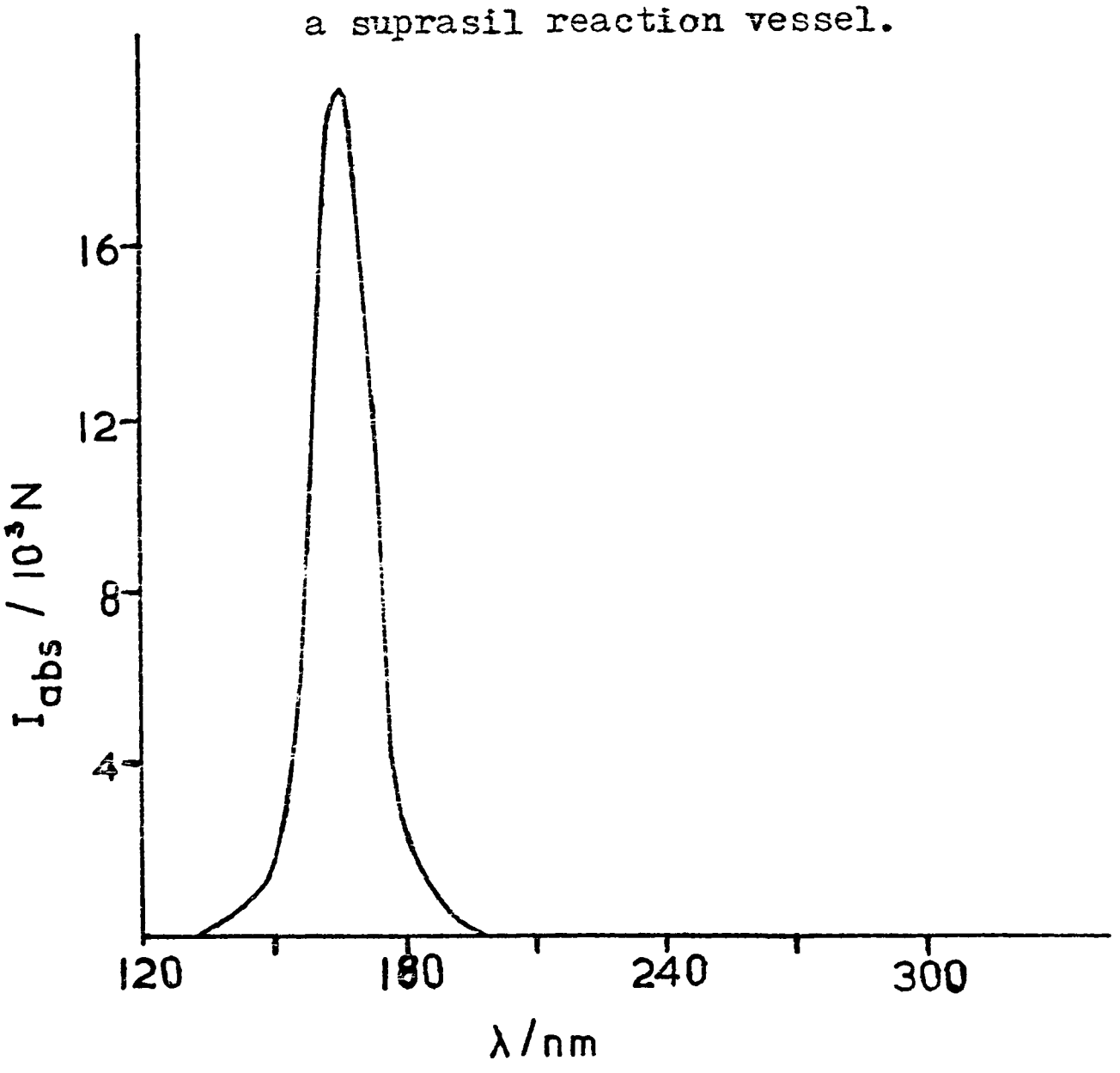



Fig. A2.2. $I_{abs}$ versus $\lambda$ for 10 mTorr $C_2H_4$ in a suprasil reaction vessel.



APPENDIX A3

## Rate of cooling of the reaction vessel.

The reaction vessel may be approximated by a cylinder of radius a.

Let the temperature of the surroundings be $\theta_1$ and suppose that the surroundings act as an infinite heat sink so that the cylinder has its surface maintained at a constant temperature $\theta_1$. At t = 0 the temperature inside the cylinder is $\theta_1 + \theta_o$. Assume that the only means of heat loss from the cylinder is conduction.

In the idealised case of an infinitely long cylinder the distribution of temperature has cylindrical symmetry and is governed by the equation,

$$\frac{\partial\theta}{\partial t} = \kappa\left(\frac{\partial^2\theta}{\partial r^2} + \frac{1}{r}\frac{\partial\theta}{\partial r}\right) \qquad 0 \le r < a, t > 0$$

with boundary conditions,

$$\theta = \theta_1 + \theta_o \qquad \text{at } t = 0,\ 0 \le r < a$$
$$\theta = \theta_1 \qquad \text{at } t \ge 0,\ r = a$$

where $\kappa = K/c\rho$

K is the thermal conductivity of the cylinder.

c is the specific heat of the cylinder.

$\rho$ is the density of the cylinder.

The equation has a solution [138]

$$\theta = \theta_1 - \theta_o \frac{2}{a} \sum_{s=1}^{\infty} \exp\left(-\kappa\alpha_s^2 t\right) \frac{J_o(\alpha_s r)}{\alpha_s J_o'(\alpha_s a)}$$

where $J_o(x)$ is a first order Bessel function and $J_o'(x)$ is the first derivative of $J_o(x)$.

$\alpha_s$ are the roots of the equation, $J_o(\alpha_s a) = 0$.

The solution was computed using the convergence test,

$$\sum_{s=1}^{n+1} f(r,t) - \sum_{s=1}^{n} f(r,t) \leq 10^{-8}$$

The values used in the solution were:

Radius of the cylinder , $a = 2.0$ cm.

Thermal conductivity of argon, $K = 50.0 \times 10^{-6}$ cal $s^{-1}$ $cm^{-1}$ $K^{-1}$

Specific heat of argon , $c = 3.0$ cal $K^{-1}$ $mol^{-1}$

Density of argon , $\rho = 5.4 \times 10^{-8}$ p mol $cm^{-3}$

where p is the pressure in Torr.

Fig. A3.1 shows $\theta$ as a function of t for r = 0 at p = 10 Torr. The curve for p = 100 Torr is identical if the scale on the abscissa is multiplied by a factor of 10 i.e. $\theta \rightarrow \theta_1$ at $t \simeq 10^{-1}$ s for p = 10 Torr, $\theta \rightarrow \theta_1$ at $t \simeq 1$ s for p = 100 Torr.

Fig. A3.2 shows $\theta$ as a function of r at a series of times, $t > 0$.

Fig. A3.1. $\theta$ as a function of t at r = 0, for p = 10 Torr.

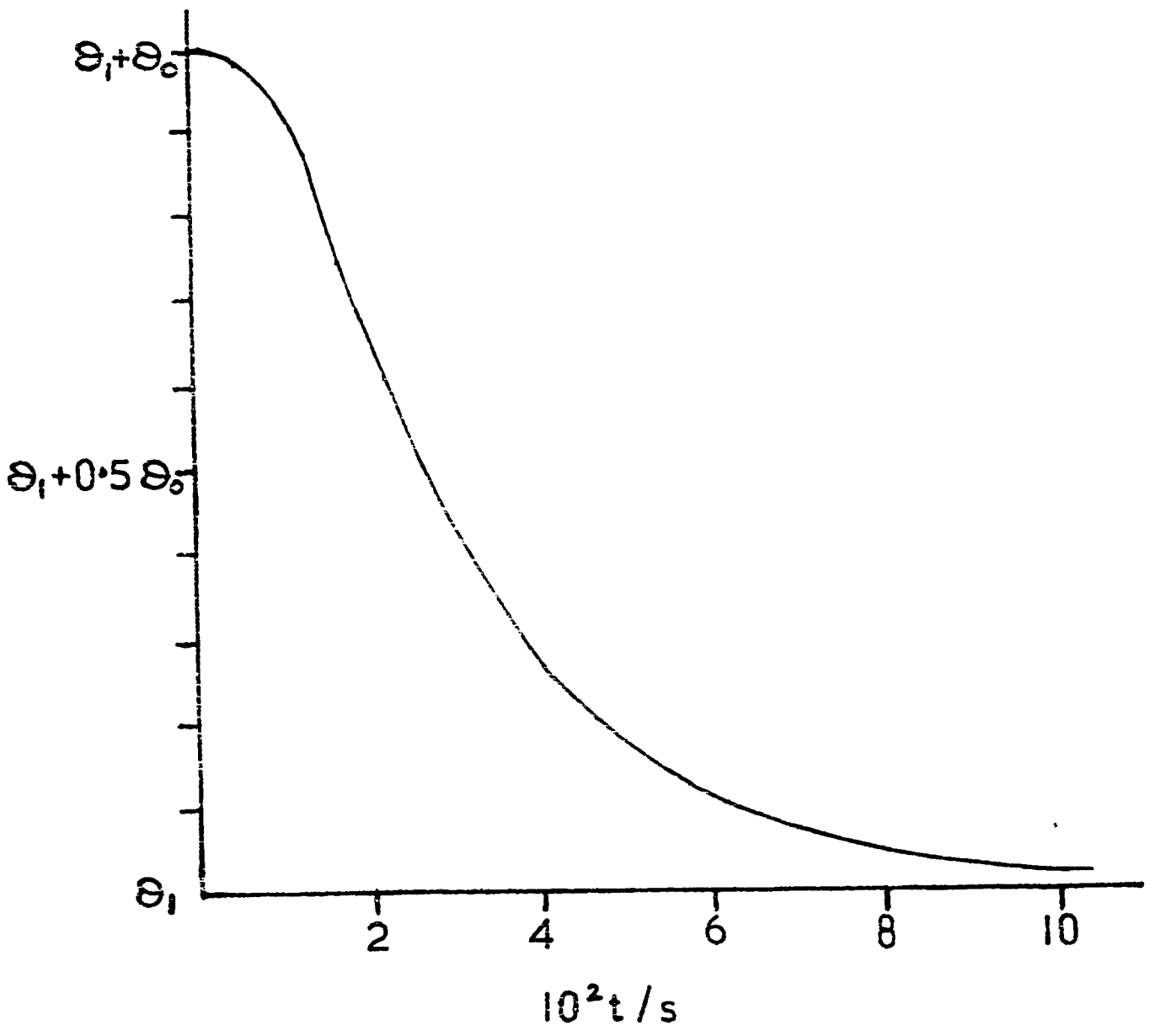
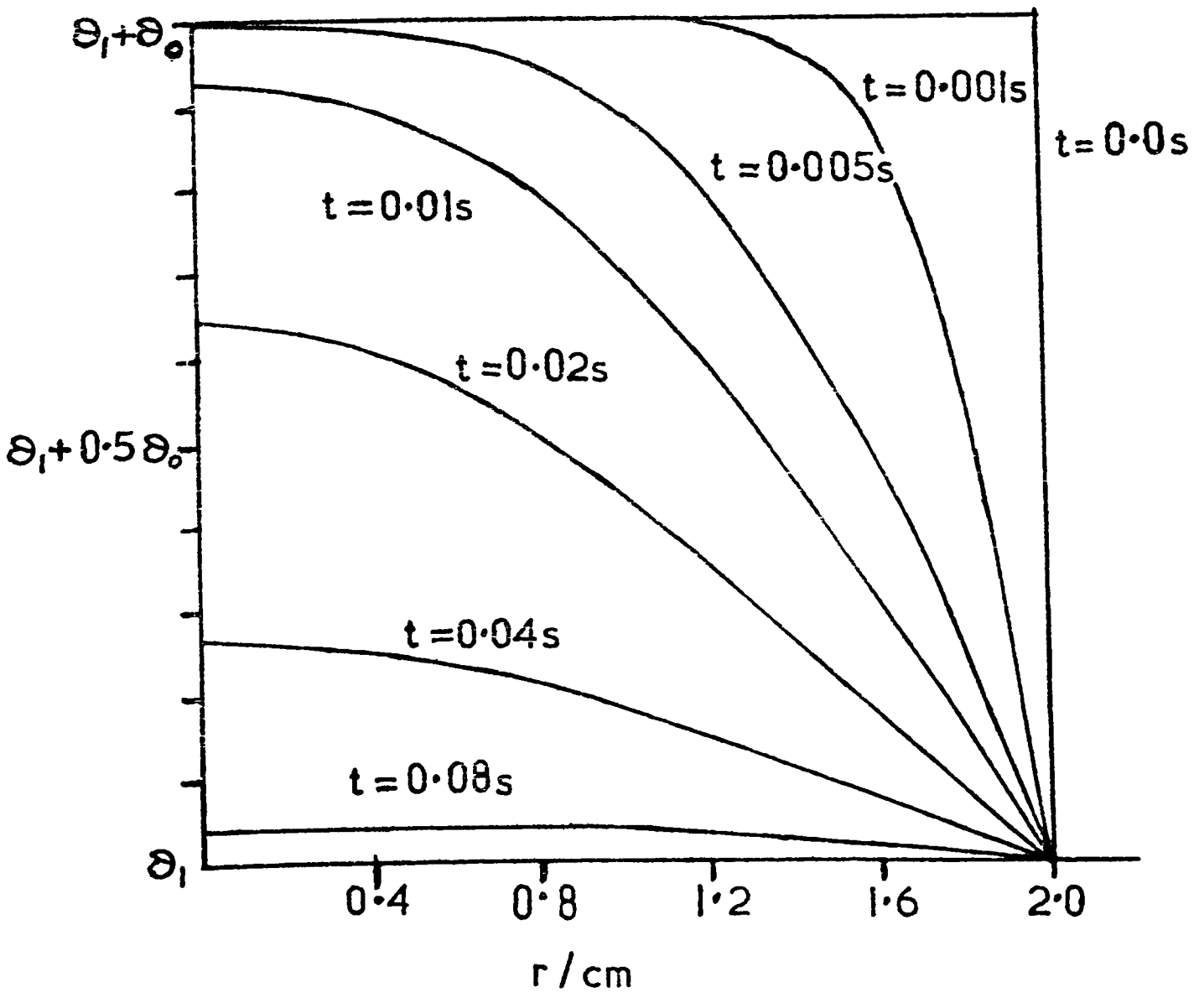


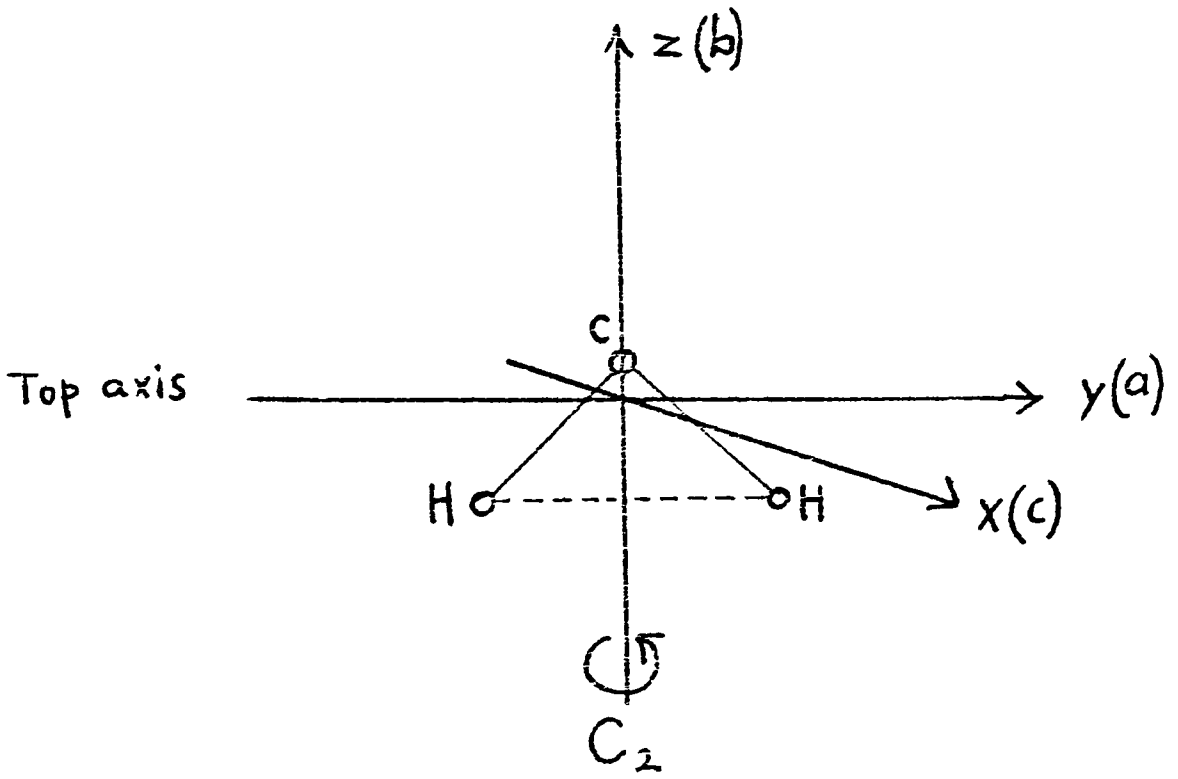

Fig. A3.2. $\theta$ as a function of r at various t, for p = 10 Torr.



APPENDIX A4

## Partition functions for $CH_2$ ($^3B_1$) and $CH_2$ ($^1A_1$).

A. 4.1. $CH_2$ ($^3B_1$). From the geometry of $CH_2$ ($^3B_1$) defined by HCH = 136°, and r (C-H) = 1.078 A, the rotational constants were calculated. The coordinate system is shown below.




A = 60.26 $cm^{-1}$, B = 8.44 $cm^{-1}$, C = 7.40 $cm^{-1}$.

Since B≃C, $CH_2$ ($^3B_1$) approximates a prolate symmetric top. The energy levels may be represented to a fairly good approximation by the expression,

$$F(J,K) = B''J(J+1) + (A-B'')K^2 \qquad (J \geq K)$$

Each J state has 2J+1 degeneracy. For K≠0 each level is doubly degenerate (K - type doubling). Since $CH_2$ has two nuclei with spin I = ½, the overall wave function must obey Fermi statistics. Since the electronic wave function is antisymmetric with respect to exchange of the hydrogen nuclei the rotational levels which are symmetric with respect to the $C_2$ axis must be associated with symmetric nuclear spin states,

and for antisymmetric rotational levels the nuclear spin wave functions must be antisymmetric. Thus symmetric rotational levels have 3 times the statistical weight of antisymmetric rotational levels.

For K = 0, the even J levels are symmetric and are thus triply degenerate on account of nuclear spin, whereas the odd J levels are antisymmetric and remain singly degenerate. For $K \neq 0$, one component of the doubly degenerate level is symmetric and the other antisymmetric giving an overall degeneracy of 4.

The general expression for a partition function is

$$Q = \sum_i g_i \exp( -E_i / kT )$$

where $g_i$ is the statistical weight of the $i^{th}$ level of energy $E_i$. The partition function in this case is most readily evaluated if the K = 0 and $K \neq 0$ levels are considered separately.

$$Q = 3 ( A + B + C ) - 6.0$$

where

$$A = \sum_{\text{even } J} 3(2J+1)\exp(-B''J(J+1)hc/kT)$$

$$B = \sum_{\text{odd } J} (2J+1)\exp(-B''J(J+1)hc/kT)$$

$$C = \sum_{K=1}^{\infty} \sum_{J=K}^{\infty} 4(2J+1)\exp(-\left[B''J(J+1)+(A-B'')K^2\right] hc/kT)$$

The factor of 3 is included to account for the electron spin degeneracy which splits all the levels except the J = 0 level (hence the term -6.0).

The value of Q, computed [139] according to the above expression, was $Q ( T = 300 K) = 521.4$.

A. 4.2. $CH_2$ ($^1A_1$). For $CH_2$ ($^1A_1$) the rotational constants are A = 20.14 $cm^{-1}$, B = 11,16 $cm^{-1}$, C = 7.06 $cm^{-1}$ [4]. The energy levels of an asymmetric top have been described by the expression [140],

$$F(J_\tau) = \tfrac{1}{2}(B + C) J(J + 1) + (A - \tfrac{1}{2}(B+C)) W_{J_\tau}$$

where $\tau$ takes the values -J, -J+1, -J+2, ..., 0, ..., J. $W_{J_\tau}$ has been tabulated for $K = 0, -0.1, -0.2, \ldots, -1.0$, where K, an asymmetry parameter is defined by

$$K = \frac{2(B - \tfrac{1}{2}(A+C))}{A - C}$$

For $CH_2$ ($^1A_1$), $K = -0.373$ and $W_{J_\tau}$ was estimated by interpolation.

The result for Q computed [140] using the above expression for the energy levels and including appropriate degeneracy factors was $Q(T = 300\ K) = 268.32$.

REFERENCES.


1. G. Herzberg and J. Shoosmith, Nature, 1959, 183, 1801.

2. G. Herzberg, Proc. Roy. Soc. (London), 1961, A262, 291.

3. G. Herzberg, "Molecular Spectra and Molecular Structure III", D. Van. Nostrand Co., 1966.

4. G. Herzberg and J.W.C. Johns, Proc. Roy. Soc.(London), 1966, A295, 107.

5. G. Herzberg, Can. J. Phys., 1961, 39, 1511.

6. A.D. Walsh, J. Chem. Soc., 1953, 2260.

7. R.A. Bernheim, H.W. Bernard, P.S. Wang, L.S. Wood, P.S. Skell, J. Chem. Phys., 1970, 53, 1280.

8. E. Wasserman, W.A. Yager, V.J. Kuck, Chem. Phys. Lett., 1970, 7, 409.

9. E. Wasserman, V.J. Kuck, R.S. Hutton, W.A. Yager, J. Am. Chem. Soc., 1970, 92, 7491.

10. G. Herzberg and J.W.C. Johns, J. Chem. Phys., 1971, 54, 2276.

11. J.F. Harrison and J.C. Allen, J. Am. Chem. Soc., 1969, 91, 807.

12. C.F. Bender and H.F. Schaefer, J. Am. Chem. Soc., 1970, 92, 4984.

13. V. O'Neil, H.F. Schaefer, C.F. Bender, J.Chem.Phys., 1971, 55, 162.

14. J.M. Foster and S.F. Boys, Rev. Mod. Phys., 1960, 32, 305.

15. P.J. Hay, N.J. Hunt, W.A. Goddard III, Chem. Phys. Lett., 1972, 13, 30.

16. S.Y. Chu, A.K.Q. Siu, E.F. Hayes, J. Am. Chem. Soc., 1972, 94, 2969.

17. C.F. Bender, H.F. Schaefer, D.R. Franceschetti, L.C. Allen, J. Am. Chem. Soc., 1972, 94, 6888.

18. R. Hoffmann, G.D. Zeiss, G.W. Van Dine, J. Am. Chem. Soc., 1968, 90, 1485.

19. W.A. Lathan, W.J. Hehre, L.A. Curtiss, J.A. Pople, J. Am. Chem. Soc., 1971, 93, 6377.

20. V. Staemmler, Theor. Chim. Acta, 1973, 31, 49.

21. J.F. Harrison, Accounts of Chemical Research, 1974, 7, 378.

22. R.C. Gordon, W. Klemperer, J.I. Steinfeld, Ann. Rev. Phys. Chem., 1968, 19, 215.

23. W.A. Chupka and C. Lifshitz, J. Chem. Phys., 1968, 48, 1109.

24. N.B.S. Technical Note 270-3, Jan. 1968, Selected Values of Chemical Thermodynamic Properties.

25. R.L. Nuttall, A.H. Laufer, M.V. Kilday, J. Chem. Thermodyn., 1971, 3, 167.

26. A.H. Laufer and H. Okabe, J. Am. Chem. Soc., 1971, 93, 4137.

27. W.A. Chupka, J. Berkowitz, K.M.A. Refaey, J. Chem. Phys., 1969, 50, 1938.

28. V.H. Dibeler, M. Krauss, R.M. Reese, F.M. Harlee, J. Chem. Phys., 1965, 42, 3791.

29. R.N. Dixon and G.H. Kirby, Trans. Farad. Soc., 1966, 62, 1406.

30. A.H. Laufer and R.A. Keller, J. Am. Chem. Soc., 1971, 93, 61.

31. W.A. Noyes and I. Unger, J. Pure and App. Chem., 1964, 9, 461.

32. S. Ho, I. Unger, W.A. Noyes, J. Am. Chem. Soc., 1965, 87, 2297.

33. B.A. Degraff and G.B. Kistiakowsky, J. Phys. Chem., 1967, 71, 3984.

34. R.W. Carr and G.B. Kistiakowsky, J. Phys. Chem., 1966, 70, 118.

35. T.W. Eder and R.W. Carr, J. Phys. Chem., 1969, 73, 2074.

36. F.H. Dorer and B.S. Rabinovitch, J. Phys. Chem., 1965, 69, 1964.

37. K. Dees and D.W. Setser, J. Chem. Phys., 1971, 75, 2240.

38. R.A. Cox and K.F. Preston, Can. J. Chem., 1969, 47, 3345.

39. A.N. Strachan and D.E. Thornton, Can. J. Chem., 1968, 46, 2353.

40. G.B. Kistiakowsky and T.A. Walter, J. Phys. Chem., 1968, 72, 3952.

41. W. Braun, A.M. Bass, M.J. Pilling, J. Chem. Phys., 1970, 52, 5131.

42. A.H. Laufer, J. Phys. Chem., 1969, 73, 959.

43. R.K. Briston and D.H. Volman, J. Chem. Phys., 1951, 19, 1394.

44. J.G. Calvert and J.N. Pitts, "Photochemistry", J.Wiley & Sons, 1966.

45. A.J. Merer, Can. J. Phys., 1964, 42, 1242.

46. Published as a private communication in Ref. 44.

47. J.A. Bell, J. Phys. Chem., 1971, 75, 1537.

48. H. Okabe and D.A. Becker, J. Chem. Phys., 1963, 39, 2549.

49. P. Ausloos and S.G. Lias, J. Chem. Phys., 1966, 44, 521.

50. H. Okabe and J.R. McNesby, J. Chem. Phys., 1962, 37, 1340.

51. K. Obi, H. Akimoto, Y. Ogata, I. Tanaka, J. Chem. Phys., 1971, 55, 3822.

52. R.D. Koob, J. Phys. Chem., 1972, 76, 9.

53. C.L. Currie, H. Okabe, J.R. McNesby, J. Phys. Chem., 1963, 67, 1494.

54. L.W. Richards and D.H. Sigafoos, J. Chem. Phys., 1965, 43, 492.

55. P. Ausloos, R. Gorden, S.G. Lias, J. Chem. Phys,, 1964, 40, 1854.

56. R. Gorden and P. Ausloos, J. Chem. Phys., 1967, 46, 4823.

57. L. Hellner, J. Masanet, C. Kermeil, J. Chem. Phys., 1971, 55, 1022.

58. A.R. Welch and D.L. Judge, J. Chem. Phys., 1972, 57, 286.

59. W. Braun, J.R. McNesby, A.M. Bass, J. Chem. Phys., 1967, 46, 2071.

60. W. Braun, K.H. Welge, J.R. McNesby, J. Chem. Phys., 1966, 45, 2650.

61. S. Karplus and R. Bersohn, J. Chem. Phys., 1969, 51, 2040.

62. E. Lindholm, J. Chem. Phys., 1970, 52, 4921.

63. R.F.W. Bader and J.I. Generosa, Can. J. Chem., 1965, 43, 1631.

64. P.S. Skell and R.C. Woodworth, J. Am. Chem. Soc., 1956, 78, 4496, 6427.

65. P.S. Skell and R.C. Woodworth, J. Am. Chem. Soc., 1959, 81, 3383.

66. H.M. Frey, Proc. Roy. Soc. (London), 1959, A251, 575.

67. D.F. Ring and B.S. Rabinovitch, Can. J. Chem., 1968, 46, 2435.

68. D.F. Ring and B.S. Rabinovitch, J. Phys. Chem., 1968, 72, 191.

69. H.M. Frey, Proc. Roy. Soc. (London), 1959, A250, 409.

70. J.A. Bell and G.B. Kistiakowsky, J. Am. Chem. Soc., 1962, 84, 3417.

71. T.W. Eder and R.W. Carr, J. Chem. Phys., 1970, 53, 2258.

72. T.W. Eder, R.W. Carr, J.W. Koenst, Chem. Phys. Lett., 1969, 3, 520.

73. M.L. Halberstadt and J. Crump, J. Photochemistry, 1972, 1, 295.

74. R.D. Koob, J. Phys. Chem., 1969, 73, 3168.

75. A. K. Dhingra and R.D. Koob, J. Phys. Chem., 1970, 74, 4490.

76. W.L. Hase, J. Chem. Phys., 1972, 57, 730.

77. H.M. Frey and R. Walsh, J. Chem. Soc.(A), 1970, 2115.

78. F.S. Rowland, P.S-T. Lee, D.C. Montague, R.L. Russell, Farad. Disc. of Chem. Soc., 1972, 53, 111.

79. R.L. Russell and F.S. Rowland, J. Am. Chem. Soc., 1968, 90, 1671.

80. A.H. Laufer and A.M. Bass, J. Phys. Chem., 1974, 78, 1344.

81. R.A. Cox and R.J. Cvetanovic, J. Phys. Chem., 1968, 74, 2236.

82. D.C. Montague and F.S. Rowland, J. Am. Chem. Soc., 1971, 93, 5381.

83. G.B. Kistiakowsky and S.B. Saunders, J. Phys. Chem., 1973, 77, 427.

84. H.M. Frey, G.R. Jackson, M. Thomson, R. Walsh, J.C.S. Faraday I, 1973, 69, 2054.

85. R.L. Johnson, W.L. Hase, J.W. Simons, J. Chem. Phys., 1970, 52, 3911.

86. A.K. Dhingra, J.H. Vdrachek, R.D. Koob, Chem. Phys. Lett., 1971, 9, 17.

87. M.G. Topor and R.W. Carr, J. Chem. Phys., 1973, 58, 757.

88. R.E. Rebbert, S.G. Lias, P. Ausloos, Chem. Phys. Lett., 1971, 12, 323.

89. W.L. Hase, R.J. Phillips, J.W. Simons, Chem. Phys. Lett., 1971, 12, 161.

90. H.M. Frey, J.C.S. Chem. Comm., 1972, 1024.

91. H.M. Frey and G.J. Kennedy, J.C.S. Chem. Comm., 1975, 233.

92. H.M. Frey, J. Am. Chem. Soc., 1960, 82, 5947.

93. W.L. Hase and J.W. Simons, J. Chem. Phys., 1971, 54, 1277.

94. R.W. Carr, T.W. Eder, M.G. Topor, J. Chem. Phys., 1970, 53, 4716.

95. M.L. Halberstadt and J.R. McNesby, J. Am. Chem. Soc., 1967, 89, 3417.

96. P.C.H. Jordan and H.C. Longuet-Higgins, Mol. Phys., 1962, 5, 121.

97. L.D. Landau and E.M. Lifshitz, "Quantum Mechanics", Addison-Wesley, 1958, p. 304.

98. T.Y. Chang and H. Basch, Chem. Phys. Lett., 1970, 5, 147.

99. G. Herzberg, "Molecular Spectra and Molecular Structure II", D. Van Nostrand Co., 1945, Table 37.

100. A.B. Callear and H.E. van den Bergh, Chem. Phys. Lett., 1970, 5, 23.

101. P.W. Atkins, "Molecular Quantum Mechanics", Oxford, 1970, p. 222.

102. R.W. Carr, J. Phys. Chem., 1972, 76, 1581.

103. C.P. Baskin, C.F. Bender, C.W. Bauschlicher, H.F. Schaefer, J. Am. Chem. Soc., 1974, 96, 2709.

104. P. Cremaschi and M. Simonetta, J.C.S. Faraday II, 1974, 70, 1801.

105. J.N. Murrell, J.B. Pedley, S. Durmaz, J.C.S. Faraday II, 1973, 69, 1370.

106. R.B. Woodward and R. Hoffmann, "The Conservation of Orbital Symmetry", Verlay Chemie GmbH, Academic Press Inc., 1970.

107. H. Kollmar, Tetrahedron, 1972, 28, 5893.

108. R.C. Dobson, D.M. Hayes, R. Hoffmann, J. Am. Chem. Soc., 1971, 93, 6188.

109. F.W. Dalby, J. Chem. Phys., 1964, 41, 2297.

110. J.P. Simons, Nature, 1965, 205, 1308.

111. R. Hoffmann, R. Gleiter, F.B. Mallory, J. Am. Chem. Soc., 1970, 92, 1460.

112. G.F. Tantardini and M. Simonetta, Israel. J. Chem., 1972, 10, 582.

113. H. Kollmar, Tetrahedron Lett., 1970, 3337.

114. H. Basch, J. Chem. Phys., 1971, 55. 1700.

115. N.F. Mott and H.S.W. Massey, "The Theory of Atomic Collisions", Oxford, 1965, p. 349, p. 687.

116. G.J. Fisher, A.F. Maclean, A.W. Schizer, J. Org. Chem., 1953, 18, 1055.

117. S. Andreadas and H.D. Carlson, Org. Syntheses, 1965, 45, 50.

118. R. Renaud and L.C. Leitch, Can. J. Chem., 1954, 32, 545.

119. D. Ambrose, "Gas Chromatography", Butterworths, 1971, p. 252 (2nd edition).

120. R.N. Lewis, E.A. Jung, G.L. Chapman, L.S. Von Loon, I. E. E. E. Trans. on Nuclear Science, April 1966, 84.

121. K.H. Welge, J. Wanner, F. Stuhl, A. Heindrichs, Rev. Sci. Instr., 1967, 38, 1728.

122. J.W. Boag, Photochemistry and Photobiology, 1968, 8, 565.

123. N. Basco, D.G.L. James, R.D. Suart, Int. J. Chem. Kinetics, 1970, 2, 215.

124. F.K. Truby and J.K. Rice, Int. J. Chem. Kinetics, 1973, 5, 721.

125. H. E. Van den Bergh, A.B. Callear, R.J. Norstron, Chem. Phys. Lett., 1969, 4, 101.

126. R.W. Carr, I.D. Gay, G.P. Glass, H. Niki, J. Chem. Phys., 1968, 49, 846.

127. H.E. Avery and R.J. Cvetanovic, J. Chem. Phys., 1968, 48, 380.

128. J.V. Michael, D.T. Osborne, G.N. Suess, J. Chem. Phys., 1973, 58, 2800.

129. Published by Numerical Analysis Group, Oxford.

130. D.F. Mayers, "Numerical Solution of Ordinary and Partial Differential Equations", (ed. L. Fox), Pergamon, 1962, pp. 16-27.

131. A. Jones, Reaction Kinetics Vol. 1, Chemical Society Specialist Periodical Reports, 1975, p. 291.

132. F.A. Melamed, L.S. Polak, Yu L. Khait, Trans. Farad. Soc., 1968, 64, 1877.

133. R.H. Snow, J. Phys. Chem., 1966, 70, 2780.

134. J.R. McNesby, W. Braun, J. Ball, "Creation and Detection of the Excited state", ed. A.A. Lamola, Vol. 1, p. 503.

135. M.J. Pilling, A.M. Bass, W. Braun, Chem. Phys. Lett., 1971, 9, 147.

136. A.M. Bass and A.H. Laufer, Int. J. Chem. Kinetics, 1973, 5, 1053.

137. B.S. Rabinovitch and D.W. Setser, Adv. Photochem., 1964, 3, 1.

138. A.N. Tikhonov and A.A. Samarski, "Equations of Mathematical Physics" (International series of monographs on pure and applied mathematics, 39), Pergamon, 1963, p. 516.

139. J.K. Little, Part II Thesis, Oxford University, June 1972.

140. G.W. King, R.M. Hainer, P.C. Cross, J. Chem. Phys., 1943, 11, 27.

141. P.W. Atkins, "Molecular Quantum Mechanics", Oxford, 1970, p. 224, p. 389.

142. J.E. Bennet and D.R. Blackmore, 13th Symposium on Combustion, 1970, p. 51.

143. P.W. Atkins, "Molecular Quantum Mechanics", Oxford, 1970, p. 8.

144. H.M. Frey, Chem. and Ind., 1960, 1266.

145. T. Terao, N. Sakai, S. Shida, J. Am. Chem. Soc., 1963, 85, 3919.

146. M.E. Jacox and D.E. Milligan, J. Am. Chem. Soc., 1963, 85, 278.

147. G. Herzberg "Molecular Spectra and Molecular Structure I", 2nd ed., D. Van Nostrand, 1950, p. 558.

148. H.E. van den Bergh and A.B. Callear, Trans. Farad. Soc., 1971, 67, 2017.

149. R.D. Hudson, Rev. Geophys. and Space Phys., 1971, 9, 305.

150. C. Willis and K.D. Bayes, J. Phys. Chem., 1967, 71, 3367.

151. A. Forchioni and C. Willis, J. Phys. Chem., 1968, 72, 3105.

152. I.T.N. Jones and K.D. Bayes, Proc. Roy. Soc. (London), 1973, A335, 547.

153. P.J. Robinson and K.A. Holbrook, "Unimolecular Reactions", Wiley-Interscience, 1972.

154. P.J. Robinson, Reaction Kinetics, Vol 1, Specialist Periodical Reports, The Chemical Society, 1975, p. 73.

155. R.A. Marcus, J. Chem. Phys., 1970, 52, 1018.

156. W. L. Hase, J. Chem. Phys., 1972, 57. 730.

157. G.Z. Whitten and B.S. Rabinovitch, J. Chem. Phys., 1968, 48, 1427; 1964, 41, 1883; 1963, 38, 2466.

158. P.C. Haarhoff, Mol. Phys., 1963, 7, 101.

159. D.L. Bunker and M. Pattengill, J. Chem. Phys., 1968, 48, 772.

160. D.L. Bunker, J. Chem. Phys., 1964, 40, 1946.

161. W.L. Hase and D.L. Bunker, Quantum Chemistry Program Exchange, QCPE Program 234.

162. G. Herzberg, "Molecular Spectra and Molecular Structure I", D. Van Nostrand, 1950, p. 101.

163. G.J. Janz, "Thermochemical Properties of Organic Compounds", Academic Press, New York, revised edition, 1967, p. 21.

164. G. Herzberg, "Molecular Spectra and Molecular Structure II", D. Van Nostrand, 1945, p. 168.

165. H.S. Johnston, "Gas Phase Reaction Rate Theory", Ronald Press, New York, 1966, pp. 77 - 87.

166. E.B. Wilson, J.C. Decius, P.C. Cross, "Molecular Vibrations", McGraw-Hill, New York, 1955.

167. D.E. Milligan, M.E. Jacox, J. Chem. Phys., 1967, 47, 5146.

168. G. Herzberg, "Molecular Spectra and Molecular Structure II" D. Van Nostrand, 1945, p. 173, equation (II,200).

169. G. Herzberg, "Molecular Spectra and Molecular Structure II", D. Van Nostrand, 1945, p. 438, equation (IV,72).

170. D. Halliday and R. Resnick, "Physics", Wiley & Sons, Inc., 1967, p. 273.

171. H.S. Johnston, "Gas Phase Reaction Rate Theory", Ronald Press, New York, 1966, p. 125.

172. G. Herzberg, "Molecular Spectra and Molecular Structure II", D. Van Nostrand, 1945, p. 412.

173. H.C. Longuet-Higgins, Mol. Phys., 1963, 6, 446.

174. A.J. Merer and R.S. Mulliken, Chem. Rev., 1969, 69, 639.

175. G. Herzberg, "Molecular Spectra and Molecular Structure II", D. Van Nostrand, 1945, p. 288.

176. P.H. Kasai, J. Am. Chem. Soc., 1972, 94, 5950.

177. G.B. Skinner and E.M. Sokolski, J. Phys. Chem., 1960, 64, 1028.

178. G. Herzberg, "Molecular Spectra and Molecular Structure III", D. Van Nostrand, 1966, p. 442.

179. L.J. Weimann and R.E. Christoffersen, J. Am. Chem. Soc., 1973, 95, 2074.

180. J.E. Del Bene, J. Am. Chem. Soc., 1972, 94, 3713.

181. H. Basch, Theor. Chim. Acta, 1973, 28, 151.

182. R. McDiarmid, Theor. Chim. Acta, 1971, 20, 282.

183. G.W. Robinson, J. Chem. Phys., 1967, 47, 1967.

184. R.J. Donovan and D. Husain, Chem. Rev., 1970, 70, 489.